ISSN:2146-0957
eISSN:2146-5703

Volume:9 Number:2
July 2019

An International Journal of Optimization and Control: Theories & Applications

www.ijocta.com

IJOCTA
An International Journal of Optimization and Control: Theories & Applications
2010

www.ijocta.com
info@ijocta.com

An International Journal of Optimization and Control: Theories & Applications

Volume: 9, Number: 2

July 2019

Publisher & Owner *(Yayımcı & Sahibi)*:

Prof. Dr. Ramazan YAMAN
Istanbul Gelisim University, Faculty of Engineering and Architecture, Department of Industrial Engineering, Avcilar, Istanbul, Turkey
İstanbul Gelişim Üniversitesi, Mühendislik ve Mimarlık Fakültesi, Endüstri Mühendisliği Bölümü, Avcılar, İstanbul, Türkiye

ISSN: 2146-0957

eISSN: 2146-5703

Press *(Basımevi)*:

Bizim Dijital Matbaa (SAGE Publishing), Kazım Karabekir Street, Kültür Market, No:7 / 101-102, İskitler, Ankara, Turkey
Bizim Dijital Matbaa (SAGE Yayıncılık), Kazım Karabekir Caddesi, Kültür Çarşısı, No:7 / 101-102, İskitler, Ankara, Türkiye

Date Printed *(Basım Tarihi)*:

July 2019
Temmuz 2019

Responsible Director (Sorumlu Müdür):

Prof. Dr. Ramazan YAMAN

IJOCTA is an international, bi-annual, and peer-reviewed journal indexed/ abstracted by *(IJOCTA, yılda iki kez yayımlanan ve aşağıdaki indekslerce taranan/dizinlenen uluslararası hakemli bir dergidir)*:
Cabell's Directories, DOAJ, EBSCO Databases, JournalSeek, Google Scholar, Index Copernicus, International Abstracts in Operations Research, JournalTOCs, Mathematical Reviews (MathSciNet), ProQuest, Scopus, Ulakbim Engineering and Basic Sciences Database (Tubitak), Ulrich's Periodical Directory, and Zentralblatt Math.

We Use Plagiarism Detection iThenticate Learn More »

iThenticate and ijocta.balikesir.edu.tr are granted by Balikesir University.

An International Journal of Optimization and Control:
Theories & Applications
Volume: 9 Number: 2
July 2019

CONTENTS

An International Journal of Optimization and Control:
Theories & Applications
Volume: 9 Number: 2
July 2019

CONTENTS

An International Journal of Optimization and Control: Theories & Applications
ISSN: 2146-0957 eISSN: 2146-5703
Vol.9, No.2, pp.82-88 (2019)
https://doi.org/10.11121/ijocta.01.2019.00703

RESEARCH ARTICLE

Control and application of accuracy positioning estimation based real-time location system

Ahmet Aktas *

Department of Electrical Electronic Engineering, Simav Technology Faculty, Kutahya Dumlupinar University, Turkey
ahmet.aktas@dpu.edu.tr

ARTICLE INFO

Article history:
Received: 31 August 2018
Accepted: 11 December 2018
Available Online: 4 February 2019

Keywords:
Real-time location system
Accuracy positioning
Ultra-wide band
Positioning control algorithm
Worker tracking

AMS Classification 2010:
68U35, 93C95

ABSTRACT

Nowadays, with the development of ultra-wide band antennas and internet of thing technologies, tracing systems are being developed in many fields such as security, health, mining and transportation. The accuracy location estimation issue is becoming very important in areas of application where occupational health and safety are high. In these applications, the transfer of information between the target and the manager, whose location must be accuracy known, has become indispensable. Especially when the target person is human, the movement parameters such as speed, acceleration, position and altitude compose the calculation parameters of the central management system. The information to be sent by the worker in emergency situations and warnings explain the need for real-time location systems to avoid a possible occupational accident. This paper includes real-time location system structure and improved accuracy location control algorithm, which are being used in occupational health and safety, hospital, storage, mine and tracing areas. The real-time location system was designed using a DWM1000 location sensor module with an ultra-wide band integrated antenna. Product usage time has been extended in designed real-time location cards with low power consuming processors. An accuracy positioning control algorithm has been improved to quickly and exactly locate the target to be tracked. With this algorithm, a new approach to real-time location systems has been introduced and worker tracing, information and warning systems are made with fast response time. The control cards developed in a sample workspace were tested and the application results on the developed computer virtual map interface were given.

1. Introduction

The major role of the real-time location systems (RTLS) in its growth phase is the development of technologies for radio frequency identification (RFID), ultra-wide band (UWB) and bluetooth low energy (BLE). The reduction in the cost of RTLS technology and the improved data accuracy ensure more efficient, widespread and secure use [1].

Together with technological improvements, actual sensor applications such as RFID ensure the correct and proper use of worker protective equipment. In the literature, systems for remote tracing, pressure sensors and location technologies are integrated for occupational health and safety. The RTLS platform was created to evaluate the personal safety performances of workers with the virtual structure realized. It has been observed that there is a problem in transferring data transfer depending on weather conditions in a system using bluetooth communication network. In addition, the biggest problem in the implementation phase is that workers have shown that they need more time to using the RTLS system, which can delay the program of the projects to be carried out [2].

RTLS is also used to help multiple animals take their positions simultaneously and automatically evaluate them. With the work done, a RTLS was realized by integrating an animal into the ear tag. It has been determined that an average of 9% of the data losses is taken in the animal tracking system. In this system, which operates with the Euclidean distance measurement algorithm, the average accuracy of the measured data is increased to 2.7 m before filtering and 2.0 m after filtering [3].

*Corresponding author

In another study, a statistical case sequence model was developed to estimate different safety situations. An effective monitoring system has been established for managers with a method of predicting dangerous situations with recorded past data. With RTLS, an algorithm was developed to analyze the walking paths of the field workers in advance. It is defined as dangerous, risky or safe according to the status of the target object in the danger zone according to the predefined work areas [4].

Another use of RTLS is hospitals. Some hospitals in the U.S. have used RFID, ultrasound, ZigBee, and UWB based RTLS technologies to track staff and patients. At 23 hospitals, a technology infrastructure using RTLS for 3 years, analysis of the functionality and degree of functionality of the software has been examined. In hospitals using UWB technology, high accuracy positioning has been achieved. These technologies have resulted in many advantages such as staff and patient tracking in hospitals. However, as a result of the analysis, it had serious barriers to the use of the systems, due to the substandard functionality of low-cost used RTLS and administrative constraints of the hospitals [5].

A decision-making model has been developed that can select financial, technical and application factor parameters for the selection of RTLS to be used in different areas. A model for the selection of the correct RTLS was created using fuzzy logic in the study. Regarding the selection of the RTLS system planned for use in hospitals in Turkey compared to others with the proposed algorithm it has been chosen as the best alternative [6].

In another work, a virtual map is designed using RTLS. The study of the system with eight virtual workstations for the positioning of production resources has been examined [7].

National Institute of Occupational Health and Safety have developed smart software on the RTLS system. This smart software determines how work-based workers will settle around dangerous machines. The smart software, which is tested in the field of mines, evaluates the working site security conditions by reporting the locations of the workers to the system in real time. When the mine worker enters a dangerous machine or work area, the algorithm alerts. It has been found that the use of a smart proximity determining system, especially in hazardous and narrow working areas, helps to prevent possible work and worker accidents. For the safety of miners, the use of such proximity determining systems has come to the conclusion that workers should be accepted [8, 9].

Different RTLS systems have been developed for RFID based closed area positioning. Since the position accuracy is low in RFID systems, the position deviation error is eliminated by using the Kalman filter in the system for real locating. RFID readers have been used in areas limited by dual effective RFID tags. It has been shown that fast results are obtained with RFID location information system which is calculated using Kalman filter method. In addition, the system is combined with a bluetooth-based RFID reader for viewing on an Android-based smart phone [10].

In this study, wireless fidelity (Wi-Fi) and UWB network technology infrastructure were used together so there was no disconnection or delay during data transfer. It is sufficient to have the designed RTLS transmitter on the user or worker. In case of emergency, the operator informs the manager by pressing the emergency button which is easy to reach on the worker. In addition, when a situation such as a fall is encountered thanks to the acceleration sensor in the tag, the system emits an emergency signal via the central information screen very quickly. At the same time, emergency sirens in the anchor are used to inform people that there is a work accident. Thus, with this accuracy positioning control algorithm, it provides early intervention by receiving very fast feedback in a possible job accident (timely warning). Designed with these features, RTLS has a serious commitment in the occupational health and safety. This study presents a new approach to RTLS application areas, with the complete accuracy positioning algorithm developed together with the designed product, to the need for the accuracy location technology that has just begun to be used.

2. Real-time location system

By using evolving sensor technology, many techniques, methods and products have been designed to effectively tracing personnel and equipment. RFID tags are provided to ensure materials to be monitored when the scanners pass through predetermined points. Although materials can be traced through RFID technological infrastructure, it is insufficient in terms of personnel location in real time with this technology. In order to more accurate and precise location tracking, real-time location system technology has been developed. GPS based tracking systems have limited tracking accuracy. In addition, they have limited their use because their indoor performance is lower than the outside. Cameras and image processing technology tracking systems are also being developed in RTLS systems. There are limited uses since cameras and image processing technologies have very high data intensities and they are insufficient at edge points. Other alternative technologies are used in RTLS; such as 2.4 GHz BLE, Wi-Fi, ZigBee and Classic Bluetooth. UWB has become an innovative application area for RTLS because of its high accuracy positioning in large areas. In addition, one of the most important advantages of these tracing sensors is wearable technologies. As an example of its use, it can be easily used even in confined areas by placing it in the helmet used by the worker. These designed tracing sensor devices low power consuming and low weight [11, 12].

In this study, UWB based signal generating sensors are used which are low power and accuracy location estimation. There are tags and anchors in the RTLS structure. UWB is used in the tags; UWB and Wi-Fi wireless network communication architecture are used in the anchors. The short UWB signal sent by the tags is received by anchors. Each slave anchor, after calculating the distance traveled by the tag, it transmits it to the main anchor using the Wi-Fi infrastructure. Then the master anchor sends all the data to the server via Wi-Fi. Thanks to the improved accuracy positioning control algorithm, the distance to tag from anchor is calculated using at least three anchor data. The manager or administrator traces the target in real time with a RTLS interface, which is a virtual map of the work area. In the same way, using tags and anchors, emergency information is transmitted between the target and the manager to create a structure that gives timely warning. Thus, a RTLS structure is established that can operate in both open and closed areas. Architecture of RTLS used in this study is given in Figure 1.

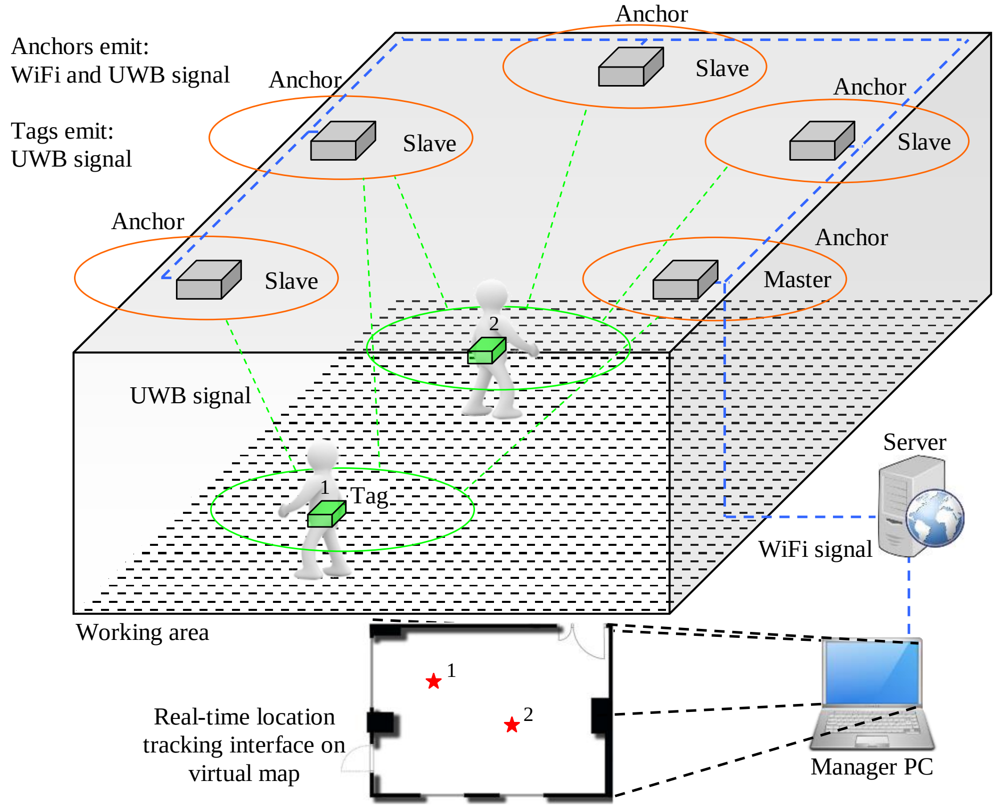

Figure 1. Architecture of real-time location system.

3. Accuracy positioning control algorithm

The mathematical algorithm to be used for accuracy location estimation in RTLS is very important for accuracy. In this paper, a unique accuracy positioning control algorithm has been developed to determine a precise location. This algorithm estimates the location with the data received using at least three anchors. This is why the intersection points of the anchors are important. There should be no blind point between the coverage of anchors. Therefore, the distance between each anchor should be 20-30 m depending on the working area to be installed. This limit is the communication distance of the DWM1000 location sensor module. This distance value should not be exceeded to get good quality and interference-free data.

When measuring the distance with 3 anchors, it appears that each of them generates areas of intersection of diameters. When a tag is placed in an area with a known distance between the anchors, the accuracy location can be determined by calculating the distances of the tag to the anchors. Figure 2 shows the positioning method between the anchors and tags required for the accuracy positioning control algorithm. Some calculations are made according to the accuracy positioning control algorithm to calculate the position of tag as in Figure 2. The target of tag to be traced will be expressed by T and its position in the x-y coordinate system will be determined. More than one anchor can be found on the same coordinate system. The distance between target tag T_1 and anchor is given by Eq. (1).

$$s_{T1} = \sqrt{(x - x_{T1})^2 + (y - y_{T1})^2} \tag{1}$$

In Eq. (1), s_{T1} is the distance between tag and anchor. x_{T1} and y_{T1} are the position of T_1 on the space coordinate system. Eq. (2) is obtained when Eq. (1) is continued.

$$s_{T1}{}^2 = x^2 - 2xx_{T1} + x_{T1}^2 + y^2 - 2yy_{T1} + y_{T1}^2 \quad (2)$$

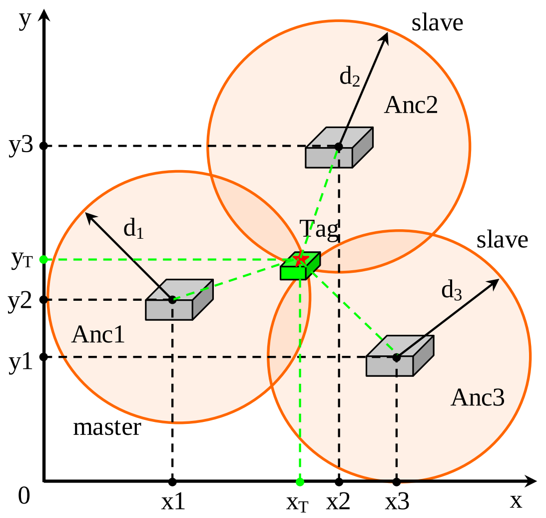

Figure 2. The positioning method between anchors and tags.

In order to convert an equation containing x^2 and y^2 to a linear equation, it is necessary to subtract s_{T1}^2 from s_n^2 as in Eq. (3). The s_n^2 is the new position value of the anchor that changes over time. In order to simplify the square expression in the Eq. (2) and to determine the tag that changed the position in time, the Eq. (3) is written.

$$\begin{aligned} s_{T1}^2 - s_n^2 &= -2(x_{T1} - x_n) + x_{T1}^2 - x_n^2 \\ &\quad - 2y(y_{T1} - y_n) + y_{T1}^2 - y_n^2 \end{aligned} \quad (3)$$

A linear series of equations are generated for determining the tag location. These linear equation solutions especially enable processors to perform fast processing at the computational stages. Eq. (3) is written in matrix form as in Eq. (4) for convenience in processors. Since a lot of samples are received over time, it is written in Eq. (4) to more easily calculate these values to the processor.

$$m = K\begin{bmatrix} x \\ y \end{bmatrix} \quad (4)$$

The matrix of Eq. (4) is written in detail as in Eq. (5).

$$m = \begin{bmatrix} s_1^2 - x_1^2 - y_1^2 - s_n^2 + x_n^2 + y_n^2 \\ s_2^2 - x_2^2 - y_2^2 - s_n^2 + x_n^2 + y_n^2 \\ \vdots \\ s_{n-1}^2 - x_{n-1}^2 - y_{n-1}^2 - s_n^2 + x_n^2 + y_n^2 \end{bmatrix} \quad (5)$$

The matrix K is given in Eq. (6).

$$K = -2\begin{bmatrix} x_1 - x_n & y_1 - y_n \\ x_2 - x_n & y_2 - y_n \\ \vdots & \vdots \\ x_{n-1} - x_n & y_{n-1} - y_n \end{bmatrix} \quad (6)$$

If there are 3 anchors in the RTLS as in Figure 4, n=3.

The location of tag to be traced T is calculated by Eq. (7).

$$T = K^{-1}m \quad (7)$$

If there are more than 3 anchors in RTLS, the unknown number in the equation will increase. However, it will be ensured that the target is more sensitive to the determination of T location. Eq. (8) gives the equation of T location calculation when there are more than 3 anchors.

$$T = \left(K^T K\right)^{-1} K^T m \quad (8)$$

K^T takes the transpose form of the K matrix.

The estimation model developed for accuracy positioning control algorithm finds the target location with the smallest error. During the anchors measurements with tag, although the working area is ideal, sometimes there can be some noise. This problem can be overcome by bringing exactly intersecting areas, especially with anchors. Also the distance data collected by the anchors is reduced by the Kalman filter. The proposed algorithm collects data at intervals of 100 milliseconds. After each of the collected data is filtered, accuracy position calculation is performed for each. After the mathematical operations given in the study, every 100 millisecond position is recorded in the registers. Then, these position values are compared and high error rate data is filtered. Thus, by using an accuracy positioning control algorithm, a RTLS is created providing fast, accuracy and timely warnings and a new approach is taken by the studies in RTLS area. The flowchart of the accuracy positioning control algorithm is given in Figure 3.

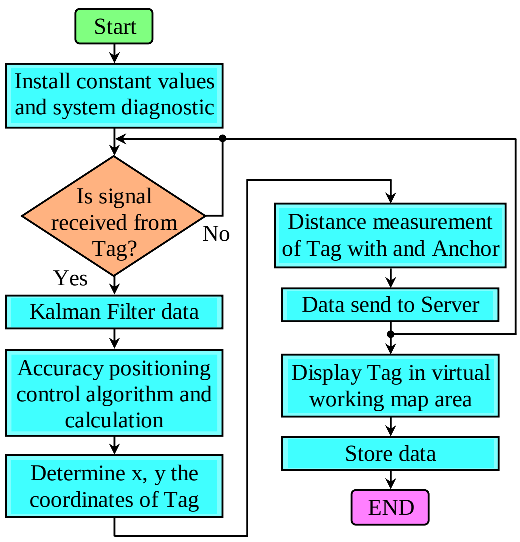

Figure 3. Flowchart of accuracy positioning control algorithm in RTLS.

4. Experimental RTLS setup and study result

The UWB based DWM1000 location sensor module produced by Decawave was used in the tags in RTLS. This sensor is compliant for the IEEE 802.15.4-2011 standard which supports multiple data transfer in high and low band. DWM1000 with low power consumption can be performed data transfer at 110 kbps, 850 kbps and 6.8 Mbps. Table 1 is given details the characteristics of the UWB based DWM1000 location sensor module [13]. This location sensor with integrated antenna, which can reduce the noise sources can accuracy determine the location. In addition, each tag uses 32-bit ARM core processors (Atmel SAM3X8E ARM Cortex-M3) which performs data transfer operations and controls. The tag topology structure and photograph used in RTLS are given in Figure 4.

Table 1. DWM1000 module technical speciation [13].

UWB based DWM1000 module
IEEE802.15.4-2011 UWB compliant
Promote 4 radio frequency band from 6.5 Ghz
Determines targets to a sensitive of 10cm closed area
Integrated radio frequency antenna
Large transmission range (290 m)
Low power consumption (TX, RX: 150 mA)
Cost-effective RTLS application

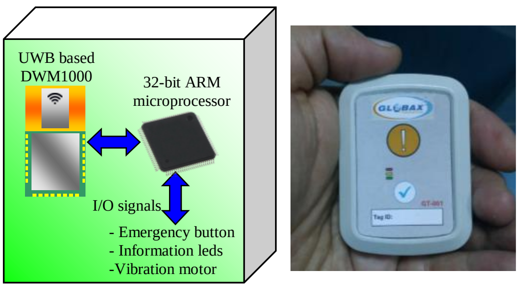

Figure 4. Tag topology structure and photograph in used RTLS.

The anchors in RTLS also include both UWB based DWM1000 location sensor module and Wi-Fi module. The ESP-12 Wi-Fi module is used as the Wi-Fi communication network. This ESP-12 Wi-Fi module is very suitable for use in RTLS thanks to its low power consumption and compact dimensions. It is also becoming more affordable for anchor networks to be installed in large working areas. As with the tags, 32-bit ARM core based processors are used in anchors. After the distance of the tags is measured, the wireless network technology transfers the data to the master Wi-Fi very quickly and the necessary data is sent for the accuracy positioning control algorithm. Depending on the working area, it is necessary to be 20-30 m between the anchors in order to be able to make accuracy location tracing. Through the wireless network infrastructure to be created, it is possible to trace a target in the ratio of mm-cm sensitivity. The anchor topology structure and photograph used in RTLS are given in Figure 5.

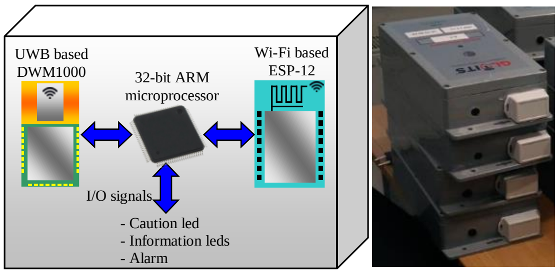

Figure 5. Anchor topology structure and photograph in used RTLS.

RTLS performance has been studied by performing worker tracing on a sample construction working area. The designed tags were produced as a wearable device so as not to interrupt the working program of the worker's construction area. Thus, both the worker is fulfilling occupational health and safety, and the position of the worker can be monitored in real time. In figure 6 is given a photograph of the worker tracing application in the construction working area where RTLS is installed. Here, tags and anchors are placed in the working area between 10 m and 15 m intervals. The system is then operated via the UWB network. Data were collected in a single center via server using Wi-fi infrastructure. The manager follows this data in detail on the virtual map.

Figure 6. RTLS application in working area.

Figure 7 shows the values of the tag position in the x and y coordinates, which are received 100 ms frequently during RTLS application. Accuracy location algorithm allows the tag location to be measured with an error of approximately 10-20 cm.

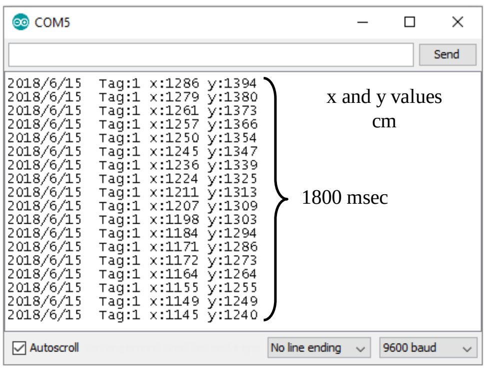

Figure 7. Tag location values in x and y coordinates.

In the implemented RTLS study, accuracy positioning control algorithm is used to determine the target location and send it to the server over the wireless network. The location of worker with data sent to server is presented in real time on the previously prepared virtual map to the manager. Real-time location tracking interface on virtual map is given in Figure 8. In addition to monitoring RTLS, it also ensures bidirectional communication support, thus providing a timely alert infrastructure. The low power consumption of RTLS effectively supports the use of these technologies. Moreover, thanks to this wearable technology, which can be easily placed inside the helmets, it has been given a different dimension to occupational health and safety, work quality and productivity.

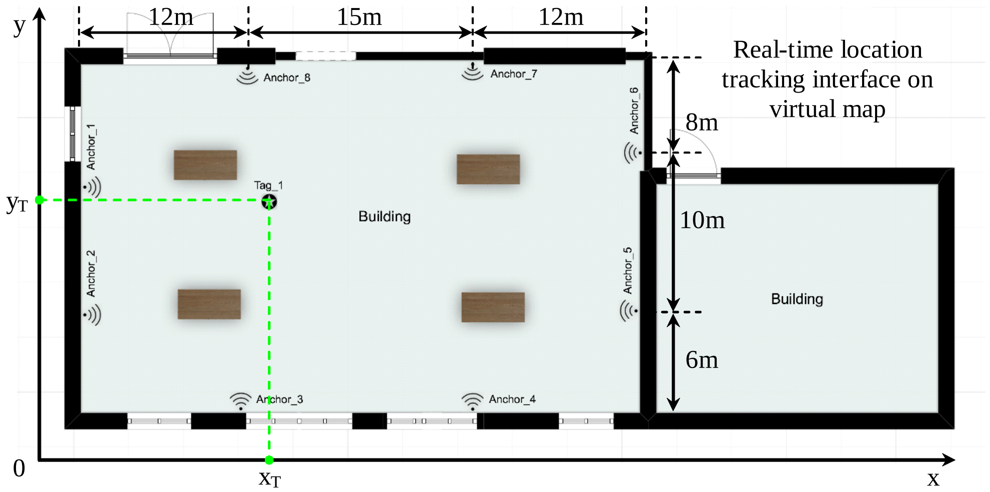

Figure 8. Real-time location tracking interface on virtual map, PC of manager.

5. Conclusion

Recently, with the increase of wearable technologies, many innovations have emerged in the area of accuracy positioning studies. In this study, an accuracy positioning sensor was used to examination that could be used especially in the area of occupational health and safety. The location of the target to be tracked by the developed accuracy positioning control algorithm is monitored in real time. This algorithm also reduces the computation time on the processor by means of fast processing, thus allowing the target to be tracked more frequently and accurately. This study also provided bidirectional data transfer between the worker and the manager by providing quick feedback which is one of the vital issues in terms of occupational health and safety.

A wireless infrastructure was created with UWB based DWM1000 location sensor module and Wi-Fi based ESP-12 module. Thanks to wireless architecture, RTLS can be installed easily and stable, fast and accurate data transfer can be realized. In addition, a virtual map of the working area has been created with the RTLS interface developed for the manager. The location of the target is monitored in real time on the virtual map and in case of emergency, the target is quickly reached and the warning sensors in the area are used to make audible and illuminated notification to the surrounding area. A new perspective has been introduced in the accuracy location estimation with this RTLS study.

In this paper, the worker position was monitored at intervals of 100 ms and the location was traced with a sensitivity of approximately 10-20 cm. In future works, camera can be added to this RTLS to provide real-time monitoring of the working area. Thus, it is possible to lead the working ergonomics by observing the working movements of the workers.

Acknowledgment

This study was supported by within Globax Technology Group company.

References

[1] Li, H., Yang, X., Wang, F., Rose, T., Chan, G., & Dong, S. (2016). Stochastic state sequence model to predict construction site safety states through Real-Time Location Systems. *Safety Science*, 84(1), 78-87.

[2] Donga, S., Lib, H., & Yinb, Q. (2018). Building information modeling in combination with real time location systems and sensors for safety performance enhancement. *Safety Science*, 102(1), 226-237.

[3] Willa, M.K., Büttner, K., Kaufholz, T., Müller-Graf, C., Selhorst, T., & Krietera, J. (2017). Accuracy of a real-time location system in static positions under practical conditions: Prospects to track group-housed sows. *Computers and Electronics in Agriculture*, 142(1), 473–484.

[4] Sunderman, C., & Waynert, J. (2012). An Overview of Underground Coal Miner Electronic Tracking System Technologies. *IEEE Industry Applications Society Annual Meeting*, Las Vegas, USA, 1-5.

[5] Fisher, J.A., & Monahan, T. (2012). Evaluation of real-time location systems in their hospital contexts. *International Journal of Medical Informatics*, 81(10), 705-712.

[6] Budak, A., & Ustundag, A. (2015). Fuzzy decision making model for selection of real time location systems. *Applied Soft Computing*, 36(1), 177-184.

[7] Huanga, S., Guo, Y., Zha, S., Wang, F., & Fang, W. (2017). A real-time location system based on RFID and UWB for digital manufacturing workshop. *Procedia CIRP*, 63(1), 132-137.

[8] Jobes, C., Carr, J., DuCarme, J., & Patts J. (2011). Determining Proximity Warning and Action Zones for a Magnetic Proximity Detection System. *IEEE Industry Applications Society Annual Meeting*, Orlando, USA, 1-7.

[9] Rashid, K.M., & Datta, S. (2017). Coupling Risk Attitude and Motion Data Mining In A Preemtive Construction Safety Framework. *Winter Simulation Conference (WSC)*, Las Vegas, USA, 2413-2424.

[10] Huang, C.H., Lee, L.H., Ho, C.C., Wu, L.L., & Lai, Z.H. (2015). Real-Time RFID Indoor Positioning System Based on Kalman-Filter Drift Removal and Heron-Bilateration Location Estimation. *IEEE Transactions on Instrumentation and Measurement*, 64(3), 728-739.

[11] Xiong, T., Liu, J., Yang, Y., Tan, X., Min H. (2010). Design and Implementation of a Passive UHF RFID-Based Real Time Location System. *Automation and Test Proceedings of 2010 International Symposium on VLSI Design*, Hsin Chu, Taiwan, 95-98.

[12] Sarrafan, K., Muttaqi, K.M., Sutanto, D., & Town, G.E. (2017). An Intelligent Driver Alerting System for Real-Time Range Indicator Embedded in Electric Vehicles. *IEEE Transactions on Industry Applications*, 53(3), 1751-1760.

[13] Decawave. (2018). *DWM100 Module. Available at*: https://www.decawave.com/products/dwm1000-module, Accessed 18 July 2018.

***Ahmet Aktas** received his B.Sc. in Electrical Education from Kocaeli University in 2010. He received the M.Sc. degree from department of Energy Systems Engineering, Kocaeli University in 2013. Finally, he got his PhD in Energy Systems Engineering at Kocaeli University in 2016. He has published many papers in different subjects including multilevel inverters, photovoltaic power generation systems, renewable energy sources, energy storage technologies, battery and ultra-capacitor modeling, smart energy management, microcontroller programming, smart grid integration, microprocessor-based application systems, offshore wind turbine and flow energy. He is a member of IEEE and a reviewer at the IEEE Transactions on Sustainable Energy and IEEE Transitions on Energy Conversion magazine. He designs custom cards for military vehicles in the defense industry. He is listed in Editorial Team of the International Journal of Electric Power Science Development. He is currently a Department of Electrical and Electronics Engineering, Kutahya Dumlupinar University.*

An International Journal of Optimization and Control: Theories & Applications
ISSN: 2146-0957 eISSN: 2146-5703
Vol.9, No.2, pp.89-99 (2019)
https://doi.org/10.11121/ijocta.01.2019.00718

RESEARCH ARTICLE

A bi-objective model for sustainable logistics and operations planning of WEEE recovery

Emine Nisa Kapukaya [a], Alperen Bal [b], Sule Itir Satoglu [a *]

[a] *Department of Industrial Engineering, Istanbul Technical University, Turkey*
[b] *Department of Industrial Engineering, Yalova University, Turkey*
eminenisacann@gmail.com, alperenbal@live.com, onbaslis@itu.edu.tr

ARTICLE INFO

Article history:
Received: 25 September 2018
Accepted: 24 December 2018
Available Online: 6 February 2019

Keywords:
Waste recovery
Sustainable operations planning
Bi-objective model
Waste electrical-electronic equipment

AMS Classification 2010:
90C29, 90C05

ABSTRACT

The Triple-bottom-line concept suggests that firms must consider the environmental and social impacts of their decisions, beside the economic aspects. Hence, the sustainability of the firms' operations can be reached. The purpose of this study is to develop a bi-objective, multi-product and multi-period mixed-integer model for the operations planning of electrical-electronic waste (WEEE) recovery facilities, by considering social (workforce) constraints. Main objective is the minimization of net recycling and logistics costs offset by the profit earned by recovered material sales, and second objective is the maximization of hazardous materials recovery. Collection of used products from the specified regions is decided and the required machine-hours, inventory and workforce decisions are made. Besides, both weight-based and unit-based WEEE recovery targets are separately considered, as a unique aspect. A sensitivity analysis is conducted with various scrap prices to understand operations planning in changing conditions. Results show that weight-based targets enhance recovery amounts.

1. Introduction

In today's world, because of the rapid increase in consumption of the commercial products, the natural resources are depleting. Therefore, many countries search for new natural sources or intend to reuse the existing ones. Waste materials that are recovered and recycled may provide a solution for this problem. In accordance, the paradigm has now become "cradle-to-cradle" waste management by means of evaluation, recycling and reuse of the end-of-life products' wastes [1].

The term of Triple-bottom-line (TBL) first proposed by Elkington [2], suggests that firms must consider the environmental and social impacts of their decisions, in addition to the economic aspects. Hence, the sustainability of the businesses can be achieved. Nikolaou et al. [3] also mentioned that companies must have social responsibility beside their profitability targets.

The reverse logistics (RL) enhances the application of the TBL approach, and concerns flow of end-of-life products to the special facilities for recovery of the waste material. The formal definition is as follows: "Reverse Logistics is the process of planning, implementing, and controlling the efficient, effective inbound flow and storage of secondary goods and related information opposite to the traditional supply chain direction for the purpose of recovering value or proper disposal." [4]. In this context, sustainability, as defined by its TBL factors of economic, environmental, and social dimensions is the underlying framework that we use in this study, during the reverse logistics and operations planning [5].

In this study, especially the Cooling and Freezing (CFC) product wastes are considered, because according to the report of the United Nations University, by the application of European Union's 2002 WEEE Recovery Directive, from the estimated 36 million tons of avoided CO emissions, 34 million tons results from removing CFC based cooling agents [6]. Therefore, CFC recovery is the most remarkable issue in WEEE recovery.

The purpose of this study is to develop a bi-objective, multi-product and multi-period mixed-integer model

*Corresponding author

for the sustainable operations planning of WEEE (especially refrigerator) recovery facilities, by considering social (workforce) constraints. Main objective is the minimization of net recycling and logistics costs offset by the profit earned by recovered material sales, and second objective is the maximization of hazardous materials recovery. Based on the region distances and amount of WEEE, whether to collect used products from the specified regions is decided and the required machine-hours, inventory and workforce decisions are made. Besides, both weight-based and unit-based WEEE recovery targets are separately considered, in different scenarios, as a unique aspect. A sensitivity analysis is conducted with various scrap prices to have better understanding of the operations planning in changing conditions.

The paper is organized as follows: The driving forces of WEEE recovery are discussed in Section 2. Later, the most relevant reverse logistics studies are reviewed. In Section 4, the bi-objective model is proposed and explained. In Section 5 , a real life application of the proposed model for reverse logistics operations planning of a refrigerator recovery plant is explained that shows applicability of our study. The Results are discussed in Section 6. An extensive Sensitivity Analysis is performed to analyze the impact of uncertainty in scrap prices and recovery cost of hazardous wastes. Finally, the Conclusion is made.

2. Driving forces of WEEE recovery

Development of third world countries led to increase in the consumption, so some of the natural sources and raw materials are expected to be depleted soon. Reusing these sources will provide a new dimension to this problem. In some developed countries, waste management and prevention are being pursued with legal legislations. These directives also put obligations on issues such as how much the product must be recycled.

Firms are collecting end-of-life products especially because of the legislations. Since the reverse logistics have complex structure and processes are hard to implement, it is rather challenging for the firms to make profit from RL. Establishing an efficient RL network is very costly when considering the small amount of profit, it provides (if any). In some developing countries, the periodically applied ‘bring old take new one’ campaigns are implemented mainly to increase the market share of the company, not to reuse or recycle the products. Since there is not any financial penalty in legislations, environmental obligations are also not very encouraging. Driving force for RL is not the economy; legislations and environmental concerns are the factors that make RL compulsory.

2.1. Economy

Many developed countries put legislations to increase the returned and recovered end-of-life product amount [6-8]. Other developing countries are also working on these types of legislations[9-10]. Being prepared for these legal obligations in advance is a step that can provide superiority to other firms. Improving the firms’ image can be one of the indirect contribution of the RL. Direct and indirect incomes, sales of the materials obtained and the cost reduction in energy are the economic gains.

2.2. Legislations

There has to be legal legislations to force the firms to recover the waste. With obligations, public should be made aware of the importance of the collection of recyclable wastes. Legislation will set certain standards and companies will have to follow up on collection, disposal, recycling, and marketing their products. Many companies in developing countries have accelerated their recycling activities due to new sanctions that will come with directives.

2.3. Environmental concerns

To minimize the negative impacts of waste, proper management strategies should be followed. By reusing, recycling and remanufacturing the WEEE, social and environmental benefits are obtained at the same time. In addition, green company image and advanced customer supplier relationship are profitable for the firms. Environmental issues that are considered in logistics are nonrenewable resources, gas emissions, density and road use, noise pollution, destruction of both harmful and harmless wastes. Besides, CO emission reduction by means of WEEE recycling was reported as much as 36 million tons [11].

3. Literature review

In this section, mathematical modeling studies in RL are discussed. As there are several papers in this field, interested readers can refer to the literature review papers. Especially, Fleischman et. al. [12] reviewed the quantitative models of distribution, production planning, and inventory control in the reverse logistics field. Later, Ilgin and Gupta [13] examined environmentally conscious manufacturing and product recovery papers published between 1998 and 2010. Agrawal et al. [14] reviewed advances in reverse logistics, especially RL studies and perspectives. Recently, Govindan and Soleimani [15] made a review about the reverse and closed-loop supply chain studies.

We would like to mention a few important RL papers and books, here. Hu et al. [16] proposed a cost minimization model recovery of multiple types of hazardous wastes, in multiple discrete time periods. Besides, e-waste types are defined and legislations and the incentives to increase the amount of returned WEEE were discussed [17]. Kumar et. al. [1] examined the closed loop supply chain with SWOT analysis, especially in the successful industry segments, such as, automotive, consumer appliances and electronic and showed the effect of the legislations upon them. Bal et.

al. [18] analyzed WEEE recovery data of Turkey, by neural networks and ANOVA. Kahhat et. al. [19] investigated the WEEE recovery practices and factors affecting the e-waste return in USA. Contributions of OR to the green logistic are mentioned and discussed with many aspects; such as transportation, inventories, supply chain design and planning [20]. Now, the studies pertaining the Single-Objective Models and Multi-objective models are discussed.

3.1. Single-objective models

In this sub-section, single-objective models developed after year-2000 are mentioned. Shih [21] developed a cost-minimization model for reverse logistics planning of WEEE and computers, in Taiwan in 2001. Listes and Dekker [22] created deterministic and stochastic MILP location-allocation models and two-stage and three-stage solution approaches were applied. Stochastic and deterministic models were compared with each other. Additionally, Listes [23] proposed a generic two stage closed loop supply return network model and the L-shape method to maximize the net revenue based on a stochastic approach.

El-Sayed et al. [24] suggested a single objective, multi period multi echelon closed loop supply chain model and the effects of mean demand and return ratio changes were evaluated. Problem was formulated by a Stochastic Mixed Integer Linear Programming (MILP). Furthermore, Achillas et. al. [25] also formulated a MILP model for WEEE collection based on the existing facilities supply chains. Dondo and Mendez [26] developed a cost-minimization model for planning of forward and reverse logistics activities. Recently, Pedram et al. [27] formulated a model to design a closed-loop supply chain including facility location and material flow decisions by maximizing the total profit.

3.2. Multi-objective models

The RL is naturally a multi-objective problem where the environmental and economic aspects must be considered. In addition to these factors, the social aspect is also important. Therefore, there is an increasing number of RL literature with multiple objectives.

Tuzkaya et. al. [28] proposed a model with two objective functions and performed an application in white good industry in Turkey. First objective function aimed to minimize the net cost and the second one maximized the amount of weighted product assigned to the centralized return centers from the initial collection centers. A Genetic Algorithm was applied to solve the problem. Ahluwalia and Nema [29] proposed a multi-objective model for recovery of the computers based on life-cycle assessment. Later, the same authors developed a multi-time-step multi-objective decision-support model minimizing the cost, environmental risk, socially perceived risk and health risk at the same time to decide the optimum waste collection locations [30].

In the model of Ramezani et al. [31], different parameters such as price, production costs, operating costs, collection costs, disposal costs, demands and return rates are assumed to be uncertain. ε-constraint method was used to generate a set of Pareto-optimal solutions for solving this three-objective problem. Objectives of the model were maximizing the total profit, maximizing the customer service level and minimizing the defected products that are provided by suppliers.

A bi-objective, single period, non-linear model was reformulated as a MIP [32]. Environmental protection level was described for the first time in the literature. The model aimed to minimize total cost and total CO emission within the supply chain. Türkay et. al. [33] modified the traditional aggregate production and operations planning approach by considering the environmental and social dimensions, based on the TBL perspective.

A closed loop facility location model was proposed by Amin and Zhang [34] in a supply chain network with multiple facilities and multiple products, and was solved by weighted sums and ε-constraint methods. Authors shown that ε-constraint method provided more efficient solutions. After uncertainties in demand and returns taken into account, it was solved with a scenario-based stochastic programming model.

Another multi-objective MIP model was proposed for location-routing with three objective functions by Samanlioglu [35]. Objectives were minimizing total cost, total transportation risk of hazardous materials and site risk. Ene and Ozturk [36] developed a bi-objective model for network design of recovery facilities of the end-of-life vehicles where maximization of the revenue and minimization of the pollution due to recovery operations were aimed.

To sum up, there is an increasing number of multi-objective RL studies in the literature. However, most of them were deterministic. To the best of authors' knowledge, in none of the deterministic studies, a sensitivity analysis was performed. This is a contribution of our study to the literature.

4. Proposed bi-objective model

The assumptions for proposed bi-objective model are presented as follows :

Additional workforce always exists, when needed.

The manufacturer does not have to collect products from every region; if it can reach the given goal by collecting goods from some of the regions.

There is no capacity limit for inventory and the demand of the secondary market of recovered material is unlimited.

Collected refrigerators are directly transferred to the RL facility.

The disposal cost of harmful materials includes the cost of transportation.

The amount of the material obtained from the recycling of the product is directly proportional to the weight of the product.

Machine process times are deterministic.

Recycle facility location is already determined.

This model answers the following questions:

1. How much is the company's net gain when it reaches the target collection numbers or how much does it cost if it has loss?

2. How much of the harmful wastes to be properly disposed are sent to the licensed firms?

3. In which period (month), from which region, how much product will be collected?

4. When and how much capacity increase is needed(if any)?

5. What are the inventory levels and required labor sources?

4.1. Indices

i: $Product\ index\ (i \in I)(i = 1,2)$

b: $Geographical\ regions\ \ index\ (b \in B)(= 1,..,7)$

t: $Periods\ index(Months)\ (t \in T)(t = 1,..,12)$

j: Recovered material index (j∈J)(j = 1,..,9)

m: Machine index $(m \in M)(m = 1,..,6)$

S: $Subset\ of\ hazardous\ materials\ (S \subset J)(= 7,8)$

4.2. Decision Variables

$Y_b = \begin{Bmatrix} 1, if\ product\ is\ collected\ from\ region\ b \\ 0, \quad otherwise \end{Bmatrix}$

x_{itb}: $Number\ of\ from\ product\ i\ collected\ \ from\ region - b, in\ period\ t.$

L_t: $Required\ labor\ source\ in\ period\ t\ (man * hour)$

I_{it}: $Inventory\ of\ product - i\ that\ is\ held\ at\ the\ end\ of\ period\ t.$

$z_1 = Objective - 1$

$z_2 = Objective - 2$

4.3. Parameters

LC_t: $Labor\ cost\ per\ worker\ in\ period\ t$

F_b: $Fixed\ cost\ of\ working\ with\ a\ 3rd\ party\ provider\ to\ collect\ waste\ product\ from\ region\ b.$

T_{im}: $Time\ required\ to\ process\ the\ product\ i\ in\ machine\ m$

G_i: $Manual\ operational\ time\ per\ one\ piece\ of\ product - i.$

$Cap_{m,t}$: $Capacity\ of\ machine\ m\ in\ period\ t\ (hour)$

H_i: $Unit\ Inventory\ Holding\ cost\ of\ one\ piece\ of\ product\ per\ month$

Dis_b: $Distance\ of\ center\ of\ the\ region\ b\ from\ the\ facility$

R_j: $Revenue\ that\ is\ gained\ by\ sales\ of\ material\ j\ per\ kg$

d_{it}: $Amount\ of\ product\ i\ that\ can\ be\ collected\ in\ period\ t$

TC: $Unit\ transportation\ cost\ per\ km\ for\ one\ full - truck\ load.$

Mij: Material j obtained from one piece of product i.

Cm: $Cost\ of\ processing\ for\ one\ machinem\ per\ hour.$

$weight_i$: $Weight\ of\ product\ type\ i\ (kg).$

4.4. Scalars

FTL: $Full\ truck - load\ (kg).$

$Legco$: $Targeted\ collection\ amount\ according\ to\ legislation.$

TC: $Transportation\ cost\ per\ km.$

FCT: $Fixed\ cost\ of\ a\ truck.$

$FiCost$: $Annually\ fixed\ cost\ of\ the\ facility\ (maintanance, office, management..)$

$Legcoweight$: $Weight\ based\ targeted\ collection\ coefficient.$

4.5. Objectives

Objective 1 (Cost minimization)

$$minz = \sum_t L_t LC_t + \sum_{b \in B} F_b * Y_b + \sum_{b \in B} \sum_{t \in T} \sum_{i \in I} \frac{x_{itb}}{FTL} * TC * Dis_b * weight_i + \sum_{b \in B} \sum_{t \in T} \sum_{i \in I} \frac{x_{itb}}{FTL} * weight_i * \mathrm{FCT} + \sum_{b \in B} \sum_{t \in T} \sum_{i \in I} \sum_{m \in M} x_{itb} * T_{im} C_m + \sum_i \sum_t H_i I_{i,t} + - \sum_{j \in J} \sum_i \sum_t \sum_b (R_j) M_{ij} x_{itb} + FiCost \tag{4.1}$$

Objective 2 (Recovery of the most hazardous materials must be maximized)

$$\max z = \sum_{j \in S} \sum_i \sum_t \sum_b x_{itb} * M_{ij} \tag{4.2}$$

4.6. Constraints

Capacity constraint for the machines

$$\sum_i \sum_b x_{itb} * T_{im} \le Cap_{m,t};\ \forall t, \forall m \tag{4.3}$$

Legislation target constraint

$$\sum_b \sum_t x_{itb} \ge \sum_t d_{it} \times Legco; (\forall i \in I) \tag{4.4}$$

Collection constraint

$$x_{itb} \le d_{it} * Y_b; (\forall i \in I)\ (\forall b \in B\ )(\forall t \in T\ ) \tag{4.5}$$

Stock balance constraint

$$I_{i(t-1)} + d_{it} - \sum_{b \in B} x_{itb} = I_{it};\ \ (\forall i \in I)\ (\forall t \in T\ ) \tag{4.6}$$

Labor constraints

$$\sum_{i \in I} \sum_{b \in B} x_{itb} G_i = L_t\ ; (\forall t \in T) \tag{4.7}$$

Truck constraints

$$\sum_i weight_i * x_{itb} \leq FTL \ (\forall b \in B)(\forall t \in T) \tag{4.8}$$

Sign constraints:

$$x_{itb} \in Z^+; \quad \forall i \in I; \ \forall t \in T; \forall b \in B \tag{4.9}$$

$$L_t \geq 0; \ \forall t \in T \tag{4.10}$$

$$I_{i,t} \geq 0 \forall i \in I; \forall t \in T \tag{4.11}$$

$$Y_b \in \{0, 1\}; \ \forall b \in B \tag{4.12}$$

In equation 5.1, in the first objective function, total cost is minimized. Labor cost, normal disassembly cost of the collected, products logistics cost (transportation and fixed cost of a truck for every tour), machining cost, total inventory holding cost, annual fixed cost of the facility and disposal cost of hazardous waste are the cost terms considered. Revenue gained from the sales of the recycled materials is subtracted from the sum of the total cost to find the first objective. In the equation 4.2, amount of materials that properly disposed is maximized as second objective. Since not all of the materials are hazardous, only the most dangerous ones are taken into account, this is an environmental objective.

Equation 4.3 satisfies that the required machine hour is no more than capacity of the machines. In equation 4.4 at least target amount of product is recycled that is set by legislations. This target is formulated by product of sales amount and legislative target ratio. Note that, recovery targets are defined in terms of number of products recovered, here. This is called unit-based recovery target. However, alternatively, this constraint is formulated as a weight based target which means at least same tons of WEEE must be recovered. The alternative formulation as the constraint is as follows where Legcoweight shows legislated coefficient for weight-based target [10] :

$$\sum_b \sum_t x_{itb} * weight_i \geq \sum_t d_{it} \ Legcoweight * weight_i; \ (\forall i \in I) \tag{4.13}$$

Equation 4.5 ensures that maximum amount that can be collected from a region is less than the available amount of products in that region. Available amount is equal to electrical-electronic equipment that comes to end-of-life, so the producer can collect them. The amount of recycled product cannot be more than the product that can be collected.

In the stock balance constraint equation 4.6, the inventory of period-t equals to the previous period's inventory plus collection amount at period-t minus the collection amount at period t.

In the equation 4.7 which is a labor constraint shows the work force amount in man-hour.

Truck constraint stipulate that the total collected amount of a region-b in period-t cannot be greater than the full truck load. Equations 4.9, 4.10 and 4.11 are non-negativity and integer constraints, x_{itb} amount of the collected product is integer and L_t and $I_{i,t}$ are greater than or equal to zero. It is shown that Y_b(whether to collect from a region-b) is binary variable in equation (4.12). The legislative weight-based targets are announced in [10].

5. An application for the white goods industry

In this study, the proposed model is implemented to a Reverse Logistics Facility that recovers waste material and safely collects hazardous substances from the refrigerators. In this section, results will be explained after solving the proposed model using GAMS®. In RL, more than one objective may be targeted. The proposed model that is bi-objective, has both economic and environmental concerns. Besides it has a workforce constraint pertaining to the social aspect. Here it is intended to show our model's applicability with a real world data set.

In Figure 1, the costs of different RL stages are shown (transportation and collection, shredding-sorting-dismantling-pretreatment, recycling-recovery, and incineration and landfill) for different product categories, namely cooling& freezing (C&F), lamps, large household appliances (LHHA), small household appliances (SHA), CRT-FDP tubes. Here, the negative values in the bar diagram show the benefit earned out of one unit of this type of product. One can conclude that cooling &freezing products have the greatest benefit potential, if the waste material can be recovered. The reason of selecting the refrigerator in this study is this great benefit potential. In this study there are two types of refrigerators to be recovered: Type-1 is big-size and type-2 is bar-type with a smaller size.

To estimate the amount of waste refrigerator we use production and domestic sales data. The previous years (1992 to 2015) semi-annual production and domestic sales data of refrigerator are available. Since the production and sales amounts are required for the coming years, forecasting method is used. Average lifetime of a refrigerator is accepted as 11 years [38].

The stages of a refrigerator recovery are shown in Figure 2. The first group of stages are manual dismantling, sorting, and separation, and the second one is called mechanical shredding and separation. In yellow rectangles, the waste material that are recovered from the product at each stage are shown.

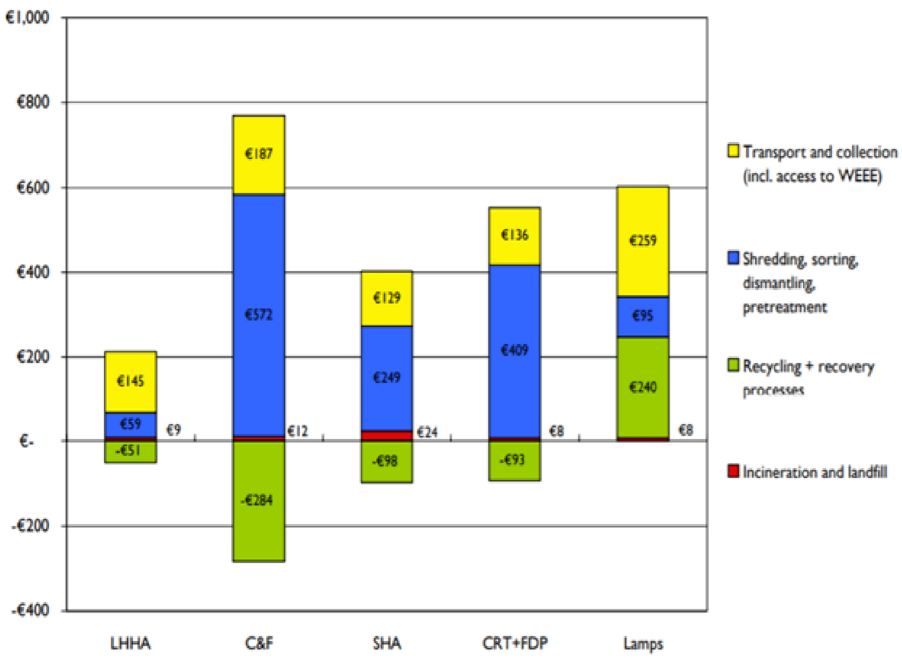

Figure 1. Technical costs for the five main categories in RL per ton in 2007 [37].

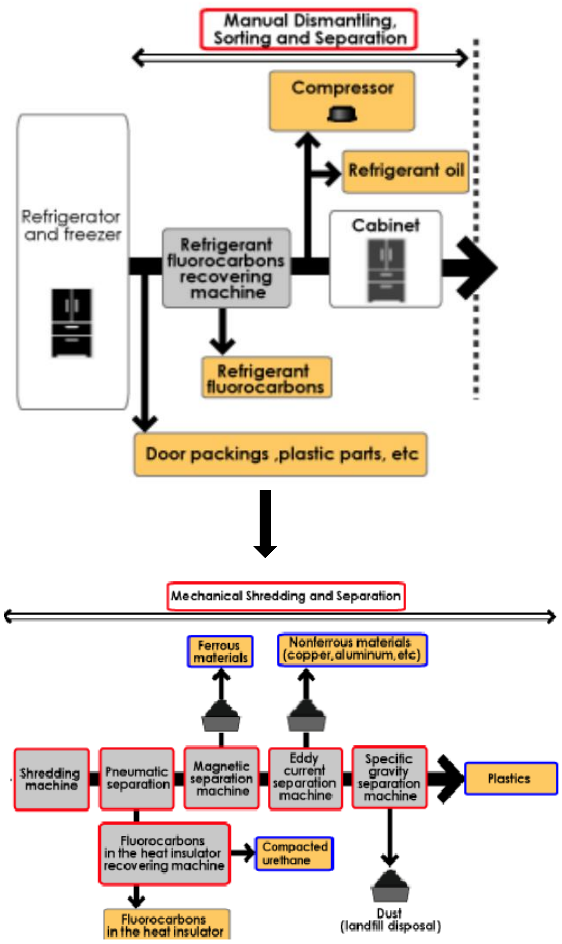

Figure 2. Recovery Stages of the Refrigerators Waste Materials [39].

Table 1. Material composition and scrap value prices for Type-1 and Type-2.

Material	Composition ratio	Disposal cost of hazardous material	Price of scrap material per kg	Revenue obtained for product 1 (30 kg)	Revenue obtained for product 2 (110 kg)
Steel	60%	-	0,5	15.3	56.2
Copper	3%	-	15	16.2	59.5
Aluminum	3%	-	4	2.7	9.9
Polyurethane	10%	-	1.1	3.3	12.1
PVC (cable)	1%	-	5	1.5	5.5
Glass	1%	-	0.4	0.12	0.45
Refrigerant oil	1%	3.5	-	1.05	-3.85
Refrigerant gas	1%	14	-	-4.2	15.4
Plastic	13%	-	1	3.9	14.3
Other	7%	-	0	0	0

Firms make agreements with scrap dealers and second-handlers for scrap metals and parts resulting from the separation of products. According to these agreements, during the return of these products to the market, this company, which carries out RL activities, does not pay an extra fee, contracted firms come and take scrap materials and second hand products.

Harmful materials in the end-of-life products (such as fluorocarbons, urethane) should completely removed from the product and destroyed in such a way not to damage the environment. These activitiees are held in the specialized facilities for a certain price.Our model this price is included in the disposal cost.

Scrap value prices of the materials for the refrigerator recovery are shown in Table 1. Disposal cost values are gathered firm licensed firms and scrap prices are determined based on the current values [40-41].

Distances between the centers of the regions and the WEEE recovery facility located in Eskisehir City are shown in Table 2.

Table 2. Distances from Eskisehir City to the Centers of the Regions(km)

Regions						
(1)	(2)	(3)	(4)	(5)	(6)	(7)
155	340	412	680	975	1030	1116

6. Results and discussion

The model is solved in GAMS® using CoinCbc and Clp Solvers. All computational work is performed in a 64-bit operating system, Intel(R) Core™ i7-6500U 2.50 GHz CPU, and 8.00 GB RAM personnel computer. For the 2017-2018, the aim is to optimize two objective functions. As these functions have a trade-off between each other, when one gets better than the other gets worse. For years between 2014-2018 years data, the model solved with AUGMECON method [42], five different Pareto Optimal Solutions were obtained for each year. Since the first objective function (net cost minimization) is more important than the second one, priority is given to the first objective during the calculations.

In some directives, recovery and recycling targets are given in terms of weight while in some others, targets are given in terms of unit. In WEEE directive that is published by Turkish Government, weight-based targets for companies are defined for every year with increasing rates[10]. However, it has been considered that the revised WEEE target is given in terms of the number of sold products. Therefore, both alternatives are tried separately and compared with each other. Legcoweight stands for target legislation coefficient if weight-based target is given, while Legco is for if uni-based target is given.

Legcoweight and Legco are 0.06 for years 2017 and 2018. The targeted collection amount is calculated as products sold at that period multiplying that legislation coefficients. The payoff table for years 2017 and 2018 is shown in Table 3, according to the weight-based recovery targets. Then, the range of Objective 2 is split into four segments with a length of 11536.75 and five Pareto optimal solutions are obtained for year-2017, as denoted in Table 4. These solutions for 2017 are close alternatives.

Table 3. Payoff table of 2017 and 2018 for weight based target.

		Objective 1	Objective 2
2017	Min Objective-1	1448556	330053
	Max Objective-2	1543446	376200
2018	Min Objective-1	1573116	390644
	Max Objective-2	1801261	501600

For year 2018, the range of Objective 2 is split into four segments with an equal length of 27739, and these five Pareto optimal solutions are also denoted in Table 4. It has been determined that the capacity is insufficient to reach the specified recovery-target of 2018.

Table 4. Trade off table of 2017 and 2018 for weight based target.

	Tradeoffs	Objective 1 (Monetary units)	Objective 2 (kg)	Labor source per month	Total collected WEEE
2017	1	1543446	376200	1500	114000
	2	1519722	364663	1500	109800
	3	1496000	353127	1500	106900
	4	1472272	341590	1500	103510
	5	1448556	330053	1500	100056
2018	1	1801261	501600	2006	152004
	2	1744220	473861	2006	143592
	3	1687183	446122	2006	135143
	4	1630149	418383	2006	126780
	5	1573117	390644	2006	118371

The capacity of bottleneck operations should be increased. To do this, the number of machines 1, 3 and 6 should be increased. All products recycled are Type-1, meaning that it will be sufficient to collect only Type-1 products in zone 1 to achieve the intended collection goal. This decision is made, since the number of products affects both the total cost and the amount of harmful waste recycled. Besides, in terms of workforce requirement, the results show that in year 2017, 1500 hr/month, and in 2018, 2006 hours/month is needed. This increase in workforce requirement is due to the increase in recovery targets.

According to the WEEE directive, 5.5% of the previous year's annual sales must be recovered by a white-goods manufacturer. For year-2018, this target percentage is set as 6%. So, these percentages are multiplied with the annual sales and divided into the twelve to find the monthly unit-based recovery targets. Hence, the recovery targets are found in terms of number of products for 2017 and 2018, and the model is solved, the pay-off is achieved as shown in Table 5.

Table 5. Payoff table of 2017 and 2018 for unit-based target.

		Objective 1	Objective 2
2017	Min Objective 1	946203	119749
	Max Objective 2	959368	130239
2018	Min Objective 1	1002153	123355
	Max Objective 2	1012256	167640

The range of objective 2 is divided into four parts, and five Pareto optimal solutions are achieved as shown in Table 6.

Table 6. Trade off table of 2017 and 2018 for unit-based target.

	Tradeoffs	Objective 1(Monetary units)	Objective 2 (kg)	Labor source per month	Total collected WEEE
2017	1	1292330	130239	832	111391
	2	1230987	127617	832	111392
	3	1198727	124994	832	111392
	4	1139876	122372	832	111990
	5	1082348	119749	832	111990
2018	1	1481091	167640	1045	139280
	2	1397643	156569	1045	137202
	3	1356783	145498	1045	137193
	4	1309845	134426	1169	137121
	5	1264341	123355	1169	137060

For the year-2018, the number of machines of type-1 the bottleneck is increased into two machines. During the 2017, 832 hours/month workforce is required. However, for the year-2018, some results require 1045 and some need 1169 hours/month workforce. The increase in workforce requirement from 2017 to 2018 is similarly due to the increase in recovery targets.

6.1. Comparison of the two target types

If the targets are given in units, products that are more advantageous (bar type fridges) will be preferred in terms of the value gained/unit. Other products may not be preferred because WEEEs are usually collected which are either light in weight or more valuable when recycled. In our model, bar type (Type-2) products are collected firstly if target is given in units. If the target is not reached, Type-1 (bigger size) refrigerators are collected from the regions.

When the weight-based target is given, only the Type-1 product is collected because it is heavier in weight and enough to reach the targets that are set by the legislations.

7. Sensitivity analysis for scrap prices and disposal cost

The sensitivity of total cost of the model to the steel prices is analyzed, both for the unit-based target recovery and for weight based target cases, for years 2018. In Figure 3, X axis shows the change in steel prices, (-20%, -10%, current value, 10%, 20%) and Y axis shows the total cost of the RL model.

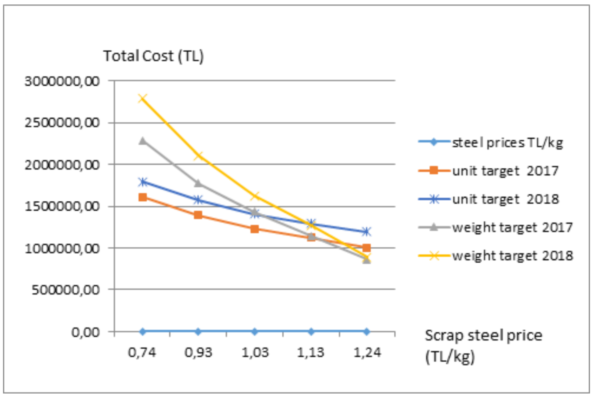

Figure 3. Sensitivity analysis for the scrap steel prices

There is no direct linear relationship between steel metal price and total cost. However, as the steel price increases, the cost decreases to a certain extent. If the target is given in terms of units, the total cost is smaller in all of the scrap values.

The cost decreases with the increase in scrap metal prices. Even though it decreases for both types of targets, if the target is defined on weight based, the reduction will be sharper. If there is a 20% increase in the current scrap metal price, the costs will be close for two target types. Moreover, if the steel price increases by more than 20 percent, total cost of the weight based target case is less than the unit based target case.

The same procedure with α coefficients is applied to copper scrap prices. In the case of the copper price change, the cost of the firm will also decrease as the income from the copper scrap rate increases. The reduction is almost linear. If the copper scrap prices increase by 20%, the costs become equal for the two target types. The results are illustrated in Figure 4.

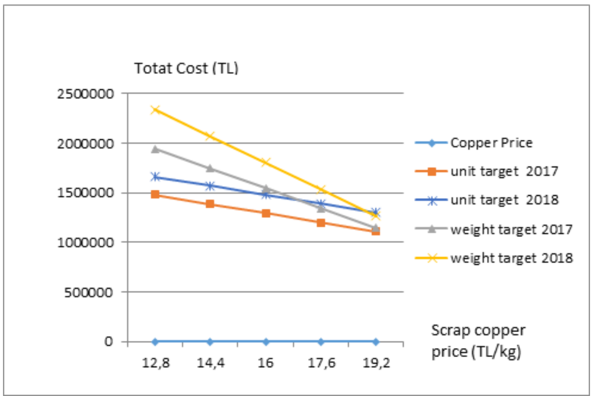

Figure 4. Sensitivity analysis for the scrap prices of copper metal

As seen in the graph in Figure 5, the disposal cost of refrigerant gas is one of the basic units of cost. The 20% reduction in the price of destruction of this harmful chemical can reduce the cost to almost zero. Producers have to send this harmful substance to the licensed company and + 20% change can double the cost. As seen in the analysis, RL activities for firms become much more favorable if the state financially supports the firm with the disposal of these harmful chemicals. Even small support to the firms for the disposal of these wastes can reduce the costs of firms' RL activities and even make them profitable.

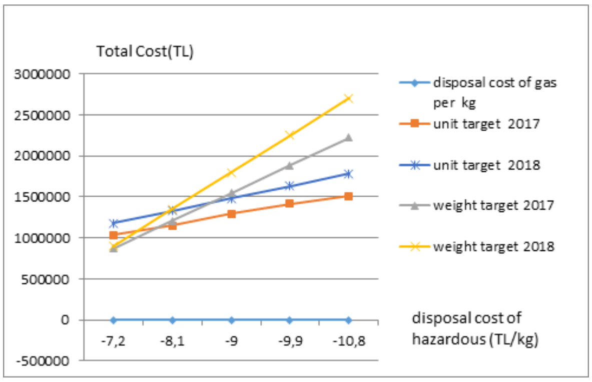

Figure 5. Sensitivity analysis of disposal cost of refrigerant gas.

8. Conclusion

RL is a popular subject, which includes all of the operations related with returned products collection, inspection and recovery to gain value from them. In this study, a bi-objective model is proposed to make an operations planning of an existing reverse logistics facility. In this deterministic MIP mathematical model, cost minimization and maximization of properly disposed hazardous material amount are targeted. The economic objective is accepted as more important where the transportation costs, labor and energy requirements and plant costs are intended to be minimized. Here, the objectives are conflicting, such that one of them become worse while the other one improves. In addition, the real application for operations planning of a real refrigerator recycling facility showed the validity and applicability of the proposed bi-objective model.

In addition, as a novel aspect, the recycling targets are considered in terms of both number of WEE products and weight of the WEEE to be recovered separately, and the model was solved for both of the cases. If the recovery targets are given in terms of number of WEEE products units, the total cost is smaller for the companies. The recycled products are preferred from those that are lighter in weight or easier to carry. Unit-based target model is less affected by the scrap value changes and fuel prices fluctuations. However, recycled materials and properly disposed hazardous materials are comparatively less when this type of target is set by the government.

If targets are given in terms of WEEE weight, firms prefer heavier products. If the value of the scrap increases, a sharper decrease in cost is observed. We can conclude that; it is important to set the target according to the product type.

For every situation, RL incurs an additional cost to the company. The company has not made any profit at all. As the years have passed and the target has increased, there has also been an increase in total cost. In order to prevent this, the state may open its own facilities for the hazardous waste materials recovery. As seen in the sensitivity analysis; the change in disposal cost is causing serious changes in cost. A financial incentive can make RL more attractive to the companies.

In order to increase the number of products collected, incentive may be given per person to give back their used products. However, this is a burden for the companies. If the state imposes a legal sanction to prevent these wastes from being discarded, people will have to deliver these wastes to the competent authorities.

Nature of the reverse supply chain is uncertain. In recent studies, the amount of returned products, costs and scrap prices are considered as uncertain. In our study, a sensitivity analysis conducted for the varying scrap prices and disposal costs of the refrigerant gas. In future studies, stochastic programming can be used as a more advanced technique to model the uncertainty in the RL. Furthermore, if more historical data can be obtained for the returned product quantity and the returned product quality, the model can be installed more accurately and more realistic results can be obtained.

References

[1] Kumar, S. & Putnam, V. (2008). Cradle to cradle: Reverse logistics strategies and opportunities across three industry sectors. International Journal of Production Economics, 115, 305–315.

[2] Elkington, J. (1994). Towards the sustainable corporation: Win-win-win business strategies for sustainable development. California Management Review, 36(2), 90-100.

[3] Nikolaou, I.E., Evangelinos, K.I. & Allan, S., (2013). A reverse logistics social responsibility evaluation framework based on the triple bottom line approach. Journal of Cleaner Production, 56, 173–184.

[4] Fleischmann, M., Bloemhof-Ruwaard, J. M., Dekker, R., Van der Laan, E., Van Nunen, J. A., & Van Wassenhove, L. N. (1997). Quantitative models for reverse logistics: A review. European Journal of Operational Research, 103(1), 1-17.

[5] Presley, A., Meade, L., & Sarkis, J. (2007). A strategic sustainability justification methodology for organizational decisions: a reverse logistics illustration. International Journal of Production Research, 45(18-19), 4595-4620.

[6] Url-1 https://eur-lex.europa.eu/resource.html?uri=cellar:ac89e64f-a4a5-4c13-8d96-1fd1d6bcaa49.0004.02/DOC_1&format=PDF Accessed 15.11.2017.

[7] Url-2 https://www.initial.co.uk/waste-legislation/ Accessed 15.11.2018.

[8] Url-3 http://www.environmentlaw.org.uk/rte.asp?id=82 Accessed 15.11.2018.

[9] Url-4 https://www.environment.gov.za/sites/default/files/legislations/nema_amendment_act59.pdf Accessed 15.11.2018.

[10] Url-5 http://www.resmigazete.gov.tr/eskiler/2012/05/20120522-5.htm Accessed 15.11.2018.

[11] Url-6 http://ec.europa.eu/environment/waste/weee/pdf/final_rep_unu.pdf Accessed 25.06.2017.

[12] Fleischmann, M., Bloemhof-Ruwaard, J. M., Dekker, R., Van der Laan, E., Van Nunen, J. A., & Van Wassenhove, L. N. (1997). Quantitative models for reverse logistics: A review. European Journal of Operational Research, 103(1), 1-17.

[13] Ilgin, M. A., & Gupta, S. M. (2010). Environmentally conscious manufacturing and product recovery (ECMPRO): A review of the state of the art. Journal of Environmental Management, 91(3), 563-591.

[14] Agrawal, S., Singh, R. K., & Murtaza, Q. (2015). A literature review and perspectives in reverse logistics. Resources, Conservation and Recycling, 97, 76-92.

[15] Govindan, K., & Soleimani, H. (2017). A review of reverse logistics and closed-loop supply chains: a Journal of Cleaner Production focus. Journal of Cleaner Production, 142, 371-384.

[16] Hu, T.-L., Sheu, J.-B. & Huang, K.-H., (2002) . A reverse logistics cost minimization model for the treatment of hazardous wastes. Transportation Research Part E: Logistics and Transportation Review, 38(6), 457–473.

[17] Widmer, R., Oswald-Krapf, H., Sinha-Khetriwal, D., Schnellmann, M., Böni, H. (2005), Global perspectives on e-waste. Environmental Impact Assessment Review, 25(5), 436-458.

[18] Bal, A., Sarvari, P. A., & Satoglu, S. I. (2018). Analyzing the Recycling Operations Data of the White Appliances Industry in the Turkish Market. In Industrial Engineering in the Industry 4.0 Era (pp. 147-157). Springer.

[19] Kahhat, R., Kim, J., Xu, M., Allenby, B., Williams, E., & Zhang, P. (2008). Exploring e-waste management systems in the United States. Resources, Conservation and Recycling, 52(7), 955-964.

[20] Dekker, R., Bloemhof, J. & Mallidis, I. (2012). Operations Research for green logistics - An overview of aspects, issues, contributions and challenges. European Journal of Operational Research, 219(3), 671–679.

[21] Shih, Li-Hsing. (2001). Reverse logistics system planning for recycling electrical appliances and computers in Taiwan. Resources, Conservation and Recycling, 32(1), 55-72.

[22] Listes, O. & Dekker, R. (2005). A stochastic approach to a case study for product recovery network design. European Journal of Operational Research, 160(1), 268–287.

[23] Listes, O. (2007). A generic stochastic model for supply-and-return network design. Computers & Operations Research, 34(2), 417–442.

[24] El-Sayed, M., Afia, N. & El-Kharbotly, A. (2010). A stochastic model for forward-reverse logistics network design under risk. Computers & Industrial Engineering, 58(3), 423–431.

[25] Achillas, C., Vlachokostas, C., Aidonis, D., Moussiopoulos, N., Iakovou, E., & Banias, G. (2010). Optimizing reverse logistics network to support policy-making in the case of electrical and electronic equipment. Waste Management, 30(12), 2592-2600.

[26] Dondo, R. G., & Méndez, C. A. (2016). Operational

planning of forward and reverse logistic activities on multi-echelon supply-chain networks. Computers & Chemical Engineering, 88, 170-184.

[27] Pedram, A., Yusoff, N. B., Udoncy, O. E., Mahat, A. B., Pedram, P., & Babalola, A. (2017). Integrated forward and reverse supply chain: A tire case study. Waste Management, 60, 460-470.

[28] Tuzkaya, G., Gülsün, B. & Önsel, Ş. (2011). A methodology for the strategic design of reverse logistics networks and its application in the Turkish white goods industry. International Journal of Production Research, 49(15), 4543–4571.

[29] Ahluwalia, P. K., Nema, A. K. (2007). A life cycle based multi-objective optimization model for the management of computer waste. Resources, Conservation and Recycling, 51(4), 792-826.

[30] Ahluwalia, P. K., & Nema, A. K. (2011). Capacity planning for electronic waste management facilities under uncertainty: multi-objective multi-time-step model development. Waste Management & Research, 29(7), 694-709.

[31] Ramezani, M., Bashiri, M., Tavakkoli-Moghaddam, R. (2013). A new multi-objective stochastic model for a forward / reverse logistic network design with responsiveness and quality level. Applied Mathematical Modelling, 37(1–2), 328–344.

[32] Wang, F., Lai, X. & Shi, N. (2011). A multi-objective optimization for green supply chain network design. Decision Support System, 51(2), 262–269.

[33] Türkay, M., Saraçoğlu, Ö., & Arslan, M. C. (2016). Sustainability in Supply Chain Management: Aggregate Planning from Sustainability Perspective. PloS One, 11(1), e0147502.

[34] Amin, S.H. & Zhang, G. (2013). A multi-objective facility location model for closed-loop supply chain network under uncertain demand and return. Applied Mathematical Modelling, 37(6), 4165–4176.

[35] Samanlioglu, F. (2013), A multi-objective mathematical model for the industrial hazardous waste location–routing problem. European Journal of Operational Research, 226(2), 332–340.

[36] Ene, S., & Öztürk, N. (2015). Network modeling for reverse flows of end-of-life vehicles. Waste Management, 38, 284-296.

[37] Url-7 http://ec.europa.eu/eurostat/statisticsexplained/index.php/File:Domestically_treated_waste_excluding_major_mineral_wastes_by_country_and_by_type_of_treatment,_2014.png#file Accessed 05.06.2017.

[38] Url-8 http://homeguides.sfgate.com/average-life-sidebyside-fridge-82650.html Accessed 25.09.2017

[39] Url-9 http://www.aeha.or.jp/assessment/en/english_flame_rp.html#Refrigerator Accessed 11.06.2018.

[40] Url-10 http://eco3e.eu/en/base/refrigerator/ Accessed 05.06.2017.

[41] Url-11 http://hurdafiyatlarim.com/ Accessed 25.06.2017.

[42] Mavrotas, G. (2009). Effective implementation of the ε-constraint method in Multi-Objective Mathematical Programming problems. Applied Mathematics and Computation. 213(2), 455–465.

***Emine Nisa Kapukaya** earned her master's degree from Istanbul Technical University, Industrial Engineering Department. She has been working as a research assistant, and continuing her PhD studies at the same department.*

***Alperen Bal** earned his master's degree from Istanbul Tehcnical University, Industrial Engineering Department. He has been working as a research assistant in Yalova University, Industrial Engineering Department, and continuing his PhD studies in Istanbul Technical University.*

***Sule Itir Satoglu** is a professor of Industrial Engineering, in Istanbul Technical University, Faculty of Management.. Her research interests include sustainable supply chains, lean production systems and humanitarian logistics.*

An International Journal of Optimization and Control: Theories & Applications
ISSN: 2146-0957 eISSN: 2146-5703
Vol.9, No.2, pp.100-104 (2019)
https://doi.org/10.11121/ijocta.01.2019.00597

RESEARCH ARTICLE

Analytical studies on waves in nonlinear transmission line media

Zehra Pinar *

Department of Mathematics, Tekirdağ Namık Kemal University, Turkey
zpinar@nku.edu.tr

ARTICLE INFO

Article history:
Received: 27 March 2018
Accepted: 11 October 2018
Available Online: 14 February 2019

Keywords:
Chebyshev equation
Auxiliary equation method
Lossy transmission line equation
Travelling wave solutions

AMS Classification 2010:
35C05, 35C11

ABSTRACT

In this study, we introduce the lossy nonlinear transmission line equation, which is the dissipative-dispersive equation and an important problem of electrical transmission lines. For the engineers and physicist, the equation and its exact solutions are important so to obtain the exact solutions; one of the modifications of auxiliary equation method based on Chebyshev differential equation is studied. The results are discussed and given in details. Recently, the studies of lossy transmission line equation have been challenging, thus, it is believed that the proposed solutions will be key part of further studies for waves in nonlinear transmission line media, which has mixed dissipative-dispersive behavior.

1. Introduction

Solitary waves are common subject among the engineers and physicians especially for who studies on elementary particle physics and electrical engineering. Solitons surviving collisions promise to be effective tools to deliver single waves, spreading skills without small scatter, modulated data at short distances in short distances with minimal loss.

Distributed electrical transmission lines composed of many identical parts were used to experimentally investigate the propagation of solitons conforming to the Korteweg-de-Vries (KdV) equation. The lines have been used in many areas such as for the regular behavior, the nonlinear transmission lines (NLTLs) is seen in electronics.

The solutions of NLTLs are investigated via mathematical models and physical experiments since 1970s. In the literature, there are many works to analyze either analytically [1, 2, 6] or numerically [3-5].

In this work, our aim is to get the exact solutions of the model of the lossy nonlinear transmission lines composed of small circuits. The inductance and capacitance are preceded from magnetic field effects and electric filed coupling between lines, respectively. The losses in the transmission lines depend on the series and shunt resistors. Corresponds to the transmission line losses constants are r and g, the circuit parameters are c and l determined for the voltage-dependent capacitance and the linear inductance, respectively.

Kengne [2] and Rosenau [7] give the similar models, which has mixed dispersive dissipative behavior. The difference between two models is depended on the capacitor's voltages determined as $c(V)=C_0\left(1-2bV\right)$ and $c(V)=C_0\left(1-V/V_0\right)^{\alpha}$, respectively. In addition to these capacitor's voltages, $c(V)=C_0\left(1+2\alpha+3\beta V^2\right)$ is determined by Tchier et al. [3] In the view of physical laws, the lossy NLTL model is given

$$l\frac{d}{dt}\left(c(V)\frac{dV_n}{dt}\right)+r\left(c(V_n)\frac{dV_n}{dt}+gV_n\right)+gl\frac{dV_n}{dt}=V_{n-1}-2V_n+V_{n+1} \tag{1}$$

where the right-side of the equation can be given approximately with the partial derivative of the distance x, and substituting the capacitor's voltages in Eq.(1), the nonlinear models are obtained. Respect to the capacitor's voltages the nonlinear models includes inductance, resistance, conductance and capacitance terms.

In our work, we will consider the model given by Kengne [4] includes the all terms

*Corresponding author

$$V_{tt}-\frac{1}{C_0L}V_{xx}+\frac{RG}{C_0L}V=\frac{1}{12C_0L}\delta^2V_{xxxx} \tag{2}$$
$$+b\left(V^2\right)_{tt}-\left(\frac{R}{L}+\frac{G}{C_0}\right)V_t+\frac{Rb}{L}\left(V^2\right)_t$$

where $L=\dfrac{l}{\delta}, R=\dfrac{r}{\delta}, G=\dfrac{g}{\delta}$ and C_0, b are corresponding to inductance, resistance, conductance and capacitance terms, respectively. When $R=0, G=0$, the Eq. (2) corresponds to an ideal transmission line and analytical solutions are given by Afsharia in [4]. Tchier et al. [1] considered the model includes inductance, resistance and capacitance terms, they obtained the analytical solution via Riccati-Bernoulli sub-ODE method and Lie symmetry reduction method. But for Eq. (2), i.e. the lossy nonlinear transmission line equation, analytical solutions could not been find so Kengne et al. [2] try to reduce Eq. (2) into integrable partial differential equation (PDE), which is solved analytically.

As it is seen that in this study, we will also investigate the exact solutions of Eq. (2) in the manner of the variant of auxiliary equation method. The auxiliary equation is generally a first-order ordinary differential equation (ODE) that its solutions are the special functions. In the literature, many methods are known as tanh-method [14-17], Jacobi method [18], Riccati expansion method [11], sub-equation method [8, 19], Bernoulli approximation method [13, 23] and auxiliary equation method [9, 10, 12]. In this study, we consider the auxiliary equation as a second-order ordinary differential equation known as Chebyshev differential equation. Therefore, our choice is correspond to our aim, to get exact solutions of the lossy transmission line equation.

The general methodology for the auxiliary equation method, first step is reducing a nonlinear PDE to a nonlinear ODE by the transformation $u(x,t)=u(\xi)$, $\xi=(x-\eta t)$.

$$u(\xi)=\sum_i^N c_i z^i(\xi) \tag{3}$$

the finite series expansion is considered as the exact solution of the reduced equation where c_i are unknown constants to be determined later. Also, $z(\xi)$ is the exact solution of the proposed auxiliary equation.

The determination of the parameters c_i is done in three main steps:

- First is substituting the proposed auxiliary equation into the reduced equation.
- Second is equating each coefficient of power of $z(\xi)$ to zero.
- Third, solving the corresponding algebraic system to obtain the coefficients.

Also, the integer N, which indicates the number of terms will be used in Eq. (3), is determined basically by balancing the term with the highest order derivative and the term with the highest power nonlinearity in Eq. (2) [20].

It is also known that the function $z(\xi)$ is the exact solution of proposed auxilary equation. Since nonlinear PDEs cannot be recovered by only one auxiliary ordinary differential equation, there have been many studies utilizing different exactly solvable auxiliary equations.

In this work, we consider the Chebyshev equation,

$$(1-\zeta^2)z''(\zeta)-\zeta z'(\zeta)+n^2z(\zeta)=0 \tag{4}$$

with the transformation $\omega=\cos\zeta$ reducing Eq. (4) to

$$z''(\omega)+n^2z(\omega)=0 \tag{5}$$

which is considered as the auxiliary equation to solve the nonlinear partial differential equation and has a solution $T_n(\omega)$ known as Chebyshev function.

It is clear that determination of the elementary function $T_n(\omega)$ by auxiliary equation is essential and plays very important role finding new travelling wave solutions of nonlinear evolution equations. This fact forces the researchers to seek a new auxiliary equation with definite solutions.

The basic idea is that if elementary function, $T_n(\omega)$, is orthogonal function, which forms complete orthogonal sets in L^2 then, the solution series will be convergent series therefore the series (3) will converge rapidly [21, 22] .

In this study, we take aim at getting the exact solutions of the lossy nonlinear transmission line equation, see Eq. (2), which has mixed dispersive-dissipative behavior. To the best of our knowledge, this is the first attempt to consider the auxiliary equation as Chebyshev equation and investigating the exact solutions of the dispersive-dissipative equation. In the literature, as we mentioned above, the analytical solutions are investigated for ideal transmission line and the lossy nonlinear transmission line equation without conductance term [1, 2]. This equation will become one of the reference equations of paper and monograph in the literature, like our previous work on scattered-Fisher-type equations. [13, 23, 24].

2. The solutions

We represent the exact solutions of the lossy nonlinear transmission line equation by the given method above. Considering the transformation $u(x,t)=u(\xi)$, $\xi=(x-\eta t)$, Eq. (2) is reduced into ODE,

$$\eta^2 V'' - \frac{1}{C_0 L}V'' + \frac{RG}{C_0 L}V = \frac{1}{12C_0 L}\delta^2 V^{(4)} + 2b\eta^2\left(V'\right)^2 + 2b\eta^2 VV'' - \left(\frac{R}{L}+\frac{G}{C_0}\right)V_t + \frac{2Rb\eta}{L}VV' \qquad (6)$$

Applying the proposed steps and from the balancing principle $N=2$ is obtained. There are many solutions as a result of algebraic system of equations. But only two of them satisfy our conditions. Some of them give trivial solution, some of them give constant solution and some of them reduce the equation classical wave equation.

Case 1. The parameters for the solution is obtained as

$$n=\frac{2\sqrt{21}}{7\delta}, C_2=0, L=84,$$

$$\eta=-\frac{R}{196\left(Rc_0+42G\right)}, \delta=\frac{4\sqrt{21}\cos\left(\frac{196xRc_0+8232xG-Rt}{196\left(Rc_0+42G\right)}\right)}{7\pi},$$

$$g_0=-\frac{1}{392b\eta c_0}, g_1=\pm 2Ig_2\sqrt{-\frac{g_0}{2g_2}}, g_2=\frac{I\left(Rc_0+42G\right)}{2C_1^2 bRc_0}.$$

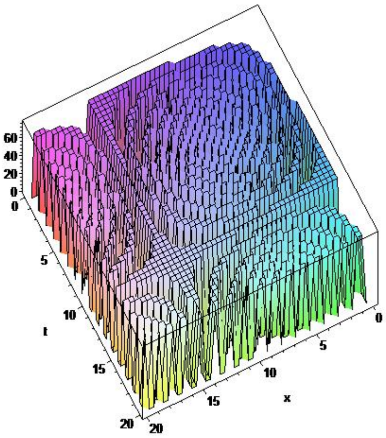

(a) For long ranges.

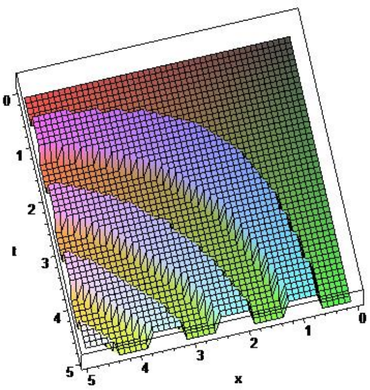

(b) For short ranges.

Figure 1. The behavior of Case 1 solution for $R=0.2, c_0=540, b=0.16, G=10^{-4}, C_1=\sin(xt)$

The exact solution is

$$V(x,t)=\frac{Rc_0+42G}{2bRc_0} - \frac{\left(Rc_0+42G\right)\sqrt{784\left(392IC_1^2\right)}\sin\left(\frac{\pi\cos\left(x-\frac{Rt}{196\left(Rc_0+42G\right)}\right)}{\cos\left(\frac{196xRc_0+8232xG-Rt}{196\left(Rc_0+42G\right)}\right)}\right)}{784bRc_0C_1} + \frac{I\left(Rc_0+42G\right)\sin\left(\frac{\pi\cos\left(x-\frac{Rt}{196\left(Rc_0+42G\right)}\right)}{\cos\left(\frac{196xRc_0+8232xG-Rt}{196\left(Rc_0+42G\right)}\right)}\right)^2}{2bRc_0}$$

For the special values of the parameters, the behavior of the solution is given by Figure 1.

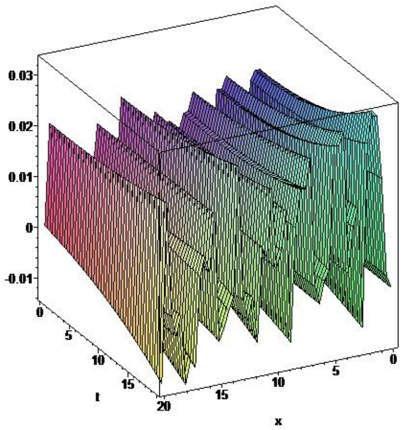

(a) For long ranges.

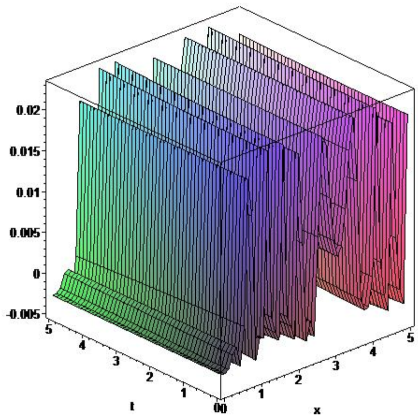

(b) For short ranges

Figure 2. The solution for $R=0.1, L=63, \delta=0.1, c_0=540, b=0.16, G=10^{-4}, g_2=exp(-x)$

Case 2. The parameters for the solution is obtained as

$$n=\frac{4\sqrt{246}}{41\delta},C_2=0,g_0=-\frac{69}{574b\eta c_0\left(2\eta+49\right)},$$

$$g_1=\pm\frac{3\sqrt{42}}{7}I\sqrt{\frac{1}{82g_2b\eta^2c_0+2009g_2b\eta c_0}}g_2,g_2=g_2$$

$$\eta=\frac{1}{1722}\left(\left(\begin{array}{l}1842182685R\\-45955971432G-2781210948047Rc_0\\+861\sqrt{861}\left(\left(\begin{array}{l}1331000R^2\\-3021083975R^2c_0+1356688267340R^2{c_0}^2\\-265274306640GRc_0\\+3308829943104G^2c_0\\+400494376518768GR{c_0}^2\end{array}\right)\Big/c_0\right)^{1/2}\end{array}\right)R^2{c_0}^2\right)^{1/3}\Big/\left(R+c_0\right)$$

$$+\left(-55+\frac{689087}{6}c_0\right)R\Big/\left(\left(\begin{array}{l}1842182685R\\-45955971432G-2781210948047Rc_0\\+861\sqrt{861}\left(\left(\begin{array}{l}1331000R^2\\-3021083975R^2c_0+1356688267340R^2{c_0}^2\\-265274306640GRc_0\\+3308829943104G^2c_0\\+400494376518768GR{c_0}^2\end{array}\right)\Big/c_0\right)^{1/2}\end{array}\right)R^2{c_0}^2\right)^{1/3}$$

$$-\frac{49}{6}$$

For this case, the behavior of the solution is given by Figure 2.

3. Conclusion

The main idea of this study is based on obtaining the exact solutions of the lossy transmission line equation, which has mixed dispersive-dissipative behavior, by using the exact solutions of different type equations as an ansatz. To the best of our knowledge, this is the first attempt to consider the auxiliary equation as the Chebyshev equation and to investigate the exact solutions of the dispersed-dispersion equation. In the literature, as we mentioned above, the analytical solutions are only investigated for ideal transmission line and the lossy nonlinear transmission line equation without conductance term [1, 2]. Whereas to our knowledge, the analytical solutions of the considered equation, Eq. (2), is obtained for the first time in the literature.

References

[1] Tchier, F., Yusuf, A., Aliyu, A. I. & Inc, M. (2017). Soliton solutions and conservation laws for lossy nonlineartransmission line equation. *Superlattices and Microstructures*, 107, 320-336.

[2] Kengne, E. & Vaillancourt, R. (2007). Propagation of solitary waves on lossy nonlinear transmission lines. *International Journal of Modern Physics B,* 23, 1-18.

[3] Koon, K.T.V., Leon, J., Marquie, P. & Tchofo-Dinda, P. (2007). Cutoff solitons and bistability of the discrete inductance- capacitance electrical line: theory and experiments. *Physical review. E*, 75, 1-8.

[4] Afshari, E. & Hajimiri, A. (2005). Nonlinear transmission lines for pulse shaping in silicon. *IEEE Journal of Solid-State Circuits, 40*, (3) : 744-752.

[5] Sataric, M.V., Bednar, N., Sataric, B.M. & Stojanovic, G.A. (2009). Filaments as nonlinear RLC transmission lines. *International Journal of Modern Physics B*, 23(22), 4697-4711.

[6] Mostafa, S.I. (2009). Analytical study for the ability of nonlinear transmission lines to generate solitons. *Chaos, Solitons & Fractals,* 39(5), 2125-2132.

[7] Rosenau, P. (1986). A Quasi-Continuous Description of a Nonlinear Transmission Line. *Physica Scripta*, 34, 827-829.

[8] Yomba, E. (2006). The modified extended Fan sub-equation method and its application to the (2+1)-dimensional Broer-Kaup-Kupershmidt equation. *Chaos, Solitons & Fractals,* 27, 187-196.

[9] Sirendaoreji. (2007). Auxiliary equation method and new solutions of Klein–Gordon equations. *Chaos, Solitons and Fractals*, 31, 943–950.

[10] Yomba, E. (2007). A generalized auxiliary equation method and its application to nonlinear Klein–Gordon and generalized nonlinear Camassa–Holm equations. *Physics Letters A*, 372, 1048–1060.

[11] Yong, C., Biao, L. & Hong-Quing Z. (2003). Generalized Riccati equation expansion method and its application to Bogoyaylenskii's generalized breaking soliton equation. *Chinese Physics*, 12, 940–946.

[12] Pinar, Z., Öziş, T. (2013). An Observation on the Periodic Solutions to Nonlinear Physical models by means of the auxiliary equation with a sixth-degree nonlinear term. *Communications in Nonlinear Science and Numerical Simulation*, 18, 2177-2187.

[13] Pinar, Z. & Öziş, T. (2015). A remark on a variable-coefficient Bernoulli equation based on auxiliary equation method for nonlinear physical systems. arXiv:1511.02154v1

[14] Wazwaz, A. M. (2009). *Partial Differential Equations and Solitary Wave Theory*. Higher Education Press - Springer-Verlag, Beijing and Berlin.

[15] Wazwaz, A. M. (2002). *Partial Differential Equations: Methods and Applications*. Balkema, Leiden.

[16] Wazwaz, A. M. (2008). The tanh method for travelling wave solutions to the Zhiber–Shabat equation and other related equations. *Communications in Nonlinear Science and Numerical Simulation*, 13, 584–592.

[17] Wazwaz, A. M. (2007). The Tanh-Coth Method Combined with the Riccati Equation for Solving the KDV Equation. *Arab Journal of Mathematics and Mathematical Sciences*, 1, 27–34.

[18] Yong, X., Zeng, X., Zhang, Z. & Chen, Y. (2009). Symbolic computation of Jacobi elliptic function solutions to nonlinear differential-difference equations. *Computers & Mathematics with Applications*, 57, 1107-1114.

[19] Zhang, H. (2009). A Note on Some Sub-Equation Methods and New Types of Exact Travelling Wave Solutions for Two Nonlinear Partial Differential Equations. *Acta Applicandae Mathematicae*, 106, 241-249.

[20] Pinar, Z. & Öziş, T. (2015). Observations on the class of ''Balancing Principle'' for nonlinear PDEs that can be treated by the auxiliary equation method. *Nonlinear Analysis: Real World Applications*, 23, 9–16.

[21] Rivlin, Theodore J. (1974). *The Chebyshev polynomials. Pure and Applied Mathematics*. Wiley-Interscience [John Wiley & Sons], New York-London-Sydney.

[22] Krall, A. M. (2002). *Hilbert Space, Boundary Value Problems and Orthogonal Polynomials*. Birkhäuser Verlag, Basel-Boston – Berlin

[23] Pinar, Z. & Kocak, H. (2018). Exact solutions for the third-order dispersive-Fisher equations. *Nonlinear Dynamics*, 91(1), 421-426.

[24] Kocak, H. & Pinar, Z. (2018). On solutions of the fifth-order dispersive equations with porous medium type non-linearity. *Waves in Random and Complex Media*, 28(3), 516-522.

***Zehra Pinar** received her B.S. degree in Applied Mathematics from Ege University, İzmir, Turkey in 2007 and her M.S. and PhDdegrees also from the same university in 2009 and 2013, respectively. In January 2014, she joined Tekirdağ Namık Kemal University, Tekirdağ, Turkey as an Assistant Professor. Current research interests include analytically-approximate and numerical methods for nonlinear problems in physics and engineering.*

An International Journal of Optimization and Control: Theories & Applications
ISSN: 2146-0957 eISSN: 2146-5703
Vol.9, No.2, pp.105-112 (2019)
https://doi.org/10.11121/ijocta.01.2019.00642

RESEARCH ARTICLE

Fitting intravoxel incoherent motion model to diffusion MR signals of the human breast tissue using particle swarm optimization

Gokhan Ertas*

Department of Biomedical Engineering, Yeditepe University, Turkey
gokhan.ertas@yeditepe.edu.tr

ARTICLE INFO

Article history:
Received: 25 July 2018
Accepted: 25 January 2019
Available Online: 15 February 2019

Keywords:
Breast
Diffusion
Intravoxel Incoherent Motion
Fit
Optimization

AMS Classification 2010:
65D10, 65Y20

ABSTRACT

Intravoxel incoherent motion (IVIM) modeling offers the parameters f, D and D^* from diffusion MR signals as biomarkers for different lesion types and cancer stages. Challenges in fitting the model to the signals using the available optimization algorithms motivate new studies for improved parameter estimations. In this study, one thousand value sets of f, D, D^* for human breast tissue are assembled and used to generate five thousand diffusion MR signals considering noise-free and noisy situations exhibiting signal-to-noise ratios (SNR) of 20, 40, 80 and 160. The estimates of f, D, D^* are obtained using Levenberg-Marquardt (LM), trust-region (TR) and particle swarm (PS) algorithms. On average, the algorithms provide the highest fitting performance for the noise-free signals (R^2_{adj}=1.000) and great fitting performances for the noisy signals with SNR>20 (R^2_{adj}>0.988). TR algorithm performs slightly better for SNR=20 (R^2_{adj}=0.947). TR and PS algorithms achieve the highest parameter estimation performance for all the parameters, while LM algorithm reveals the highest performance for f and D only on the noise-free signals (r=1.00). For the noisy signals, performances increase with an increase in SNR. All algorithms accomplish poor performances for D^* (r=0.01-0.20) while TR and PS algorithms perform same for f (r=0.48-0.97) and D (r=0.85-0.99) but remarkably better than LM algorithm for f (r=0.08-0.97) and D (r=0.53-0.99). Overall, TR and PS algorithms demonstrate better but indistinguishable performances. Without requiring any user-given initial value, PS algorithm may facilitate improved estimation of IVIM parameters of the human breast tissue. Further studies are needed to determine its benefit in clinical practice.

1. Introduction

Diffusion-weighted MR imaging traces random displacements of water within living tissues using the exponential decay of the diffusion signal amplitude with respect to the degree of field gradient encoding exposed to the tissues during imaging [1]. This imaging technique uses no ionizing radiation and requires no contrast agent administration to the patient for quantitative tissue characterization and therefore has become a very popular medical imaging technique in diagnosis and treatment of cancer [2, 3]. To assess the volume fraction of incoherently flowing blood in the tissue, the diffusion coefficient of water in the tissue and the sum of the pseudo-diffusion coefficient associated to the motion effect and the diffusion coefficient of water in blood, the diffusion MR signal of the tissue needs be processed using intravoxel incoherent motion (IVIM) model [4]. This process conventionally involves nonlinear least squares fitting of a bi-exponential decay function to the diffusion MR signal [5]. Among the optimization strategies proposed for the fittings, the Levenberg-Marquardt and the trust-region optimization algorithms stand forward due to their easy implementation.

The Levenberg-Marquardt algorithm [6] uses a search direction that is a cross between the Gauss-Newton direction and the steepest descent direction that reveals increased robustness. However, the algorithm does not consider any boundary constraints and therefore an estimate may be out of physiologically acceptable range. The trust-region algorithm [7] inherited from the Levenberg-Marquardt algorithm employs a search space restricted to a subset of the domain of a cost function. The algorithm offers estimates within acceptable ranges by incorporating boundary constraints that can be determined easily from the

*Corresponding author

recent research on breast diffusion MR imaging. Both algorithms suffer from the same concern: the initial value of any model parameter to be estimated should be pre-selected correctly to minimize the possible disruptive effect of local minima during fitting. The selection process is quite complicated and requires decent experience on excessive trials with different values. There is a need for an optimization algorithm that requires no user given initial values and that utilizes boundary constraints. Such an algorithm holds a priceless potential to improve the use of IVIM modeling in distinguishing different lesion types and cancer stages of the human breast tissue.

The particle swarm optimization algorithm [8] performs search behavior of a swarm of particles hovering through a multidimensional search space. The algorithm eliminates the need for user given initial values while making use of boundary constraints. It has been suggested to optimize several tasks in medicine, such as medical image segmentation, image enhancement and image registration [9-11]. However, to the best of our knowledge, its use in fitting diffusion MR signals to the IVIM model has not yet been explored.

In the current study, a particle swarm optimization algorithm is proposed and compared with the Levenberg-Marquardt and the trust-region optimization algorithms in least squares fitting of the IVIM model to breast diffusion MR signals.

2. Materials and methods

2.1. Synthetic diffusion MR signal generation using intravoxel incoherent motion model

The intravoxel incoherent motion (IVIM) model expresses the attenuation in the diffusion MR signal strength acquired for a specific diffusion weighting determined by a *b*-value, $s(b)$, with respect to the signal strength captured without any diffusion weighting, $s(0)$. The model is formulated using a bi-exponential decay function giving a normalized diffusion signal [12]:

$$\frac{s(b)}{s(0)} = (1-f)\exp^{-bD} + f\exp^{-bD^*} \tag{1}$$

Here f, D and D^* are the three free model parameters. f represents the volume fraction of incoherently flowing blood in the tissue. Meanwhile, D denotes the diffusion coefficient of water in the tissue and D^* is the sum of the pseudo-diffusion coefficient associated to the IVIM effect and the diffusion coefficient of water in blood.

Using the IVIM model, synthetic diffusion MR signals of human breast tissue are generated by Monte Carlo trials performed 1000 times in the current study. During each trial, values for the model parameters are first determined randomly using the pre-defined mean and standard deviation values for each parameter considering the malignant and the benign lesions, the cysts and the healthy glandular tissue of the human breast reported in the literature [13]: f= 0.10±0.03, D= 1.38±0.25μm²/ms and D^*= 110±20μm²/ms. Next, the synthetic noise-free diffusion signal is generated with ten different *b*-values of 0, 30, 70, 100, 150, 200, 300, 400, 500, 800s/mm² [14] using the determined parameter values. Finally, the noisy forms of the signal are obtained by adding Gaussian noise at four different signal-to-noise ratios (SNR) of 20, 40, 80 and 160 (The SNR is defined as the ratio of the normalized diffusion signal strength obtained without any diffusion weighting to the standard deviation of the noise [14]).

2.2. Nonlinear least squares fitting

The diffusion MR signals obtained are fitted to the IVIM model using the bi-exponential decay function in a nonlinear least squares fashion. The process involves minimizing the difference between the signal fed to fitting and the signal predicted during fitting:

$$\min_{\beta} \sum_{i=1}^{n} \left(s_i - \hat{s}_i(\beta)\right)^2 = \min_{\beta} \left\| r(\beta) \right\|_2^2 \tag{2}$$

Here, β = [f, D, D^*]. s_i and $\hat{s}_i(\beta)$ denote the signal strength given and the signal strength predicted using a set of values for β for the *i*-th *b*-value respectively. n is the total number of *b*-values considered for the diffusion signal. In the current study, the nonlinear least squares fittings are performed by using three different optimization algorithms, namely Levenberg-Marquardt, trust-region and particle swarm.

2.2.1. Levenberg-Marquardt algorithm

The Levenberg-Marquardt (LM) algorithm [6] uses a search direction that is a cross between the Gauss-Newton direction and the steepest descent direction and therefore offers increased robustness:

$$\left(J_k^T J_k + \lambda_k I\right) d_k = -J_k^T r_k \tag{3}$$

Here J_k and λ_k are the Jacobian matrix of derivatives of the residuals with respect to β and the Marquardt parameter both for the *k*-th iteration. d_k is a direction of descent satisfying $\beta_{k+1}= \beta_k+d_k$. λ is updated from iteration to iteration; increasing the value has the effect of changing both the direction and the length of the shift vector. In the current implementation, λ is initially set to 0.01. After an iteration, if the difference takes a lower value, λ is decreased by a factor of 10; otherwise, it is increased by a factor of 10 for the next iteration. The iteration is stopped when the gradient of the difference reaches its minimum of 10^{-12} or the change in model parameters for finite difference gradients reaches its minimum of 10^{-9}. No bound constraints are considered during iterations; however, the optimization is started with 0.10, 1.38μm²/ms and 110μm²/ms as the initial values for f, D and D^* respectively.

2.2.2. Trust-region algorithm

The trust-region (TR) algorithm [7] is inherited from LM algorithm and potentially offers better and faster solutions especially when the fitting process is far from the correct solution. Let Δ_k be the two-norm of the solution to Eq. 3 updated by each iteration according to standard rules, then d_k may be the solution as follows:

$$\min_{d_k} \left\| J_k d_k + r_k \right\|_2^2 \quad \text{subject to } \left\| d \right\|_\infty \le \Delta_k \qquad (4)$$

In the current implementation, the TR algorithm considers the same stopping criteria and the same initial values set for the LM algorithm. Besides, the algorithm also makes use of lower and upper limits for the parameters set as $0\leq f\leq 0.25$, $0.25\leq D\leq 3.50$ (×μm²/ms) and $25\leq D^*\leq 250$ (×μm²/ms).

2.2.3. Particle swarm algorithm

The particle swarm (PS) algorithm [8] performs search behavior of a swarm of particles hovering through a multidimensional search space to find a solution. During this search, a particle iteratively adjusts its velocity (v) and position (x) according to

$$v_{k+1} = wv_k + c_1 r_1 (x^b - x_k) + c_2 r_2 (x^{ba} - x_k) \qquad (5a)$$

$$x_{k+1} = x_k + \mu v_{k+1} \qquad (5b)$$

Here, w is an inertia weight that balances the global search and local search while c_1 and c_2 are two scaling factors and r_1 and r_2 are the randomly generated numbers uniformly distributed between 0 and 1. x^b and x^{ba} denote respectively the best previous position of the particle and the best position among all the particles that gives the minimum difference. μ presents the flying time for the particle. In the current implementation, the number of particles in the swarm is set to 100 while μ= 1, w= 1.1 and c_1=c_2= 1.49. The lower and the upper limits for the parameters are set to the values considered for the TR algorithm. The iteration is stopped when the gradient of the difference reaches its minimum of 10^{-12}.

2.3. Performance assessment

Success of each optimization algorithm studied is assessed with respect to the model fitting and the parameter estimation performances. The model fitting performance is measured by goodness-of-fit given by adjusted R-squared [15]:

$$R_{adj}^2 = 1 - \left(\frac{n-1}{n-m} \right) \left(\frac{\sum_{i=1}^{n} (s_i - \hat{s}_i)^2}{\sum_{i=1}^{n} (s_i - \bar{s})^2} \right) \qquad (6)$$

Here, n and m represent respectively the number of diffusion signal strength measurements and the number of parameters within the model fitted (for the current study, n= 10 and m= 3). $\bar{s}$ denotes the average of the diffusion signal strength for different b-values. R^2_{adj} ranges from 0 to 1 with a higher value indicating a better fit (i.e. better similarity between the diffusion signal predicted by the estimated parameter values and the diffusion signal given by the ground truth parameter values for a specific noise level). To assess the parameter estimation performance of the optimization algorithms, correlations between the estimates by the algorithms and the true simulated values are measured by Person's correlation coefficient (r). The coefficient value ranges between -1 and +1 and a higher absolute value designates a better estimate. The fitting algorithms are numerically implemented and performance metrics are computed using the existing libraries of MATLAB (v8.2; Natick, MA) on a standard PC (Intel i5-4460 3.20GHz processor, 6GB memory and 64-bit OS).

3. Results

A total of one thousand different value sets for f, D and D^* are synthetically generated to mimic the diffusion characteristics of the human breast tissue regarding to the IVIM model. Statistical summary for each parameter is as shown in Table 1. The value sets are used to simulate diffusion MR signals considering noise-free and noisy imaging conditions with four different levels of SNR (i.e. 20, 40, 80 and 160) resulting in the generation of five thousand synthetic breast diffusion MR signals in total.

Table 1. Statistics for the IVIM model parameters f, D and D^* simulated.

Parameter	Mean ± SD	Min - Max
f	0.10 ± 0.03	0.01 - 0.21
D	1.38 ± 0.25	0.51 - 2.25
D^*	110 ± 20	49 - 181

Units of D and D^* are μm²/ms and f is dimensionless.

All the signals generated are fitted by using the IVIM model and by carrying out numerous nonlinear least squares fittings with LM, TR and PS based optimization algorithms. All of the optimization methods provide the highest fitting performance for the noise-free signals, (R^2_{adj}=1.000). However, for the noisy signals, their performances decrease with the increase in noise level (see Table 2). The LM and the PS optimization algorithms provide almost the same very good fitting performances (R^2_{adj}=0.947-0.999). Though, the TR algorithm offers the best performance among all of the algorithms (R^2_{adj}=0.951-0.999).

Table 2. Model fitting performances of the optimization algorithms assessed by R^2_{adj}

Algorithm	SNR20	SNR40	SNR80	SNR160
LM	0.947 ± 0.019 (0.775-0.991)	0.988 ± 0.005 (0.954-0.998)	0.997 ± 0.001 (0.989-0.999)	0.999 ± 0.000 (0.997-1.000)
TR	0.951 ± 0.017 (0.775-0.991)	*	*	*
PS	**	*	*	*

Results are the same for all the algorithms for the dedicated SNR value (*) and as the ones for the LM algorithm (**).

Table 3. Estimates of *f*, *D* and D^* by the optimization algorithms.

Parameter	Algorithm	SNR20	SNR40	SNR80	SNR160	Noise-Free
f	LM	0.16 ± 0.17 (0.00 - 0.97)	0.12 ± 0.08 (0.00 - 0.94)	0.10 ± 0.04 (0.01 - 0.92)	0.10 ± 0.03 (0.01 - 0.22)	0.10 ± 0.03 (0.01 - 0.21)
	TR	0.11 ± 0.06 (0.00 - 0.25)	0.10 ± 0.04 (0.00 - 0.25)	0.10 ± 0.03 (0.00 - 0.24)	*	*
	PS	**	**	**	*	*
D	LM	1.24 ± 0.43 (0.00 - 2.33)	1.34 ± 0.29 (0.00 - 2.29)	1.38 ± 0.25 (0.47 - 2.27)	1.38 ± 0.25 (0.49 - 2.26)	1.38 ± 0.25 (0.51 - 2.25)
	TR	1.35 ± 0.29 (0.35 - 2.32)	1.37 ± 0.26 (0.43 - 2.29)	*	*	*
	PS	**	**	*	*	*
*D**	LM	2472 ± 4068 (0 - 10669)	3090 ± 4468 (1 - 11685)	2222 ± 3815 (2 - 12162)	1551 ± 3143 (14 - 12234)	384 ± 1483 (49 - 10432)
	TR	136 ± 105 (25 - 250)	142 ± 100 (25 - 250)	144 ± 91 (25 - 250)	143 ± 80 (25 - 250)	110 ± 20 (49 - 181)
	PS	138 ± 102 (25 - 250)	**	**	**	**

Units of *D* and *D** are [μm^2/ms] and *f* is dimensionless. Results are the same for all the algorithms (*) and as the ones estimated by the TR algorithm (**).

Table 4. Parameter estimation performances the optimization algorithms assessed by *r*

Parameter	Algorithm	SNR20	SNR40	SNR80	SNR160	Noise-Free
f	LM	0.08	0.21	0.65	0.97	1.00
	TR	0.48	0.73	0.90	0.97	*
	PS	**	**	**	**	*
D	LM	0.53	0.83	0.97	0.99	1.00
	TR	0.85	0.95	0.99	0.99	*
	PS	**	**	**	**	*
*D**	LM	0.01	0.03	0.05	0.14	0.08
	TR	0.02	0.06	0.10	0.20	1.00
	PS	0.04	**	**	**	**

Results are the same for all the algorithms (*) and as the ones estimated by the TR algorithm (**).

However, for the signals having SNR≥ 40, very good fitting performances are attained by all the algorithms (R^2_{adj}≥ 0.954). The LM, TR and PS algorithms require respectively 35ms, 39ms and 353ms on average for fitting the IVIM model to a noise-free signal. For a noisy signal, the average computation time for the LM, TR and PS algorithms increases respectively from 40ms to 71ms, 42ms to 58ms and 356ms to 360ms with the decrease in SNR from 160 to 20. The PS algorithm always requires a considerably longer computation time when compared to the LM and the TR algorithms.

Estimates of *f*, *D* and *D** from all diffusion MR signals obtained by the LM, TR and PS algorithms are given in Table 3. For *f* and *D*, the same statistical measures (i.e. Mean±SD, the minimum and the maximum) are provided by all the algorithms. However, for *D**, the LM algorithm often provides remarkably different statistical measures when compared to the TR and the PS algorithms that reveal indistinguishable measures. In addition, noise has a certain impact on the estimates by the algorithms; when the level of noise increases (i.e. SNR decreases), higher values for *f*, lower values for *D* and remarkably higher values for *D** are estimated. Table 4 shows the results of parameter estimation performances of the optimization algorithms (i.e. the correlations between the estimated and the true simulated values for *f*, *D* and *D**). For the noise-free signals, the strongest positive correlation exists for *f* and *D* (*r*=1.00) regardless of the optimization algorithm. However, for *D**, very strong positive correlations are recognizable between the true simulated values and their estimates by the TR and the PS algorithms only (*r*=1.00). Besides, a very weak positive correlation is obtained for the LM algorithm (*r*=0.08). For the noisy signals, varying positive correlations are observable for *f*, *D* and *D**. When compared to the LM algorithm, the TR algorithm always offers better correlations. Besides, the TR and the PS algorithms demonstrate almost the same correlations. These algorithms permit very strong correlations for D from the noisy signals with SNR$\geq$ 40 ($r\geq$ 0.95) meanwhile for f from the noisy signals with SNR$\geq$ 80 ($r\geq$ 0.90). However, for D^*, they demonstrate very weak correlations (r= 0.02-0.20) as the LM algorithm does (r=0.01-0.14) regardless of the SNR.

In a general sense, the TR and the PS algorithms provide better parameter estimates than the LM algorithm. However, the PS algorithm shows almost the same estimation performance as the TR algorithm. In contrast to the TR algorithm, the PS algorithm does not require any user-given initial value, therefore it offers a priceless tool in nonlinear least squares fitting of IVIM model to the diffusion MR signals of the human breast tissue especially for low SNRs. Scatter plots of the estimates by the PS algorithm against the true simulated values are presented in Figure 1.

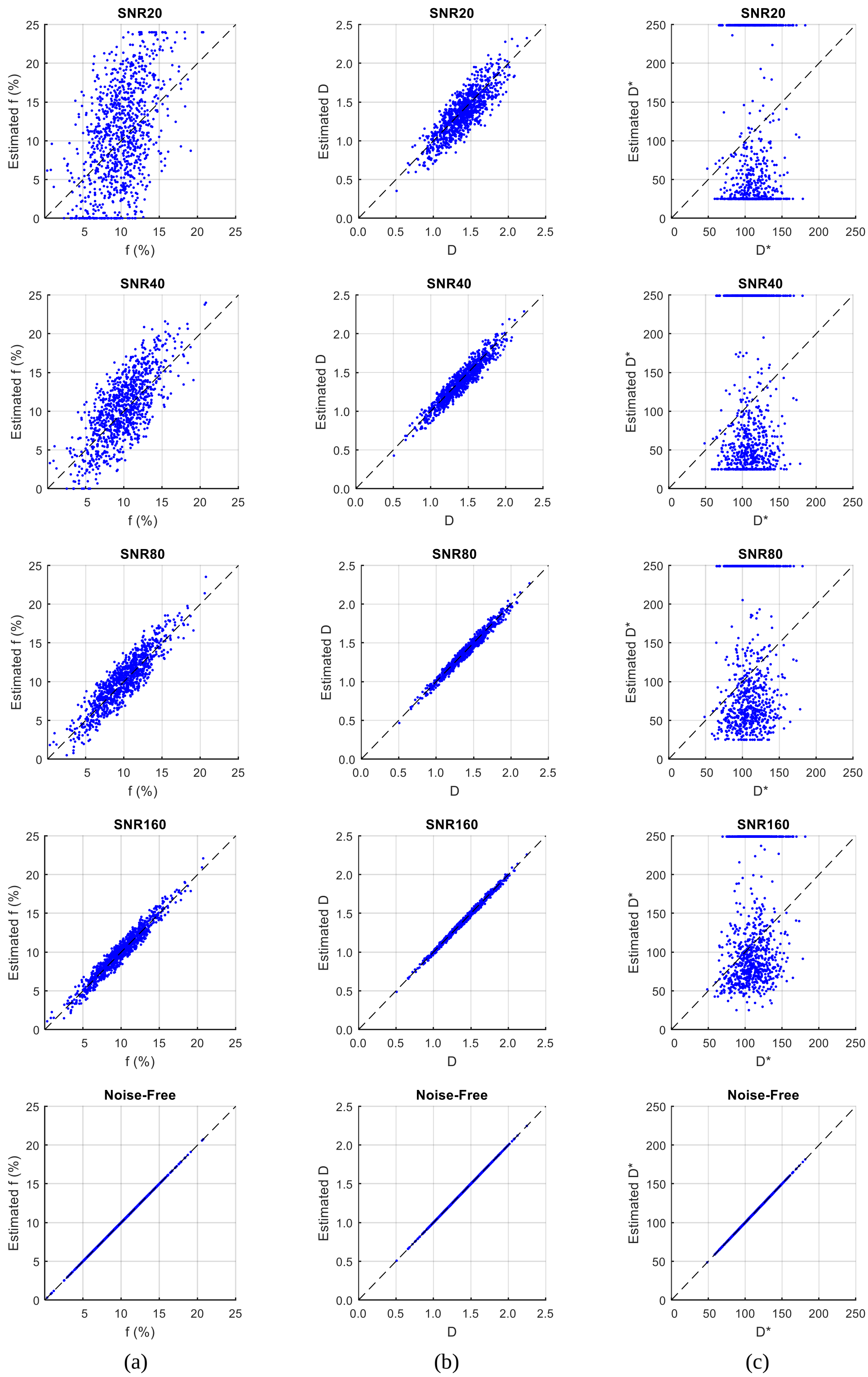

Figure 1. Scatter plots of (a) f, (b) D and (c) D^* estimated by the PS algorithm against the true simulated values.

4. Conclusion

The intravoxel incoherent motion (IVIM) modeling for the diffusion MR signals of the human breast tissue enables assessment of volume fraction of the incoherently flowing blood in the tissue (*f*), the diffusion coefficient of water in the tissue (*D*) and the sum of the pseudo-diffusion coefficient associated to the motion effect and the diffusion coefficient of water in blood (D^*) as the potential biomarkers for different types of breast lesions and different stages of breast cancer. In the current study, the model fitting and the model parameter estimation performances of three optimization algorithms, namely Levenberg-Marquart (LM), trust-region (TR) and particle swarm (PS), in nonlinear least squares based fitting the IVIM model to the diffusion MR signals are investigated.

Our results from five thousand breast diffusion MR signals generated synthetically show that all the optimization algorithms achieve very good model fitting performances for both noise-free and noisy diffusion signals. However, computation time spent by all the algorithms for fitting the IVIM model increase with the increase in noise level. When compared to the LM and the TR algorithms, the PS optimization algorithm always requires a considerably longer computation time. On the other hand, our results also demonstrate that the optimization algorithms play a very important role in getting reliable and precise estimates of the three model parameters *f*, *D* and D^*. On the noise-free signals, the LM, TR and PS algorithms all exhibit the highest performance in estimating *f* and *D*. However, for D^*, most of the estimates by the LM algorithm are out of the physiologically acceptable range and therefore the algorithm shows a remarkably lower performance then the TR and PS algorithms both of which reveal the highest performance possible. In presence of noise, the TR algorithm performs better than the LM algorithm; the PS algorithm possesses the same estimation performance as the TR algorithm. The TR and the PS algorithms perform remarkably better in estimating *f* and *D*, especially in presence of high noise levels. However, their performances for *f* are not as good as for *D*. In addition to these, all the three algorithms suffer from very poor performances in estimating D^* regardless of the noise level. These findings verify the wide use of the estimates of *D* in recent research on quantitative diffusion weighted imaging, arising the question that *f* and D^* may also offer valuable information under low noise conditions.

Overall, the TR algorithm performs better than the LM algorithm while the PS algorithm shows almost the same performance as the TR algorithm. Revealing a very good performance without requiring any user-given initial value, the PS algorithm can be preferably used in nonlinear least squares fitting of the IVIM model to the diffusion MR signals of the human breast tissue, especially in presence of high levels of noise.

The current study has some limitations. First of all, the results are from synthetic MR signals generated for the IVIM model parameters with certain mean and standard deviation values that satisfy ranges reported from a single-center study performed with a 3.0T MR scanner. Ranges recognized by different scanners at different centers may differ and therefore dissimilar MR signals can be of concern. Second, noisy MR signals are obtained for SNRs of 20, 40, 80 and 160 using Gaussian noise. 3T MR scanners with optimized imaging protocols easily provide these high SNRs. However, lower SNRs may be experienced in some cases and for signals with SNR<5, it might be questionable to use of Gaussian noise instead of Rician noise. Another issue is that the mean values of the IVIM model parameters generated are later used as the user-given initial values for the LM and the TR algorithms. For most of the fittings by these algorithms, the initial values might be very close to the solution of the model and this might minimize the disruptive effect of local minima during fitting while leading to convergence to a precise solution. Consequently, performances of the LM and the TR algorithms might be over assessed. In addition, current implementation of the PS algorithm consumes considerably large amount of time in fitting the IVIM model. The use of faster computers or programming techniques dedicated to PS optimizations might lead to much shorter computation time. On the other hand, adjusted R-squared measure gives almost the same model fitting performances for all the algorithms. The use of an alternative measure such as the Akaike Information Criterion or Bayesian Information Criterion may give remarkably different fitting performances.

There are some issues awaiting further exploration and improvement. Noise has undesirable impact on most of the IVIM model parameter estimates limiting their use in the detection of different types of breast lesions and stages of breast cancer. To cope with this, an additional parameter estimation may be performed from a "reference" healthy tissue to get a normalized parameter that may be less corrupted by noise. Another solution may be the use of alternative fitting techniques less sensitive to noise then the least squares fitting. For instance, artificial neural networks can be developed to approximate the IVIM model parameters by approximating the bi-exponential decay function. On the other hand, improved methods based on least squares fitting such as segmented least squares fitting [16] or weighted least squares fitting may also be used to minimize the effect of noise [17].

In conclusion, by facilitating the estimation of IVIM model parameters from diffusion MR signals of the human breast, the particle swarm optimization algorithm holds a priceless potential to improve quantitative characterization of human breast tissue. Further studies with real clinical data are needed to determine its benefit in distinguishing types of breast tissue and lesions in the diagnosis of breast cancer.

References

[1] Le Bihan, D. & Lima, M. (2015). Diffusion magnetic resonance imaging: What water tells us about biological tissues. *PLoS Biology*, 13(7): e1002203. http://doi.org/10.1371/journal.pbio.1002203.

[2] Pinker, K., Moy, L., Sutton, E.J., Mann, R.M., Weber, M., Thakur, S.B., Jochelson, M.S., Bago-Horvath, Z., Morris, E.A., Baltzer, P.A. & Helbich, T.H. (2018). Diffusion-weighted imaging with apparent diffusion coefficient mapping for breast cancer detection as a stand-alone parameter: comparison with dynamic contrast-enhanced and multiparametric magnetic resonance imaging. *Investigative Radiology*. http://doi:10.1097/RLI.0000000000000465.

[3] Pasquier, D., Hadj Henni, A., Escande, A., Tresch, E., Reynaert, N., Colot, O., Lartigau, E. & Betrouni, N. (2018). Diffusion weighted MRI as an early predictor of tumor response to hypofractionated stereotactic boost for prostate cancer. *Scientific Reports*, 8, 10407. http://doi.org/10.1038/s41598-018-28817-9.

[4] Keil, V. C., Mädler, B. , Gielen, G. H., Pintea, B. , Hiththetiya, K. , Gaspranova, A. R., Gieseke, J. , Simon, M. , Schild, H. H. & Hadizadeh, D. R. (2017). Intravoxel incoherent motion MRI in the brain: Impact of the fitting model on perfusion fraction and lesion differentiability. *Journal of Magnetic Resonance Imaging*, 46(4), 1187-1199.

[5] Barbieri, S., Donati, O.F., Froehlich, J.M. & Thoeny, H.C. (2016). Impact of the calculation algorithm on bi-exponential fitting of diffusion-weighted MRI in upper abdominal organs. *Magnetic Resonance in Medicine*, 75(5), 2175-2184.

[6] Marquardt, D.W. (1963). An algorithm for least-squares estimation of nonlinear parameters. *Journal of the Society for Industrial and Applied Mathematics*, 11(1), 431-441.

[7] Coleman, T.F. & Li, Y. (1996). An interior, trust region approach for nonlinear minimization subject to bounds. *SIAM Journal on Optimization*, 6(1), 418-445.

[8] Kennedy, J. & Eberhart, R. (1995). Particle swarm optimization. *Proceedings of the IEEE International Conference on Neural Networks*, 1942-1945.

[9] Devraj Mandal, D., Chatterjee, A. & Maitra, M. (2014). Robust medical image segmentation using particle swarm optimization aided level set based global fitting energy active contour approach. *Engineering Applications of Artificial Intelligence*, 35(1), 199-214.

[10] Kaur, S. & Kaur, M. (2010) Medical image enhancement using particle swarm optimization. *Artificial Intelligent Systems and Machine Learning*, 2(5), 54-59.

[11] Lin, C.-L., Mimori, A. & Chen, Y.-W. (2012). Hybrid particle swarm optimization and its application to multimodal 3D medical image registration. *Computational Intelligence and Neuroscience*, 561406. http://doi.org/10.1155/2012/561406.

[12] Le Bihan, D., Breton, E., Lallemand, D., Grenier, P., Cabanis, E. & Laval-Jeantet, M. (1986). MR imaging of intravoxel incoherent motions: application to diffusion and perfusion in neurologic disorders. *Radiology*, 161(2), 401-417.

[13] Liu, C., Liang, C., Liu, Z., Zhang, S. & Huang, B. (2013). Intravoxel incoherent motion (IVIM) in evaluation of breast lesions: comparison with conventional DWI. *European Journal of Radiology*, 82(12): e782-9. http://doi:10.1016/j.ejrad.2013.08.006.

[14] Cho, G. Y., Moy, L., Zhang, J. L., Baete, S., Lattanzi, R., Moccaldi, M. & Sigmund, E.E. (2015). Comparison of Fitting Methods and b-Value Sampling Strategies for Intravoxel Incoherent Motion in Breast Cancer. *Magnetic Resonance in Medicine*, 74(4), 1077–1085.

[15] Harel, O. (2009). The estimation of R2 and adjusted R2 in incomplete data sets using multiple imputation. *Journal of Applied Statistics*, 36(10), 1109-1118.

[16] Zhou, T. & Han, D. (2008). A weighted least squares method for scattered data fitting. *Journal of Computational and Applied Mathematics*, 217(1), 56-63.

[17] While, P. T. (2017). A comparative simulation study of bayesian fitting approaches to intravoxel incoherent motion modeling in diffusion-weighted MRI. *Magnetic Resonance in Medicine*, 78(6), 2373-2387.

Gokhan Ertas *received his B.S. degree from Erciyes University in Electronics Engineering in 1998 and his M.S. and Ph.D. degrees from Bogazici University in Biomedical Engineering in 2001 and 2007, respectively. He led efforts in developing computational methods to comparing breast MR images at the Institute of Cancer Research and the Royal Marsden Hospital, UK. He is currently the vice chairman of the Biomedical Engineering Department at Yeditepe University. His interests include development of new diffusion estimation methods for better diagnosis of breast diseases.*

An International Journal of Optimization and Control: Theories & Applications (http://ijocta.balikesir.edu.tr)

An International Journal of Optimization and Control: Theories & Applications
ISSN: 2146-0957 eISSN: 2146-5703
Vol.9, No.2, pp.113-124 (2019)
https://doi.org/10.11121/ijocta.01.2019.00655

RESEARCH ARTICLE

Analyzing occupational risks of pharmaceutical industry under uncertainty using a Bow-Tie analysis

Sukran Seker *

Department of Industrial Engineering, Yildiz Technical University, Turkey
sseker@yildiz.edu.tr

ARTICLE INFO

Article history:
Received: 30 July 2018
Accepted: 12 December 2018
Available Online: 19 February 2019

Keywords:
Risk analysis
Bow-tie
Fuzzy sets
Pharmaceutical industry

AMS Classification 2010:
90C70, 90B25

ABSTRACT

Risk analysis is a systematic and widespread methodology to analyze and evaluate risks which are exposed in many working areas. One of the Quantitative Risk Analysis (QRA) methods for risk assessment is Bow-Tie analysis which combines features of fault-tree analysis and event-tree analysis to identify the top event; its causes and consequences (outcomes); and possible preventive and protective control measures or barriers. This study proposes an occupational risk assessment approach, which is known as Fuzzy Bow-Tie analysis, for pharmaceutical industry processes and work units. The aim is to evaluate critical risks and risky pharmaceutical work units and take safety precautions against accidents which caused by risky conditions. Thus, this methodology combines the concept of uncertainty which comes from different (Decision Maker) DM's evaluations and the whole performance of the Bow-Tie analysis for hazard identification and risk assessment. To apply and validate the proposed method, a case study is performed for pharmaceutical industry processes and work units. Based on the computed risk score, which is calculated by multiplying probability ranking and impact ranking of criterion, the risks are prioritized and some measures are suggested for management to prevent accidents occur in the industry.

1. Introduction

Pharmaceutical industry is usually considered to have high quality levels since healthcare products require manufacturing processes in safe conditions, protection under a substantial control hygiene against chemical and biological contaminants, and keeping equipments at optimum working conditions [1]. Since the main aim is to produce medical substances with pharmacological processes, many factors in pharmaceutical Research and Development (R&D) and manufacturing are hazardous for employees. Pharmaceutical workers are at risk because occupational direct/indirect exposure is considered to be high among workers who used biological, chemical/radiological, or pharmacological agents in their working areas [2]. Risk factors and impact of these risks lead to occupational risks in Pharmaceutical industry. Fire or explosion risks during pharmaceutical production of dosage arrangements are associated with process safety. These processes are generally related to bed drying, slugging, granulation, blending, compounding and drying etc. and they produce pharmaceutical dusts due to flammable liquids. Coating, wet granulation, compounding operations may cause solvent vapor exposure. Also, once pharmaceutical workers expose to complex mixtures including high amounts of active drug substances, they are physically and chemically damaged. Moving machine parts (exposed equipment e.g., belts and shafts), manual handling of materials and equipments, unsafe energy systems (electrical, thermal, pneumatic, etc.); high-pressure vapor, hot water and heated areas; combustible and corrosive liquids; and high sound degree are other health and safety risks for workers during manufacturing process in pharmaceutical industry. These occupational risks cause illnesses, including occupational asthma, adverse reproductive concerns, pharmacologic impacts and dermatitis among pharmaceutical workers [2].

Appropriate mitigation measures need to be implemented for occupational risks in pharmaceutical industry to protect workers from industrial chemicals and drug matters throughout manufacturing, R&D and quality control processes [3,4].

*Corresponding author

Consequently, in pharmaceutical industry, risk assessment methodologies play an important role to analyze occupational risks with other work environment components, including technical and organizational parts, production activities as well as implementation procedures [5].

The main objective of this paper is to propose a Risk Assessment framework and develop extensive risk analysis methodology to assess and prioritize risk factors for occupational safety in pharmaceutical industry. For this purpose, Bow-Tie risk assessment analysis, which includes two main risk assessment methods named Fault Tree Analysis (FTA), Event Tree Analysis (ETA), have combined with Fuzzy Set Theory (FST) to analyze the risk factors associated with the pharmaceutical industry. FST is used to handle data uncertainty in risk analysis. Thus, fuzzy linguistic probabilities are used for associating possibilities of failures, since probability theory alone was found insufficient to represent all types of uncertainties due to lack of ability to model human conceptualizations in the real world applications [6].

2. Literature review

Risk assessment is an efficient and methodological approach to assess and minimize the risks of an accident for any industry [7]. A quantity of qualitative and quantitative methods including Event Tree Analysis (ETA), Fault Tree Analysis (FTA), HAZOP analysis, and barrier block diagrams [8], Bow-Tie diagrams [9,10] have been used for risk assessment process [11].

The Bow-Tie diagrams and other risk assessment techniques have been used due to effective implementation in many real world applications such as accident risk assessment [12-17], human error risk analysis [18,19], dynamic risk analysis [20], risk management [21,22], safety barrier implementation [23-25]. However, the applications of all these techniques aren't efficient in terms of satisfying results because the safety risk data are often vague, imprecise or incomplete to determine risk levels [26]. Therefore FST, probability theory, and evidence theory etc. have been suggested to handle vagueness in risk analysis because of their efficiencies [27-32]. In this study, combination of FTA and ETA is introduced as Bow-Tie analysis to solve the risk assessment problem using fuzzy numbers to deal with uncertain and vague information.

The use of FST has been implemented in different fields of the process risk assessment [29,33-38]. However, uncertainty is seldom carried out in all other risk assessment studies, especially in consequence analysis [39]. The uncertainty-based methods of ETA, FTA and Bow-Tie analysis have been studied in literature for risk analysis of different systems [29,37,38,40-42].

Some researchers suggested certain novel methods to recognize barriers in Bow-Tie diagram [12, 23,24]. For instance, [24] presented a new approach using crossing matrices (checklist filled by experts) to suggest preventive and protective measures by considering the Bow-Tie construction. Aqlan and Mustafa Ali [43] proposed the Fuzzy Bow-Tie analysis to compute the aggregated risk scores for likelihood and impacts that have been used to decide the position of risk in risk prioritization matrix. Markowski et al. [44] presented a fuzzy based methodology for Bow-Tie analysis; however, this methodology is not useful to handle vagueness due to inconsistency in the knowledge. This study also was incapable to capture model uncertainty owing to the individual difference among the input events in FTA or ETA.

There is limited research in the literature related to workers health and safety assessment in pharmaceutical industry [1,5,45-49] since the quality risk management is commonly studied in this industry.

As it is evident in the previous studies in the literature, this paper is the first QRA study performing Fuzzy Bow-Tie for pharmaceutical industry to analyze and visualize risks, causes and consequences of potential risk events and their impacts with possible preventive and protective control measures or barriers in prospective manner.

Accordingly, the aim of the current study is to introduce a comprehensive framework based on Bow-Tie analysis and FST with three important points in risk analysis a) combination of multiple expert knowledge, and b) handling and managing uncertainty for risk analysis c) prioritizing risks based on probability and impact of the risks.

3. Risk analysis under uncertainty

3.1. Bow-tie analysis for risk assessment

Bow-Tie analysis was proposed by SHELL Company in the early nineties to analyze the whole scenario of an accident based on Swiss Cheese Model [9]. Bow-Tie analysis is a combined probabilistic method that assesses accident consequences due to evaluating the probability and impact of risk events [22].

Bow-Tie combines the features of fault and event trees used in QRA [50]. In the center of the diagram there is a top event. While the left side of the "Bow-Tie" diagram (fault tree) represents the potential parallel and consecutive combination of faults (causes), the right side of the ''Bow-Tie'' diagram (event tree) represents the potential consequences (outcomes) of corresponding top event [44]. After identifying risk events, hazards and consequences also preventive and protective measures or barriers are determined to mitigate hazards [50].

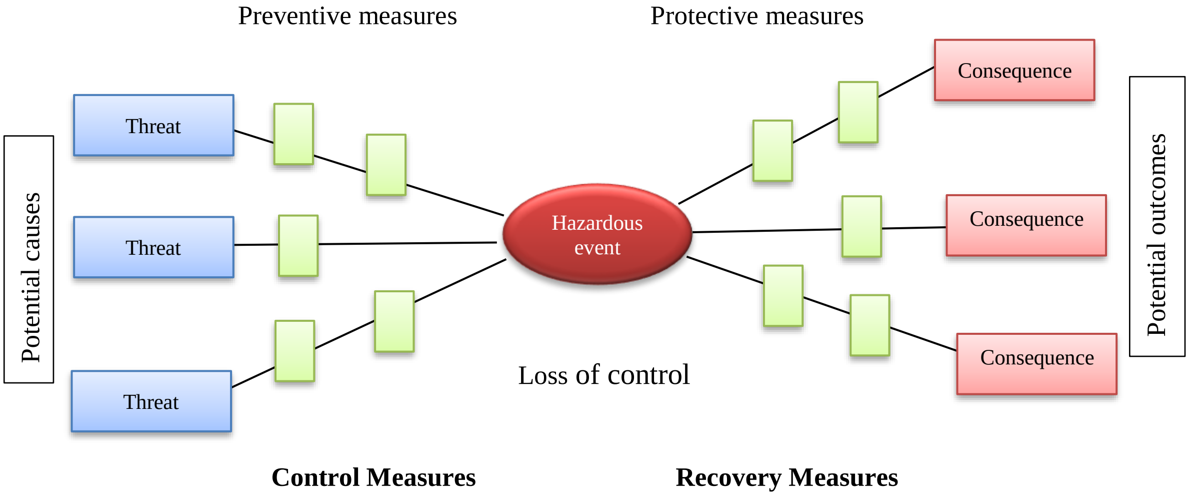

Figure 1. Implementation of Bow-Tie structure [9].

Figure 1 shows the implementation of Bow-Tie structure. As a part of Bow-Tie analysis, determination of preventive and protective barriers can be difficult since they are continuously contact with each other. Also, their performance depends on several criteria such as efficiency, being safe, ease of use and cost etc. [9].

The main advantage of performing the Bow-Tie analysis is that it ensures a visual illustration to evaluate and analyze the potential hazards and risks with their potential interactions. This relationship illustration provides many advantage when compared with word-based or tabular risk information in QRA [51]. However, data and model uncertainty are prevalent and generally inevitable, in fault tree and event tree and consequently in Bow-Tie analysis [52]. In the current study, to deal with the data and model uncertainty, Bow-Tie analysis is conducted based on the principles of FST.

3.2. Fuzzy set theory

The FST is suggested by L.A. Zadeh [53] in 1965. FST is performed to deal with vague and uncertain information. A FST in probability space symbolizes a fuzzy number which is between zero and one for the likelihood of an event. There are various representations of fuzzy numbers such as Triangular Fuzzy Number (TFN) and Trapezoidal Fuzzy Number (TrFN) which are generally used in reliability analysis. To quantify subjectivity of the DM's evaluations, TFNs are used in this study. A TFN can be represented by a vector (a_1, a_2, a_3) that shows the lower bound, most likely value, and upper bound.

A fuzzy set $\breve{A}$ identified on R must have the following features to represent a fuzzy number: [53-57].

(a) $\mu_{\breve{A}}(x) = 0$ for all $x \in (-\infty, c] \cup [d, \infty)$, where c<d.

(b) $\mu_{\breve{A}}(x)$ is hardly increasing on [c, a] and hardly decreasing on [b, d] for $c \leq a \leq b \leq d$.

(c) $\mu_{\breve{A}}(x) = 1$ for all $x \in [a, b]$ ensured $a \leq b$.

While a fuzzy number ($\breve{A}$) is represented as TFN, the membership function of fuzzy number A is denoted by the Expression (1):

$$\mu_{\tilde{A}}(x)=\begin{cases} 0 & if\ x \leq a_1\ or\ x \geq a_2 \\ \frac{x-a_1}{a_2-a_1} & if\ a_1 \leq x \leq a_2 \\ \frac{a_3-x}{a_3-a_2} & if\ a_2 \leq x \leq a_3,\quad x, a_1, a_2, a_3\ \in R \end{cases} \tag{1}$$

A triplet (a_1, a_2, a_3) might be used to illustrate any TFN seen above.

A trapezoidal fuzzy number $\breve{A}$ represented by a quadruple (a1, a2, a3, a4) can be identified as follows:

$$\mu_{\tilde{A}}(x)=\begin{cases} 0 & if\ x \leq a_1\ or\ x \geq a_2 \\ \frac{x-a_1}{a_2-a_1} & if\ a_1 \leq x \leq a_2 \\ 1 & if\ a_2 \leq x \leq a_3 \\ \frac{a_3-x}{a_3-a_2} & if\ a_2 \leq x \leq a_3,\quad x, a_1, a_2, a_3\ \in R \end{cases} \tag{2}$$

(TFN) $\breve{A}$ = (a, b, c) and (TrFN) $\breve{A}$ = (a, b, c, d) are illustrated in Figure 2.

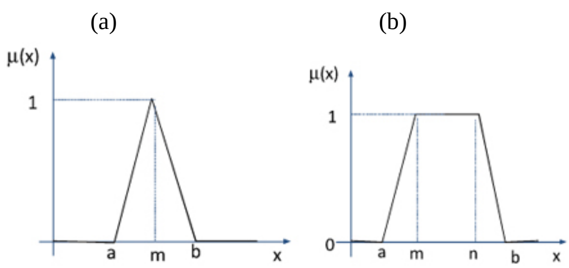

Figure 2. Illustration of (a) TFN and (b) TrFN.

Linguistic expression is representeed with words or sentences. For example, ''probability of failure'' might be shown with linguistic terms whose values are: ''very low'', ''low'', ''medium'', ''high'' and ''very high''. As shown in Figure 3, these variables can be represented by fuzzy numbers whose members are probability of risks [58].

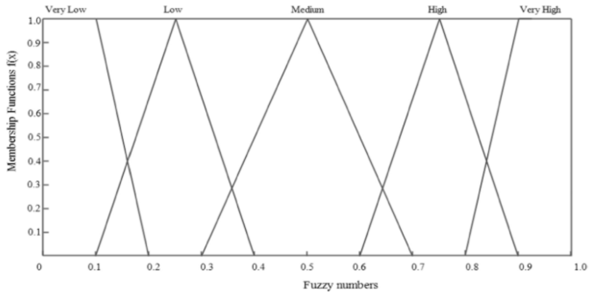

Figure 3. Linguistic values of fuzzy numbers.

In the implementation of the Bow-Tie analysis, the risk factors associated with each risk need to be identified. A fuzzy evaluation for the probability of occurrence and impact of the risk factors are determined. The probability of occurrence is calculated using the estimated evaluations given in Table 1. The impact or severity of each risk is also calculated. Table 2 shows the fuzzy probabilities for risk impacts.

Once two TFNs are summed, again a TFN is obtained. Likewise, when one TFN subtract from other TFN, a TFN is obtained again. Suppose $\breve{A}$ =(a_1, a_2, a_3) and $\breve{B}$ =(b_1, b_2, b_3) are two TFNs. The operations of TFNs are shown in Equation (3-5) [59].

$$\tilde{A} + \tilde{B} = (a_1+b_1,\ a_2+b_2,\ a_3+b_3) \quad (3)$$

$$\tilde{A} - \tilde{B} = (a_1-b_1,\ a_2-b_2,\ a_3-b_3) \quad (4)$$

The multiplication of two fuzzy numbers A=(a_1, a_2, a_3) and B =(b_1, b_2, b_3) represented as A*B can be denoted as:

$$\mu\tilde{A} * \tilde{B}(x) = \begin{cases} -D_1 + [D_1^2 + (x-P)/T_1]^{1/2} & P \le x \le Q \\ -D_1 + [D_{21}^2 + (x-R)/U_1]^{1/2} & Q \le x \le R \\ 0 & otherwise \end{cases} \quad (5)$$

where $T_1 = (a_2 - a_1)(b_2 - b_1), T_1 = a_1(a_2 - a_1) + ab_2(b_2 - b_1)$, $U_1 = (a_2 - a_1)(b_2 - b_1)$, $U_2 = b_3(a_2 - a_1) + a_3(b_2 - b_1)$, $D_1 = \frac{T_2}{2T_1}$, $D_2 = -\frac{U_2}{2U_1}$, $P = a_1b_1$, $Q = a_2b_2$, $R = a_3b_3$

Supposing that the probability of a risk factor 'i' is assessed by n different number of DMs, the fuzzy probability can be computed as $\breve{P}(t) = (a_i - c_{1i}, a_i, a_i + c_{2i})$ where $i = 1,2,\dots,n$; while $(a_i - c_{1i})$ is the minimum value of the fuzzy number, a_i is the mid value of the fuzzy number and $(a_i + c_{2i})$ is the maximum value of the fuzzy number. The fuzzy probabilities can be aggregated using aggregation operator. Thus, a single fuzzy probability has been obtained as $\breve{P}A(t) = (b - d_1, b, b + d_2)$ that best fits all DMs' forecasts. The values of b, d_1 and d_2 are estimated in such a way that $\breve{P}A$ has minimum variance with all $\breve{P}i(t)'s$. The square of deviations (S) can be computed as follows :

$$S_1 = \sum_{i=1}^{n}[2(d_1 - c_{1i})]^2 \quad (6)$$

$$S_2 = \sum_{i=1}^{n}[2(d_2 - c_{2i})]^2 \quad (7)$$

The minimum deviation can be computed using $d_1 = 1/n\sum_{i=1}^{n} c_{1i}$ and $d_2 = 1/n\sum_{i=1}^{n} c_{2i}$. The parameter b can be obtained by using equation $D = max_{1\le i\le n}|b - a_i|$ where D is the absolute deviation. Then, D is the minimum for $b = min_{1<i<n}a_i + max_{1<i<n}a_i/2$ [43].

The fault tree consist of 'AND' and 'OR' gates. The 'AND' gate express that the out-put event will occur if all the input events occur, while the 'OR' gate express that the output event will occur if any one of the input events occurs. Therefore, in Bow-Tie analysis total probability for each failure is calculated when the connecting gate is either AND or OR [58].

In FTA, "AND gate" operator is: ($P_{AND} = \Pi$ Pi) in which Pi (i = 1,2….n) recognizes the certain probability of the event i. Fuzzy operator for P_{AND} can be represented by the following equation:

$$P_{AND} = \prod_{i=1}^{n} P_i = [\prod_{i=1}^{n} a_i, \prod_{i=1}^{n} b_i, \prod_{i=1}^{n} c_i] \quad (8)$$

If the events are interdependent, then the mathematical expression is $P_{AND} = \min(P_1, P_2, \dots P_n)$.

In FTA, "OR gate" operator is: $P_{OR} = \Pi$ (1-Pi) in which Pi (i = 1,2….n) recognizes the certain probability of event i. Fuzzy operator for P_{OR} can be represented by the following equation:

$$P_{OR} = 1 - \prod_{i=1}^{n}(1 - P_i)$$

$$P_{OR} = 1 - \left[\prod_{i=1}^{n}(1 - a_i), \prod_{i=1}^{n}(1 - b_i), \prod_{i=1}^{n}(1 - c_i)\right] \quad (9)$$

if the events are dependent, then the algorithm is P_{OR} = max(P1, P2,…,Pn) [43].

4. Framework of the fuzzy Bow-Tie analysis

The proposed framework is applied to pharmaceutical industry to prevent occupational accidents in the pharmaceutical industry.

The aim is to propose a risk analysis framework which can be used in any pharmacy firm as a risk analysis tool. The steps of the proposed Fuzzy Bow-Tie risk analysis approach for pharmaceutical industry are explained in Figure 4. Before the implementation of this approach, five DMs, who actively work in the pharmaceutical industry, evaluated the risk events which can cause fatal or non-fatal occupational accidents. The DMs made judgments by expressing their opinions based on their experience, knowledge, and expertise. All potential occupational risk types and their impacts in any pharmaceutical industry processes are identified in Appendix A.

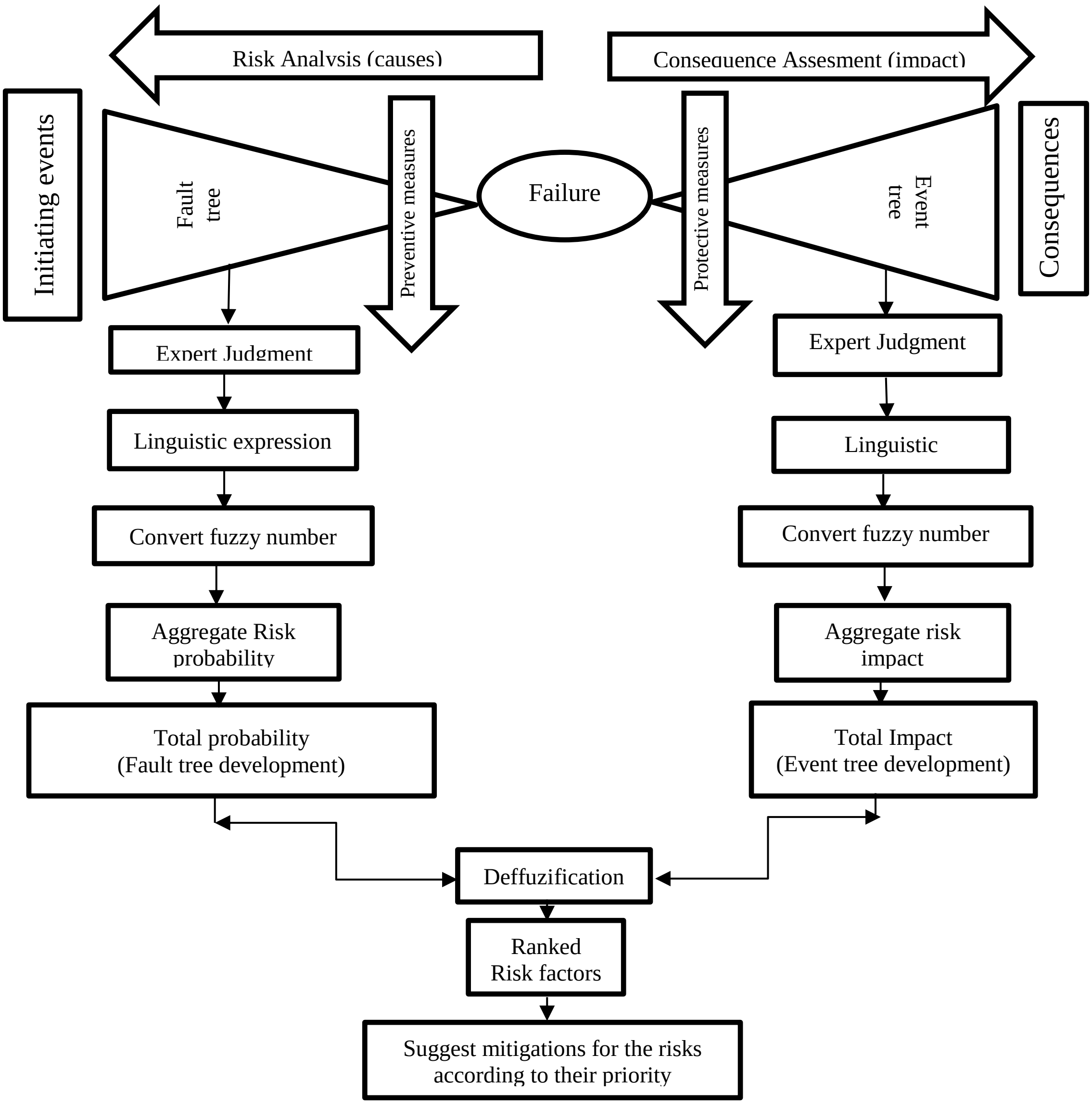

Figure 4. Implementation of Fuzzy Bow-Tie risk analysis approach.

The proposed framework based on FST and Bow-Tie analysis is as follows:

Step 1. Identify potential risks. The risks, risk factors, and risks' impacts are identified based on reported events and DMs' experience and knowledge in pharmaceutical industry.

Step 2. Collect linguistic expressions of DMs. DMs are interviewed about potential risk factors and their impacts by using qualitative linguistic terms because of the highly subjective and imprecise information. Therefore, DMs express their opinions for the probability of occurrence and impact of the risk events using linguistic variables. The linguistic expressions for the probability of occurrence of each risk event are 'Expected, 'Possible', 'Unlikely', 'Very unlikely' and 'Not expected'. The linguistic expressions for the impact of each risk event are 'High, 'Medium', 'Low', 'Very low' and 'None'.

Step 3. Convert linguistic variables into numerical values using TFNs. Each linguistic variable is converted into a TFN using Table 1 and Table 2 for the probabilities of occurrence and impacts of the risk events, respectively.

Step 4. Calculate fuzzy aggregated values for the probability of the occurrence and impact of each identified risk. If two or more DM judgments are available, it is needed to integrate their opinions into a single opinion to deal with non-homogeneous situations [60]. Accordingly, the individual DM fuzzy values are aggregated in this step. Fuzzy probabilistic value for the probability of the occurrence of each risk event is calculated using Equations (6) and (7). The same calculation is carried out for the impacts of the risk factors.

Table 1. Linguistic expressions and their corresponding fuzzy numbers for probabilistic occurrence [43,59].

Linguistic assessment variables	Corresponding fuzzy numbers	Characteristic function of fuzzy numbers
Expected (E)	$\widetilde{0.9}$	(0.7,0.9,1.0)
Possible (P)	$\widetilde{0.7}$	(0.5,0.7,0.9)
Unlikely (U)	$\widetilde{0.5}$	(0.3,0.5,0.7)
Very Unlikely(VU)	$\widetilde{0.3}$	(0.1,0.3,0.5)
Not Expected (NE)	$\widetilde{0.1}$	(0.0,0.1,0.3)

Table 2. Linguistic expressions and fuzzy numbers for impact of risks [43].

Linguistic assessment variables	Corresponding fuzzy numbers	Characteristic function of fuzzy numbers
High (H)	$\tilde{9}$	(7,9,10)
Medium (M)	$\tilde{7}$	(5,7,9)
Low (L)	$\tilde{5}$	(3,5,7)
Very low (VL)	$\tilde{3}$	(1,3,5)
None (N)	$\tilde{1}$	(0,1,3)

Step 5. Calculate the total risk probability for each identified risk event. In Bow-Tie analysis, after the probability of occurrence of each risk event is determined, the total risk probability for each event is calculated. The total probability value for each identified risk is calculated according to the relationship among risk factors (OR or AND). In the proposed framework, the total risk probability is calculated using Equation (8,9).

Step 6. Calculate the total impact for each identified risk event. The right side of the Bow-Tie diagram is event tree and it recognizes the estimated impact of each risk event. If the risk has multiple impacts $\widetilde{L_j}$ each with probability $\widetilde{P_j}(t)$, the total fuzzy impact can be calculated using Equation (10) in event tree diagram [43].

$$\widetilde{L_k} = \frac{\sum_{j=1}^{N} \widetilde{P_j}(t) * \widetilde{L_j}(t)}{\sum_{j=1}^{N} \widetilde{P_j}(t)} \tag{10}$$

Step 7. Defuzzify the fuzzy values for the probability of occurrence and the impact of each risk event. Defuzzification is the process of converting the fuzzy numbers into a crisp (exact) value. The aim is to determine the risk event priorities more easily using defuzzified values for the probability of occurrence, impact and total risk in the Fuzzy Bow-Tie analysis. The bigger the defuzzified value, the bigger the overall risk and the higher risk priority [58]

In this study, Centre of Area (COA) is used to defuzzify TFN output. A crisp output is obtained by calculating the center of symmetry of the area delimited by aggregating the consequences of such fuzzy set. A is a fuzzy set denoted on the output dimension (x), N is the number of quantization levels of the output. Equation (11) shows the COA formula [61].

$$x_0 = \frac{\sum_{j=1}^{N} \mu_A(x_0).\, x_0}{\sum_{j=1}^{N} \mu_A(x_0)} \tag{11}$$

Step 8. Calculate the risk score and prioritize the risk events. The aim of this step is to determine the risk level after calculating total risk score for each risk event. After defuzzification process, risk score is calculated by multiplying total risk probability and impact of the risks [43].

Step 9. Suggest risk mitigation strategies for safety management. After prioritizing risk events, appropriate mitigation plan can be implemented to reduce or eliminate the risk events.

4.1. Illustrative example

In this section, applicability and efficiency of the proposed Fuzzy Bow-Tie analysis is demonstrated through risk analysis in real pharmaceutical industry.

Step 1. Identify potential risks. Five DMs are organized as a team from pharmaceutical industry. These DMs are denoted as DM 1, DM 2, DM 3, DM 4, and DM 5. The DMs make judgments for potential risk events that cause the top event and their impacts based on their experience, knowledge, and expertise.

The profiles of DMs' from Pharmaceutical industry are shown in Table 3.

Table 3. The profile of DMs'.

DM	Age (years)	Education	Experience (years)	Professional Position
DM1	55	PhD	20	R&D manager
DM2	40	Bachelor	15	Synthesis/Process chemist
DM3	35	Master	10	Occupational safety expert
DM4	40	Master	10	Pharmaceutical operator
DM5	30	Bachelor	5	R&D Laboratory technician

Potential occupational risk events and their impacts during any pharmaceutical industry processes are identified as given in Appendix A. Risk factors, impacts, preventive and protective strategies are also identified by DMs as presented in Appendix A. According to their risk classification, the framework for risk assessment has been divided into six main risk types.

Step 2. Collect linguistic expressions of DMs. In this phase, DMs express their judgements and assessments for the probability of occurrence and impact of the risk events using linguistic variables.

Step 3. Convert linguistic variables into numerical values by TFNs. In this step, each linguistic expression has been transformed into a corresponding fuzzy number. Linguistic variables and corresponding fuzzy numbers for risk probability and risk impact are given in Table 1 and Table 2, respectively.

Step 4. Calculate fuzzy aggregated values for both the probability of occurrence and impact of each risk event. The individual DM fuzzy values for the probability of occurrence and impact of each risk event are aggregated with Equations (6) and (7). The aggregated fuzzy probabilistic values for the probability of occurrence of risk events are shown in Table 4. The estimation values for the impacts and associated probabilities are shown in Table 5.

Step 5. Determine the total risk probability for each identified risk event. Total probability for the identified risks is calculated using Equation (8-9). In Bow-Tie analysis, the left side is related to the relationship among the risk factors (OR or AND) for all the identified risks.

Step 6. Calculate the total impact for risk events. Total impact for each risk event is calculated using event tree diagram with Equation (10). The total risk probability of occurrence and total impact for each identified risk are given in Table 6.

Step 7. Defuzzify the fuzzy values for the probability of occurrence and the impact of each risk event. In order to obtain crisp value, TFNs are defuzzified using COA defuzzification method. The risk priority is obtained using defuzzified values for the probability of occurrence, impact and total risk in the Fuzzy Bow-Tie analysis. The results are seen in Table 7.

Step 8. Calculate the total risk score and prioritize the risks. In this step, total score for each risk event is calculated by multiplying total risk probability and impact of the risk after defuzzification process. The aim is to determine risk level of each risk event. Accordingly, Risk events are ranked based on the calculated total risk scores. Table 7 shows the total risk score and risk level for each risk event.

Step 9. Suggest mitigation strategies for safety management. After prioritize risks, appropriate mitigation plans must be implemented firstly for the high priority risks.

5. Results

According to the total risk scores, R1 is the most hazardous risk due to its higher score and the others have medium scores. The critical risks in descending order are R1, R3, R5, R6, R4 and R2. In order to mitigate the effect of risks, the risk mitigation plans must be developed for the high priority risks. However, managers have to identify preventive and protective mitigation measures to reduce risk scores to lower level. Preventive measures and protective strategies should be implemented to avoid the risk event occurs and minimize the impact of risk event, respectively. Hence mitigation plans related to R1 must be implemented firstly. R1 is associated with chemical hazards. According to this result, firstly, health and safety management team should implement a multifaceted prevention program and educate and inform employees about environmental health and safety risks, safe working instructions and the use of personal protective equipment and ventilators, gasmask etc. Training must include the drugs and chemical awareness. Chemicals must be stored in a separate storage area to reduce the risks of chemical practices, worker exposure to hazardous chemicals, and fire and explosion. Manual handling system must be replaced with an automated handling equipment for safety. Smoke or heat alarms and automated sprinkler systems must be installed to detect and prevent fire. Construction of suitable flooring, safe maintenance activities and appropriate cleaning and hygiene for work place are other key prevention and mitigation strategies for chemical risks. Other preventive protective measures about other risks are as follows:

Arrange design of workstations, hand tools, equipment etc.

Provide ergonomically designed equipment and furniture.

Install safeguards which protect workers against contact with potentially dangerous machine motions via physical guard.

Implement electrical safety program which designs and manages electrical installations.

6. Conclusions and discussions

The objective of this research is to propose a QRA framework which can be implemented effectively in any pharmacy company as a risk analysis tool. The Bow-Tie analysis is used to combine quality features of both FTA and ETA for risk assessment. It noticeably analyzes causes and consequences of an accident, then develops prevention and mitigation measures accordingly. Fuzzy sets and probability theories have been performed to handle the ambiguity of data since estimating the impact and occurrence probability of events are imprecise. Hence, this study combines the Bow-Tie analysis and FST to identify an initiating event; its causes and consequences; and potential preventive and protective control strategies or barriers to mitigate harms. The proposed methodology is easy to understand, clear, and practical that combines the features of handling vagueness, aggregation of different DM' data and prioritizing risks based on the probability of occurrence and impact of the risks.

The proposed method provides satisfactory risk assessment to evaluate and then prevent, control and mitigate occupational risks for pharmacy industry. A risk matrix, which shows the comparison of results obtained by above procedures, defines the level of risks related to ranking probability and impacts. In order to mitigate effect of risks, the risk mitigation plans must be developed for the high priority risks.

Table 4. The aggregated fuzzy probabilistic values for the probability of the occurrence of each risk event.

Risks	Factors	DM 1	DM 2	DM 3	DM 4	DM 5	Aggregated
R1	R11	P	P	U	P	P	(0.4,0.6,0.8)
	R12	U	U	U	U	VU	(0.2,0.4,0.6)
	R13	U	VU	P	U	U	(0.3,0.5,0.7)
R2	R21	NE	NE	NE	NE	NE	(0,0.1,0.3)
	R22	NE	NE	VU	NE	NE	(0.08, 0.2,0.4)
	R23	U	U	U	U	VU	(0.2,0.4,0.6)
R3	R31	U	U	U	U	VU	(0.2,0.4,0.6)
	R32	U	P	P	P	P	(0.4,0.6,0.8)
	R33	U	NE	U	U	U	(0.12,0.3,0.5)
R4	R41	VU	VU	U	U	U	(0.2,0.4,0.6)
	R42	NE	U	U	U	U	(0.12,0.3,0.5)
R5	R51	E	U	P	U	U	(0.5,0.7,0.88)
	R52	U	U	U	U	VU	(0.2,0.4,0.6)
	R53	U	NE	U	U	U	(0.12,0.3,0.5)
R6	R61	P	P	U	P	P	(0.4,0.6,0.8)
	R62	U	P	VU	U	U	(0.3,0.5,0.7)

Table 5. The estimation values for impacts and associated probabilities.

Risks	Factors	Impact /Probability	DM 1	DM 2	DM 3	DM 4	DM 5	Aggregated
R1	R11	Impact	L	M	H	M	H	(5,7.8.6)
		Probability	P	U	U	P	P	(0.4,0.6,0.8)
	R12	Impact	L	L	VL	M	M	(3,5,7)
		Probability	P	P	P	P	U	(0.4,0.6,0.8)
	R13	Impact	M	M	H	M	M	(6,8,9.8)
		Probability	P	P	U	P	P	(0.4,0.6,0.8)
	R14	Impact	M	M	H	M	M	(6,8,9.8)
		Probability	P	U	P	U	P	(0.4,0.6,0.8)
R2	R21	Impact	H	M	H	M	M	(6,8,9.6)
		Probability	P	E	P	P	P	(0.6,0.8,0.98)
	R22	Impact	L	L	L	VL	L	(2,4,6)
		Probability	NE	P	E	NE	P	(0.34,0.5,0.68)
	R23	Impact	L	M	H	M	H	(5,7,8.6)
		Probability	P	U	U	P	P	(0.4,0.6,0.8)
R3	R31	Impact	L	M	H	M	H	(5,7,8.6)
		Probability	P	U	U	P	P	(0.4,0.6,0.8)
	R32	Impact	L	L	VL	M	M	(3,5,7)
		Probability	P	P	P	P	U	(0.4,0.6,0.8)
	R33	Impact	M	M	H	M	M	(6,8,9.8)
		Probability	P	P	U	P	P	(0.4,0.6,0.8)
R4	R41	Impact	L	L	L	VL	L	(2,4,6)
		Probability	U	P	P	U	P	(0.4,0.6,0.8)

	R42	Impact	H	M	H	M	M	(6,8,9.6)
		Probability	P	E	P	P	P	(0.6,0.8,0.98)
R5	R51	Impact	M	VL	L	L	L	(3,5,7)
		Probability	U	U	U	P	E	(0.5,0.7,0.88)
	R52	Impact	M	M	H	H	M	(3,5,7)
		Probability	U	U	U	U	P	(0.4,0.6,0.8)
	R53	Impact	L	M	H	M	H	(5,7,8.6)
		Probability	P	U	U	P	P	(0.4,0.6,0.8)
R6	R61	Impact	L	M	L	L	L	(4,6,8)
		Probability	P	E	P	P	P	(0.6,0.8,0.98)
	R62	Impact	L	M	L	L	L	(4,6,8)
		Probability	U	P	P	U	P	(0.4,0.6,0.8)

Table 6. Calculated total probabilities and impacts for each risk.

Risk Type	Total Probability	Total Impact
R1	(0.66,0.88,0.98)	(5,7,8.8)
R2	(0.26,057,0.83)	(4.45,6.63,7.43)
R3	(0.58,0.83,0.96)	(4.67,6.67,8.47)
R4	(0.30,0.58,0.8)	(4.4,6.28,7.98)
R5	(0.65,0.87,0.98)	(4.4,6.28,7.98)
R6	(0.58,0.8,0.94)	(4,6,8)

Table 7. Determination of ratings for risk occurrence probability and impact.

Risk Type	Probability (COA)	Probability level	Impact (COA)	Impact level	Total risk score	Risk level
R1	0,84	VH	6,93	H	5,82	H
R2	0,55	H	6,17	M	3,42	M
R3	0,79	VH	6,6	M	5,22	M
R4	0,56	H	6,22	M	3,47	M
R5	0,83	VH	6,22	M	5,18	M
R6	0,77	VH	6	M	4,64	M

According to results, R1 is more hazardous risk due to higher its higher score. Hence mitigation plans related to R1 must be implemented at first. However, to reduce future risks, and human and material losses, other mitigation strategies must be implemented for other risks. Therefore, all risks needed to be reduced to low risk scores. For further research, the proposed approach can be used for safety and risk analysis in different industry areas that are faced with uncertainty in data and model.

References

[1] Attaianese, E. & Duca, G. (2012). The integrated assessment of occupational risks in a pharmaceutical manufacturing plant. *Work*, IOS press, 41, 1733-1738. DOI: 10.3233/WOR-2012-0377-1733.

[2] Keith, T. (1998). *Encyclopaedia of Occupational Health and Safety*. Fourth Edition Edited Jeanne Mager Stelman, International Labour Office, Chapter 79.

[3] Naumann, B., Sargent, EV., Starkman, BS., Fraser, WJ . Becker, GT & Kirk, GD. (1996). Performance-based exposure control limits for pharmaceutical active ingredients. *American Industrial Hyjgiene Association Journal,* 57: 33-42.

[4] Evelyn, N., Cristophe, R., Nathalie, B. & Alessandro, S. (2018). Chemical Risk Assessment Screening Tool of a Global Chemical Company. *Safety and Health at Work,* 9(1) 84-94.

[5] Binks, S.P. (2003). Occupational toxicology and the control of exposure to pharmaceutical agents at work. *Occupational Medicine,* 53:363–370.

[6] Shahriar , A., Sadiq, R. Tesfamariam, S. (2012). Risk analysis for oil & gas pipelines: A sustainability assessment approach using fuzzy based Bow-Tie analysis. *Journal of Loss Prevention in the Process Industries*, 25(3), 505–523.

[7] Khan, FI., Abbasi SA. (2001). Risk analysis of a typical chemical industry using ORA procedure. *Journal of Loss Prevention in the Process Industries*, 14, 43–59.

[8] Sklet S. (2004). Comparison of some selected methods for accident investigation. *Journal of Hazardous Materials*. 111 (1-3), 29-37.

[9] Couronneau, J.C., Tripathi, A. (2003). Implementation of the new approach of risk analysis in France. *Proceedings of the 41st International Petroleum Conference*, Bratislava, Slovakia.

[10] Jacinto, C., Silva, C. (2010). A semi-quantitative assessment of occupational risks using Bow-Tie representation. *Safety Science*, 48, 973–979.

[11] Khan FI, Abbasi SA. (1998). Techniques and methodologies for risk analysis in chemical process industries. *Journal of Loss Prevention in the Process Industries*, 11: 261–277.

[12] Delvosalle, C., Fievez, C., Pipart, A., Fabreg, C.J., Debray, B. (2006). ARAMIS project: a comprehensive methodology for the identification of reference accident scenarios in process industries. *Journal of Hazardous Materials*, 130, 200–219.

[13] Montano, D. (2014). Chemical and biological work-related risks across occupations in Europe: a review. Montano *Journal of Occupational Medicine and Toxicology* 2014, 9:28.

[14] Gowland, R. (2006). The accidental risk assessment methodology for industries (ARAMIS)/layer of protection analysis (LOPA) methodology: a step forward towards convergent practices in risk assessment? *Journal of Hazardous Materials*, 130, 307–310.

[15] Khan, F. (2001). Use maximum-credible accident scenario for realistic and reliable risk assessment. *Chemical Engineering Progress*, 11, 56–64.

[16] Chevreau, F. R., Wybo, J. L., & Cauchois, D. (2006). Organizing learning processes on risks by using the Bow-Tie representation. *Journal of Hazardous Materials*, 130(3), 276. doi:10.1016/j.jhazmat.2005.07.018.

[17] Khakzad, N., Khan, F., Amyotte, P. (2013). Quantitative risk analysis of offshore drilling operations: a Bayesian approach. *Safety Science*, 57, 108-117.

[18] Deacon, T., Amyotte, P.R., Khan, F.I. (2013). A framework for human error analysis of offshore evacuations. *Safety Science*, 51 (1), 319-327.

[19] Deacon, T., Amyotte, P.R., Khan, F.I. (2010). Human error risk analysis in offshore emergencies. *Safety Science*, 48 (6), 803-818.

[20] Khakzad, N., Khan, F., Amyotte, P. (2012). Dynamic risk analysis using Bow-Tie approach. *Reliability Engineering and System Safety*, 104, 36-44.

[21] Cockshott, J.E. (2005). Probability Bow-Ties: a transparent risk management tool. *Process Safety and Environmental Protection*, 83 (4), 307-316.

[22] Duijm, N. J. (2009). Safety-barrier diagrams as a safety management tool. *Reliability Engineering & System Safety*, 94(2), 332-341. doi:10.1016/j.ress.2008.03.031.

[23] Badreddine, A., Ben HajKacem, M.A., Ben Amor, N. (2014). A three stages to implement barriers in Bayesian-based Bow-Tie diagram. *27rd International Conference on Industrial Engineering and Other Applications of Applied Intelligent Systems, IEA/AIE* 2014, 32-41.

[24] Dianous, V., Fivez, C. (2006). ARAMIS project: a more explicit demonstration of risk control through the use of Bow-Tie diagrams and the evaluation of safety barrier performance. *Journal of Hazardous Materials*, 130(3), 220-233.

[25] Mokhtari, K., Ren, J., Roberts, C., Wang, J. (2011). Application of a generic Bow-Tie based risk analysis framework on risk management of sea ports and offshore terminals. *Journal of Hazardous Materials*, 192(2), 465-475.

[26] Preeda S., Min A. (2015). Development of Risk Assessment and Occupational Safety Management Model for Building Construction Projects. World Academy of Science. *Engineering and Technology International Journal of Civil and Environmental Engineering* Vol.9, No.9.

[27] Agarwal, H., Renaud, J. E., Preston, E. L., & Padmanabhan, D. (2004). Uncertainty quantification using evidence theory in multidisciplinary design optimization. *Reliability Engineering & System Safety*, 85(1-3), 281-294. doi:10.1016/j.ress.2004.03.017.

[28] Ayyub, B. M., & Klir, G. J. (2006). *Uncertainty modeling and analysis in engineering and the sciences.* Boca Raton, FL 33487-2742, US: Chapman & Hall.

[29] Wilcox, C.R., Ayyub, M.B. (2003). Uncertainty modeling of data and uncertainty propagation for risk studies. *IEEE Proceedings on Uncertainty Modeling and Analysis*, 184–191.

[30] Bae, H., Grandhi, R. V., & Canfield, R. A. (2004). An approximation approach for uncertainty quantification using evidence theory. *Reliability Engineering & System Safety*, 86(3), 215. doi:10.1016/j.ress.2004.01.011.

[31] Boudraa, A., Bentabet, A., Salzenstein, F., & Guillon, L. (2004). Dempster-Shafer's basic probability assignment based on fuzzy membership functions. *Electronic Letters on Computer Vision and Image Analysis*, 4(1), 1-10.

[32] Sentz, K., & Ferson, S. (2002). Combination of evidence in Dempster-Shafer theory. *Technical US Department of Energy*. Sandia National Laboratories.

[33] Gentile, M., Rogers, W. J., & Mannan, M. S. (2003). Development of an inherent safety index based on fuzzy logic. *Process Safety and Environmental Protection*, 81(6), 444-456.

[34] Markowski, A. S. (2006). Layer of protection analysis for the process industry. *Lodz: PAN, ISBN 83-86-492-36-8*.

[35] Salzano, E., & Cozzani, V. (2006). A fuzzy set analysis to estimate loss intensity following blast wave interaction with process equipment. *Journal of Loss Prevention in the Process Industries, 19, 343-*

352.

[36] Abrahamsson, M. (2002). *Uncertainty in Quantitative Risk Analysis—Characterization and Methods of Treatment. Department of Fire Safety Engineering.* Lund University, Sweden.

[37] Ferdous, R., Khan, F., Sadiq, R., Amyotte, P., Veitch, B. (2009). Methodology for computer aided fuzzy fault tree analysis. *Process Safety and Environment Protection*, 87(4), 217–226.

[38] Ferdous, R., Khan, F., Sadiq, R., Amyotte, P., Veitch, B. (2010). Fault and event tree analyses for process systems risk analysis: uncertainty handling formulations. *Risk Analysis: An International Journal*, 31(1), 86–107.

[39] Markowski, A., Sam Mannan, M., Kotynia, A. (Bigoszewska)., Siuta, D (2010). Uncertainty aspects in process safety analysis. *Journal of Loss Prevention in the Process Industries,* 23, 446-464.

[40] Ferdous, R., Khan, F., Sadiq, R., Amyotte, P., Veitch, B. (2011). Analyzing system safety and risks under uncertainty using a Bow-Tie diagram: an innovative approach. *Process Safety and Environmental Protection,* doi:10.1016/j.psep.2011.08.010.

[41] Tanaka, H., Fan, T.L., Lai, F.S., Toughi, K. (1983). Fault tree analysis by fuzzy probability. *IEEE Transactions on Reliability 32(5), 455–457.*

[42] Singer, D. (1990). A fuzzy approach to fault tree and reliability analysis. *Fuzzy Sets and Systems 34, 145–155.*

[43] Aqlan, F., Mustafa Ali, E. (2014). Integrating lean principles and fuzzy Bow-Tie analysis for risk assessment in chemical industry. Jou*rnal of Loss Prevention in the Process Industries*, *29, 39-48.*

[44] Markowski, A. S., Mannan, M. S., & Bigoszewska, A. (2009). Fuzzy logic for process safety analysis. *Journal of Loss Prevention in the Process Industries*, 22(6), 695-702. doi:10.1016/j.jlp.2008.11.011.

[45] Bhusnure, O. G., Dongare, R. B., Gholve, S. B., Giram, P. S. (2018). Chemical hazards and safety management in pharmaceutical industry. *Journal of Pharmacy Research,* Vol. 12, Issue 3.

[46] Gathuru, I.M., Buchanich, J., Marsh, G., Dolan, D. (2015). Health Hazards in the Pharmaceutical Industry. *Pharmaceutical Regulatory Affairs,* 4:3, DOI: 10.4172/2167-7689.1000145.

[47] Kumar, P., Shukla, J. (2010). Rısk Analysis and Risk Management In Pharmaceutıcal Industry. *Internatıonal Journal of Pharma World Research,* Vol. 1, Issue 1.

[48] Urushihara H, Kobashi G, Masuda H, Taneichi S, Yamamoto M, Nakayama T, Kawakami K, Matsuda T, Ohta K, Sugimori H. (2014). *Pharmaceutical company perspectives on current safety risk communications in Japan*. SpringerPlus, 3:51.

[49] Bhowmik, D., Durai Vel, S., Rajalakshmi A.N, Sampath Kumar, K. (2014). Recent Trends in Hazards in the Pharmaceutical Industry and Safety Precaution. *Elixir Pharmacy,* 69, 23688-23691.

[50] Patrick T.W., Guchelaar, H., Guchelaar, H. (2003). Risk assessment in clinical pharmacy. *Pharmacy World and Science*; 25(3), 98–103.

[51] Anthony P. Acfield and Dr. Robert A. Weaver (2012). Integrating Safety Management through the Bow-Tie Concept A move away from the Safety Case focus. *Australian System Safety Conferrence (ASSC 2012).*

[52] Shuang, C., Jinqiu, H., Laibin, Z. (2016). Risk analysis of refining equipment based on fuzzy theory and Bow-Tie model. *Proceedings of the 35th Chinese Control Conference July 27-29, 2016,* Chengdu, China.

[53] Zadeh, L.A. (1965). Fuzzy sets. *Information and Control,* 8, 339-353, 1965.

[54] Zadeh, L.A. (1978). Fuzzy sets as a basis for a theory of possibility. *Fuzzy sets and systems,* 1, 3-28.

[55] Lin, C., Wang, M.J. (1997). Hybrid fault tree analysis using fuzzy sets. *Reliability Engineering and System Safety,* 58, 205–213.

[56] Lee, K. (2005). *First Course on Fuzzy Theory and Applications*. Springer, ISBN 978-3-540-32366-2.

[57] L.X. Wang, (1997). *A Course in Fuzzy Systems and Control.* Prentice-Hall International Inc.

[58] Cheliyan, A.S., Bhattacharyya, S.K. (2018). Fuzzy fault tree analysis of oil and gas leakage in subsea production systems. *Journal of Ocean Engineering and Science,* 3(1), 38-48.

[59] Tyagi, S., Pandey D., Tyagi, R. (2010). Fuzzy set theoretic approach to fault tree analysis. *International Journal of Engineering, Science and Technology,* 2(5), 276-283.

[60] Sangaiah, A., Kumar, A., Thangavelu, A. (2013). An exploration of FMCDM approach for evaluating the outcome/success of GSD projects. *Central European Journal of Engineering,* 3(3), 419-435. DOI: 10.2478/s13531-012-0070-9.

[61] Tsenga, T., Konadaa , U., Kwon Y. (2016). A novel approach to predict surface roughness in machining operations using fuzzy set theory. *Journal of Computational Design and Engineering,* 3, 1–13.

***Sukran Seker** is Assistant Professor in the Department of Industrial Engineering at Yildiz Technical University. She received her Ph.D. degree in Department of Industrial Engineering from Yildiz Technical University. She has many research papers about Multi Criteria Decision Making under Uncertainty, Risk Analysis, and Production Management.*

An International Journal of Optimization and Control: Theories & Applications
ISSN:2146-0957 eISSN:2146-5703
Vol.9, No.2, pp.125-131 (2019)
http://doi.org/10.11121/ijocta.01.2019.00628

RESEARCH ARTICLE

Stability of delay differential equations in the sense of Ulam on unbounded intervals

Süleyman Öğrekçi

Department of Mathematics, Faculty of Arts and Science, Amasya University, Amasya, Turkey
suleyman.ogrekci@amasya.edu.tr

ARTICLE INFO

Article History:
Received 28 June 2018
Accepted 01 November 2018
Available 13 March 2019

Keywords:
Delay Differential equations
Stability theory
Hyers-Ulam-Rassias Stability
Fixed point theory
Generalized metric spaces

AMS Classification 2010:
34D20; 34D23

ABSTRACT

In this paper, we consider the stability problem of delay differential equations in the sense of Hyers-Ulam-Rassias. Recently this problem has been solved for bounded intervals, our result extends and improve the literature by obtaining stability in unbounded intervals. An illustrative example is also given to compare these results and visualize the improvement.

1. Introduction

In 1940, Ulam [1] raised the following stability problem of functional equations: Assume one has a function $f(t)$ which is very close to solve an equation. Is there an exact solution $h(t)$ which is relatively close to $f(t)$? More precisely, Ulam raised the question: Given a group G_1 and a metric group (G_2, ρ). Given $\varepsilon > 0$, does there exist a $\delta > 0$ such that if $f : G_1 \to G_2$ satisfies $\rho(f(xy), f(x)f(y)) < \delta$ for all $x, y \in G_1$, then a homomorphism $h : G_1 \to G_2$ exists with $\rho(f(x), h(x)) < k\varepsilon$ for all $x \in G_1$ and some $k > 0$? If the answer is affirmative, the equation $h(xy) = h(x)h(y)$ is called *stable* in the sense of Ulam. One year later, Hyers [2] gave an answer to this problem for linear functional equations on Banach spaces: Let G_1, G_2 be real Banach spaces and $\varepsilon > 0$. Then, for each mapping $f : G_1 \to G_2$ satisfying $\|f(x+y) - f(x) - f(y)\| \leq \varepsilon$ for all $x, y \in G_1$, there exists a unique additive mapping $g : G_1 \to G_2$ such that $\|f(x) - h(x)\| \leq \varepsilon$ holds for all $x \in G_1$. The above result of Hyers [2] was extended by Aoki [3] and Bourgin [4]. In 1978, Rassias [5] provided a remarkable generalization, which known as Hyers-Ulam-Rassias stability today, by considering the constant ε as a variable in Ulam's problem (see for example [3, 6–8]). After Hyers' answer, a new concept of stability for functional equations established, called today Hyers-Ulam stability, and is one of the central topics in mathematical analysis (see for example [9–12]).

The first result on Hyers-Ulam stability of differential equations was given by Obloza [13, 14]. Thereafter, in 1998, Alsina and Ger [15] investigated the Hyers-Ulam stability for the linear differential equation $y' = y$. They proved that if a differentiable function $y : I \to R$ satisfies

$$\left|y'(t) - y(t)\right| \leq \varepsilon$$

for all $t \in I$, then there exists a differentiable function $f : I \to R$ satisfying $f'(t) = f(t)$ for any $t \in I$ such that

$$|y(t) - f(t)| \leq 3\varepsilon$$

for all $t \in I$. Here, I is an open interval and $\varepsilon > 0$.

Furthermore, Miura et al. [16], Miura [17] and Takahasi et al. [18] generalized the above result of Alsina and Ger [15]. Indeed, they proved the Hyers-Ulam stability of the dynamic equation $y' = \lambda y$.

In 2004, Jung [19] obtained a similar result for the differential equation $\varphi(t)\, y = y$. More later, the result of the Hyers-Ulam stability for first-order linear differential equations has been generalized by Miura et al. [20], Takahasi et al. [21] and Jung [22]. They studied the nonhomogeneous linear differential equation of first-order

$$y' + p(t)\, y + q(t) = 0. \qquad (1)$$

In 2006, Jung [22] proved the Hyers-Ulam-Rassias stability of Eq. (1). Also, Jung [23] studied the generalized Hyers-Ulam stability of the differential equation of the form

$$ty'(t) + \alpha y(t) + \beta t^r x_0 = 0.$$

In 2008, Wang et al. [24] studied the first-order nonhomogeneous linear differential equation

$$p(t)\, y' - q(t)\, y - r(t) = 0. \qquad (2)$$

Using the method of the integral factor, they proved the Hyers-Ulam stability of Eq. (2) and extend the existing results. In 2008, Jung and Rassias [25] generalized the Hyers-Ulam stability of the Riccati equation of the form

$$y' + g(t)\, y + h(t)\, y^2 = k(t)$$

under the some additional conditions. In 2009 and 2010, Rus [26, 27] gave four types of Ulam stability: Ulam-Hyers stability, generalized Ulam-Hyers stability, Ulam-Hyers-Rassias stability and generalized Ulam-Hyers-Rassias stability for the ordinary differential equations

$$y' = f(t, y(t)) \qquad (3)$$

and

$$y'(t) = p(t) + f(t, y(t)),$$

respectively. Also, in 2010, by using the fixed point method and adopting the idea used in Cădariu and Radu [9], Jung [28] proved the Hyers-Ulam sability for Eq. (3) defined on a finite and closed interval, and he also investigated the Hyers-Ulam-Rassias for Eq. (3). In 2013, Li and Wang [29] obtained Hyers-Ulm-Rassias and Ulam-Hyers stability results for the following semilinear differential equations with impulses on a compact interval:

$$y'(t) = \lambda y(t) + f(t, y(t)).$$

In 2014, Qarawani [30] established the stability of linear and nonlinear differential equations of first-order in the sense of Hyers-Ulam-Rassia. Also, he investigated stability and asymptotic stability in the sense of Hyers-Ulam-Rassias for a Bernoulli's differential equation. Same year, Alqifiary [31] gave a necessary and sufficient condition in order that the first order linear system of differential equations

$$y'(t) + A(t)\, y(t) + B(t) = 0$$

has the Hyers-Ulam-Rassias stability and find Hyers-Ulam stability constant under those conditions. In 2017, Onitsuka and Shoji [32] studied the Hyers-Ulam stability of the first-order linear differential equation

$$y' - ay = 0, \qquad (4)$$

where a is a nonzero reel number. They find an explicit solution $y(t)$ of Eq. (4) satisfying $|\phi(t) - y(t)| \leq \varepsilon/|a|$ for all $t \in R$ under the assumption that a differential function $\phi(t)$ satisfies $|\phi'(t) - a\phi(t)| \leq \varepsilon$ for all $t \in R$.

Serious studies on the stability problem of differential equations have been started since 2000s. Stability has been investigated for the different classes of differential equations with different approaches. For example, delay differential equations are a special type of ordinary differential equations. To our knowledge, in 2010, the first mathematicians who investigated the stability of delay differential equations are Jung and J.Brzdek [33]. Motivated by the above mentioned outcomes on Hyers-Ulam stability, they investigated the Hyers-Ulam stability of $y'(t) = \lambda y(t-\tau)$ for $[-\tau, \infty)$ with an initial condition, where $\lambda > 0$ and $\tau > 0$ are real constants. Thereafter, Otrocol and Ilea [34] investigated Ulam-Hyers stability and generalized Ulam-Hyers-Rassias for the following functional differential equation

$$y'(t) = f(t, y(t), y(g(t))).$$

In 2015, by using the fixed point method, Tunç and Biçer [35] proved two new results on the Hyers-Ulam-Rassias and the Hyers-Ulam stability for the first-order delay differential equation

$$y'(t) = F(t, y(t), y(t - \tau)).$$

Recently, in the last two decades, the theory time scale and related dynamic equations have been systematically studied. To our knowledge, only in 2013, András and Mészáros [36] studied the Ulam-Hyers stability of some linear and nonlinear dynamic equations and integral equations on time scales. They used both direct and operational methods. In 2013, Shen [37] established the Ulam stability of the first-order linear dynamic equation

$$y^{\Delta} = p\,(t)\, y + f\,(t)$$

and its adjoint equation

$$x^{\Delta} = -p\,(t)\, x^{\sigma} + f\,(t)$$

on a finite interval in the time scale by using the integrating factor method. Same year, by using the idea of time scale Zada et al. [38] studied a relationship between the Hyers-Ulam stability and dichotomy of the first-order linear dynamic system

$$x^{\Delta} = Gx\,(t)\,.$$

In the last decade, there has been a significant development in the theory of fractional differential equations. We refer to the papers [39–43] for qualitative study of fractional equations, including stability theory.

2. Preliminaries

As it is outlined in Introduction section, stability problem of differential equations in the sense of Hyers-Ulam was initiated by the papers of Obloza [13,14]. Later Alsina and Ger [15] proved that, with assuming I is an open interval of reals, every differentiable mapping $y : I \to \mathbb{R}$ satisfying $|y'(x) - y(x)| \le \varepsilon$ for all $x \in I$ and for a given $\varepsilon > 0$, there exists a solution y_0 of the differential equation $y'(x) = y(x)$ such that $|y(x) - y_0(x)| \le 3\varepsilon$ for all $x \in I$. This result was later extended by Takahasi, Miura and Miyajima [18] to the equation $y'(x) = \lambda y(x)$ in Banach spaces, and [20, 44] to higher order linear differential equations with constant coefficients.

Recently Jung [28] proved Hyers-Ulam stability as well as Hyers-Ulam-Rassias stability of the equation

$$y' = f(t, y)$$

which extends the above mentioned results to nonlinear differential equations. Jung also shoved that some of his results are valid also on unbounded intervals. Jung's technique has been modified also for functional equations in the form

$$y'(t) = F\,(t, y(t), y(t - \tau)) \tag{5}$$

by Tun and Bier [35]. They obtained the following significant result for delay differential equations.

Theorem 1. *Let $I_0 := [t_0 - \tau, T]$ for given real numbers t_0, T and τ with $T > t_0$. Suppose that the continous function $F : I_0 \times \mathbb{R} \times \mathbb{R} \to \mathbb{R}$ satisfies the Lipschitz condition*

$$\begin{aligned} |F\,(t, x_1, y_1)\;\; F\,(t, x_2, y_2)| &\le L_1\,|x_1 - x_2| \\ &+ L_2\,|y_1 - y_2| \end{aligned}$$

for all $(t, x_1, y_1), (t, x_2, y_2) \in I_0 \times \mathbb{R} \times \mathbb{R}$ and some $L_1, L_2 > 0$. Suppose also that $\Psi : [t_0 - \tau, t_0] \to \mathbb{R}$ is a continuous function. Let $\varphi : I_0 \to \mathbb{R}$ be a continuous and nondecreasing function satisfying

$$\left| \int_{t_0}^{t} \varphi(s) \underset{\cdot}{s} \right| \le K\varphi(t) \tag{6}$$

for all $t \in I_0$ and some $K > 0$ satisfying $0 < K\,(L_1 + L_2) < 1$. If a continuous function $y : I_0 \to \mathbb{R}$ satisfies

$$\begin{cases} |y'(t) - F\,(t, y(t), y(t - \tau))| < \varphi(t), & t \in [t_0, T], \\ |y(t) - \Psi(t)| < \varphi(t), & t \in [t_0 - \tau, t_0], \end{cases}$$

then there exists a unique continuous function $y_0 : I_0 \to \mathbb{R}$ satisfying Eq.

$$\begin{cases} y_0'(t) = F\,(t, y_0(t), y_0(t - \tau))\,, & t \in [t_0, T], \\ y_0(t) = \Psi(t), & t \in [t_0 - \tau, t_0] \end{cases}$$

and

$$|y(t) - y_0(t)| \le \frac{K}{1 - K(L_1 + L_2)} \varphi(t)$$

for all $t \in I_0$ and any number L with $L > L_1 + L_2$.

In this paper, we will extend and improve these result by proving the stability results for delay differential equations for unbounded intervals. To achive stability results on unbounded intervals, we will use the inspiring techniques used in the above mentioned papers [7] and [35].

3. Main result

Before stating our main result, let us define the Ulam-Hyers-Rassias stability precisely for the differential equation (5).

For some $\varepsilon \geq 0$, $\Psi \in C[t_0 - \tau, t_0]$ and $t_0, T \in \mathbb{R}$ with $T > t_0$, assume that for any continous function $f : [t_0 - \tau, T] \to \mathbb{R}$ satisfying

$$\begin{cases} |f'(t) - F(t, f(t), f(t-\tau))| < \varepsilon, & t \in [t_0, T], \\ |f(t) - \Psi(t)| < \varepsilon, & t \in [t_0 - \tau, t_0]. \end{cases}$$

If there exists a continuous function $f_0 : [t_0 - \tau, T] \to \mathbb{R}$ satisfying

$$\begin{cases} f_0'(t) = F(t, f_0(t), f_0(t-\tau)), & t \in [t_0, T], \\ f_0(t) = \Psi(t), & t \in [t_0 - \tau, t_0] \end{cases}$$

and

$$|f(t) - f_0(t)| < K(\varepsilon), \quad t \in [t_0 - \tau, T],$$

where $K(\varepsilon)$ is an expression of ε only, we say that Eq. (5) has the Hyers-Ulam stability. If the above statement is also true when we replace ε and $K(\varepsilon)$ by φ and Φ, where $\varphi, \Phi \in C[t_0 - \tau, T]$ are functions not depending f and f_0 explicitly, then we say that Eq. (5) has the Hyers-Ulam-Rassias stability. These definitons may be applied to different classes of differential equations, we refer to Jung [28], Tun and Bier [35] and references cited therein for more detailed definitions of Hyers-Ulam stability and Hyers-Ulam-Rassias stability.

Our main result concerning the Ulam-Hyers-Rassias stability of delay differential equations on unbounded intervals reads as follows.

Theorem 2. *For a given real number t_0, let $I := [t_0 - \tau, \infty)$. Let K, L_1 and L_2 be positive constants with $0 < K(L_1 + L_2) < 1$. Assume that $F : I \times \mathbb{R} \times \mathbb{R} \to \mathbb{R}$ is a continuous function which satisfies the Lipschitz condition (6) for all $(t, x_1, y_1), (t, x_2, y_2) \in I \times \mathbb{R} \times \mathbb{R}$. If a continuously differentiable function $y : I \to \mathbb{R}$ satisfies,*

$$\begin{cases} |y'(t) - F(t, y(t), y(t-\tau))| < \varphi(t), & t \in [t_0, \infty), \\ |y(t) - \Psi(t)| < \varphi(t), & t \in [t_0 - \tau, t_0], \end{cases} \tag{7}$$

where $\varphi : I \to (0, \infty)$ is a continuous function satisfying the condition (6) for all $t \in I$, then there exists a unique continuous function $y_0 : I \to \mathbb{R}$ which satisfies

$$\begin{cases} y_0'(t) = F(t, y_0(t), y_0(t-\tau)), & t \in [t_0, \infty), \\ y_0(t) = \Psi(t), & t \in [t_0 - \tau, t_0] \end{cases} \tag{8}$$

and

$$|y(t) - y_0(t)| \leq \frac{K}{1 - K(L_1 + L_2)} \varphi(t) \tag{9}$$

for all $t \in I$.

Proof. For any $n \in \mathbb{N}$, define the sets $I_n := [t_0, t_0 + n]$. Then according to Theorem 1, for each n, there exists a unique continuous function $y_n : I_n \to \mathbb{R}$ such that

$$y_n(t) = y(t_0) + \int_{t_0}^{t} F(s, y_n(s), y_n(s-\tau))\, ș \tag{10}$$

and

$$|y(t) - y_n(t)| \leq \frac{K}{1 - K(L_1 + L_2)} \varphi(t) \tag{11}$$

for all $t \in I_n$. Keep in mind that $y(t) = y_0(t) = \Psi(t)$ for $t \in [t_0 - \tau, t_0]$. If $t \in I_n$, uniqueness of the functions y_n implies that

$$y_n(t) = y_{n+1}(t) = y_{n+2}(t) = \cdots. \tag{12}$$

Now, for any $t \in \mathbb{R}$, define the number $n(t) \in \mathbb{N}$ as

$$n(t) := \min\{n \in \mathbb{N} \,:\, t \in I_n\}.$$

Moreover, we define the function $y_0 : \mathbb{R} \to \mathbb{R}$ with

$$y_0(t) = y_{n(t)}(t) \tag{13}$$

and we claim that y_0 is continuous. To prove this, for arbitrary $t_1 \in \mathbb{R}$, we choose the integer $n_1 := n(t_1)$. Then n_1 belongs to interior of I_{n+1} and there exists an $\varepsilon > 0$ such that $y_0(t) = y_{n+1}(t)$ for all $t \in (t_1 - \varepsilon, t_1 + \varepsilon)$. Since y_{n+1} is continuous at t_1, so is y_0. That is, y_0 is continuous at t_1 for any $t_1 \in \mathbb{R}$.

Now, for arbitrary $t \in I$, we choose the number $n(t)$. Then, we have $t \in I_{n(t)}$ and it follows from (10) and (13) that

$$\begin{aligned} y_0(t) &= y_{n(t)}(t) \\ &= y(t_0) + \int_{t_0}^{t} F\left(s, y_{n(t)}(s), y_{n(t)}(s-\tau)\right) ș \\ &= y(t_0) + \int_{t_0}^{t} F(s, y_0(s), y_0(s-\tau))\, ș. \end{aligned} \tag{14}$$

Here, the last equality is valid because $n(s) \leq n(t)$ for any $s \in I_{n(t)}$ and it follows from (12) and (13) that

$$y_{n(t)}(t)(s) = y_{n(s)}(s) = y_0(s).$$

The equality (14) implies that the function y_0 satisfies the equations (8).

Now we will show that the function y_0 satisfies the inequality (9). Since $t \in I_{n(t)}$ for all $t \in I$, from (11) and (13), we have

$$\begin{aligned} |y(t) - y_0(t)| &= \left|y(t) - y_{n(t)}(t)\right| \\ &\leq \frac{K}{1 - K(L_1 + L_2)}\varphi(t) \end{aligned}$$

for all $t \in I_n$.

Finally, we will now show that the function y_0 is unique. Let $u_0 : I \to \mathbb{R}$ be another continuous function satisfies (8) and (9), with u_0 in place of y_0, for all $t \in I$. For arbitrary $t \in I$, the restrictions $y_0|_{I_{n(t)}}$ $\left(= y_{n(t)}\right)$ and $u_0|_{I_{n(t)}}$ both satisfy (8) and (9) for all $t \in I_{n(t)}$. Then, it follows from the uniqueness of $y_{n(t)} = y_0|_{I_{n(t)}}$ that

$$y_0(t) = y_0|_{I_{n(t)}} = u_0|_{I_{n(t)}} = u_0(t),$$

which completes the proof. $\square$

4. Example

Example 1. For any $\lambda_1, \lambda_2 > 0$, consider the following delay differential equation

$$y'(t) + \lambda_1 y(t) + \lambda_2 y(t - \tau) = q(t) \tag{15}$$

on the interval $I := [t_0 - \tau, \infty]$, where t_0 and τ are arbitrary real numbers. Since

$$F\left(t, y(t), y(t-\tau)\right) = y(t) + y(t-\tau) - q(t),$$

we have

$$\begin{aligned} |F\left(t, x_1, y_1\right) &- F\left(t, x_2, y_2\right)| \\ &= |\lambda_1 x_1 + \lambda_2 y_1 - q(t) \\ &\qquad -\lambda_1 x_2 - \lambda_2 y_2 + q(t)| \\ &= |\lambda_1 \left(x_1 - x_2\right) + \lambda_2 \left(y_1 - y_2\right)| \\ &\leq \lambda_1 \left|x_1 - x_2\right| + \lambda_2 \left|y_1 - y_2\right| \end{aligned}$$

for all $t \in I$. So all the conditions of Theorem 2 are satisfied and we obtain stability of the differential equation (15) in the sense of Hyers-Ulam.

Now, if we define the function $\varphi(t) := \mathrm{e}^{\lambda t}$ $(K > 0)$, we have

$$\begin{aligned} \left|\int_{t_0}^{t} \varphi(t)\d{s}\right| &= \int_0^t \mathrm{e}^{\lambda t}\d{s} \\ &= \frac{1}{\lambda}\left(\mathrm{e}^{\lambda t} - 1\right) \leq \frac{1}{\lambda}\mathrm{e}^{\lambda t} \\ &= \frac{1}{\lambda}\varphi(t) \end{aligned}$$

for all $t \in I$. Then, according to Theorem 2, the equation (1) is stable in the sense of Hyers-Ulam-Rassias.

It should be remarked that Theorem 2 guarantees the stability of (15) for any $T \leq \infty$, while the result of Tun and Bier [35] can guarantee stability in only a bounded subset of I. In this example, their result works only for $T < \infty$.

References

[1] Ulam, S.M. (1960) A Collection of Mathematical Problems. Interscience, New York.

[2] Hyers, D. (1941) On the stability of the linear functional equation. Proceedings of National Academy of Sciences of the United States of America, 27(4), 222–224.

[3] Aoki, T. (1951) On the stability of the linear transformations in banach spaces. Bulletin of the American Mathematical Society, 57(1), 223–237.

[4] Bourgin, T.G. (1950) Classes of transformations and bordering transformations. Journal of the Mathematical Society of Japan, 2(1), 64–66.

[5] Rassias, T. (1978) On the stability of linear mappings in Banach spaces. Proceedings of the American Mathematical Society, 72(1), 297–300.

[6] Popa, D. (2005) Hyers-Ulam-Rassias stability of a linear recurrence. Journal of Mathematical Analysis and Applications, 309(2), 591–597.

[7] Jung, S.M. (2001) Hyers-Ulam-Rassias Stability of Functional Equations in Mathematical Analysis. Hadronic Press, London.

[8] Rassias, T. (1953) Handbook of Functional Equations: Stability Theory. Springer, London.

[9] Cadariu, L., & Radu, V. (2008) Fixed point methods for the generalized stability of functional equations on a single variable. Fixed Point Theory and Applications, article ID749392, 15 pages.

[10] Forti, G.L. (2004) Comments on the core of the direct method for proving Hyers-Ulam stability of functional equations. Journal of Mathematical Analysis and Applications, 295(1), 127–133.

[11] Brzdek, J., Popa, D., & Xu, B. (2007) The Hyers-Ulam stability of nonlinear recurrences. Journal of Mathematical Analysis and Applications, 335(1), 443–449.

[12] Petru, T.P., Petruel, A., & Yao, Y.C. (2011) Ulam-Hyers stability for operatorial equations and inclusions via nonself operators.

Taiwanese Journal of Mathematics, 15(5), 2195–2212.

[13] Obloza, M. (1993) Hyers-Ulam stability of the linear differential equations. Rocznik Nauk-Dydakt Prace Matematik, 19(1), 259–270.

[14] Obloza, M. (1997) Connections between Hyers and Lyapunov stability of the ordinary differential equations. Rocznik Nauk-Dydakt Prace Matematik, 14(1), 141–146.

[15] Alsina, C., & Ger, R. (1998) On some inequalities and stability results related to the exponential function. Journal of Inequalities and Applications, 2(1), 373–380.

[16] Miura, T., Takahasi, S.E., & Choda, H. (2001) On the Hyers-Ulam stability of real continuous function valued differentiable map. Tokyo Journal of Mathematics, 24(2), 467–476.

[17] Miura, T. (2002) On the Hyers-Ulam stability of a differentiable map. Japanese Journal of Mathematics, 55(1), 17–24.

[18] Takahasi, S.H., Miura, T., & Miyajima, S. (2002) The Hyers-Ulam stability constants of first order linear differential operators. Bulletin of Korean Mathematical Society, 39(1), 309–315.

[19] Jung, S.M. (2004) Hyers-Ulam stability of linear differential equations of first order. Applied Mathematics Letters, 17(10), 1135–1140.

[20] Miura, T., Miyajima, S., & Takahasi, S.H. (2003) A characterization of Hyers-Ulam stability of first order linear differential operators. Journal of Mathematical Analysis and Applications, 286(1), 136–146.

[21] Takahasi, S.E., Takagi, H., Miura, T., & Miyajima, S. (2004) The Hyers-Ulam stability constants of first order linear differential operators. Journal of Mathematical Analysis and Applications, 296(2), 403–409.

[22] Jung, S.M. (2006) Hyers-Ulam stability of linear differential equations of first order. ii. Applied Mathematics Letters, 19(9), 854–858.

[23] Jung, S.M. (2005) Hyers-Ulam stability of linear differential equations of first order. iii. Applied Mathematics Letters, 18(2), 139–146.

[24] Wang, G., Zhou, M., & Sun, L. (2008) Hyers-Ulam stability of linear differential equations of first order. Applied Mathematics Letters, 21(10), 1024–1028.

[25] Jung, S.M., & Rassias, T.M. (2008) Generalized Hyers-Ulam stability of riccati differential equation. Mathematical Inequalities & Applications, 11(4), 777–782.

[26] Rus, I.A. (2009) Ulam stability of ordinary differential equations. Studia Universitatis Babe-Bolyai Mathematica, 54(4), 297–300.

[27] Rus, I.A. (2010) Ulam stabilities of ordinary differential equations in a Banach space. Carpathian Journal of Mathematics, 26(1), 103–107.

[28] Jung, S.M. (2010) A fixed point approach to the stability of differential equations $y' = f(x,y)$. Bulletin of the Malaysian Mathematical Sciences Society, 33(1), 47–56.

[29] Li, X & Wang, J. (2013) Ulam-Hyers-Rassias stability of semilinear differential equations with impulses. Electronic Journal of Differential Equations, 2013(172), 1–8.

[30] Qarawani, M.N. (2014) On Hyers-Ulam-Rassias stability for bernoulli's and first order linear and nonlinear differential equations. British Journal of Mathematics and Computer Science, 4(11), 1615–1628.

[31] Alqifiary, Q.H. (2014) Note on the stability for linear systems of differential equations. International Journal of Applied Mathematical Research, 3(1), 15–22.

[32] Onitsuka, M., & Shoji, T. (2017) Hyers-ulam stability of first-order homogeneous linear differential equations with a real-valued coefficient. Applied Mathematics Letters, 63(1), 102–108.

[33] Jung, S.M., & Brzdek, J. (2010) Hyers-Ulam stability of the delay equation $y'(t) = \lambda y(t-\tau)$. Abstract and Applied Analysis, 2010(3), 10 pages.

[34] Otrocol, D., & Ilea, V. (2013) Ulam stability for a delay differential equation. Central European Journal of Mathematics, 11(7), 1296–1303.

[35] Tun, C., & Bier, E. (2015) Hyers-Ulam-Rassias stability for a first order functional differential equation. Journal of Mathematical and Fundamental Sciences, 47(2), 143–153.

[36] András, S., & Mészáros, A.R. (2013) Ulam-Hyers stability of dynamic equations on time scales via Picard operators. Applied Mathematics and Computation, 219(4), 4853–4864.

[37] Shen, Y. (2017) The Ulam stability of first order linear dynamic equations on time scales. Results in Mathematics, Online first.

[38] Zada, A., Shah, S.O., Ismail, S., & Li, T. (2017) Hyers-Ulam stability in terms of dichotomy of first order linear dynamic system. Punjab University Journal of Mathematics, 49(3), 37-47.

[39] Trigeassou, J.C., Maamri, N., Sabatier, J., & Oustaloupa, A. (2011) A Lyapunov approach to the stability of fractional differential equations. Signal Processing, 91(3), 437–445.

[40] Li, C.P., & Zhang, F.R. (2011) A survey on the stability of fractional differential equations. The European Physical Journal Special Topics, 193(1), 27–47.

[41] Bayram, M,. Seer, A., & Adgzel, H. (2017) Oscillatory behavior of solutions of differential equations with fractional order. Applied Mathematics & Information Sciences, 11(3), 683–691.

[42] Bayram, M., Adgzel, H., & Seer, A. (2016) Oscillation criteria for nonlinear fractional differential equation with damping term. Open Physics, 14(1), 119–128.

[43] Seer, A., & Adgzel, H. (2016) Oscillation of solutions for a class of nonlinear fractional difference equations. The Journal of Nonlinear Science and Applications, 9(11), 5862–5869.

[44] Miura, T., Miyajima, S., & Takahasi, S.H. (2003) Hyers-Ulam stability of linear differential operator with constant coefficients. Mathematische Nachrichten, 258(2), 90–96.

Süleyman Öğrekçi *received the Ph.D degree in mathematics from Gazi University Instute of Science and Technology in 2014. He is currently working as assistant professor in the Department of Mathematics, Arts and Science Faculty, Amasya University, Amasya, Turkey. His current research interests include stability theory of dynamical systems, theory of fractional differential equations and scientific computing.*

An International Journal of Optimization and Control: Theories & Applications
ISSN: 2146-0957 eISSN: 2146-5703
Vol.9, No.2, pp.142-147 (2019)
https://doi.org/10.11121/ijocta.01.2019.00780

Evaluation of wind energy investment with artificial neural networks

Hasan Huseyin Yildirim [a], Mehmet Yavuz [b*]

[a] *Department of Banking and Finance, Balikesir University, Turkey*
[b] *Department of Mathematics-Computer, Necmettin Erbakan University, Turkey*
hhyildirim@balikesir.edu.tr, mehmetyavuz@erbakan.edu.tr

ARTICLE INFO

Article history:
Received: 31 January 2019
Accepted: 12 March 2019
Available Online: 17 March 2019

Keywords:
Energy
Wind energy
Forecasting
Energy investment evaluation
Artificial neural networks

AMS Classification 2010:
97R40, 97M30

ABSTRACT

Countries aiming for sustainability in economic growth and development ensure the reliability of energy supplies. For countries to provide their energy needs uninterruptedly, it is important for domestic and renewable energy sources to be utilised. For this reason, the supply of reliable and sustainable energy has become an important issue that concerns and occupies mankind. Of the renewable energy sources, wind energy is a clean, reliable and inexhaustible source of energy with low operating costs. Turkey is a rich nation in terms of wind energy potential. Forecasting of investment efficiency is an important issue before and during the investment period in wind energy investment process because of high investment costs. It is aimed to forecast the wind energy products monthly with multilayer neural network approach in this study. For this aim a feed forward back propagation neural network model has been established. As a set of data, wind speed values 48 months (January 2012-December 2015) have been used. The training data set occurs from 36 monthly wind speed values (January 2012-December 2014) and the test data set occurs from other values (January-December 2015). Analysis findings show that the trained Artificial Neural Networks (ANNs) have the ability of accurate prediction for the samples that are not used at training phase. The prediction errors for the wind energy plantation values are ranged between 0.00494-0.015035. Also the overall mean prediction error for this prediction is calculated as 0.004818 (0.48%). In general, we can say that ANNs be able to estimate the aspect of wind energy plant productions.

1. Introduction

Turkey is one of the developing countries, the economic change experienced in recent years has led to a rapid increase in demand in the energy sector, as it has in other sectors. While electricity production in Turkey showed an average annual increase of 3.6% between the years 1970 and 2000, electricity production increased annually by 8.9% on average between 2000 and 2017 years. In this regard, Turkey was one of the OECD countries in which energy demand increased the most rapidly. Electricity production in Turkey in 2017 increased by 5.6% to 294.8 GWh compared with the previous year. 37% of this production was obtained from natural gas, 33% was obtained from coal, 20% from hydraulic energy, 6% from wind energy, 2% from geothermal energy and 2% from other sources [1]. In 2017, approximately 70% of electricity production came from fossil sources, namely coal, liquid fuels and natural gas, while about 28% was obtained from renewable energy sources. Between the years 1996 and 2017, energy imports made up an average of 20% of total annual imports. When evaluating Turkey's energy situation, the high percentage of the required energy is provided by imports has a negative effect on the balance of payments in a national economic sense. If Turkey's energy needs were obtained from domestic sources instead of imported sources, the foreign trade deficit would be reduced by approximately 48%. Considering the overall picture of energy in Turkey in recent years, providing the required energy from domestic and renewable sources has become essential.

With regard to renewable energy potential, Turkey is a country with high potential for obtaining electricity production from wind and solar energy. According to the criteria specified, wind potential at a height of 50 metres on Turkey's wind atlas ranges from good to excellent, approaching 48 GW [2]. By July 2018, Turkey's wind-based energy capacity had reached 7 GW [3]. Turkey's wind-based power is about 15% of the energy potential that can be obtained from wind.

Within the scope of the 2015-2019 Strategic Plan

*Corresponding author

prepared by the Ministry of Energy and Natural Resources, based on the diversification of resources in energy consumption with continuous, sustainable, environmentally friendly, good quality, reliable and low-cost energy for final consumers, the greatest possible utilisation of domestic and renewable energy sources was included among the main aims. In the 2015-2019 Strategic Plan, in the area of Energy and Natural Resources, common development needs such as good governance and stakeholder interaction, regional and international activity, technological research, development and innovation, and improvement of the investment environment are emphasised, while in the Energy field, security of supply and energy efficiency and saving are given priority. Moreover, in the field of Natural Resources, the subjects of security of supply of raw materials and efficient and effective use of raw materials are given attention. The subject of sustainability, which is regarded as an indispensable approach in the process of acquiring energy and natural resources for the economy and of their consumption, is designed not as a separate theme, but as a framework which covers all the themes [4].

The use of domestic and renewable energy sources ensures diversification of resources within the energy portfolio, thereby allowing important progress to be made in reducing dependence on foreign energy sources and developing an environment that provides security of energy supply [5].

In evaluating a wind energy project in an economic sense, a project estimate of the installation costs must be made. In the technical evaluation of a WPP investment, the subjects in which there is insufficient knowledge and uncertainties regarding the WPP investment are factors such as when it will be completed, when the installation of the investment will begin, when the installation period of the investment will be completed, future changes in prices of materials to be used in the investment and how long the supply of the turbine from the manufacturer will take. Businesses have to make decisions under the existence of uncertainties like these. It is important for companies to make decisions that are as correct as possible and that will gain the most profit.

This study is aimed to forecast the wind energy products monthly with multilayer neural network approach. For this aim a feed forward back propagation neural network model has been established. As a set of data, wind speed values 48 months (January 2012-December 2015) have been used. The training data set occurs from 36 monthly wind speed values (January 2012-December 2014) and the test data set occurs from other values (January-December 2015).

2. Literature review

Wind power is the most common, widely applicable and productive renewable energy source. Studies about energy investments, wind speed predictions and renewable energy systems application with neural networks have been investigated especially about for a quarter century. In [6], Kalogirou et al. modeled the heat-up response of a solar steam generation plant and they were able to forecast pre-heat completion times within 3.9%. This is considered very adequate and thus the neural network can be used effectively for this type of predictions. In another work [7], Kalogirou et al. estimated successfully the performance of a parabolic trough collector steam generation system by using ANN. Kemmoku et al. [8] developed a multi-stage neural network with back-propagation and by using it they forecasted daily insolation of next day. They also compared the mean errors of the insolation forecast obtained by single-stage and multi-stage neural networks. The results showed that the mean error by the single-stage was about 30% while by the multi-stage it was about 20%. In [9], the authors developed a new Neural network model which helps to perform quickly and easily the estimations of office building energy consumption. Datta et al. [10] presented preliminary results on the estimation of electricity consumption with different independent input variables in a supermarket. Also they compared the prediction performance of one hidden layer-neural networks with the more traditional multiple regression techniques. Besides they founded the correlation coefficient as 0.95 with ANNs and 0.79 with the regression analysis. Dorvlo et al. [11] investigated a multilayer perceptron ANN model in order to estimate the solar radiation at any location in Oman. In other study [12], Aydinalp et al. developed a NN based energy consumption model for the Canadian residential sector. They presented the NN methodology used in developing the appliances, lighting, and space-cooling component of the model and the accuracy of its predictions. The study of More and Deo [13] employed the technique of neural networks in order to forecast daily, weekly as well as monthly wind speeds at two coastal locations in India. Öztopal [14] presented an artificial neural network (ANN) technique in order to determine weighting factors of surrounding stations necessary for the estimation of a pivot station. He compared the wind speed prediction results with measured values at a pivot station. Ermis et al. [15] developed a back-propagation feed forward ANN model in order to forecast world green energy consumption to the year 2050, and derived the consumption equations for different energy sources. Amrouche and Le Pivert [16] proposed a new neural network model for local forecasting of daily global solar radiation with satisfactory accuracy. Velazquez et al. [17] developed a new ANN model with back propagation by using Levenberg-Marquardt algorithm in order to determine influence of the input layer signals of ANNs on wind power estimation for a target site. They concluded from the study that the use of ANN models was helpful to estimate the wind energy potential of a site for which no long-term wind records are available. Zhao et al. [18] used in their ANN model the tan hyperbolic and sigmoid function and obtained that the error an average value of 16.47% in a whole month. The authors declared that the proposed system has a good wind power forecasting performance. Bigdeli et al. [19] showed that the hybrid ICA-neural network model is better than the others when prediction the wind power. Castellani et al. [20] obtained that the R2 between target test data and forecasted data is systematically higher using the pure NN approach. Qin et al. [21] demonstrated that the Cuckoo Search Optimization (CSO)-based Back Propagation Neural Network (BPNN) model can obtain higher quality interval forecasts for short-term wind speed forecasts. Wang et al. [22] presented a medium-term wind speed forecasting performance analysis for three different sites in the Xinjiang region of China, utilizing daily wind speed data collected over a period of eight years. The experimental results of their study suggested that the hybrid models forecast the daily wind velocities with a higher degree of accuracy over the prediction horizon compared to the other models. The studies on the application of artificial neural networks to the wind energy plant and renewable energy sources are not limited to these. Detailed information can be found in [23] for other studies in this regard.

3. Materials and methods

In this section of the study, the main method related in this study will be described briefly, including ANN model developed, the algorithm and the activation functions used.

3.1. Wind power plant information

For this analyses of a WPP investment that maintains its activity in Balıkesir province in the Southern Marmara region have been made by utilizing actual data. The data for thirty 3 MW wind turbines in the installed plants of the wind power company have been used in the study.

3.2. Application steps of research

Under this heading, explanations were made about the implementation steps of the research. The application steps of the research consist of two steps, step 1 and step 2, as shown in Figure 1.

Step 1: The distribution of wind speeds of each turbine was determined by using the arena input analyzer. Then monthly wind speeds for 2015 were estimated by the MiniTab program with reference to the distributions between 2012-2014 for each wind turbine.

Figure 2 shows the 36-month distribution results of one of the thirty turbines WTG01. Based on these results, wind turbines of WTG01 coded for 2015 were estimated with minitab program.

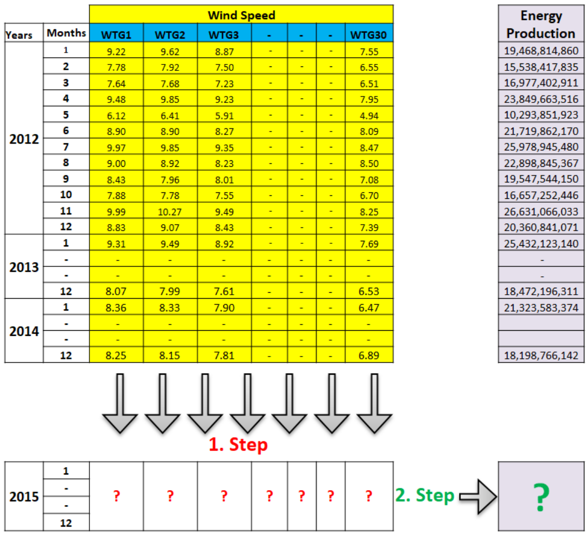

Years	Months	Wind Speed WTG1	WTG2	WTG3	-	-	-	WTG30	Energy Production
2012	1	9.22	9.62	8.87	-	-	-	7.55	19,468,814,860
	2	7.78	7.92	7.50	-	-	-	6.55	15,538,417,835
	3	7.64	7.68	7.23	-	-	-	6.51	16,977,402,911
	4	9.48	9.85	9.23	-	-	-	7.95	23,849,663,516
	5	6.12	6.41	5.91	-	-	-	4.94	10,293,851,923
	6	8.90	8.90	8.27	-	-	-	8.09	21,719,862,170
	7	9.97	9.85	9.35	-	-	-	8.47	25,978,945,480
	8	9.00	8.92	8.23	-	-	-	8.50	22,898,845,367
	9	8.43	7.96	8.01	-	-	-	7.08	19,547,544,150
	10	7.88	7.78	7.55	-	-	-	6.70	16,657,252,446
	11	9.99	10.27	9.49	-	-	-	8.25	26,631,066,033
	12	8.83	9.07	8.43	-	-	-	7.39	20,360,841,071
2013	1	9.31	9.49	8.92	-	-	-	7.69	25,432,123,140
	-	-	-	-	-	-	-	-	-
	-	-	-	-	-	-	-	-	-
	12	8.07	7.99	7.61	-	-	-	6.53	18,472,196,311
2014	1	8.36	8.33	7.90	-	-	-	6.47	21,323,583,374
	-	-	-	-	-	-	-	-	
	-	-	-	-	-	-	-	-	
	12	8.25	8.15	7.81	-	-	-	6.89	18,198,766,142

Figure 1. Research stages and framework

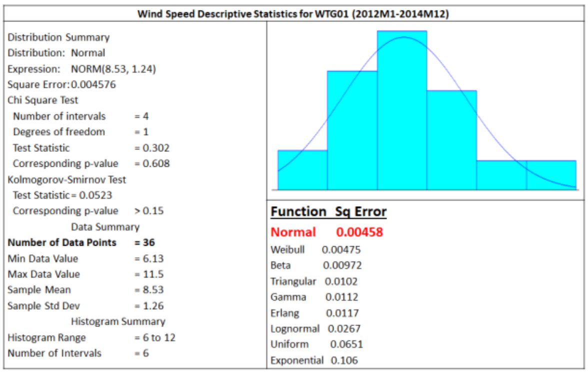

Figure 2. Arena input analyzer results of WTG1 coded turbine

Step 2: Artificial neural networks have been trained with production data realized in relation to wind speeds between 2012 and 2014. Monthly production for the year 2015 was estimated with reference to the trained network results.

3.3. Proposed neural network model

In this study it is aimed to forecast the wind energy products with multilayer neural network approach. For this aim a feed forward back propagation neural network model has been established. As a set of data, wind speed values 48 months (January 2012-December 2015) have been used.

The training data set occurs from 36 monthly wind speed values (January 2012-December 2015) and the test data set occurs from other values (January-December 2015). The topology of the neural network is composed of 1 input layer, 3 hidden layers and 1 output layer. The number of neurons located in each layer 15, 20, 25 and 1, respectively. The topology of the network used in this study is given in Figure 3 [24].

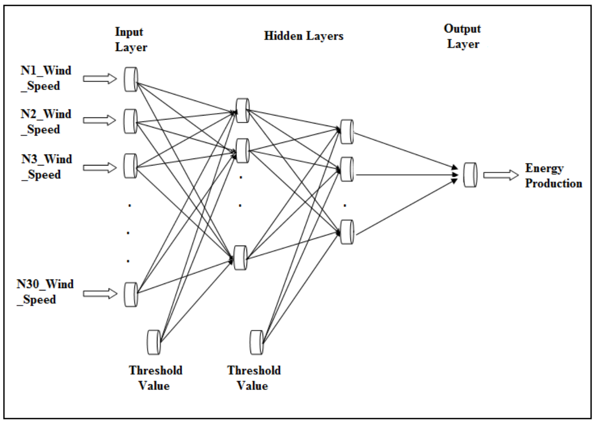

Figure 3. Network topology for the energy production prediction

In the layers purelin function, tangent hyperbolic function and tangent sigmoid function are used as activation function. The structures of purelin function and tangent hyperbolic function are presented in Figures 4(a) and 4(b).

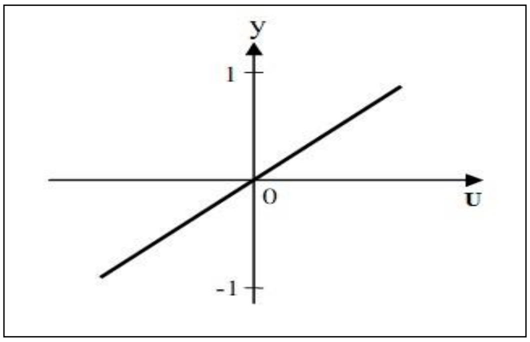

Figure 4(a). Purelin function

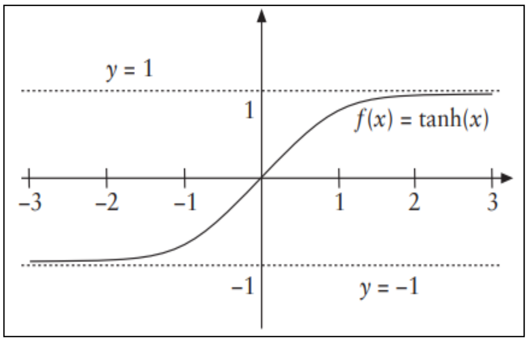

Figure 4(b). Tangent hyperbolic function

Purelin function can be defined in two different types such as $\omega_{1,2} = \sum_{i=1}^{n} x_i w_i \pm \theta$ and $y = f(\omega) = A\omega$, where A is constant, θ is the threshold value and ω is the sum of the net input. Tangent hyperbolic function can be represented as $y = \tanh(\omega) = \dfrac{e^{\omega} - e^{-\omega}}{e^{\omega} + e^{-\omega}}$ [25].

The training of the ANN is performed by using Microsoft Visual Studio C#.NET 2013. The normalized data, structure of ANNs used and mean square errors (mse) are presented for wind energy plantation prediction in Figure 5:

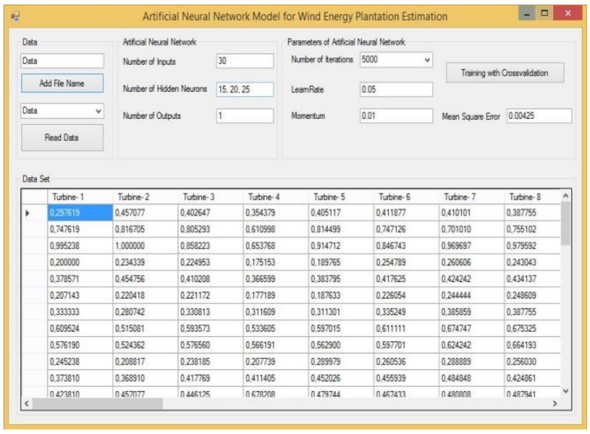

Figure 5. Structure of ANN used for wind energy plantation estimation

The pseudo-code for the given ANN is coded as [19]:

```
Define the input matrix as (P0) and calculate its transpose as (P)
Define the output matrix as (T0) and calculate its transpose as (T)
Determine the number of neurons of the input layer as (S0)
Determine the number of neurons of the hidden layers as (S1, S2, S3)
Determine the number of neurons of the output layer as (S4)
Construct the network topology and using the initialized weights between
  -1 and 1
start to training by using the given code below:
[Pn, minP, maxP, tn, minT, maxT] = premnmx (P,T);
[Net = newff(minmax(P), [S0, S1, S2, S3, S4], 'traingd'];
net.trainParam.epochs = …;
net.trainParam.goal = …;
net.trainParam.show = …;
net.trainParam.mc = …;
net.trainParam.lr = …;
net.trainParam.lr_inc = …;
net = train(net,P,T);
save training result.
```

4. Analysis findings and discussions

In this study the amount of energy produced between January 2012–December 2014 is used as the test values. Using the amount of energy production of 30 turbines, returns of these turbines are predicted with an ANN model that we developed. The test results are given in Table 1.

Table 1. Comparing the energy production values and ANN findings

Year	Months	(A) Amount of energy production (kw)	(B) Predicted value of energy with ANN	$(C = \lvert A - B \rvert / A)$ Absolute Error
2015	January	17629023301	17576045381	0.003005
	February	17582464880	17541452365	0.002333
	March	14995980995	15221447853	0.015035
	April	17609981947	17582614252	0.001554
	May	14169262992	14142598562	0.001882
	June	16036506273	15946251235	0.005628
	July	22976464967	22965124526	0.000494
	August	23972837201	24135689541	0.006793
	September	15211951424	15304523688	0.006085
	October	20874601700	20702569555	0.008241
	November	18726339588	18736258954	0.000530
	December	19920942346	20045258922	0.006240
			Mean Absolute Error	**0.004818**

The wind energy plantation prediction is performed for January 2012 and December 2014. The prediction errors between the observed values are given in (C) column in Table-3. When these error values are examined the overall error rate for a long time period is lower than 0.5%. These results show that the trained ANN has the ability of accurate prediction for the samples that is not used at training phase. The prediction errors for the wind energy plantation values are ranged between 0.000494-0.015035. Also the overall mean prediction error for this prediction is calculated as 0.004818 (0.48%). In general, we can say that ANNs be able to estimate the aspect of wind energy plantation.

5. Conclusion and recommendations

Countries aiming for sustainability in economic growth and development ensure the reliability of energy supplies. For countries to provide their energy needs uninterruptedly, it is important for domestic and renewable energy sources to be utilised. Turkey, which is one of the developing countries, is the world's 17th largest and Europe's 6th largest economy. Together with its growing economy and increasing population, demand for energy in Turkey is rising rapidly. To meet this increasing energy need and to reduce foreign dependence on energy, the use of domestic and renewable energy sources must be increased. From this perspective, realistic targets for renewable energy sources should be set, and to reach these targets, the barriers preventing investments should be lifted.

When its potential for renewable energy sources is assessed, Turkey is a rich country. Before companies make an investment in a renewable energy area, it is important that they undertake technical and economic feasibility studies of the investment. A pre-feasibility study will form a reference for the practicability of the investment. Following the pre-feasibility study, high-productivity renewable energy investments are important for providers of liability in terms of repayment of the credit they are to provide.

In this respect, it is very important to estimate the future energy generation for those who invest in wind energy. It is aimed to forecast the wind energy products monthly with multilayer neural network approach in this paper. For this aim a feed forward back propagation neural network model has been established. As a set of data, wind speed values 48 months (January 2012-December 2015) have been used. The training data set occurs from 36 monthly wind speed values (January 2012-December 2014) and the test data set occurs from other values (January-December 2015). Analysis findings show that the trained Artificial Neural Networks (ANNs) has the ability of accurate prediction for the samples that is not used at training phase. The prediction errors for the wind energy plantation values are ranged between 0.00494-0.015035. Also the overall mean prediction error for this prediction is calculated as 0.004818 (0.48%). In general, we can say that ANNs be able to estimate the aspect of wind energy plant productions.

The results obtained suggest that ANN model can be used quite successfully in this area and it can forecast correctly the value for wind power with an accuracy margin error even for unknown samples.

References

[1] http://www.enerji.gov.tr [Accessed 11 October 2018].

[2] Develi, A. & Kaynak, S. (2012). Energy Economics, Frankfurt am Main, ISBN 3631633335, DEU:Peter Lang AG.

[3] Turkish Wind Energy Association, Turkish Wind Statistic Report 2018 July, https://www.tureb.com.tr/yayinlar/turkiye-ruzgar-enerjisi-istatistik-raporu-temmuz-2018.

[4] Ministry of Energy and Natural Resources (2014). 2015-2019 Strategy Plan, http://sp.enerji.gov.tr/ETKB_2015_2019_Stratejik_Plani.pdf, 26.

[5] Bahgat, G. (2006). Europe's energy security: challanges and opportunities, *International Affairs*, 82(5), 961-975.

[6] Kalogirou, S.A., Neocleous, C.C., & Schizas, C.N. (1996). Artificial neural networks in modelling the heat-up response of a solar steam generation plant, *Proceedings of the International Conference EANN*, 1-4.

[7] Kalogirou, S.A., Neocleous, C.C., & Schizas, C.N. (1997). Artificial neural networks for the estimation of the performance of a parabolic trough collector steam generation system, *Proceedings of the International Conference EANN*, 227-232.

[8] Kemmoku, Y., Orita, S., Nakagawa, S., & Sakakibara, T. (1999). Daily insolation forecasting using a multi-stage neural network, *Solar Energy*, 66(3), 193-199.

[9] Kajl, S., Roberge, M.A., Lamarche, L., & Malinowski, P. (1997). Evaluation of building energy consumption based on fuzzy logic and neural networks applications, *Proceedings of the International Conference CLIMA 2000*, 264-274.

[10] Datta, D., Tassou, S.A., & Marriott, D. (2000). Application of neural networks for the prediction of the energy consumption in a supermarket, *Proceedings of the International Conference CLIMA 2000*, 98-107.

[11] Dorvlo, A.S., Jervase, J.A., & Al-Lawati, A. (2002). Solar radiation estimation using artificial neural networks, *Applied Energy*, 71(4), 307-319.

[12] Aydinalp, M., Ugursal, V.I., & Fung, A.S. (2002). Modeling of the Appliance, Lighting, and Space-Cooling Energy Consumptions in the Residential Sector Using Neural Networks, *Applied Energy*, 71(2), 87-110.

[13] More, A., & Deo M. (2003). Forecasting Wind with Neural Networks, *Marine Structures*, 16(1), 35-49.

[14] Öztopal, A. (2006). Artificial Neural Network Approach to Spatial Estimation of Wind Velocity Data, *Energy Conversion and Management*, 47(4), 395-406.

[15] Ermis, K., Midilli, A., Dincer, I., & Rosen, M.A. (2007). Artificial neural network analysis of world green energy use. *Energy Policy*, 35(3), 1731-1743.

[16] Amrouche, B., & Le Pivert, X. (2014). Artificial neural network based daily local forecasting for global solar radiation. *Applied Energy*, 130, 333-341.

[17] Velázquez, S., Carta, J. A., & Matías, J. M. (2011). Influence of the input layer signals of ANNs on wind power estimation for a target site: A case study. *Renewable and Sustainable Energy Reviews*, 15(3), 1556-1566.

[18] Zhao, P., Wang, J., Xia, J., Dai, Y., Sheng, Y., & Yue, J. (2012). Performance evaluation and accuracy enhancement of a day-ahead wind power forecasting system in China. *Renewable Energy*, 43, 234-241.

[19] Bigdeli, N., Afshar, K., Gazafroudi, A.S., & Ramandi, M.Y. (2013). A comparative study of optimal hybrid methods for wind power prediction in wind farm of Alberta, Canada. *Renewable and sustainable energy reviews*, 27, 20-29.

[20] Castellani, F., Burlando, M., Taghizadeh, S., Astolfi, D., & Piccioni, E. (2014). Wind energy forecast in complex sites with a hybrid neural network and CFD based method. *Energy Procedia*, 45, 188-197.

[21] Qin, S., Liu, F., Wang, J., & Song, Y. (2015). Interval forecasts of a novelty hybrid model for wind speeds. *Energy Reports*, 1, 8-16.

[22] Wang, J., Qin, S., Zhou, Q., & Jiang, H. (2015). Medium-term wind speeds forecasting utilizing hybrid models for three different sites in Xinjiang, China. *Renewable Energy*, 76, 91-101.

[23] Ata, R. (2015). Artificial Neural Networks Applications in Wind Energy Systems: A Review, *Renewable and Sustainable Energy Reviews*, 49, 534-562.

[24] Sakarya, S., Yavuz, M., Karaoglan, A.D., & Özdemir, N. (2015). Stock market index prediction with neural network during financial crises: a review on BIST-100. *Financial Risk and Management Reviews*, 1(2), 53-67.

[25] Yavuz, M., Sakarya, S., & Özdemir, N. (2015). Yapay Sinir Ağları ile Risk-Getiri Tahmini ve Portföy Analizi, *Ömer Halisdemir Üniversitesi İktisadi ve İdari Bilimler Fakültesi Dergisi*, 8(4), 87-107.

Hasan Huseyin Yildirim *received his Master's Degree (2011) in Finance from Marmara University and obtained a PhD Degree (2016) from Istanbul University. Mr. Yildirim is Assist. Prof. in the Burhaniye School of Applied Sciences at Balikesir University. His research interests include the economy, finance and banking sector and renewable energy investments.*

Mehmet Yavuz *is an Assistant Professor at the Department of Mathematics-Computer, Faculty of Science, Necmettin Erbakan University, Turkey. He received his B.Sc. (2009) degree from Department of Mathematics, Bulent Ecevit University, Turkey. He received his M.Sc. (2012) and Ph.D. (2016) degrees from Applied Mathematics, Balikesir University, Turkey. His research areas include fractional calculus, differential equations, artificial intelligence and financial mathematics.*

An International Journal of Optimization and Control: Theories & Applications
ISSN: 2146-0957 eISSN: 2146-5703
Vol.9, No.2, pp.148-153 (2019)
https://doi.org/10.11121/ijocta.01.2019.00602

RESEARCH ARTICLE

Hermite-Hadamard type inequalities for p-convex stochastic processes

Nurgul Okur [a] *, Imdat Iscan [b], Emine Yuksek Dizdar [c]

[a] *Department of Statistics, Giresun University, Turkey*
[b] *Department of Mathematics, Giresun University, Turkey*
[c] *Institute of Sciences, Giresun University, Turkey*
nrgokur@gmail.com, imdati@yahoo.com, eminee_yuksekk@hotmail.com

ARTICLE INFO

Article history:
Received: 10 April 2018
Accepted: 26 January 2019
Available Online: 19 March 2019

Keywords:
p-convexity
Stochastic process
Hermite-Hadamard type inequality
Mean-square integralibility

AMS Classification 2010:
37A50, 32F17

ABSTRACT

In this study are investigated p-convex stochastic processes which are extensions of convex stochastic processes. A suitable example is also given for this process. In addition, in this case a p-convex stochastic process is increasing or decreasing, the relation with convexity is revealed. The concept of inequality as convexity has an important place in literature, since it provides a broader setting to study the optimization and mathematical programming problems. Therefore, Hermite-Hadamard type inequalities for p-convex stochastic processes and some boundaries for these inequalities are obtained in present study. It is used the concept of mean-square integrability for stochastic processes to obtain the above mentioned results.

1. Introduction and preliminaries

The convexity for stochastic processes is of great importance in optimization, especially in optimal designs, and also useful for numerical approximations when there exist probabilistic quantities in the literature.

In 1980 Nikodem defined convex stochastic processes and gave some properties which are also known for classical convex functions. Some types of convex stochastic processes were introduced by Skowronski in 1992. In 2012 Kotrys obtained the classical Hermite-Hadamard inequality to convex stochastic processes. There are many studies in recent years on the above mentioned processes. A lot of definitions of various convexity and some new inequalities were for these stochastic processes in the literature [7-13].

The author's findings led to our motivation to build our work.The main goal is to introduce p-convex stochastic processes. Moreover, we prove Hermite-Hadamard type inequalities for p-convex stochastic processes and obtain some important results for these processes.

Let us show the definition of a stochhastic process:

Definition 1 ([5]). *The process $\{X(t): t \in I\}$ is a parameterized collection of random variables defined on a common probability space$(\Omega, \mathfrak{I}, P)$. Its parameter t is considered to be time. Then $X(t)$, which can also be shown as $X(t,\omega)$ for $\omega \in \Omega$, is considered to be state or position of the process at time t. For any fixed outcome ω of sample spaceΩ, the deterministic mapping $t \to X(t,\omega)$ denotes a realization, trajectory or sample path of the process. For any particular $t \in I$the mapping depends ω alone, i.e., then we obtain a random variable. It can be said that, $X(t,\omega)$ changes in time in a random manner. We restrict our attention to continuous time stochastic processes, i.e., index set is I: $[0,\infty)$.*

Definition 2 ([5]). *The process $X: I \subset \mathbb{R} \times \Omega \to \mathbb{R}$ is called convex stochastic process if*

$$X(\lambda u + (1-\lambda)v,\cdot) \leq \lambda X(u,\cdot) + (1-\lambda)X(v,\cdot) \text{ (a.e.)}$$

for all $u, v \in I, \lambda \in [0,1]$. If the above inequality is reversed, then $X(t,\cdot)$ is called concave.

Let us give some basic definitions:

Definition 3 ([5]). *The process $X: I \times \Omega \to \mathbb{R}$ is called*
(i) *continuous in probability in I if for all $t_0 \in I$ if*

$$P - \lim_{t \to t_o} X(t,\cdot) = X(t_0,\cdot)$$

where $P - \lim$ denotes limit in probability,

*Corresponding author

(ii) *mean-square continuous in I if for all $t_0 \in I$ if*

$$\lim_{t \to t_o} E[X(t,\cdot) - X(t_0,\cdot)]^2 = 0$$

where $E[X(t,\cdot)]$ denotes expectation value of the random variable $X(t,\cdot)$,

(iii) *increasing (decreasing) if for all $u, v \in I$ such that $u < v$ if*

$$X(u,\cdot) \le X(v,\cdot) \quad (X(u,\cdot) \ge X(v,\cdot)) \text{ (a.e.)},$$

(iv) *mean-square differentiable at a point $t \in I$ if there is random variable $X'(t,\cdot): I \times \Omega \to \mathbb{R}$ such that*

$$X'(t,\cdot) = P - \lim_{t \to t_o} \frac{X(t,\cdot) - X(t_0,\cdot)}{t - t_0}$$

The stochastic process $X: I \times \Omega \to \mathbb{R}$ is continuous (differentiable) if it is continuous (differentiable) at every point of interval I.

The concept "mean-square convergence" is used as the statement "almost everywhere" in this paper.

Definition 4 ([5]). *Let $X: I \times \Omega \to \mathbb{R}$ be Theprocess with $E[X(t)^2] < \infty$ and $u = t_0 < t_1 < \cdots < t_n = v$ be a partition of $[u, v] \subset I$, $\Theta_k \in [t_{k-1}, t_k]$, $k = 1, \dots, n$. A random variable $Y: \Omega \to \mathbb{R}$ is called mean-square integral of the process $X(t,\cdot)$ on $[u, v]$ if the following identity holds:*

$$\lim_{n \to \infty} E[\left(\sum_{k=1}^{n} X(\Theta_k) \cdot (t_k - t_{k-1}) - Y\right)^2] = 0.$$

Then we can write $\int_u^v X(t,\cdot)dt = Y(\cdot)$(a.e..).

For the existence of the mean-square integral it is enough to assume the mean-square continuity of the stochastic process X.

Now, we give the well-known Hermite-Hadamard integral inequality for convex stochastic processes:

Theorem 1 ([5]). *If $X: I \times \Omega \to \mathbb{R}$ is a Jensen-convex stochastic process and mean square continuous in the interval I, then we have almost everywhere*

$$X\left(\frac{u+v}{2},\cdot\right) \le \frac{1}{v-u} \int_u^v X(t,\cdot)dt \le \frac{X(u,\cdot) + X(v,\cdot)}{2}$$

for any $u, v \in I$, $u < v$.

Definition 5 ([7]). *Let $I \subset \mathbb{R}\backslash\{0\}$ be a real interval. The process $X: I \times \Omega \to \mathbb{R}$ is called a harmonically convex stochastic process, if the following inequality holds almost everywhere:*

$$X\left(\frac{uv}{\lambda u + (1-\lambda)v},\cdot\right) \le \lambda X(v,\cdot) + (1-\lambda)X(u,\cdot)$$

for all $u, v \in I$ and $\lambda \in [0,1]$. If the above inequality is reversed, then X is called a harmonically concave stochastic process.

Definition 6 ([13]). *Let I be a p-convex set. A function $f: I \to \mathbb{R}$ is called a p-convex function or belongs to the class $PC(I)$, if the following inequality holds:*

$$f\left([tx^p + (1-t)y^p]^{\frac{1}{p}}\right) \le tf(x) + (1-t)f(y)$$

for all $x, y \in I$ and $t \in [0,1]$.

Theorem 2 ([12]). *Let $f: I \subset (0,\infty) \to \mathbb{R}$ be a p-convex function. Iff $\in L[a,b]$, $a, b \in I$, $a < b$, then we have*

$$f\left(\left[\frac{a^p + b^p}{2}\right]^{\frac{1}{p}}\right) \le \frac{p}{b^p - a^p} \int_a^b \frac{f(x)}{x^{1-p}} dx \le \frac{f(a) + f(b)}{2}.$$

Remark 1 ([9]). *Let us define the following functions:*

(1) The Beta function:

$$\beta(x,y) = \frac{\Gamma(x)\Gamma(y)}{\Gamma(x+y)} = \int_0^1 \lambda^{x-1}(1-\lambda)^{y-1} d\lambda.$$

(2) The hypergeometric function $c > b > 0$; $|z| < 1$: :

$$ {}_2F_1(a, b; c; z) = \frac{1}{\beta(b, c-b)} \int_0^1 \lambda^{b-1}(1-\lambda)^{c-b-1}(1-z\lambda)^{-a} d\lambda.$$

2. Main results

The main subject of this paper is to adapt some well-known related results p-convex functions on p-convex stochastic processes. Also, we purpose to obtain Hermite-Hadamard type inequalities for p-convex stochastic processes.

Definition 7. *Let I be a p-convex set. The process $X: I \times \Omega \to \mathbb{R}$ is called a p-convex stochastic process, if the following inequality holds almost everywhere:*

$$X\left([\lambda u^p + (1-\lambda)v^p]^{\frac{1}{p}},\cdot\right) \le \lambda X(u,\cdot) + (1-\lambda)X(v,\cdot)$$

for all $u, v \in I$ and $\lambda \in [0,1]$.

Remark 2. *The interval I is called a p-convex set, if $[\lambda u^p + (1-\lambda)v^p]^{\frac{1}{p}} \in I$ for all $u, v \in I$ and $\lambda \in [0,1]$, where $p = 2k+1$ or, $p = \frac{n}{m} n = 2r+1$, $m = 2t+1$ and $k, r, t \in \mathbb{N}$.*

Remark 3. *If $I \subset (0,\infty)$ and $p \in \mathbb{R}\backslash\{0\}$, then $[\lambda u^p + (1-\lambda)v^p]^{\frac{1}{p}} \in I$ for all $u, v \in I$ and $\lambda \in [0,1]$.*

Thus, we can also define p-convex stochastic processes as follows:

Definition 8. *The process $X: I \times \Omega \to \mathbb{R}$ is called a p-convex stochastic process, if the following inequality holds almost everywhere:*

$$X\left([\lambda u^p + (1-\lambda)v^p]^{\frac{1}{p}},\cdot\right) \le \lambda X(u,\cdot) + (1-\lambda)X(v,\cdot) \quad (1)$$

for all $u, v \in I \subset (0,\infty)$, $\lambda \in [0,1]$, $p \in \mathbb{R}\backslash\{0\}$. If the inequality in Eq. (1) is reversed, then the process X is called p-concave.

According to Definition 8, it can be easily seen that for $p = 1$ or $p = -1$, a p-convex stochastic process reduces to convex and harmonically convex stochastic process on $I \subset (0,\infty)$, respectively.

Example 1. *Let $X: (0,\infty) \times \Omega \to \mathbb{R}$, $X(u,\cdot) = u^p$, $p \ne$*

0 and $Y:(0,\infty)\times\Omega\to\mathbb{R}$, $Y(u,\cdot)=c$, $c\in\mathbb{R}$, then X and Y are both p-convex and p-concave stochastic processes.

Lemma 1. *Let $X: I\subset(0,\infty)\times\Omega\to\mathbb{R}$ be a p-convex stochastic process and mean-square integrable on I°. Then the following equality holds almost everywhere:*

$$\frac{p}{v^p-u^p}\int_u^v \frac{X(t,\cdot)}{t^{1-p}}dt$$

$$=\frac{1}{v-u}\int_u^v X\left(\left[\frac{y-u}{v-u}v^p+\frac{v-y}{v-u}u^p\right]^{\frac{1}{p}},\cdot\right)dy$$

for all $u,v\in I$,$p\in\mathbb{R}\backslash\{0\}$.

Proof. Changing of $t^p=\frac{y-u}{v-u}v^p+\frac{v-y}{v-u}u^p$ in

$$\frac{p}{v^p-u^p}\int_u^v \frac{X(t,\cdot)}{t^{1-p}}dt,$$

then the proof of Lemma 1 is completed.

Theorem 3. *Let $X: I\subset(0,\infty)\times\Omega\to\mathbb{R}$ be a p-convex stochastic process. If $X$is mean-square integrable on $[u,v]$, then we have almost everywhere*

$$X\left(\left[\frac{u^p+v^p}{2}\right]^{\frac{1}{p}},\cdot\right)\leq\frac{p}{v^p-u^p}\int_u^v\frac{X(t,\cdot)}{t^{1-p}}dt\leq\frac{X(u,\cdot)+X(v,\cdot)}{2}$$

for all $u,v\in I$, $u<v$.

Proof. Changing of $\lambda=\frac{v-y}{v-u}$ in Eq. (1), we get

$$X\left(\left[\frac{v-y}{v-u}u^p+\frac{y-u}{v-u}v^p\right]^{\frac{1}{p}},\cdot\right)$$

$$\leq\left(\frac{v-y}{v-u}\right)X(u,\cdot)+\left(\frac{y-u}{v-u}\right)X(v,\cdot).$$

Integrating on $[u,v]$and using Lemma 1, we have

$$\frac{1}{v-u}\int_u^v X\left(\left[\frac{y-u}{v-u}v^p+\frac{v-y}{v-u}u^p\right]^{\frac{1}{p}},\cdot\right)dy$$

$$=\frac{p}{v^p-u^p}\int_u^v\frac{X(t,\cdot)}{t^{1-p}}dt\leq\frac{X(u,\cdot)+X(v,\cdot)}{2}.$$

Changing of $y=\frac{1}{2}(u+v)+t$ in Lemma 1, we obtain

$$\frac{p}{v^p-u^p}\int_u^v\frac{X(t,\cdot)}{t^{1-p}}dt$$

$$=\frac{1}{v-u}\int_{-\frac{1}{2}(v-u)}^{\frac{1}{2}(v-u)}X\left(\begin{bmatrix}\frac{1}{2}(u^p+v^p)\\+\frac{v^p-u^p}{v-u}t\end{bmatrix}^{\frac{1}{p}},\cdot\right)dt$$

$$\geq\frac{2}{v-u}\int_0^{\frac{1}{2}(v-u)}X\left(\left[\frac{1}{2}(u^p+v^p)\right]^{\frac{1}{p}},\cdot\right)dt$$

$$=X\left(\left[\frac{1}{2}(u^p+v^p)\right]^{\frac{1}{p}},\cdot\right)\ (a.e.).$$

Corollary 1. *If $X$is mean-square integrable on $[u,v]$, then we have almost everywhere*

$$X\left(\frac{2uv}{u+v},\cdot\right)\leq\frac{uv}{v-u}\int_u^v\frac{X(t,\cdot)}{t^2}dt\leq\frac{X(u,\cdot)+X(v,\cdot)}{2}.$$

Proof. In Theorem 3, if $p=-1$, then the proof of Corollary 1 is completed.

Lemma 2. *Let $X: I\subset(0,\infty)\times\Omega\to\mathbb{R}$ be a mean-square differentiable stochastic process on I°. If X' is mean-square integrable on $[u,v]$, then we have almost everywhere*

$$\frac{X(u,\cdot)+X(v,\cdot)}{2}-\frac{p}{v^p-u^p}\int_u^v\frac{X(t,\cdot)}{t^{1-p}}dt$$

$$=\frac{v^p-u^p}{2p}\int_0^1\begin{bmatrix}\frac{1-2\lambda}{[\lambda u^p+(1-\lambda)v^p]^{1-\frac{1}{p}}}\\ \times X'\left([\lambda u^p+(1-\lambda)v^p]^{\frac{1}{p}},\cdot\right)\end{bmatrix}d\lambda$$

for all $u,v\in I$,$p\in\mathbb{R}\backslash\{0\}$.

Proof. It suffices to show that

$$\int_0^1\begin{bmatrix}\frac{1-2\lambda}{[\lambda u^p+(1-\lambda)v^p]^{1-\frac{1}{p}}}\\ \times X'\left([\lambda u^p+(1-\lambda)v^p]^{\frac{1}{p}},\cdot\right)\end{bmatrix}d\lambda$$

$$=\frac{X(u,\cdot)+X(v,\cdot)}{v^p-u^p}-\frac{2p}{v^p-u^p}\int_0^1 X\left(\begin{bmatrix}\lambda u^p\\+(1-\lambda)v^p\end{bmatrix}^{\frac{1}{p}},\cdot\right)d\lambda$$

$$=\frac{X(u,\cdot)+X(v,\cdot)}{v^p-u^p}-\frac{2p^2}{(v^p-u^p)^2}\int_u^v\frac{X(t,\cdot)}{t^{1-p}}dt.$$

Multiplying by $\frac{v^p-u^p}{2p}$ both sides of above equality then the proof of Lemma 2 is completed.

Corollary 2. *If $X'$is mean-square integrable on $[u,v]$, then the following equality holds almost everywhere:*

$$\frac{X(u,\cdot)+X(v,\cdot)}{2}-\frac{1}{v-u}\int_u^v X(t,\cdot)dt$$

$$=\frac{v-u}{2}\int_0^1(1-2\lambda)X'\big((\lambda u+(1-\lambda)v),\cdot\big)d\lambda.$$

Proof. In Lemma 2, if we take $p=1$, then the proof of Corollary 2 is completed.

Corollary 3. *If $X'$is mean-square integrable on $[u,v]$, then almost everywhere*

$$\frac{X(u,\cdot)+X(v,\cdot)}{2}-\frac{uv}{v-u}\int_u^v\frac{X(t,\cdot)}{t^2}dt$$

$$=\frac{uv(v-u)}{2}\int_0^1\frac{1-2\lambda}{[\lambda v+(1-\lambda)u]^2}X'\left(\frac{uv}{\lambda v+(1-\lambda)u},\cdot\right)d\lambda$$

Proof. In Lemma 2, if we take $p=-1$, then the proof of Corollary 3 is completed.

Theorem 4. *Let $X: I\subset(0,\infty)\times\Omega\to\mathbb{R}$ be a differentiable stochastic process on I° and X' be mean-square integrable on $[u,v]$. If $|X'|^q$ is a p-convex stochastic process on $[u,v]$ for $q\geq 1$, then the following inequality holds almost everywhere:*

$$\left|\frac{X(u,\cdot)+X(v,\cdot)}{2}-\frac{p}{v^p-u^p}\int_u^v\frac{X(t,\cdot)}{t^{1-p}}dt\right|$$

$$\leq\frac{v^p-u^p}{2p}C_1^{1-\frac{1}{q}}\left[C_2|X'(u,\cdot)|^q+C_3|X'(v,\cdot)|^q\right]^{\frac{1}{q}}$$

for all $u, v \in I^\circ$, $u < v$, $p \in \mathbb{R}\backslash\{0\}$ *and where*

$$C_1 = C_1(u,v;p) = \frac{1}{4}\left(\frac{u^p+v^p}{2}\right)^{\frac{1}{p}-1} \times \left[\begin{array}{l} {}_2F_1\left(1-\frac{1}{p},2;3;\frac{u^p-v^p}{u^p+v^p}\right) \\ +{}_2F_1\left(1-\frac{1}{p},2;3;\frac{v^p-u^p}{u^p+v^p}\right)\end{array}\right],$$

$$C_2 = C_2(u,v;p) = \frac{1}{24}\left(\frac{u^p+v^p}{2}\right)^{\frac{1}{p}-1} \times \left[\begin{array}{l} {}_2F_1\left(1-\frac{1}{p},2;4;\frac{u^p-v^p}{u^p+v^p}\right) \\ +{}_2F_1\left(1-\frac{1}{p},2;4;\frac{v^p-u^p}{u^p+v^p}\right)\end{array}\right],$$

$$C_3 = C_3(u,v;p) = C_1 - C_2.$$

Proof. Using the power mean integral inequality and Lemma 2, then we have

$$\left|\frac{X(u,\cdot)+X(v,\cdot)}{2} - \frac{p}{v^p-u^p}\int_u^v \frac{X(t,\cdot)}{t^{1-p}}dt\right|$$

$$\leq \frac{v^p-u^p}{2p}\int_0^1 \left[\begin{array}{l}\left|\frac{1-2\lambda}{[\lambda u^p+(1-\lambda)v^p]^{1-\frac{1}{p}}}\right| \\ \times\left|X'\left([\lambda u^p+(1-\lambda)v^p]^{\frac{1}{p}},\cdot\right)\right|\end{array}\right]d\lambda$$

$$\leq \frac{v^p-u^p}{2p}\left(\int_0^1 \frac{|1-2\lambda|}{[\lambda u^p+(1-\lambda)v^p]^{1-\frac{1}{p}}}d\lambda\right)^{1-\frac{1}{q}}$$

$$\times\left(\int_0^1 \left[\begin{array}{l}\frac{|1-2\lambda|}{[\lambda u^p+(1-\lambda)v^p]^{1-\frac{1}{p}}} \\ \times\left|X'\left([\lambda u^p+(1-\lambda)v^p]^{\frac{1}{p}},\cdot\right)\right|^q\end{array}\right]d\lambda\right)^{\frac{1}{q}}.$$

Hence, using p-convexity of the stochastic process $|X'|^q$ on $[u,v]$, we have almost everywhere

$$\left|\frac{X(u,\cdot)+X(v,\cdot)}{2} - \frac{p}{v^p-u^p}\int_u^v \frac{X(t,\cdot)}{t^{1-p}}dt\right|$$

$$\leq \frac{v^p-u^p}{2p}\left(\int_0^1 \frac{|1-2\lambda|}{[\lambda u^p+(1-\lambda)v^p]^{1-\frac{1}{p}}}d\lambda\right)^{1-\frac{1}{q}}$$

$$\times\left(\int_0^1 \frac{|1-2\lambda||\lambda X'(u,\cdot)+(1-\lambda)X'(v,\cdot)|^q}{[\lambda u^p+(1-\lambda)v^p]^{1-\frac{1}{p}}}d\lambda\right)^{\frac{1}{q}}$$

$$\leq \frac{v^p-u^p}{2p}C_1^{1-\frac{1}{q}}\left[C_2\left|X'(u,\cdot)\right|^q + C_3\left|X'(v,\cdot)\right|^q\right]^{\frac{1}{q}},$$

where $\int_0^1 \frac{|1-2\lambda|}{[\lambda u^p+(1-\lambda)v^p]^{1-\frac{1}{p}}}d\lambda = C_1(u,v;p)$,

$$\int_0^1 \frac{|1-2\lambda|\lambda}{[\lambda u^p+(1-\lambda)v^p]^{1-\frac{1}{p}}}d\lambda = C_2(u,v;p),$$

$$\int_0^1 \frac{|1-2\lambda|(1-\lambda)}{[\lambda u^p+(1-\lambda)v^p]^{1-\frac{1}{p}}}d\lambda = C_1(u,v;p) - C_2(u,v;p).$$

Corollary 4. *If* $|X'|^q$ *is a p-convex stochastic process on* $[u,v]$, *then almost everywhere*

$$\left|\frac{X(u,\cdot)+X(v,\cdot)}{2} - \frac{p}{v^p-u^p}\int_u^v \frac{X(t,\cdot)}{t^{1-p}}dt\right| \leq \frac{v^p-u^p}{2p}\left[C_2\left|X'(u,\cdot)\right| + C_3\left|X'(v,\cdot)\right|\right],$$

where C_2 *and* C_3 *are defined as in Theorem 4.*

Proof. If $q = 1$ in Theorem 4, then the proof of Corollary 4 is completed.

Theorem 5. *Let* $X: I^\circ \subset \mathbb{R}\times\Omega \to \mathbb{R}$ *be a differentiable stochastic process on* I. *If* $|X'|$ *is a convex stochastic process on* $[u,v]$, *then the following inequality holds almost everywhere:*

$$\left|\frac{X(u,\cdot)+X(v,\cdot)}{2} - \frac{1}{v-u}\int_u^v X(t,\cdot)dt\right| \leq \frac{(v-u)\left(\left|X'(u,\cdot)\right| + \left|X'(v,\cdot)\right|\right)}{8}$$

for all $u, v \in I^\circ$, $u < v$.

Proof. If $p = 1$ in Corollary 4, then then the proof of Theorem 5 is completed.

Corollary 5. *If* $|X'|^q$ *is harmonically convex stochastic process on* $[u,v]$ *for* $q \geq 1$, *then almost everywhere*

$$\left|\frac{X(u,\cdot)+X(v,\cdot)}{2} - \frac{uv}{v-u}\int_u^v \frac{X(t,\cdot)}{t^2}dt\right| \leq \frac{uv(v-u)}{2}\lambda_1^{1-\frac{1}{q}}\left[\lambda_2\left|X'(u,\cdot)\right|^q + \lambda_3\left|X'(v,\cdot)\right|^q\right]^{\frac{1}{q}},$$

where $\lambda_1 = \frac{1}{uv} - \frac{2}{(v-u)^2}ln\left(\frac{(u+v)^2}{4uv}\right)$,

$$\lambda_2 = \frac{-1}{v(v-u)} + \frac{3u+v}{(v-u)^3}ln\left(\frac{(u+v)^2}{4uv}\right),$$

$$\lambda_2 = \frac{1}{u(v-u)} - \frac{3v+u}{(v-u)^3}ln\left(\frac{(u+v)^2}{4uv}\right) = \lambda_1 - \lambda_2.$$

Proof. If $p = -1$ in Theorem 4, then the proof of Corollary 5 is completed.

Theorem 6. *Let* $X: I \subset (0,\infty)\times\Omega \to \mathbb{R}$ *be a differentiable stochastic process on* I° *and mean-square integrable on* $[u,v]$. *If* $|X'|^q$ *is a p-convex stochastic process on* $[u,v]$ *for* $q > 1, \frac{1}{r}+\frac{1}{q} = 1$, *then almost everywhere*

$$\left|\frac{X(u,\cdot)+X(v,\cdot)}{2} - \frac{p}{v^p-u^p}\int_u^v \frac{X(t,\cdot)}{t^{1-p}}dt\right| \leq \frac{v^p-u^p}{2p}\left(\frac{1}{r+1}\right)^{\frac{1}{r}}\left[C_4\left|X'(u,\cdot)\right|^q + C_5\left|X'(v,\cdot)\right|^q\right]^{\frac{1}{q}} \quad (2)$$

for all $u, v \in I^\circ$, $u < v$, $p \in \mathbb{R}\backslash\{0\}$ *and where*

$$C_4 = C_4(u,v;p;q) = \begin{cases}\frac{1}{2u^{qp-q}}\ {}_2F_1\left(q-\frac{q}{p},1;3;1-\left(\frac{v}{u}\right)^p\right), & p<0, \\ \frac{1}{2v^{qp-q}}\ {}_2F_1\left(q-\frac{q}{p},2;3;1-\left(\frac{u}{v}\right)^p\right), & p>0\end{cases},$$

$$C_5 = C_5(u,v;p;q) =$$

$$\begin{cases} \frac{1}{2u^{qp-q}}\ {}_2F_1\left(q-\frac{q}{p},2;3;1-\left(\frac{v}{u}\right)^p\right),\ p<0, \\ \frac{1}{2v^{qp-q}}\ {}_2F_1\left(q-\frac{q}{p},1;3;1-\left(\frac{u}{v}\right)^p\right),\ p>0 \end{cases}.$$

Proof. Hölder's inequality, using p-convexity of the stochastic process $|X'|^q$on $[u,v]$ from Lemma 2

$$\left|\frac{X(u,\cdot)+X(v,\cdot)}{2}-\frac{p}{v^p-u^p}\int_u^v \frac{X(t,\cdot)}{t^{1-p}}dt\right|$$

$$\leq \frac{v^p-u^p}{2p}\left(\int_0^1 |1-2\lambda|^r d\lambda\right)^{\frac{1}{r}}$$

$$\times\left(\int_0^1\left[\frac{\left|X'\left([\lambda u^p+(1-\lambda)v^p]^{\frac{1}{p}},\cdot\right)\right|^q}{[\lambda u^p+(1-\lambda)v^p]^{q-\frac{q}{p}}}\right]d\lambda\right)^{\frac{1}{q}}$$

$$\leq \frac{v^p-u^p}{2p}\left(\frac{1}{r+1}\right)^{\frac{1}{r}}$$

$$\times\left(\int_0^1 \frac{\lambda|X'(u,\cdot)|^q+(1-\lambda)|X'(v,\cdot)|^q}{[\lambda u^p+(1-\lambda)v^p]^{q-\frac{q}{p}}}d\lambda\right)^{\frac{1}{q}},$$

where $\displaystyle\int_0^1 \frac{\lambda}{[\lambda u^p+(1-\lambda)v^p]^{q-\frac{q}{p}}}d\lambda$

$$=\begin{cases} \frac{1}{2u^{qp-q}}\ {}_2F_1\left(q-\frac{q}{p},1;3;1-\left(\frac{v}{u}\right)^p\right),\ p<0, \\ \frac{1}{2v^{qp-q}}\ {}_2F_1\left(q-\frac{q}{p},2;3;1-\left(\frac{u}{v}\right)^p\right),\ p>0 \end{cases}, \quad (3)$$

$$\int_0^1 \frac{1-\lambda}{[\lambda u^p+(1-\lambda)v^p]^{q-\frac{q}{p}}}d\lambda$$

$$=\begin{cases} \frac{1}{2u^{qp-q}}\ {}_2F_1\left(q-\frac{q}{p},2;3;1-\left(\frac{v}{u}\right)^p\right),\ p<0, \\ \frac{1}{2v^{qp-q}}\ {}_2F_1\left(q-\frac{q}{p},1;3;1-\left(\frac{u}{v}\right)^p\right),\ p>0 \end{cases} \quad (4).$$

Substituting Eq. (3) and (4) in Eq. (2), then the proof is completed.

Corollary 6. *If $|X'|^q$ is a convex stohastic process on $[u,v]$ then the following inequality holds:*

$$\left|\frac{X(u,\cdot)+X(v,\cdot)}{2}-\frac{1}{v-u}\int_u^v X(t,\cdot)dt\right|$$

$$\leq \frac{(v-u)}{2(p+1)^{\frac{1}{p}}}\left[\frac{|X'(u,\cdot)|^q+|X'(v,\cdot)|^q}{2}\right]^{\frac{1}{q}}, (\mathrm{a.e.})$$

where $\frac{1}{p}+\frac{1}{q}=1$.

Proof. In Theorem 6, if we take $p=1$, then the proof of Corollary 6 is completed.

Corollary 7. *If $|X'|^q$ is a harmonically convex stochastic process on $[u,v]$ for $q>1,\frac{1}{p}+\frac{1}{q}=1$, then*

$$\left|\frac{X(u,\cdot)+X(v,\cdot)}{2}-\frac{uv}{v-u}\int_u^v \frac{X(t,\cdot)}{t^2}dt\right|$$

$$\leq \frac{uv(v-u)}{2}\left(\frac{1}{p+1}\right)^{\frac{1}{p}}\left[\mu_1|X'(u,\cdot)|^q+\mu_2|X'(v,\cdot)|^q\right]^{\frac{1}{q}},$$

where $\mu_1=\dfrac{u^{2-2q}+v^{1-2q}[(v-u)(1-2q)-u]}{2(v-u)^2(1-q)(1-2q)}$,

$$\mu_2=\frac{v^{2-2q}-u^{1-2q}[(v-u)(1-2q)+v]}{2(v-u)^2(1-q)(1-2q)}.$$

Proof. In Theorem 6, if we take $p=-1$, then the proof of Corollary 7 is completed.

Theorem 7. *Let $X: I\subset(0,\infty)\times\Omega\to\mathbb{R}$ be a differentiable stochastic process on $I°$ and X'be mean-square integrable on $[u,v]$. If $|X'|^q$ is a p-convex stochastic process on $[u,v]$ for $q>1,\frac{1}{r}+\frac{1}{q}=1$, then*

$$\left|\frac{X(u,\cdot)+X(v,\cdot)}{2}-\frac{p}{v^p-u^p}\int_u^v \frac{X(t,\cdot)}{t^{1-p}}dt\right|$$

$$\leq \frac{v^p-u^p}{2p}C_6^{\frac{1}{r}}\left(\frac{1}{q+1}\right)^{\frac{1}{q}}\left[\frac{|X'(u,\cdot)|^q+|X'(v,\cdot)|^q}{2}\right]^{\frac{1}{q}} \quad (5)$$

for all $u,v\in I°$, $u<v$,$p\in\mathbb{R}\backslash\{0\}$and where

$$C_6=C_6(u,v;p;r)$$

$$=\begin{cases} \frac{1}{u^{rp-r}}\ {}_2F_1\left(r-\frac{r}{p},1;2;1-\left(\frac{v}{u}\right)^p\right),\ p<0, \\ \frac{1}{v^{rp-r}}\ {}_2F_1\left(r-\frac{r}{p},1;2;1-\left(\frac{u}{v}\right)^p\right),\ p>0 \end{cases}.$$

Proof. Using Hölder's inequality, p-convexity of the stochastic process $|X'|^q$on $[u,v]$ and Lemma 2

$$\left|\frac{X(u,\cdot)+X(v,\cdot)}{2}-\frac{p}{v^p-u^p}\int_u^v \frac{X(t,\cdot)}{t^{1-p}}dt\right|$$

$$\leq \frac{v^p-u^p}{2p}\left(\int_0^1 \frac{1}{[\lambda u^p+(1-\lambda)v^p]^{r-\frac{r}{p}}}d\lambda\right)^{\frac{1}{r}}$$

$$\times\left(\int_0^1 |1-2\lambda|^q\left|X'\left([\lambda u^p+(1-\lambda)v^p]^{\frac{1}{p}},\cdot\right)\right|^q d\lambda\right)^{\frac{1}{q}}$$

$$\leq \frac{v^p-u^p}{2p}C_6^{\frac{1}{r}}(u,v;p;r)\left(\frac{1}{q+1}\right)^{\frac{1}{q}}\times\left(\frac{|X'(u,\cdot)|^q+|X'(v,\cdot)|^q}{2}\right)^{\frac{1}{q}},$$

where $C_6(u,v;p;r)=\int_0^1 \frac{1}{[\lambda u^p+(1-\lambda)v^p]^{r-\frac{r}{p}}}d\lambda$

$$=\begin{cases} \frac{1}{u^{rp-r}}\ {}_2F_1\left(r-\frac{r}{p},1;2;1-\left(\frac{v}{u}\right)^p\right),\ p<0, \\ \frac{1}{v^{rp-r}}\ {}_2F_1\left(r-\frac{r}{p},1;2;1-\left(\frac{u}{v}\right)^p\right),\ p>0 \end{cases}, \quad (6)$$

$$\int_0^1|1-2\lambda|^q\lambda d\lambda=\int_0^1|1-2\lambda|^q(1-\lambda)d\lambda=\frac{1}{2(q+1)}. \quad (7)$$

Substituting Eq. (6) and (7) in Eq. (5), then the proof of Theorem 7 is completed.

3. Conclusion

In this paper, we considered an important extension of convexity for stochastic processes which is called p-convex stochastic processes and obtained new Hermite-Hadamard inequalities for these processes. In the future, new inequalities for the other convex stochastic processes can be obtained using similar methods in this study.

Acknowledgments

The author is very grateful to the referees for helpful comments and valuable suggestions.

References

[1] Nikodem, K. (1980). On convex stochastic processes. *Aequationes Mathematicae*, 20, 184-197.

[2] Shaked, M., & Shanthikumar, J.G. (1988). Stochastic convexity and its applications. *Advances in Applied Probability*, 20, 427-446.

[3] Skowronski, A. (1992). On some properties of J-convex stochastic processes. *Aequationes Mathematicae*, 44, 249-258.

[4] Skowronski, A. (1995). On Wright-convex stochastic processes. *Annales Mathematicae*, 9, 29-32.

[5] Kotrys, D. (2012). Hermite-Hadamard inequality for convex stochastic processes. *Aequationes Mathematicae*, 83, 143-151.

[6] Akdemir G. H., Okur B. N., Iscan, I. (2014). On Preinvexity for Stochastic Processes. *Statistics, Journal of the Turkish Statistical Association*, 7 (1), 15-22.

[7] Okur, N., İşcan, İ., Yüksek Dizdar, E. (2018). Hermite-Hadamard Type Inequalities for Harmonically Stochastic Processes, *International Journal of Economic and Administrative studies*, 11 (18. EYI Special Issue), 281-292.

[8] Tomar, M., Set, E., & Okur B., N. (2014). On Hermite-Hadamard-Type Inequalities for Strongly Log Convex Stochastic Processes. *The Journal of Global Engineering Studies*, 1(2), 53-61.

[9] İşcan, İ. (2016). Hermite-Hadamard inequalities for p-convex functions. *International Journal of Analysis and Applications*, 11 (2), 137-145.

[10] Okur B., N., Günay Akdemir, H., & İşcan, İ. (2016). *Some Extensions of Preinvexity for Stochastic Processes*, G.A. Anastassiou and O. Duman (eds.), Computational Analysis, pp. 259-270, Springer Proceedings in Mathematics & Statistics, Vol. 155, Springer, New York.

[11] Sarikaya, M. Z., Yaldiz, H. & Budak, H. (2016). Some integral inequalities for convex stochastic processes. *Acta Mathematica Universitatis Comenianae*, 85(1), 155–164.

[12] Fang, Z. B. & Shi, R. (2014). On the (p,h)-convex function and some integral inequalities. *Journal of Inequalities and Applications*, 2014:45.

[13] Zhang, K. S. & Wan, J. P. (2007). p-convex functions and their properties. *Pure and Applied Mathematics*, 23(1), 130-133.

[14] Noor, M. A., Noor, K. I., Mihai, M. V. & Awan, M. U. (2016). *Hermite-Hadamard ineq. for differentiable p-convex functions using hypergeometric functions*. Pub. De L'institut Math. Nouvelle série, tome 100(114), 251–257.

Nurgul Okur *is an assistant professor at the department of statistics in Giresun University. She studied for doctorate in applied mathematics. She has many research papers about the theory of inequalities for some convex stochastic processes.*

Imdat Iscan *is an associate professor at the department of mathematics in Giresun University. He studied for doctorate in analysis. He has many research papers about the theory of inequalities for convex functions and stochastic processes.*

Emine Yuksek Dizdar *graduated from the department of statistics in Giresun University. She studied of master in applied mathematics. She studies for doctorate in applied mathematics in Giresun University. Her research interests focus in inequality theory, especially Hermite-Hadamard type inequalities.*

An International Journal of Optimization and Control: Theories & Applications
ISSN: 2146-0957 eISSN: 2146-5703
Vol.9, No.2, pp.154-164 (2019)
https://doi.org/10.11121/ijocta.01.2019.00614

RESEARCH ARTICLE

Developing a package for analysis and design optimization of wind turbine systems

Ulas Eminoglu[a*], Ozan Karahan[b]

[a] Department of Electrical & Electronics Engineering, Gaziosmanpasa University, Turkey
[b] Department of Electricity and Energy, Samsun University, Turkey
ulas.eminoglu@gop.edu.tr, ozankarahan60@gmail.com

ARTICLE INFO

Article history:
Received: 17 May 2018
Accepted: 27 March 2019
Available Online: 29 April 2019

Keywords:
Energy cost
Design optimization
Graphical user interface
Modelling
Wind turbine system

AMS Classification 2010:
65K99, 68N99, 90C47, 90C29, 90B23, 90B56

ABSTRACT

The installation of wind turbines and consequently the use of wind energy is increasing day by day, since the rapid development in semiconductor technology has led to more advance in the wind turbine technologies. On the other hand, it is well known that a Graphical User Interface (GUI) application provides great advantages to the user such as; the use of programming language and data input for systems without coding, getting the results with the help of symbols, icons and other visual graphics. Accordingly, in this paper, to determine the amount of energy production, cost of energy and etc., of a Wind Turbine System (WTS) that has been established or will be installed, a tool is introduced by the presented software package. Besides the analysis option, the package also offers optimization algorithms that would be used for the layout design of types of Wind Turbine Systems which are called fixed-speed and variable-speed Wind Turbine Systems seperately by keeping in consideration the wind speed and geographic features of the regions. The graphical user interface, which is the one of important features of C# program were used and called Analysis & Design Optimization Package (A&DOP).

1. Introduction

User interface implementations are crucial in providing connectivity between the user and the software or command directories. Graphical User Interface (GUI) applications provide a great advantage to the user in terms of the usage of any programming language and access to information by means of input data, icons and other visual graphics for systems without coding [1]. Accordingly, several number of tools have been developed and published on the modeling and/or simulation for different areas of electrical power systems such as; voltage stability analysis and distributed generation allocation in distribution systems [2], designing DC motor control systems [3], the simulation and control of wind turbines [4], performance estimating tool for transmission lines [5], analyses and design tools for WTS [6-9] and etc. in the literature. Although modelling and design optimization problems for WTSs are being analysed by using a number of programs i.e., developed in [6-9], these programs commonly used classical power computation model (fundamental equations of wind power) that requires determination of rotor efficiency (power coefficient) for WTSs. The determination of power coefficient for a wind turbine requires a field test with the knowledge of aerodynamic design parameters or actual power curve provided by the manufacturers. In these programs, consequently, special requirements of wind turbines, especially variable type, are not well treated.

In recent years, the increase in energy demand and government support has led to a significant increase in the use of wind turbine systems (WTS) in energy production [10]. Therefore, in order to lower the costs and the investments for the operation in a WTS, a great number of theoretical and practical applications in terms of power output controlling [11], power curve modeling and optimal designing of WTSs have been presented in the literature, i.e. [12-18]. Optimal designing of a WTS reduces the energy costs to the minimum level and/or to produce maximum amount of energy. Most of these studies were carried out by utilizing an optimization algorithm in order to obtain highest energy production with the lowest possible cost by considering the wind potential in the region.

*Corresponding author

Mathematical methods for computation of rotor power coefficient, resulting of power output [14] and modelling of power curve with respect to wind speed [13, 16-18] were also presented in these studies. Furthermore, there are some studies in the literature [19-23] which mainly focused on the reliability analyses of these mathematical methods developed for characterization of output power for WTSs.

It has been emphasized that the usage of a powerful method for characterizing the power curve for a WTS is an important task for the determining the amount of energy produced and its cost, accurately, results in determining the optimum size/value of design parameters [20]. Additionally, the size of components such as; generator, blades (rotor radius) and tower must be compatible. And, wind characteristic of the site has to be undertaken into design process to get high efficiencies in electrical energy production with lower cost [12-18]. The paper presents a package developed for power and energy cost analyses, and design optimization procedure that implements the life cycle cost model [12] with a powerful power curve method presented in [22]. The package was designed using C# [23] and it is executables to be run on a personal computer even without using any program. The package also facilitates analyzing and design optimization of fixed type of WTSs implementing our output power computation model proposed in [14]. Additionally, new mathematical formulations between the value of rated power, the size of tower and blades for a WTS are defined and used as a constraint for the purpose of increasing the reliability and the computational efficiency. Results clearly indicate that the package enables user to perform power and energy cost analyses, and design optimization to determine optimal size/value of design parameters yielding minimum cost of energy for both types of WTSs, accurately. Organization of the proposed paper can be listed as: output power and energy models for wind turbines are given in Section 2. Section 3 starts with relations between design parameters for WTSs, and a brief description of the package and its validation are then given in the same section. Section 4 relates with the conclusions.

2. Power and energy calculation for WTS

2.1 Output power calculation

A WTS is an electromechanical system and it converts the kinetic energy to the mechanical energy firstly, and then to the electrical energy through a generator. In this system, the power transmitted to the rotor shaft is described as given in following equations [6].

$$P_m = \frac{1}{2}\rho A u^3 C_p(\lambda, v) \tag{1-a}$$

$$C_p(\lambda, v) = c_1\left(c_2\frac{1}{\Lambda} - c_3 v - c_4 v^x - c_5\right)e^{\left(\frac{-c_6}{\Lambda}\right)} \tag{1-b}$$

$$\frac{1}{\Lambda} = \frac{1}{\lambda + 0.08v} - \frac{0.035}{1+v^3} \tag{1-c}$$

$$\lambda = \frac{R w_r}{u} \tag{1-d}$$

where, R and ρ stands for the rotor radius and the air density, respectively, and A is the swept area of a blade, v is the pitch angle, u shows wind speed, w_r represents the rotor angular velocity in rad/s [6]. Rotor efficiency is denoted by $C_p(\lambda, v)$. Occasionally, it is based on the aerodynamic parameters of blades (c_1 - c_6 and x), blade angle and the rotor tip-speed ratio (λ) and called power coefficient. Its maximum value is smaller than Betz limit which is the theoretical maximum value determined as 0.593 [10]. The usage of this type of methods based on the power coefficient is cumbersome to use. This is due to the fact that the determination of maximum power coefficient (rotor efficiency) is difficult, since its value varies with the blade angle and tip-speed ratio which depends on variable wind speed, as can be seen in Eq. (1). It requires a field test with the complex aerodynamic knowledge of design parameters provided by manufacturers, if the actual power curve of that WTS is not available. In some cases, accordingly, the value of power coefficient is taken as its maximum value (C_{p_max}) or constant equivalent values ($C_{p,eq}$) for all steady wind speed which is called approximate power curve model [19].

Wind turbine systems have two types of power generations, namely fixed- and variable-speed. The first type of WTS whose speed is fixed has generally operated with stall principle to keep rotor speed at constant. Even though, variable-speed WTSs is the most favorite type of the WTSs in recent years, the installed capacity of the WTSs is commonly based on the fixed-speed induction generator. Therefore, power curve modeling and analysis of this type of WTS is still an important task. For this reason, we have developed a mathematical method to estimate rotor efficiency in [14] for power curve characterization in both analyses and design optimization studies. The model has been developed by using Weibull probability function. The mathematical expression for the model is as follow:

$$C_p(u) = \frac{C_{p\_max}}{w_m}\left(\frac{u}{u_{ci}} - 1\right)\left(\frac{k}{c}\right)\left(\frac{u}{c}\right)^{k-1} exp\left[-\left(\frac{u}{c}\right)^k\right] \tag{2}$$

Here, C_{p_max} represents the maximum value of rotor efficiency, which depends on the λ_{opt} as:

$$C_{p\_max} = 0.59\left(\frac{\lambda_{opt}\, p^{0.67}}{1.48 + \lambda_{opt}(p^{0.67} - 0.04) + 0.0025\,\lambda_{opt}^{\;2}} - \frac{1.92\lambda_{opt}^{\;2}\, p}{1 + 2\lambda_{opt}\, p}\frac{C_d}{C_L}\right) \tag{3}$$

where, C_l/C_d stands for the lift-to-drag ratio, u_{ci} denotes cut in wind speed, and p is the number of blades [13].

The parameter k, c and w_m are computed with respect to design wind speed (u_{des}) for which rotor efficiency is in maximum. The model validation and the value of coefficients for these parameters are given in [14], in detail.

The second type is called variable-speed WTS. Although a fixed-speed WTS is more efficient when a single wind speed is considered, adjusting the rotor speed to wind speed is the ability of variable-speed wind turbine. As a result, it can operate in the maximum level in almost every time [11]. In order to predict the performance of this type of WTSs, various methods have been developed to calculate the output power depending on the wind speed as reviewed in [19]-[21]. These methods have been evolved by taking into account the change in power curve, and are simpler to use. Accordingly, a functional method was also developed to compute the output power for variable-speed WTSs in [22]. The method is based on the capacitor charging voltage equation and characterizes the whole power curve even without knowledge of manufacturers' data. The mathematical formulation of the model is given in following equations.

$$P = P_{rated}(1-e^{-\left(\frac{u}{a}\right)^{b}}) \tag{4-a}$$

$$a = 0.70335986 \ x\, u_r - 0.00049995 \tag{4-b}$$

where, u is the steady wind speed in m/s and P_{rated} denotes the generator rating in kW and b is a constant, $b=5$. The method has great advantages comparing to the classical computation method and other approximate methods considered in comparison in terms of number of parameters, and the necessity of the rotor efficiency or actual power provided by the manufacturers [22].

2.2 Energy model for WTSs

In order to characterize the wind potential for any site, the probability function called Weibull distribution is used commonly in the literature [12]-[17], [20]. It is characterized by two parameters as given in following equation.

$$W(u) = \left(\frac{k}{c}\right)\left(\frac{u}{c}\right)^{k-1} exp\left[-\left(\frac{u}{c}\right)^{k}\right] \tag{5}$$

Here, u represents the steady wind speed, k and c denotes the shape and scale parameter, respectively, and is defined in terms of height and ground surface friction [12-17]. For a WTS, the Annual Energy Production (AEP) is necessary for determination of energy cost, and it is computed by using the annual mean power of the WTS. The value of mean power for a WTS is determined depending on the turbines' power output and probability density function of wind speed (Generally Weibull distribution) as follow:

$$P_o(u_o) = \int_{u_{min}}^{u_{max}} P(u)W(u)du \tag{6}$$

Here, the wind speed varies between cut-in and cut-out wind speed of the WTS, (u_{min} and u_{max}), respectively [12]. It is used for determination of turbine capacity factor and the amount of energy produced. Capacity factor (C_f) is an important performance parameter in terms of energy efficiency, and defined as given in below.

$$C_f = \frac{P_o(u_o)}{P_{rated}} \tag{7}$$

It is used for determining Annual Energy Production (AEP). The AEP is the quantity of annual total energy generated by a WTS. It is used for determining the cost of energy and evaluation the performance of wind turbines for different wind conditions, and defined as:

$$AEP = 8760 \times P_o(u_o) \times \mu \times Availability\,\% \tag{8-a}$$

$$AEP = 8760 \times P_{rated} \times C_f \times \mu \times Availability\,\% \tag{8-b}$$

where, μ denotes the efficiency of the turbine including soiling and array losses, the number 8760 refers to the annual hours and the Availability% is the annual operating hours of a WTS in percentage [12]. For estimating the cost of *kWh*, the Cost of Energy Model (CEO) model reported by National Renewable Energy Laboratory (NREL) in [12] is commonly used in studies dealing with the optimization of the design and analysis [12, 14, 16-18]. In this model, the cost of energy is defined as given in below.

$$COE = \frac{FCR \times ICC + AOE}{AEP} \tag{9}$$

where, *ICC* denotes initial investment cost (*$*), *FCR* stands for fixed charge rate for one year. *AOE* stands for the operating expenses for one year ($/year). The model consists of all components of WTSs, namely rotor, drive train, tower, land lease and etc., and is detailed in [12].

3. Design methodology and software descriptios

3.1 Design methodology for WTS

In order to configure of a WTS with the ideal size/value of design parameters, the size/value of these parameters has to be optimized undertaking the wind potential of the region into the design process. For this purpose, design optimization algorithms have been developed for both fixed- and variable-speed WTS. In these algorithms, Particle Swarm Optimization (PSO) method [24] and Differential Evolution Algorithm (DEA) [25] are utilized, since they need less user input, easy and simple to use. Additionally, they are effective for obtaining the best solution for every kind of optimization problems by converging and commonly used for this type of problems [14], [16]-[17]. The algorithm developed for designing of variable-speed WTSs optimizes the size of the rotor, the tower height, the generator rating, and the value of the rated wind speed. It also determines the value of capacity factor for optimized wind turbine depending on the wind potential of a given site. The cost of energy in $/kWh is taken as the objective function. The algorithm can be summarized as follows. The rotor radius and the rated wind speed are chosen as independent parameters for the optimized WTS. The optimized parameters and their limits are given in Table 1. As given in table, the rated wind speed and the hub height are arbitrarily selected in the range of their lower and upper bounds. The rotor radius is then computed with respect to h. Using computed R_{min} and R_{max}, a range is defined and the value of R is arbitrarily selected from this range for each value of h. Similar to the computation of R, for each value of R and u_r, the range of rated power is defined for random value of $C_{p\text{-}max}$ between 0.3 and 0.4 which is defined by observing a number of practical wind turbine data collected from product brochures and company website. Rated power, P_r, is then arbitrarily selected from that range. The value of capacity factor is determined numerically by utilizing power curve model given in Eq. (4) and Weibull distribution at the selected hub height and u_r as given in following equation.

$$C_f = \frac{P_o(u_o)}{P_r} = \int_{u_{ci}}^{u_{co}} \left(1 - e^{-\left(\frac{u}{0.70335986\ x\, u_r - 0.00049995}\right)^5}\right) x \left(\frac{k}{c}\right)\left(\frac{u}{c}\right)^{k-1} exp\left[-\left(\frac{u}{c}\right)^k\right] du \tag{10}$$

Where, k and c parameters are determined using selected hub height (h), surface friction coefficient and Weibull's parameters (k_o and c_o) or mean wind speed and standard deviation at the reference height (h_o) for the region. It is repeated to create candidate solution sets for the design parameters (h, u_r, R, P_r, C_f), the amount of energy which will be produced by the WTS and the cost of energy are then computed for each set by using Eq. (8) and Eq. (9), respectively. The selection and mutation process are then performed with PSO [24] and DEA [25] algorithms and it is repeated until maximum number of iterations is met. It must be stated that At last, the solution set which has the lowest cost of energy is identified as the best (optimum) solution. It must be stated that The geographical features (altitude and mean temperature) are used for determining the value of air density which is used for computation of rated power (P_r).

Table 1. Design parameters and their range for variable-speed WTs

Design Parameters		Its range	Step
Independent Parameters	Hub height (h)	h_{min}-h_{max} (input parameters) 20-100 (m)	DEA-PSO
	Rated wind speed (u_r)	u_{r_min}- u_{r_max} (input parameters) 11-17 (ms^{-1})	DEA-PSO
Dependent Parameters	Rotor radius (R)	$\left(\frac{h}{7.711}\right)^{\frac{1}{0.6713}} \le R \le \left(\frac{h}{4.56}\right)^{\frac{1}{0.7385}}$	Random
	Rated power (P_r)	$0.195 \times \left(\frac{R}{0.5927}\right)^{\frac{1}{0.4639}} - 0.5\rho A u_r^3 C_{p\_max}$	Random
	Capacity factor (C_f)	Eq. (10)	[$k=k(h)$ and $c=c(h)$]

For a fixed-speed WTS, the size of components and the value of parameters namely generator rating, wing length, tower height, the rotor speed, tip-speed ratio and design wind speed comprise the set of optimization variables by considering constrains defined in [14]. Geographical features of the region such as; altitude and average temperature are also considered as equality constrains. The Weibull distribution, characterized shape and scale parameters (k, c), are used for computation of turbine mean power for one year by using Eq. (6). The maximum value of rotor efficiency is determined depending on the aero dynamical variables (lift to drag ratio) and the number of blades by Eq. (3). In the design process, the velocity and position of all particles (the value of design parameters) are randomly updated by taking into account the range of design parameters. After updating, all particles are checked and limited according to constrains. This process is continued until the number of iterations that are the stopping criterion is completed. The algorithm could be examined in [14], in detail.

3.2 Software description

Because of the user-friendliness that is the one of most apparent advantages of a graphical user interface, a package called *A&DOP* (**A**nalysis & **D**esign **O**ptimization **P**ackage) was developed. It has one main window that allows users to carry out energy and cost analyses, and to optimize design parameters undertaking wind potential of the site into the design process. C# is used for all program routines of the package, since it is inexpensive and supports cross-platform applications for a lot of operating system as well as 64-bit compilation on Windows [23]. Figure 1 shows main window of the package. As can be seen from the figure, the main window is divided into two main sections called *Analysis* and *Design Optimization*, on which an input and output data for considering WTS is entered and seen, respectively. The first section of the package consists of energy and its cost analyses for fixed-and variable-speed WTS, separately. This section enables the user to analyse the performance of WTS such as; mean power, resulting in AEP, turbine capacity factor and the cost of kWh, total cost of WTS and project for both types of WTS. For the variable type, however, the tip-speed ratio is not to be required with the proposed model; the parameter is used as an input parameter to compute design wind speed for which rotor efficiency is in maximum and the maximum value of rotor efficiency using Eq. (1-d) and Eq. (3), respectively. Besides geographical features of the region i.e., altitude, mean temperature and surface friction coefficient, the wind potential is entered either mean wind speed with its standard deviation or Weibull shape and scale parameters at reference height. Input data in terms of design parameters of WTS, geographical and wind features are typed in using the *Analysis and Design Optimization* windows. In addition to performance analyses in terms of energy and cost, it is also possible to analyse the power curve and Weibull distribution of the wind site graphically by clicking related button on *Graphical Analysis* Section as shown in Figure 2. In the figure Data input and performance analysis of a variable-speed WTS on the *Analysis Window* is examined. It enables to user determining power-energy and cost analysis of a WTS for a specified wind site with its geographical and wind features.

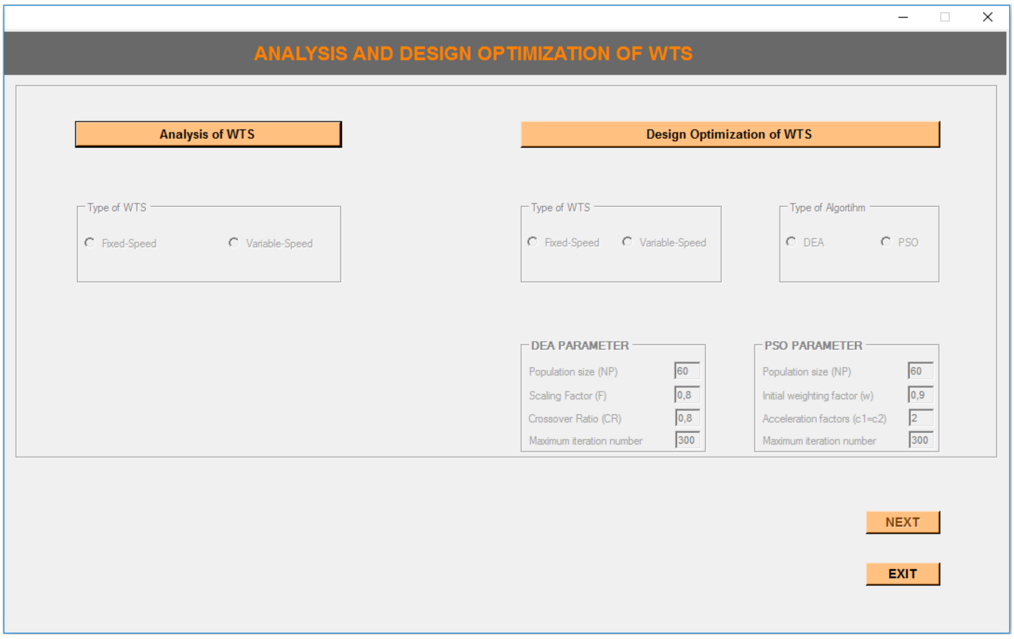

Figure 1. Main window of the package

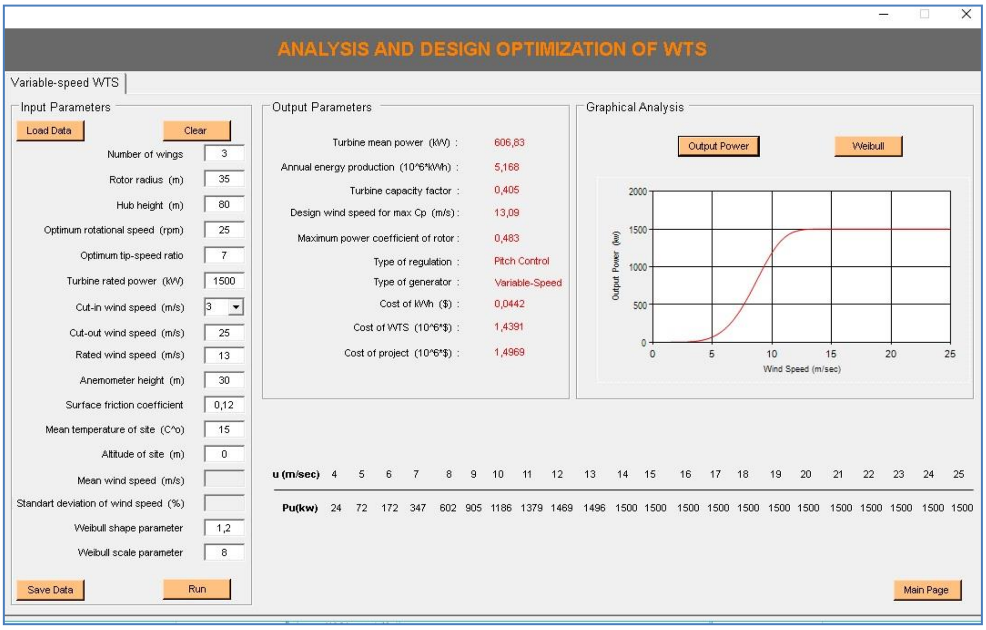

Figure 2. Data input and performance analysis of variable-speed WTS on the *Analysis* window

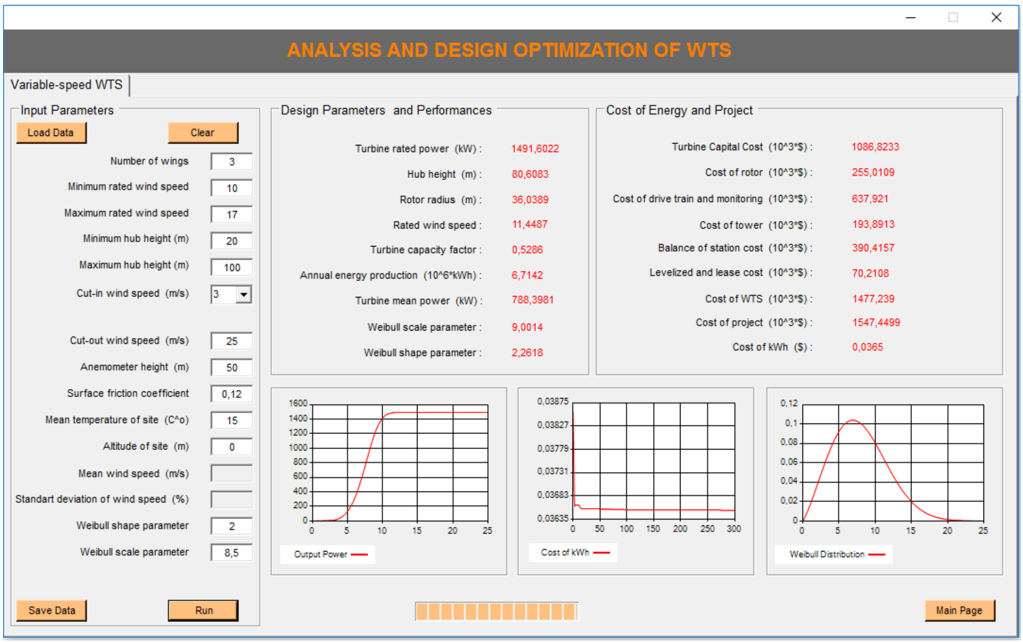

Figure 3. Data input and design optimization of variable-speed WTS on *Optimization* window

The second section of the package, called *Design Optimization of WTS*, facilitates optimal design of both fixed- and variable-speed WTS. In this section maximum iteration number of the optimization algorithm, the value of PSO and DEA parameters could be changed by the user as can be viewed in Figure 1. The *Design Optimization* section of the package consists of three sections for both types of WTS. The first section is called *Input Parameters*, and wind and geographical data of the related site, the range of some design parameters given in Table 1 are entered in this section as it can be viewed in Figure 3. In the figure data input and design optimization of a variable-speed WTS on *Optimization Window* is examined. The first section, called *Input Parameters*, includes the range of independent parameters, geographical features and wind characteristics of the site. The second section, called *Design Parameters & Performances*, provides the optimal size or value of design parameters for variable-speed WTS i.e. rated power, hub height, rotor radius, rated wind speed, and resulting in AEP applying optimization algorithm with the our power curve model as can be seen in Figure 3. The final section, called *Cost of Energy & Project*, allows user to perform cost analyses containing cost of kWh, the cost of all components of the turbine, total cost of WTS and project by using cost of energy model [12]. It also provides turbine power curve and Weibull distribution of the site, graphically.

Recently, even though variable-speed WTSs based on Double Fed Induction Generator or Permanent Magnet Synchronous Generator is the most favorite type of the WTSs, the fixed-speed WTSs are still used in rural areas. Therefore, power curve modeling and analysis of this type of WTS is still an important task. The package is also consisted of analysis and design optimization sections for fixed-speed WTSs. Similarly, the performance of the related WTS; mean power for one year, annual energy production, tip-speed ratio, maximum value of rotor efficiency, and cost of kWh and project could be analysed by using *Analysis* section of the package clicking *Fixed-Speed WTS* button. Our rotor efficiency model presented in [14] is used for power curve characterization in COE model for both *Analyses and Design Optimization* Sections. In *Analysis* section, it is also possible to perform graphical analyses i.e. power curve of the considered WTS as can be seen in Figure 4. In the figure, data input and design optimization of fixed-speed WTS on *Optimization* window is examined. As can be seen from the figure, it is similar to variable-speed type of WTS. The site specified design optimization of fixed-speed WTS could be carried out on *Design Optimization* section of the package. In the optimization algorithm, generator rating, rotor size, tower height, optimum value of rotor speed, tip-speed ratio and design wind speed comprise the set of optimization variables by considering inequality constrains as given in [14], in detail. Geographical and aero dynamical variables namely lift to drag ratio and number of wings are also used as equality constrains. It facilitates to user determining the optimal value or size of design parameters, and its performances in terms of energy and cost undertaking equality and inequality constraints as can be seen in Figure 4. Moreover, the entered data can be saved and reloaded by the Save Data and Load Data buttons in the Analysis and Design Optimization sections of the package. With the Save Data button, information is recorded in the Microsoft Access Database (.accdb) file type. The most suitable WTSs used in the practice can be selected with the *Select Wind Turbine* tab, based on the installed power for the designed WTSs and in particular the nominal wind speed as can be seen in Figure 5. As shown in Figures 1-4, the main window of the package is returned by the *Main Page* button, the screen is cleared with the *Clear* button and the program is closed by using the *Exit* button.

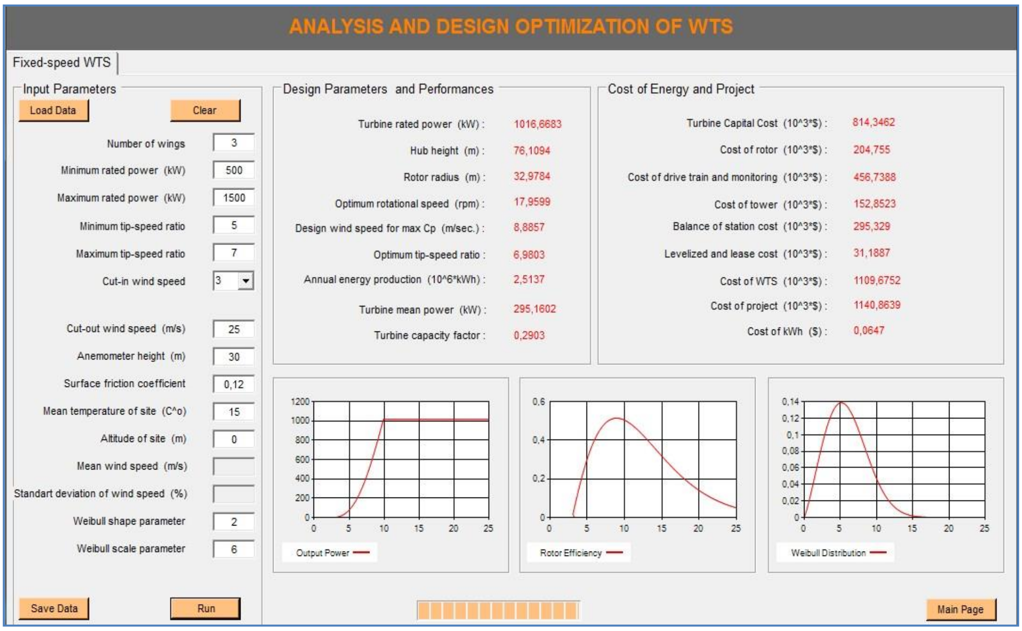

Figure 4. Data input and design optimization of fixed-speed WTS on *Optimization* window

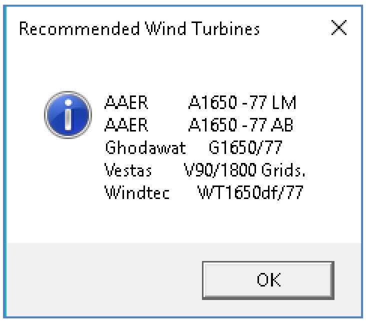

Figure 5. Optimal commercial WTS selection

3 Software testing

In this case of the study, three wind sites are considered in order to evaluate the reliability of the developed package. The size/value of design components/parameters of the WTS that should be installed are obtained by using *Design Optimization* section of the package for both types of WTS. Firstly, the design optimization is performed for variable-speed type and Mediterranean site of Europe whose Weibull parameters are k=1.2 and c=8 m.s^{-1} at the reference height of h=30 m [13]. The wind friction coefficient of the region is taken as α =0.12 [13]. The reason for this is that there is a bigger wind potential in the Mediterranean countries than in the Northern Europe. In addition, some of the Environmental Policies of the Mediterranean countries have been amended for the purpose of increasing the wind parks. A PC, which has the following characteristics, has been used for the simulations; Core™ i5-4590 CPU, 3.3-GHz processor and 8 GB/3.3-GHz memory. The design parameters for the WTS to be installed in this site are determined. Optimization results are presented in Table 2 with the ones of WTSs optimized in [13] and in [16] for this site. One can see from the table that the WTSs designed by using two different optimization methods of the package are in agreement in terms of design parameters and energy cost. Moreover, they are more advantageous in terms of the energy cost and/or the amount of energy production rather than the reference WTS given in [13]. However, both of them produces electrical energy nearly at the same cost, the capacity factor of the optimized WTSs is greater than that of the reference WTS and it generates more energy. On the other hand, when the wind turbines designed are compared with the other wind turbine that is designed for the same area given as in [16], one can see that the wind turbine designed as in [16] is slightly more advantageous in terms of energy amount and its cost. But, in the study, the value of rotor efficiency at the nominal wind speed was taken greater than 0.4, however; the rotor efficiency decreases as the wind speed increases. When the real power curves of the WTSs used in practice are examined, it is observed that taking the rotor efficiency value lower than 0.4 at the nominal wind speed in Eq. (1) is a more accurate approach. For this reason, although it has a slightly lower performance, it is possible to claim that the designed wind turbines are more realistic in terms of the power curve model, constraints and design methodology.

Secondly, the design parameters for a WTS optimized by NREL as in [12] for k=2 and c=8.5 m.s^{-1} at the reference height of h_o=50 m are considered in comparison. For this site, designed wind turbines with the value of its parameters are given in Table 3. As it may be observed in the table, the parameters of WTSs designed by using two different methods of the package and the design parameters for the reference WTS (h, u_r, R, P_r) are consistent at a great rate. On the other hand, it is observed that the designed WTSs by using the developed package are slightly more advantageous in terms of turbine capacity factors; and as a result of annual energy production. For design algorithm given in [12], here, it must be stated that the turbine power output has been determined with the classical method given in Equation (1) by using the change between the rotor efficiency according to wind speed. Since a great number of WTSs with various power rates are evaluated in design process, especially in design optimizations performed with a population-based optimization algorithm, it is not possible to use rotor efficiency in a realistic manner in forming the power curve for each WTS. For this reason, in addition the realistic results, it is possible to claim that the algorithm is also advantageous in terms of implementation.

Table 2. Optimized parameters of the variable-speed WTSs for Mediterranean site of Europe

Parameter	p	D (m)	H_{hub} (m)	U_r (m.s^{-1})	P_{rated} (kW)	AEP (kWh)	Cost of kWh ($cent)	Capacity Factor	Mean power (kw/yr)
Optimized WTS with PSO	3	68.1	79	12.17	1606	5.98×10^6	0.039	0.437	702
Optimized WTS with DEA	3	69.2	79	12.09	1624	6.09×10^6	0.039	0.440	715
WTS [13]	3	30	30	14.00	1000	2.97×10^6	0.038	0.349	349
WTS [16]	3	64.26	73.5	12.40	1705	6.57×10^6	0.0366	0.488	771

Table 3. Optimized variables of the variable-speed WTSs for k=2, c=8.5 m.s^{-1} at h=50 m.

Design Parameters	p	D (m)	h (m)	u_r (ms^{-1})	P_r (kW)	Capacity Factor	Mean power (kw/year)	AEP (kWh)	Cost of kWh ($)
Optimized WTS with DEA	3	72	80	11.44	1491	0.528	797	6.78×10^6	0.036
Optimized WTS with PSO	3	71.6	81	11.42	1460	0.531	775	6.60×10^6	0.036
WTS in Ref. [12]	3	70	65	11.39	1500	0.511	767	6.53×10^6	0.036

As can be seen from the results of both design optimization processes given in Table 2 and Table 3, different wind site has significant influence on the size of the turbine components and the value of other design parameters; rated wind speed and capacity factor. For this reason, the effect of the wind speed on these parameters is analyzed parametrically, and the results are given in Figure 6. As can be seen from the figure, it is obvious that different wind speed and its standard deviation cause different rated wind speed values for the designed wind turbines. From this analysis, we also observed similar situation for the variation of the turbine capacity factor and the amount of energy produced. They are also significantly affected with the variation of the wind speed. Consequently, it can be stated that the rated wind speed of a WTS is a very important parameters in terms of energy production and its cost; hence it must be selected as a design parameter as design in design optimization processes.

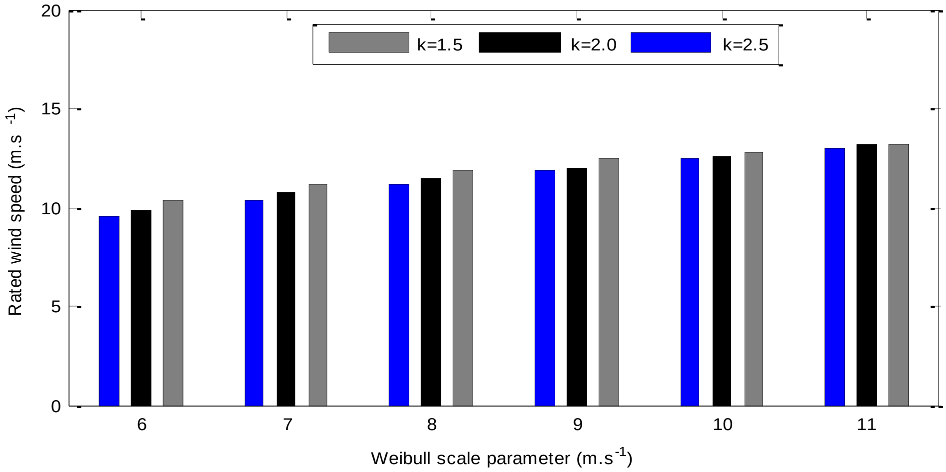

Figure 6. The value of rated wind speed of WTS designed for different wind site

In this case study, finally, Northern site of Europe which has k=2 and c=6 m.s^{-1} at h=30 m, and α=0.12 is considered to validate the optimization section of the package for the fixed-speed WTSs. Table 4 shows the optimization results that can also be seen from Figure 4. The optimized value of design parameters for reference wind turbine given in [13] and its performances are also given. One can see from the table that the value/size of the design parameters, namely design wind speed, rotor diameter, hub height and generator rating power are greater, but the design parameters; rotor speed and optimum tip-speed are lower as compared with those of the suggested WTS in [13]. The values of capacity factor are the same for both wind turbines, but the amount of energy production is more advantageous. Additionally, the results obtained for the same region are given in the last columns of the table by taking the turbine power equal to the reference WTS's power (660 kW) to test the validity of the design algorithm and the identified constraints. One can see that the size of turbine components and the value of design parameters (such as; hub height, rotor radius, design wind speed, and etc.) are matched at a great rate. On the other hand, it is possible to say that the WTS designed is more advantageous in terms of energy cost and annual energy production amount compared to the reference WTS.

Table 4. Optimized variables of the fixed-speed WTS for Northern site of Europe

Parameters	Reference WTS in [13]	Optimized WTS with DEA	Optimized WTS with PSO	Optimized WTS with DEA *(P_n=660kW)*	Optimized WTS with PSO *P_n=660kW)*
p	3	3	3	3	3
D (m)	47	65.8	63.4	53.6	52.6
H_{hub} (m)	60	76	77	69	68
N (rpm)	26	17.9	18.5	21.3	21.9
U_{des} (m.s^{-1})	8	8.88	8.83	8.0	8.29
P_{rated} (kW)	660	1016	943	660	660
AEP (kWh)x10^6	1.30	2.51	2.35	1.66	1.64
Cost of kWh ($cent)	7.12	6.47	6.46	6.44	6.49
Capacity Factor	0.23	0.29	0.29	0.29	0.29
Opt. tip-speed ratio	7.99	6.98	6.97	7.48	7.46
Mean power (kW/yr)	153.4	295	276	195	193

4. Conclusion

The installation of WTSs has been increased in recent times. Accordingly, to product electrical energy at higher efficiency with the lower cost, accurate mathematical methods and algorithms has to be used in analysis and design processes. In this paper, a software package called *A&DOP* (Analysis & Design Optimization Package) for energy system engineering was presented. It was composed by utilizing GUI environment of C#, and validated for both fixed- and variable-speed WTS at different wind sites. It enables the user to analyse and design of a WTS by using functional power curve method, mathematical models defined between the sizes of main components. It also permits the user to gain experience and knowledge in energy and cost analysis, and optimal design of fixed- and especially variable-speed WTSs by taking into account of geographical features of the region. In the optimization algorithm, population based methods; Differential Evolution Algorithm (DEA) and Particle Swarm Optimization (PSO) algorithm were used for solving such problem to determine the most appropriate size/value of design parameters. The parameters consist of the size of turbine main components (hub height, rotor diameter, rated power, and the value of the parameters that has effects on the produced energy and its cost (rated wind speed and turbine capacity factor). From results, it was concluded that the WTSs designed by using the developed package are more advantageous in terms of the energy amount that will be produced and its cost, and are more realistic as compared with those of WTSs given in the literature. Additionally, it was also observed that the DEA is more efficient to solve this type of problem, however; it requires slightly higher computation time as compared with the performance of PSO algorithm. The package is available at: https://muhendislik.gop.edu.tr/Icerik.aspx?d=tr-TR&mk=31052&m=tanitim&bidr=11151&bid=11557 and can be freely downloaded. The package will be continuously modified in terms of power computation methods, constraints defined between the design parameters and the design optimization processes. Additionally, realization of optimal hybrid system design for the regions is planned by including photovoltaic panels to the package.

Acknowledgment

This work has been supported by the Scientific and Technological Research Council of Turkey (TUBITAK) under Grant No: EEEAG-114E961.

References

[1] Depcik, C., & Assanis, D.N. (2005). Graphical User Interfaces in an Engineering Educational Environment. *Computer Applications in Engineering Education*, 13 (1), 48–59.

[2] Gozel, T., Eminoglu, U., & Hocaoglu, M.H. (2008). A tool for Voltage Stability and Optimization (VS&OP) in Radial Distribution Systems Using Matlab Graphical User Interface (GUI). *Simulation Modelling Practice and Theory*, 16 (5), 505–518.

[3] Dalibor, B., Kamil, V., Josef, C., & Tomas, D. (2000). General Three-Port Current Conveyor: A Useful Tool For Network Design. *Journal of Electrical Engineering*, 51 (1-2), 36-39.

[4] Li, W., Vanfretti, L., & Chompoobutrgool, Y. (2012). Development and Implementation of Hydro Turbine and Governor Models in a Free and Open Source Software Package. *Simulation Modelling Practice and Theory*, 24, 84-102.

[5] Ledion, B., & George, E. (2005). Pocket–PC Boolean Function Simplification. *Journal of Electrical Engineering*, 56 (7-8), 209-212.

[6] *The integrated Modular Wind Turbine Design Tool [Online]*. Available from: http://www.wmc.eu. Accessed 15 December 2018.

[7] Hassan, G. (2018). *Wind farm design software, [Online]*. Available from: http://www.glgarradhassan.com. Accessed 15 December 2018.

[8] *Wind data analyses software (WindRose) [Online]*. Available from: http://www.windrose.gr. Accessed 15 December 2018.

[9] *Wind atlas analysis and application program [Online]*, Available from: http://www.wasp.dk. Accessed 15 December 2018.

[10] Heier, S. (1998). Grid Integration of Wind Energy Conversion Systems. *Wiley*, New York.

[11] Michalke, G., & Hansen, A.D. (2010). Modelling and Control of Variable Speed Wind Turbines for Power System Studies. *Wind Energy*, 13 (4), 307-322.

[12] Fingersh, L., Hand, M., & Laxson, A. (2006). Wind Turbine Design Cost and Scaling Model. *Technical Report*, Golden, Colorado.

[13] Diveux, T., Sebastian, P., Bernard, D., Puiggali, R.J., & Grandidier, J.Y. (2001). Horizontal Axis Wind Turbine Systems: Optimization Using Genetic Algorithms. *Wind Energy*, 4 (4), 151-171.

[14] Eminoglu, U. (2016). Site Specific Design Optimization of Horizontal Axis Wind Turbine Systems. *Turkish Journal of Electrical Engineering and Computer Sciences*, 24, 1044-1060.

[15] Fuglsang, P., & Bak, C. (2002). Site-Specific Design Optimization of Wind Turbines. *Wind Energy*, 5 (4), 261-279.

[16] Eminoglu, U., & Ayasun, S. (2014). Modelling and Design Optimization of Variable-Speed Wind Turbine Systems. *Energies*, 7 (1), 402-419.

[17] Kongam, C., & Nuchprayoon, S. (2010). A Particle Swarm Optimization for Wind Energy Control Problem. *Renewable Energy*, 35, 2431-2438.

[18] Li, H., & Chen, Z. Design Optimization and Site Matching of Direct-Drive Permanent Magnet Wind

Power Generator Systems. *Renewable Energy*, 34 (4), 1175–1184.

[19] Carrillo, C., Obando Montano, A.F., & Diaz-Dorado, E. (2013). Review of Power Curve Modelling for Wind Turbines. *Renewable and Sustainable Energy Reviews*, 21, 572-581.

[20] Thapar, V., Agnihotri, G., & Sethi, V.K. (2011). Critical Analysis of Methods for Mathematical Modelling of Wind Turbines. *Renewable Energy*, 36 (11), 3166-3177.

[21] Akdag, S.A., & Guler, O. (2010). Comparison of Wind Turbine Power Curve Models. *Proceedings of International Renewable Energy Congress*, 215-219, Sousse, Tunisia.

[22] Eminoglu, U. (2015). A New Model for Output Power Calculation of Variable-Speed Wind Turbine Systems. *Proceedings of IEEE International Conference on ACEMP-OPTIM-ELECTROMOTION (ACEMP),* 141-145.

[23] *Visual Studio Enterprise*, Copyright ©2013.

[24] Kennedy, J., & Eberhart, R.C. (1995). Particle Swarm Optimization, *Proceedings of IEEE International Conference on Neural Networks*, 1942-1946, Perth, WA, Australia.

[25] Rainer, S., & Kenneth, P. (1997). Differential Evolution–A Simple and Efficient Heuristic for Global Optimization Over Continuous Spaces. *Journal of Global Optimization*, 11, 341-359.

[26] *Matlab Curve Fitting Tool*, Matlab R2010b Enterprise: Copyright©2010.

Ulas Eminoglu *received the B. Sc degree in Electrical-Electronics Engineering from Inonu University and M. Sc degree in Electrical-Electronics Eng. from Nigde Ömer Halisdemir University. He joined Gebze Institute of Technology and has studied distribution systems load flow analyses and power electronics. He has completed his PhD in 2007 at Gebze Institute of Technology. He is currently working as a Professor in Dept. of Electrical Eng. of Gaziosmanpasa University, Turkey.*

Ozan Karahan *obtained B.E. degree and M. Tech. degree in Electrical and Electronics Eng. from Dokuz Eylul University İzmir, Turkey and Gaziosmanpaşa University Tokat, Turkey respectively. He is currently a PhD student in the Department of Electrical and Electronics Eng. at Ondokuz Mayıs University in Samsun, Turkey. He is currently working at Department of Electricity and Energy in Samsun University, Turkey. His research areas of interest are distributed generation systems, optimization and energy storage.*

An International Journal of Optimization and Control: Theories & Applications
ISSN:2146-0957 eISSN:2146-5703
Vol.9, No.2, pp.165-175 (2019)
http://doi.org/10.11121/ijocta.01.2019.00659

RESEARCH ARTICLE

Parameter effect analysis of particle swarm optimization algorithm in PID controller design

Mustafa Sinasi Ayas[a*] and Erdinc Sahin[b]

[a] *Department of Electrical and Electronics Engineering, Karadeniz Technical University, Turkey*
[b] *Department of Energy Systems Engineering, Karadeniz Technical University, Turkey*
msayas@ktu.edu.tr, esahin@ktu.edu.tr

ARTICLE INFO

Article History:
Received 02 August 2018
Accepted 18 January 2019
Available 09 April 2019

Keywords:
PID controller
PSO algorithm
Controller parameter tuning
Error-based objective functions
SOPDT model

AMS Classification 2010:
90C26; 93C05; 78M50; 49N05

ABSTRACT

PID controller has still been widely-used in industrial control applications because of its advantages such as functionality, simplicity, applicability, and easy of use. To obtain desired system response in these industrial control applications, parameters of the PID controller should be well tuned by using conventional tuning methods such as Ziegler-Nichols, Cohen-Coon, and Astrom-Hagglund or by means of meta-heuristic optimization algorithms which consider a fitness function including various parameters such as overshoot, settling time, or steady-state error during the optimization process. Particle swarm optimization (PSO) algorithm is often used to tune parameters of PID controller, and studies explaining the parameter tuning process of the PID controller are available in the literature. In this study, effects of PSO algorithm parameters, i.e. inertia weight, acceleration factors, and population size, on parameter tuning process of a PID controller for a second-order process plus delay-time (SOPDT) model are analyzed. To demonstrate these effects, control of a SOPDT model is performed by the tuned controller and system response, transient response characteristics, steady-state error, and error-based performance metrics obtained from system response are provided.

1. Introduction

Meta-heuristic optimization algorithms have attracted attention in control system area, especially in controller design process. Because these algorithms have been agreed as an alternative method of solving deterministic optimization problems or stochastic programming whose solution is not feasible in most cases even though optimality is proven. Genetic algorithm (GA) [1, 2], ant colony optimization (ACO) [3], cuckoo search algorithm (CSA) [4], flower pollination algorithm (FPA) [5], differential evolution [6], artificial bee colony algorithm (ABC) [8], and particle swarm optimization (PSO) [7, 9–11] are some of meta-heuristic optimization algorithms used in controller design process in control system area.

PID controller has been preferred in industrial control applications to obtain desired transient and steady-state response of the closed loop system since 1940s. Either PID controller or its combinations have been included in almost 90% of the industrial control applications [12] because of its functionality, simplicity, applicability, and easy of use [13]. A PID controller has three different parameters required to optimally tune in order to obtain desired system response. Even though conventional tuning methods such as Ziegler-Nichols [14], Cohen-Coon, and Astrom- Hagglund [15] methods are available in the literature, meta-heuristic optimization algorithms considering a predefined fitness function have become popular in the tuning process.

*Corresponding Author

Although several meta-heuristic optimization algorithms are available, PSO algorithm is commonly used in many control applications [16]. PSO algorithm was used to design an optimum PID controller for an automatic voltage regulator (AVR) system [9] by defining a performance criterion W which contains overshoot, rise time, settling time, and steady-state error obtained from system response. In another study, to show the effectiveness of PSO algorithm in control system area, Solihin et. al designed a PID controller for a DC motor model and compared the results with Ziegler-Nichols tuning method [11]. The authors used various fitness functions to see the effect of fitness function in the optimization process. Zhao et. al [17] designed PID controllers for both a first-order process plus delay-time (FOPDT) model and a second-order process plus delay-time (SOPDT) model by proposing a novel fitness function which provides less overshoot and control input. Speed control of a DC motor was performed using PID controller whose parameters were tuned by PSO algorithm and the performance of the PID controller were compared to another PID controller tuned by differential evolution (DE) algorithm [18]. A comparative study for PID controller design with different algorithms was published in [19] where GA, DE, and PSO algorithms were used to tune the parameters of the PID controller.

Even though other studies related to PID controller design based on PSO algorithm are available in the literature, we have not come across with any study analyzing effects of PSO algorithm parameters, yet. Therefore, variable parameters of PSO algorithm such as inertia weight, acceleration factors, and population size are taken into account and effects of these variables on PID controller parameter optimization process are analyzed in this study. During the optimization process, a SOPDT model is used since most of the high order processes can be modeled by either a FOPDT model or a SOPDT model [20]. Both visual and numerical results are provided in the paper to see the effects of each variable on change of fitness value, transient response characteristics, steady-state error, and error-based performance metrics.

The rest of this paper is organized as follows: Section 2 presents a brief background about PID controller and PSO algorithm, and introduces optimization process of the PID controller. Simulation results are given in Section 3 where the effects of inertia weight, acceleration factors, and population size of PSO algorithm are analyzed separately. In addition, the obtained system responses are provided in this section. Concluding remarks are made in Section 4.

2. PID controller and optimization

2.1. PID controller

PID controller and its combinations have been still preferred in many control applications to improve system dynamic response in addition to steady-state error, although being over 100 years old. Because it has critical advantages such as functionality, simplicity, applicability, and easy of use [13]. A PID controller has three different terms: proportional, integral, and derivative. Each term has a gain called with the same name. In other words, proportional, integral, and derivative terms have the gains K_P, K_I, and K_D, respectively. In this structure, the integral term increases system type by adding a pole at the origin, whereas the derivative term adds a finite zero to the open loop transfer function. Therefore, both the steady-state error and transient response of the closed-loop system improve thanks to integral and derivative terms, respectively.

Block diagram representation of a parallel form PID controller is demonstrated in Figure 1 where E(s) and U(s) are the error and control signals in Laplace domain, respectively. The general transfer function of a parallel form PID controller in Laplace domain is:

$$U(s) = (K_p + \frac{K_i}{s} + K_d s)E(s) \tag{1}$$

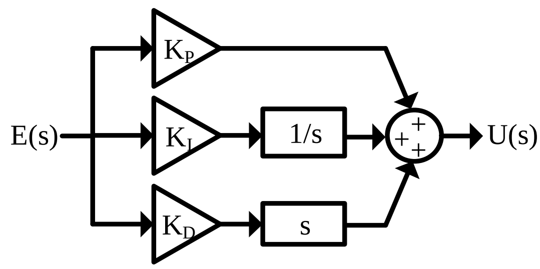

Figure 1. Block diagram of a PID controller.

2.2. Particle swarm optimization

Particle swarm optimization develop by Kennedy and Eberhart [21] is a stochastic evolutionary optimization algorithm based on simulating the movements of a swarm like fish schooling and bird flocking. In order to model the movements of the swarm, position and velocity update equations of the particles are used. The equations of the velocity and position are given below, respectively.

$$V_i^{k+1} = w^k V_i^k + c_1 r_1 (P_{best}^k - X_i^k) + c_2 r_2 (G_{best}^k - X_i^k) \quad (2)$$

$$X_i^{k+1} = X_i^k + V_i^{k+1} \quad (3)$$

where k is the iteration number, i is the number of the particle, w is the inertia weight that directly effect the velocity, c_1 and c_2 are the acceleration factors called cognition and social constants, respectively, r_1 and r_2 are the random numbers between 0 and 1, P_{best} is the best local solution, G_{best} is the best global solution, and V_i and X_i are the velocity and position of the particle i, respectively.

When considered the velocity and position equations, it can be inferred that population size, inertia weight w, and acceleration factors c_1 and c_2 effect the result of the algorithm. In general, c_1 and c_2 are set to 2 and the inertia weight w which balances the global and local search is linearly decreased from about 0.9 to 0.4 [9].

The implementation of the PSO algorithm is described as follows:

Step 1. Initialize the particles with random velocities and positions.

Step 2. Evaluate and compare fitness values of the particles in the population and obtain the local best value (P_{best}) of the population for current iteration, keep the P_{best} value in memory.

Step 3. Compare the P_{best} value to global best (G_{best}) value, which is initially assigned to P_{best} value, and assign global best (G_{best}) value to the position of the particle with the best fitness function value.

Step 4. Update the velocities of the particles by using Eq. 2

Step 5. Move each particle to their new position by using Eq. 3

Step 6. Increase iteration number, go to step 2 and repeat the steps until the stopping criterion is met.

2.3. Optimization of the controller

Three parameters of the PID controller, i.e. K_P, K_I, and K_D, were tuned by using PSO algorithm to find minimum fitness function value in Matlab/Simulink platform. As the fitness function, integral of time-weighted absolute error (ITAE) which is as error based fitness function was utilized. ITAE fitness function was preferred because it produces smaller overshoot and oscillations than the other error-based fitness function such as integral of absolute error (IAE) and integral of squared error (ISE) [22, 23]. Although ITAE value was used as the fitness function, both IAE and ISE values were calculated in simulations as error-based performance metrics in addition to ITAE value. The equations of the mentioned metrics are:

$$ITAE = \int_0^t t\,|e(t)|\,dt \quad (4)$$

$$IAE = \int_0^t |e(t)|\,dt \quad (5)$$

$$ISE = \int_0^t e(t)^2 dt \quad (6)$$

where e(t) is the error signal between reference and actual signals.

A general schematic representation of the whole system used in the parameter optimization process of the PID controller is shown in Figure 2. In this process, which was performed with a sampling time T_s of 0.001s, a classical PID controller without filter was utilized.K_P, K_I, and K_D parameters of the PID controller were optimized by PSO algorithm. The optimization process started with initializing the particles with random velocities and positions. The number of the particles were equal to population size and each particle contains three parameters called $\hat{K}_P$, $\hat{K}_I$, and $\hat{K}_D$ representing the parameters of the PID controller. As the second step, ITAE values of the particles were evaluated and compared to obtain local best value (P_{best}) of the population for current iteration and kept it in memory. Then, the P_{best} value of the population were compared to global best (G_{best}) value of the population, which is initially assigned to P_{best} value, and the position of the particle with the minimum ITAE fitness function value was assigned as the global best (G_{best}) value. The process went forward with updating the velocities of the particles and obtaining new positions for them. By using these new positions, calculating P_{best} and G_{best} values were repeated during 50 iterations. Since the algorithm starts with randomly assigned velocities and positions, the optimization process was performed 10 times for each analyses explained in detail below, i.e. effect of inertia weight, acceleration parameters, and population size. The optimization process might be performed more than 10 trials. However, it requires much more time to analyze effects of these three different parameters. Moreover, when the result figures containing fitness value (ITAE) vs. iteration, i.e. Figures 3, 5, and 7, was considered, it was seen that the fitness values generally aggregate to a common fitness value. Hence, we decided that 10 trials were sufficient to rely on the algorithm.

Mean, standard deviation, median, maximum and minimum values of obtained fitness values were considered for the 10 different trials of each analysis and the details are given in the next section.

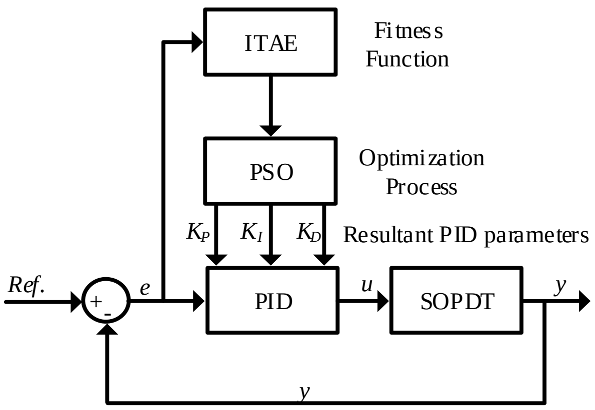

Figure 2. Schematic representation of the parameter optimization process of the PID controller.

3. Simulation results

To analyze effects of PSO algorithm parameters in PID controller design, simulation of a SOPDT model was performed in Matlab/Simulink platform. The transfer function of the SOPDT model used in the study is:

$$G(s) = \frac{0.3172}{s^2 + 1.007s + 0.9515} e^{-0.27s} \tag{7}$$

Unity step reference input was provided to the closed loop system given in Figure 2, and the best controller parameters, i.e. K_P, K_I, and K_D values, were searched considering minimum ITAE fitness function value during 10 seconds simulation.

First of all, effect of inertia weight w was considered in this section. Then effect of acceleration factors c_1 and c_2 were analyzed. Finally, effect of population size used in the PSO algorithm was investigated.

3.1. Effect of inertia weight

The inertia weight w constructs a relation between the past and current velocities of the swarms as seen in Eq. 2. Therefore, it effects the flying abilities of swarms to either in a wide-range or in a narrow-range. Global and local searching abilities are intended by wide and narrow-range flying abilities. Therefore, larger or smaller inertia weight determines the trade-off between global and local searching abilities. Smaller inertia weight is suggested to fine-tune in a smaller search space, whereas larger inertia weight is asked to global exploration in a larger search space [24]. In general, the inertia weight w is linearly decreased from about 0.9 to 0.4 depending on the maximum and current iteration numbers [9]. Eq. 8 is used to calculate the inertia weight

$$\omega = \omega_{max} - \frac{\omega_{max} - \omega_{min}}{iter_{max}} iter_{current} \tag{8}$$

where $iter_{max}$ and $iter_{current}$ represent the maximum and current iteration numbers, respectively. ω_{max} and ω_{min} are set to 0.9 and 0.4, respectively.

To see the effect of the inertia value on a SOPDT, various w values were used in optimization process. 11 different w values from 0.05 to 1.0 in addition to linearly decreased w value calculated by using Eq. 8 were utilized in the parameter optimization process of the PID controller. Since the PSO algorithm starts with random initial positions, the algorithm performed 10 times. All trials were performed with stationary acceleration factors c_1 and c_2, population size, and maximum iteration number which are set to 2, 2, 10, and 50, respectively. The change of ITAE fitness values during the optimization process with different w values are shown in Figure 3. In order to make a fair comparison and provide a more possible visual figures, both the scales of x-axis and y-axis were set to the same possible values in each subfigures. Therefore, some subfigures may not contain the 10 different trial lines as in Figures 3(a), (b), and (c) which consist of 9 different trial lines. From the figures, the minimum fitness function can not be observed clearly. Therefore, in addition to visual results, numerical results belonging to optimization process are provided in Table 1, where FV, Mean, SD, Median, Max, Min stand for the best fitness value, the mean of the fitness values, the standard deviation of the fitness values, the median of the fitness values, maximum of the fitness values and minimum of the fitness values, respectively. It can be concluded from the table that reaching to optimal solution, i. e. global best position, is more possible when $w = 0.2$ than the other inertia weights, when considered the standard deviation of the fitness values. Furthermore, the maximum ITAE fitness value obtained with $w = 0.2$ is less than the other inertia weights. As a result of the numerical results, the minimum fitness value is 0.4477 and obtained when $w = 0.2$ for this SOPDT model during 10 seconds.

The best PID controller parameters for each w value are given in Table 2. The obtained system response using these controller parameters are shown in Figure 4, where a zoomed region is also demonstrated to see the transient response characteristics more clearly. From the figure, it can be concluded that satisfactory steady-state error is obtained for each w value. However, transient response obtained for each w is required a further thought. Therefore, the transient response characteristics, i.e. maximum overshoot (MO), settling time (Ts), rise time (Tr), and peak time (Tp), are also provided in Table 2 in addition to steady-state error, and error-based performance metrics, i.e. IAE, ISE, and ITAE. The minimum steady-state error and ITAE performance metric was obtained when $w = 0.2$. However, less overshoot and settling time occurred when $w = 0.6$ and $w = 0.5$, respectively. As a result, since the fitness function of the PSO algorithm is ITAE fitness value, the best controller parameters were obtained when $w = 0.2$.

Table 1. Effect of inertia weight on fitness value.

w	FV	Mean	SD	Median	Max	Min
0.05	0.4532	0.5672	0.2456	0.4946	1.2562	0.4532
0.1	0.4484	0.5775	0.2673	0.5007	1.3333	0.4484
0.2	**0.4477**	**0.5082**	**0.1399**	**0.4593**	**0.9032**	**0.4477**
0.3	0.4484	0.5627	0.2231	0.4644	1.1247	0.4484
0.4	0.4480	0.5420	0.2110	0.4629	1.1247	0.4480
0.5	0.4500	0.5394	0.2064	0.4887	1.1247	0.4500
0.6	0.4517	0.5382	0.2066	0.4797	1.1247	0.4517
0.7	0.4502	0.5541	0.2072	0.4890	1.1263	0.4502
0.8	0.4587	0.5651	0.2202	0.4915	1.1857	0.4587
0.9	0.4673	0.5947	0.2117	0.5300	1.1857	0.4673
1.0	0.5045	0.6177	0.1884	0.5612	1.1316	0.5045
LD	0.4488	0.5367	0.2071	0.4732	1.1247	0.4488

3.2. Effect of acceleration parameters

Effect of acceleration factors c_1 and c_2 on ITAE fitness value and both transient and steady-state response of the SOPDT are considered in this section. c_1 and c_2 constants weight the acceleration ratios of the particles towards the local (P_{best}) and global (G_{best}) best positions, respectively. High acceleration constant values may cause inconsistent movement of the particle, i.e. the particles may suddenly converge to the best global position or past it towards other local best positions, whereas low values may allow the particle to go around far away from the global best position. Therefore, the acceleration factors c_1 and c_2 are set to 2.0 as a result of trial and error method in most studies.

In this study, (c_1, c_2) acceleration constant pair were set to $(0,4)$, $(1,3)$, $(2,2)$, $(3,1)$, and $(4,0)$ by keeping inertia weight w and population size stationary at 0.2 and 10, respectively. w was set to 0.2, since minimum ITAE fitness value had been obtained at that weight in the previous subsection.

The change of ITAE fitness values during the optimization process with different (c_1, c_2) pairs are given in Figure 5 where the scales of each subfigures are set to the same possible values to make a fair comparison and provide a more possible visual figures. Numerical results of the optimization process are also provided in Table 3, where FV, Mean, SD, Median, Max, Min stand for the best fitness value, the mean of the fitness values, the standard deviation of the fitness values, the median of the fitness values, maximum of the fitness values and minimum of the fitness values, respectively. The minimum fitness value is 0.4477 and obtained with $(c_1 = 2.0, c_2 = 2.0)$ for this system during 10 seconds. As a result of the numerical result, c_2 constant, which is related to the global (G_{best}) best position, has more effect on the fitness value as expected. Because the minimum fitness value is obtained with $(c_1 = 2.0, c_2 = 2.0)$ and the increase of the fitness value becomes more when the weight of c_2 constant is decreased.

The best PID controller parameters for each acceleration constant pair are given in Table 4. The obtained system response using these controller parameters are demonstrated in Figure 6, where a zoomed region is also given to see the transient response characteristics more clearly. When considered the numerical results given in Table 4, it can be concluded that the best controller parameters were obtained with $(c_1 = 2.0, c_2 = 2.0)$ pair according to defined fitness value, although the best transient response obtained with $(c_1 = 0, c_2 = 4.0)$.

Table 3. Effect of acceleration parameters on fitness value.

C1	C2	FV	Mean	SD	Median	Max	Min
0	**4**	0.4492	0.5447	0.2049	0.4890	1.1247	0.4492
1	**3**	0.4493	**0.5011**	**0.1022**	0.4785	**0.7873**	0.4493
2	**2**	**0.4477**	0.5082	0.1399	**0.4593**	0.9032	**0.4477**
3	**1**	0.4507	0.7244	0.2060	0.7580	1.1466	0.4507
4	**0**	0.5513	2.1092	1.2775	1.5627	4.8274	0.5513

Table 2. Effect of inertia weight on system dynamic response, steady-state error and performance metrics.

	Controller Parameters			Transient Response Characteristics					Error-based Metrics		
w	**Kp**	**Ki**	**Kd**	**MO (%)**	**Ts**	**Tr**	**Tp**	**Ess**	**IAE**	**ISE**	**ITAE**
0.05	12.5363	3.5191	7.7843	2.2481	2.5800	0.6900	1.5900	2.4e-06	0.8743	0.6988	0.4532
0.1	13.3055	3.5799	8.2060	2.2787	2.5600	0.6600	1.5200	3.7e-06	0.8604	0.6849	0.4484
0.2	13.6308	3.6244	8.3257	2.8301	2.5500	0.6400	1.5000	**9.02e-07**	0.8552	0.6791	**0.4477**
0.3	13.7343	3.6662	8.2867	3.6717	2.5500	0.6300	1.4900	3.1e-06	0.8539	0.6770	0.4484
0.4	13.3769	3.6077	8.1810	2.8409	2.5600	0.6600	1.5200	1.9e-06	0.8590	0.6833	0.4480
0.5	14.1622	3.6696	8.6112	3.0230	**2.5100**	0.6300	1.4500	3.7e-05	0.8485	0.6706	0.4500
0.6	12.6971	3.5296	7.8798	**2.1768**	2.5800	0.6900	1.5800	3.6e-06	0.8712	0.6958	0.4517
0.7	14.0695	3.6762	8.5284	3.2739	2.5200	0.6300	1.4600	5.0e-05	0.8495	0.6719	0.4502
0.8	14.1778	3.7780	8.2815	5.8517	2.5700	0.6100	1.4700	5.0e-05	0.8523	0.6695	0.4587
0.9	14.7846	3.8085	8.5959	6.0705	2.5300	0.5900	1.4300	1.4e-04	0.8467	0.6607	0.4673
1.0	16.5954	3.8457	10	4.0038	2.8600	**0.5500**	**1.3100**	3.0e-04	**0.8385**	**0.6394**	0.5045
LD	13.8335	3.6525	8.4119	3.1014	2.5400	0.6400	1.4800	3.3e-05	0.8524	0.6757	0.4488

Table 4. Effect of acceleration parameters on system dynamic response, steady-state error and performance metrics.

		Controller Parameters			Transient Response Characteristics					Error-based Metrics		
C1	**C2**	**Kp**	**Ki**	**Kd**	**MO (%)**	**Ts**	**Tr**	**Tp**	**Ess**	**IAE**	**ISE**	**ITAE**
0	**4**	13.9362	3.6169	8.5811	**2.1622**	**2.5200**	**0.6400**	**1.4700**	5.6e-06	**0.8519**	**0.6746**	0.4492
1	**3**	13.1337	3.6020	8.0138	3.1200	2.5800	0.6700	1.5400	5.2e-06	0.8631	0.6874	0.4493
2	**2**	13.6308	3.6244	8.3257	2.8301	2.5500	**0.6400**	1.5000	**9.0e-07**	0.8552	0.6791	**0.4477**
3	**1**	13.0244	3.6075	7.9132	3.4741	2.5900	0.6700	1.5500	2.4e-06	0.8654	0.6892	0.4507
4	**0**	11.5784	3.7322	6.6511	8.6182	2.2400	0.6900	1.7100	2.1790e-04	0.9294	0.7175	0.5513

3.3. Effect of population size

In an optimization process, if the population size is small, the algorithm require less computational effort. On the other hand, the probability of premature convergence increases [25]. Therefore, researches have a common idea of that the algorithms provide poor solutions when the population size is small [26] and require more computational effort when it is large [27].

In this section, the effect of population size parameter on the PSO algorithm is considered by keeping inertia weight w and acceleration constant pair stationary at 0.2 and $(c_1 = 2.0, c_2 = 2.0)$, respectively. As in the previous subsection, the PSO algorithm is performed for 10 times for all population sizes and the results are recorded.

Figure 7 shows the change of ITAE fitness values during the optimization process with different population sizes. It can be concluded from the figure that the standard deviation of the obtained fitness value is the smallest with the largest population size. In other words, the probability of converging global best position is higher than the others. This result can be supported by Table 5, where FV, Mean, SD, Median, Max, Min stand for the best fitness value, the mean of the fitness values, the standard deviation of the fitness values, the median of the fitness values, maximum of the fitness values and minimum of the fitness values, respectively. In addition to standard deviation, the maximum value of ITAE value is getting smaller while increasing the population size. On the other hand, the required computation time increases as the population size increase.

The obtained best PID controller parameters for each population size are given in Table 6. The obtained system response using these controller parameters are demonstrated in Figure 8, where a zoomed region is also provided. The transient response characteristics obtained from system response is also given in Table 6. That the best controller parameters were obtained with the largest population size is concluded from the numerical results in the table. In addition to ITAE fitness value, all transient response characteristics except maximum overshoot is better when the population size is equal to 50.

Table 5. Effect of population size on fitness value.

Size	FV	Mean	SD	Median	Max	Min	Time(s)
10	0.4477	0.5082	0.1399	0.4593	0.9032	0.4477	**1023.1**
25	0.4480	0.4538	0.0130	0.4483	0.4887	0.4480	2521.9
50	**0.4477**	**0.4482**	**5.8e-04**	**0.4480**	**0.4494**	**0.4477**	5375.5

4. Conclusion

In this paper, the effects of inertia weight, acceleration factors, and population size of the PSO algorithm during a PID controller design process for

Table 6. Effect of population size on system dynamic response, steady-state error and performance metrics.

Pop.	Controller Parameters			Transient Response Characteristics					Error-based Metrics		
Size	Kp	Ki	Kd	MO (%)	Ts	Tr	Tp	Ess	IAE	ISE	ITAE
10	13.6308	3.6244	8.3257	2.8301	**2.5500**	**0.6400**	1.5000	9.0e-7	0.8552	0.6791	**0.4477**
25	13.3667	3.6044	8.1821	**2.7809**	2.5600	0.6600	1.5200	6.7e-7	0.8591	0.6835	0.4480
50	13.6532	3.6306	8.3249	2.9459	**2.5500**	**0.6400**	**1.4900**	**4.8e-7**	**0.8548**	**0.6787**	**0.4477**

a SOPDT model were separately analyzed. For this SOPDT model, first the effect of the inertia weight was observed and the best PID controller parameters providing minimum ITAE fitness value were obtained with the inertia weight $w = 0.2$. Then, the effect of the acceleration factors were analyzed and it is concluded that the importance of social constant c_2 related to global best solution is higher than the cognition constant c_1. However, the best solution of the optimization process was obtained with $(c_1 = 2.0, c_2 = 2.0)$ for this system. At last, the effect of the population size were considered by keeping the inertia weight w and the acceleration constant pair stationary at 0.2 and $(c_1 = 2.0, c_2 = 2.0)$, respectively. It was observed that the probability of converging the global best solution increases as the population size increases. However, the required computation time increases.

References

[1] Krohling, R. A., & Rey, J. P. (2001). Design of optimal disturbance rejection pid controllers using genetic algorithms. *IEEE Transactions on Evolutionary Computation*, 5(1), 78–82. .

[2] Wang, P., & Kwok, D. (1994). Optimal design of pid process controllers based on genetic algorithms. *Control Engineering Practice*, 2(4), 641–648.

[3] Chiha, I., Liouane, N., & Borne, P. (2012). Tuning pid controller using multiobjective ant colony optimization. *Applied Computational Intelligence and Soft Computing*, 2012, 11.

[4] Ayas, M. S., Altas, I. H., & Sahin, E. (2018). Fractional order based trajectory tracking control of an ankle rehabilitation robot. *Transactions of the Institute of Measurement and Control*, 40(2), 550–564.

[5] Sahin, E., & Altas, I. H. (2018). Optimized fractional order control of a cascaded synchronous buck–boost converter for a wave-uc hybrid energy system. *Electrical Engineering*, 100(2), 653–665.

[6] Altinoz, O. T., (2018). Multiobjective PID controller design for active suspension system: scalarization approach. *An International Journal of Optimization and Control: Theories & Applications (IJOCTA)*, 8(2), 183–194.

[7] Erguzel, T. T., (2015). A hybrid PSO-PID approach for trajectory tracking application of a liquid level control process. *An International Journal of Optimization and Control: Theories & Applications (IJOCTA)*, 5(2), 63–73.

[8] Rajasekhar, A., Jatoth, R. K., & Abraham, A. (2014). Design of intelligent pid/piλdμ speed controller for chopper fed dc motor drive using opposition based artificial bee colony algorithm. *Engineering Applications of Artificial Intelligence*, 29, 13–32.

[9] Gaing, Z.-L. (2004). A particle swarm optimization approach for optimum design of pid controller in avr system. *IEEE transactions on energy conversion*, 19(2), 384–391.

[10] Zamani, M., Karimi-Ghartemani, M., Sadati, N., & Parniani, M. (2009). Design of a fractional order pid controller for an avr using particle swarm optimization. *Control Engineering Practice*, 17(12), 1380–1387.

[11] Solihin, M. I., Tack, L. F., & Kean, M. L. (2011). Tuning of pid controller using particle swarm optimization (pso). International Journal on Advanced Science, *Engineering and Information Technology*, 1(4), 458–461.

[12] Basu, A., Mohanty, S., & Sharma, R. (2016). Designing of the pid and fopid controllers using conventional tuning techniques. *International Conference on Inventive Computation Technologies (ICICT)*, 2, 1–6.

[13] Ang, K. H., Chong, G., & Li, Y. (2005). Pid control system analysis, design, and technology. *IEEE transactions on control systems technology*, 13(4), 559–576.

[14] Ziegler, J. G. & Nichols, N. B. (1942). Optimum settings for automatic controllers.*trans. ASME*, 64(11).

[15] Hägglund, T. & Åström, K. J. (2002). Revisiting the ziegler-nichols tuning rules for pi control. *Asian Journal of Control*, 4(4), 364–380.

[16] Zhang, Y., Wang, S., & Ji, G. (2015). A comprehensive survey on particle swarm optimization algorithm and its applications. *Mathematical Problems in Engineering*, 2015, 1–39.

[17] Zhao, J., Li, T., & Qian, J. (2005). Application of particle swarm optimization algorithm on robust pid controller tuning. *International Conference on Natural Computation*, Springer, 948–957.

[18] Idir, A., Kidouche, M., Bensafia, Y., Khettab, & Tadjer, K., S. (2018). Speed control of DC motor using PID and FOPID controllers based on differential evolution and PSO. *International Journal of Intelligent Engineering and Systems*, 11(4), 241–249.

[19] Pano, V. & Ouyang, P. R. (2014). Comparative study of ga, pso, and de for tuning position domain pid controller. *2014 IEEE International Conference on Robotics and Biomimetics (ROBIO)*, 1254–1259.

[20] Sun, L., Li, D., Zhong, Q.-C., & Lee, K. Y. (2016). Control of a class of industrial processes with time delay based on a modified uncertainty and disturbance estimator. *IEEE Transactions on Industrial Electronics*, 63(11), 7018–7028.

[21] Kennedy, J. & Eberhart, R. (1995). Pso optimization. *Proc. IEEE Int. Conf. Neural Networks*, 4, 1941–1948.

[22] Nagrath, I. (2006). *Control systems engineering*. New Age International.

[23] Schultz, W. & Rideout, V. (1961). Control system performance measures: Past, present, and future. *IRE Transactions on Automatic Control*, 1, 22–35.

[24] Shi, Y. & Eberhart, R. C.. (1998), Parameter selection in particle swarm optimization. *International conference on evolutionary programming*, Springer, 591–600.

[25] Mallipeddi, R. & Suganthan, P. N. (2008). Empirical study on the effect of population size on differential evolution algorithm. *IEEE World Congress on Computational Intelligence Evolutionary*, 3663–3670.

[26] Piszcz, A. & Soule, T. (2006). Genetic programming: Optimal population sizes for varying complexity problems. *Proceedings of the 8th annual conference on Genetic and evolutionary computation*, 953–954.

[27] Koumousis, V. K. & Katsaras, C. P. (2006). A saw-tooth genetic algorithm combining the effects of variable population size and reinitialization to enhance performance. *IEEE Transactions on Evolutionary Computation*, 10(1), 19–28.

Mustafa Sinasi Ayas *received BSc (2009) degree in Electrical and Electronics Engineering from Hacettepe University, Turkey. He obtained his MSc (2012) and PhD (2017) degrees from Karadeniz Technical University, Turkey. He is working as an assistant professor at the Department of Electrical and Electronics Engineering, Karadeniz Technical University, Turkey. His research interests includes control systems, parallel robotics, and metaheuristic optimization algorithms.*

Erdinc Sahin *is at Department of Energy Systems Engineering, Karadeniz Technical University as an assistant professor.He received his B.S. degree in Electrical and Electronics Engineering Department from Eskisehir Osmangazi University, M. S. degree in Control and Automation Department from Istanbul Technical University, and PhD degree in Electrical and Electronics Engineering Department from Karadeniz Technical University. His research interests include renewable energy systems, fractional order system modeling and controller design, power electronics and drive systems, and metaheuristic algorithms.*

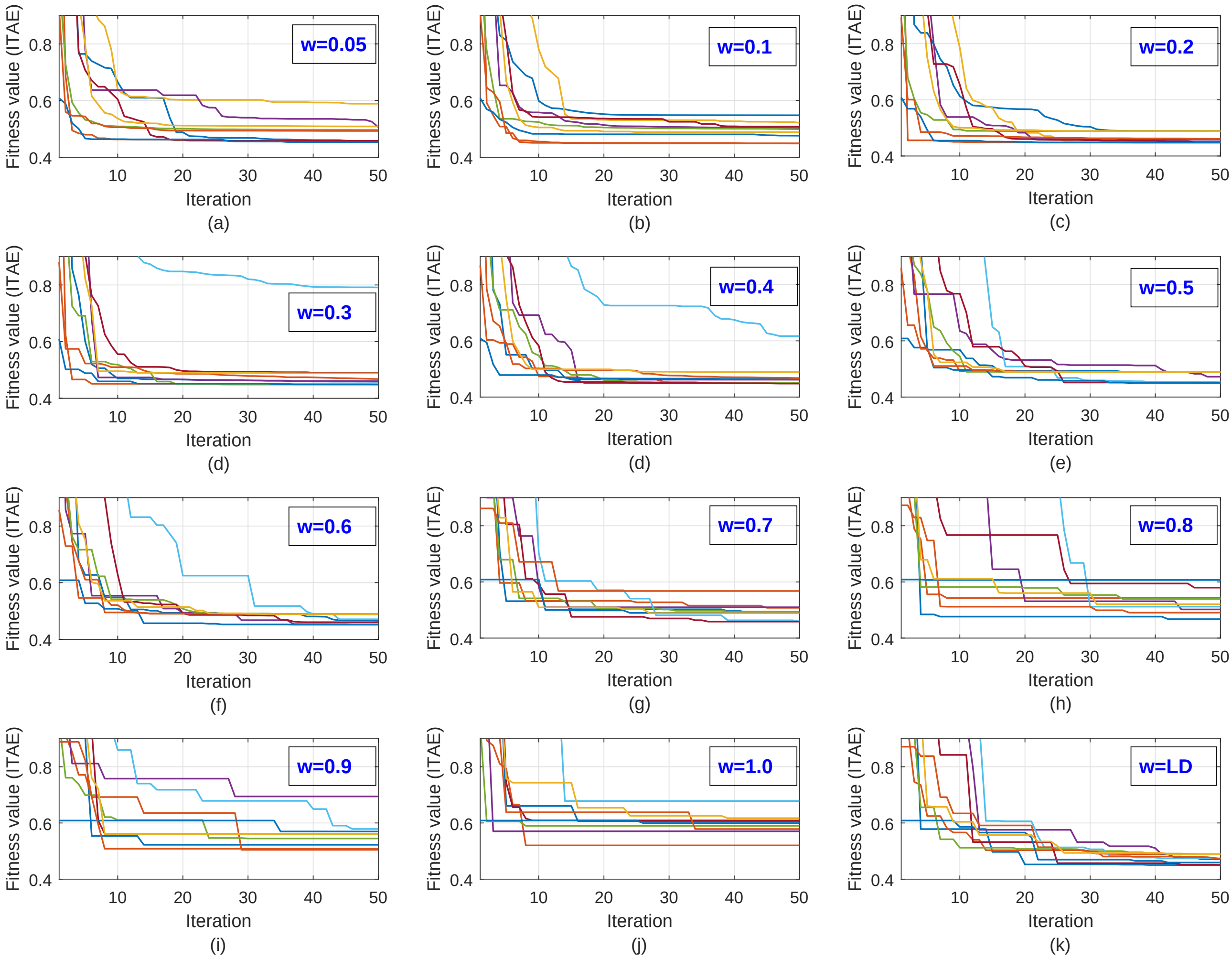

Figure 3. Fitness values obtained with different inertia weight for 10 different trial: Inertia weight is 0.05, 0.1, 0.2, 0.3, 0.4, 0.5, 0.6, 0.7, 0.8, 0.9, 1.0 and LD (linearly decreased from 0.9 to 0.4) in (a), (b), (c), (d), (e), (f), (g), (h), (i), (j) and (k), respectively.

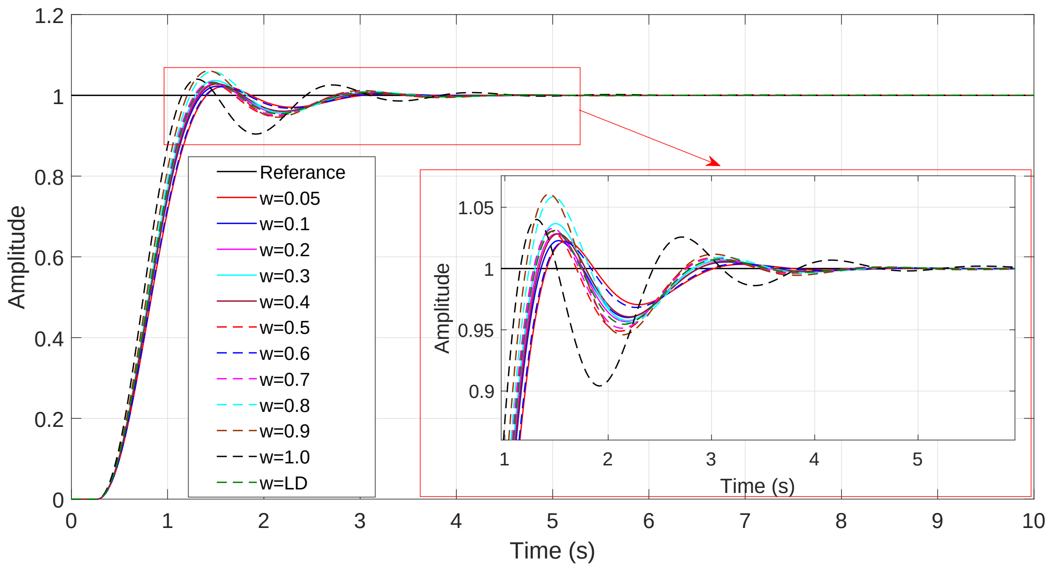

Figure 4. Obtained system responses with different inertia weights.

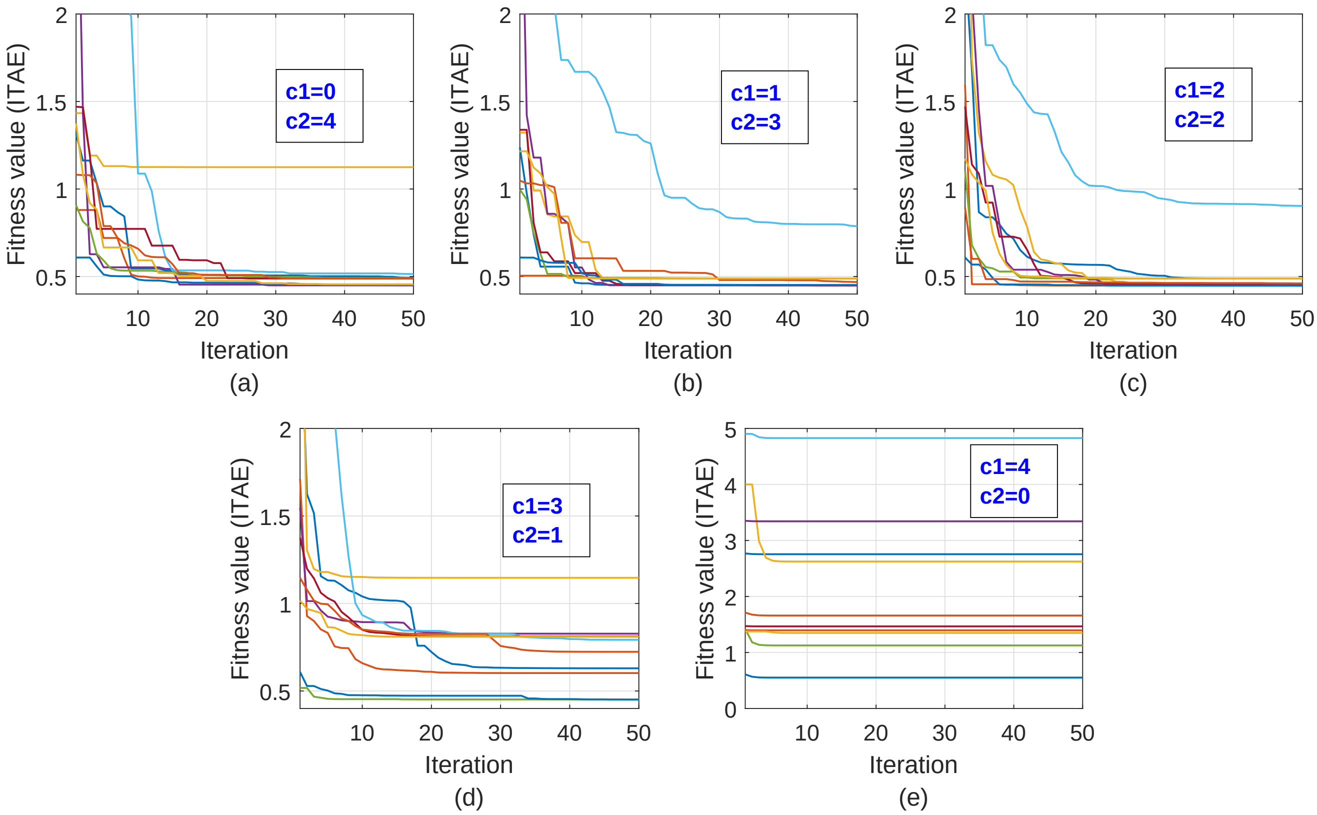

Figure 5. Fitness values obtained with different acceleration parameters for 10 different trial: (a) c1=0, c2=4; (b) c1=1, c2=3; (c) c1=2, c2=2; (d) c1=3, c2=1; (e) c1=4, c2=0.

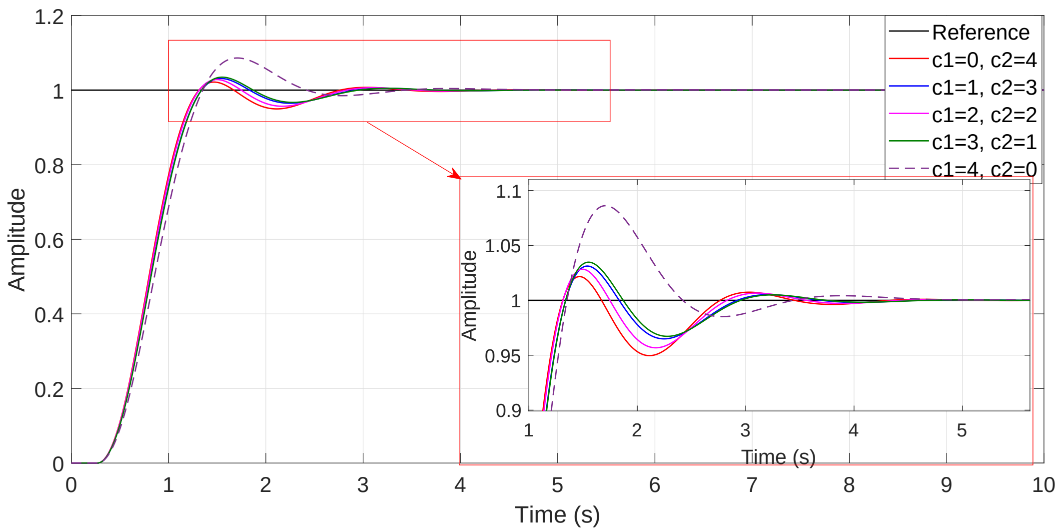

Figure 6. Obtained system responses with different acceleration parameters.

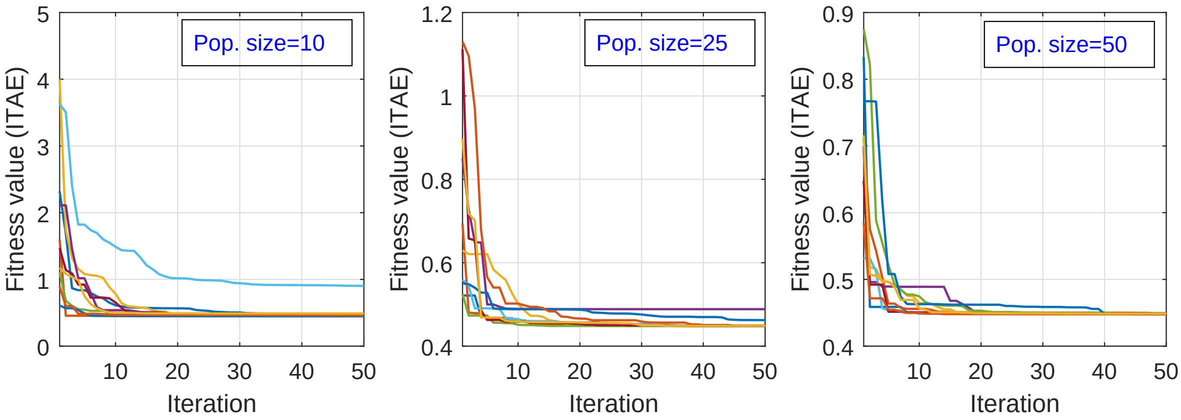

Figure 7. Fitness values obtained with different population size for 10 different trial. Population size is 10, 25, and 50 in (a), (b), and (c), respectively.

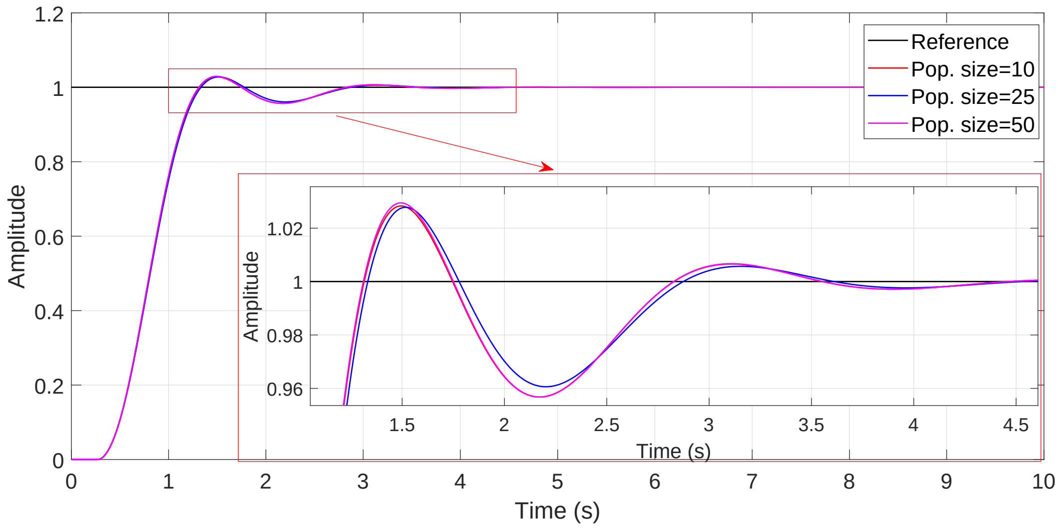

Figure 8. Obtained system responses with different population sizes.

An International Journal of Optimization and Control: Theories & Applications
ISSN:2146-0957 eISSN:2146-5703
Vol.9, No.2, pp.176-185 (2019)
http://doi.org/10.11121/ijocta.01.2019.00743

RESEARCH ARTICLE

A New Broyden rank reduction method to solve large systems of nonlinear equations

Mostafa Ouarit [a], Ali Souissi[b] and Mohammed Ziani*[b]

[a] *MACS Laboratory, Department of Mathematics and Computer Sciences, Faculty of Sciences Ain Chock, Hassan II University Of Casablanca, Morocco*
[b] *Numerical Analysis Group, LMSA, CeReMAR, Department of Mathematics, Faculty of Sciences, Mohammed V University in Rabat, Morocco*
mostafa.ouarit@univh2c.ma, souissi@fsr.ac.ma, ziani@fsr.ac.ma

ARTICLE INFO

Article History:
Received 04 November 2018
Accepted 03 February 2019
Available 09 April 2019

Keywords:
Large nonlinear systems of equations
Limited memory Broyden method
Singular values thresholding
Rank reduction
Superlinear convergence

AMS Classification 2010:
65H10; 65Y20; 15A15

ABSTRACT

We propose a modification of limited memory Broyden methods, called dynamical Broyden rank reduction method, to solve high dimensional systems of nonlinear equations. Based on a thresholding process of singular values, the proposed method determines *a priori* the rank of the reduced update matrix. It significantly reduces the number of singular values decomposition calls of the update matrix during the iterations. Local superlinear convergence of the method is proved and some numerical examples are displayed.

1. Introduction

Let us consider the problem of finding a solution of the system of nonlinear equations

$$F(x) = 0, \qquad F : \mathbb{R}^n \to \mathbb{R}^n. \tag{1}$$

The mapping F is assumed to fulfill the following classical assumptions (CA):

- it is continuously differentiable in an open convex set $\mathcal{D} \subset \mathbb{R}^n$,
- there is an x_* in $\mathcal{D}$ such that $F(x_*) = 0$,
- the Jacobian F' is Lipschitz continuous at x_* and $F'(x_*)$ is nonsingular.

Newton's method (see [1–3])

$$x_{k+1} = x_k - (F'(x_k))^{-1} F(x_k), \quad k = 0, 1, \dots, \tag{2}$$

is well suited to solve the system (1) due to its local quadratic convergence. However, this method is known to be numerically expensive. It requires the evaluation of a jacobian matrix and the solution of a linear system per iteration. An alternative to Newton's method is the Broyden's quasi-Newton method. This method uses approximations to the Jacobian matrix at each iteration by performing rank-one updates, see [4]. It requires only one F-evaluation per iteration and achieves, under the classical hypotheses (CA), local superlinear convergence as shown in [5]. Given an initial guess x_0 and an initial approximation B_0 of the jacobian matrix, Broyden iteration is given by

$$x_{k+1} = x_k - B_k^{-1} F(x_k), \quad k = 0, 1, \dots, \tag{3}$$

where B_k is updated at each iteration as

$$B_{k+1} = B_k + (y_k - B_k s_k) \frac{s_k^T}{s_k^T s_k}, \tag{4}$$

*Corresponding Author

with $y_k = F(x_{k+1}) - F(x_k)$ and $s_k = x_{k+1} - x_k$. To avoid the drawback of storing and manipulating the $(n\times n)$-matrices of Broyden, limited memory methods put restrictions on the size of systems to solve, see references [6], [7] and [8]. Equation (4) implies that if B_0 is updated p times, the resulting matrix can be written as

$$B_p = B_0 + c_1 d_1^T + \ldots + c_p d_p^T = B_0 + CD^T, \quad (5)$$

where

$$c_{j+1} = \frac{y_j - B_j s_j}{\| s_j \|}$$

and

$$d_{j+1} = \frac{s_j}{\| s_j \|},\ j = 0, ..., p-1,$$

with $C = [c_1, ..., c_p]$ and $D = [d_1, ..., d_p]$. The update matrix $Q = CD^T$ is sum of p rank-one matrices, its rank does not exceed p. The singular values decomposition of Q is then given by

$$Q = \sigma_1 u_1 v_1^T + \ldots + \sigma_p u_p v_p^T, \quad (6)$$

where $\sigma_1 \geq \ldots \geq \sigma_p \geq 0$ are the singular values. The sets $\{u_1, \ldots, u_p\}$ and $\{v_1, \ldots, v_p\}$ are, respectively, the left and right corresponding singular vectors. By choosing $B_0 = I$, the matrix B_p can be stored using $2p$ vectors of length n.

Suppose the maximal rank of Q is fixed at p with $p << n$. Broyden rank reduction (BRR) method, see [7], is a variant of limited memory Broyden methods that approximates Q by a matrix $\tilde{Q}$ with low rank $q \leq p-1$ by truncating the singular value decomposition (6).

The current number of stored updates is denoted by m $(0 \leq m \leq p)$. The maximal number of updates to the initial Broyden matrix is thus given by p. If p updates are stored $(m = p)$, the singular value decomposition of Q is computed and the last $(p-q)$ singular values are removed just before the next update is computed. In this case, the next Broyden update will proceed using the modified matrix

$$\tilde{B}_k = B_k - R,$$

where $R = \sum_{l=q+1}^{p} \sigma_l u_l v_l^T$ is the so-called round-off matrix. No reduction is performed as long as $m < p$. Thus, the liberated memory is used to store $(p-q)$ new Broyden's updates according to the scheme (7)

$$B_{k+1} = \begin{cases} B_k + (y_k - B_k s_k)\dfrac{s_k^T}{s_k^T s_k} \\ -R\left(I - \dfrac{s_k s_k^T}{s_k^T s_k}\right) & \text{if } m = q+1, \\ B_k + (y_k - B_k s_k)\dfrac{s_k^T}{s_k^T s_k}, & \text{else.} \end{cases} \quad (7)$$

The BRR method, as presented in [7], does not give any idea how to fix *a priori* the rank of the matrix $\tilde{Q}$, only the smallest singular value is removed. But, in many cases there are more than one singular value that are close to zero and so they can be removed. In this case, memory will be free to store more than one Broyden's update. We propose here a new approach using a thresholding process of singular values of the update matrix by fixing a relative accuracy for the approximation of the matrix Q. In section 2 we present the new method and prove its local superlinear convergence. Section 3 is devoted to numerical results showing the efficiency of the method.

2. The proposed method

In many nonlinear problems, the singular values of the update matrix decay rapidly to zero, and more than one singular value can be removed. In figure 3 (see problem 3 in section 3) we present the singular values distribution of Q in case of the Spedicato function for $p = 6$ and $p = 10$. For example, when $p = 6$, we can see that the two last smallest singular values are zero while the third and the fourth ones are close to zero. In this example, the four last singular values can advantageously be removed as memory will be available to store four new Broyden updates and no singular values decomposition will be needed during the following four iterations.

So, the question is how, in general, to choose the rank q of $\tilde{Q}$ and thence the number of singular values to remove. As an answer to this question, we propose to use a tresholding process by exploiting the information about the approximation error $\| R \|_2$. Given a relative accuracy $\varepsilon > 0$ of the approximation $\tilde{Q}$, i.e.,

$$||Q - \tilde{Q}||_2 < \varepsilon ||Q||_2,$$

the required rank $q(\varepsilon)$ is given, if it exists, by

$$q(\varepsilon) = \min \{k \in \{1, \ldots, p-1\} \text{ s.t. } \sigma_{k+1} < \varepsilon\sigma_1\}. \quad (8)$$

The value of $q(\varepsilon)$ is calculated each time a reduction of the update matrix is needed, and all singular values satisfying the condition $\sigma_{l+1} < \varepsilon\sigma_1$, $l = 1, \ldots, p-1$ are removed. If there is no k satisfying (8), only the smallest singular value is removed (we turn back to the BRR method), and in this case $q = p-1$. So, the rank q will be chosen as

$$q = \begin{cases} q(\varepsilon) & \text{if } q(\varepsilon) \text{ exists,} \\ p-1 & \text{otherwise.} \end{cases} \tag{9}$$

This dynamical choice of q leads to a new method, displayed in Algorithm 1, which will be called dynamical Broyden rank reduction (DBRR) method.

In DBRR algorithm, the Sherman Morrison Woodbury formula, see [1], is used in order to compute the inverse of the Broyden matrix. If we set $B_0 = I$ we get

$$(I + CD^T)^{-1} = I - C(I + D^T C)^{-1} D^T.$$

In this case, we have only to solve linear systems of equations with $p \times p$ matrices. Note also that the singular value decomposition of the update matrix is carried out using an economical process, see [7]. Note that the error that is introduced by removing the last $(p-q)$ singular values of Q equals

$$||R|| = \begin{cases} \sigma_{q+1} & \text{for} \quad m = q+2, \\ 0 & \text{else.} \end{cases}$$

Let us now prove the superlinear convergence of the proposed algorithm.

Theorem 1. *Let q be defined as in (9) with*

$$||R|| \le \alpha \parallel s_k \parallel, \;\; s_k \neq 0, \;\; k \in \mathbb{N}, \tag{10}$$

where the constant α does not depend on k. Let, in addition, the classical hypotheses (CA) hold. Then the DBRR method has local superlinear convergence.

Proof. Define $E_k = B_k - F'(x_*)$ and $e_k = x_k - x_*$ for $k = 0, 1, \ldots$. To prove linear convergence of the proposed method, we need the following lemma whose proof can be found in [1], p. 77.

Lemma 1. *Let $F : \mathbb{R}^n \to \mathbb{R}^n$ be continuously differentiable in the open convex set $\mathcal{D} \subset \mathbb{R}^n$ and F' is γ-Lipschitz in $x \in \mathcal{D}$. Then, for any $u, v \in \mathcal{D}$,*

$$\begin{aligned} &\left\|F(v) - F(u) - F'(x)(v-u)\right\| \\ &\le \frac{\gamma}{2}\left(\|v-x\| + \|u-x\|\right)\|v-u\|. \end{aligned}$$

Equation (7) can be written as

$$\begin{aligned} E_{k+1} &= E_k\left(I - \frac{s_k s_k^T}{s_k^T s_k}\right) + \left(y_k - F'(x_*)s_k\right)\frac{s_k^T}{s_k^T s_k} \\ &\quad - R\left(I - \frac{s_k s_k^T}{s_k^T s_k}\right). \end{aligned} \tag{11}$$

Using Lemma 1 we have

$$\left\|y_k - F'(x_*)s_k\right\| \le \frac{\gamma}{2}\left(||e_{k+1}|| + ||e_k||\right)||s_k||, \tag{12}$$

where γ is the constant Lipschitz for F'. Thus we obtain, from equation (11), the so-called bounded deterioration property of the DBRR method

$$||E_{k+1}|| \le ||E_k|| + \left(\alpha + \frac{\gamma}{2}\right)\left(||e_{k+1}|| + ||e_k||\right), \tag{13}$$

since $||R|| = \sigma_{q+1} \le \alpha||s_k|| \le \alpha\left(||e_{k+1}|| + ||e_k||\right)$. We have used the fact that $\left(I - \frac{s_k s_k^T}{s_k^T s_k}\right)$ is an orthogonal projection and then its norm is equal to one. Inequality (13) implies local convergence of the DBRR method. In fact, as shown in [5], any quasi-Newton method that obeys the bounded deterioration property has local linear convergence. As consequences of the linear convergence, we have

$$||e_{k+1}|| \le \frac{1}{2}||e_k||, \quad k = 0, 1, \ldots, \tag{14}$$

and

$$\sum_{k=0}^{\infty} ||e_k|| \le 2||e_0||. \tag{15}$$

Since DBRR method satisfies the secant equation ($B_{k+1}s_k = y_k$), according to Theorem 8.2.4 in [1], a sufficient condition for $\{x_k\}_k$ to converge superlinearly to the root x_* is the so-called Dennis-Moré condition

$$\lim_{k \to +\infty} \frac{||E_k s_k||}{||s_k||} = 0. \tag{16}$$

Equation (11) also implies

$$\begin{aligned} ||E_{k+1}||_F &\le \left\|E_k\left(I - \frac{s_k s_k^T}{s_k^T s_k}\right)\right\|_F \\ &\quad + \left\|\left(y_k - F'(x_*)s_k\right)\frac{s_k^T}{s_k^T s_k}\right\|_F + ||R||_F, \end{aligned}$$

Algorithm 1. *Let $x_0 \in \mathbb{R}^n$ and $B_0 \in \mathbb{R}^{n\times n}$ be given. Set the parameter p and the accuracy $\varepsilon > 0$. Let $m = 0$.*

: *For $k = 0, 1, 2, ...$ until convergence,*

1. : *Solve $B_k s_k = -F(x_k)$ for s_k*

2. : $x_{k+1} = x_k + s_k$

3. : $y_k = F(x_{k+1}) - F(x_k)$

4. : *If $m = p$ then*

4.1. : *Compute the singular values decomposition of Q as in (6)*

4.2. : *Compute q as in (9)*

4.3. : *Reduce Broyden matrix:* $B_k = B_k - \sum_{i=q+1}^{p} \sigma_i u_i v_i^T$

4.4. : *Set $m = q$*

5. : *Update matrix B_k as in (7)*

6. : *Set $m = m + 1$*

where $||.||_F$ denotes the Frobenius norm. From equation (12), we obtain

$$\begin{aligned} & \left\| \left(y_k - F'(x_*)s_k\right) \frac{s_k^T}{s_k^T s_k} \right\|_F \\ = & \left\| \left(y_k - F'(x_*)s_k\right) \frac{s_k^T}{s_k^T s_k} \right\| \\ \leq & \frac{\gamma}{2}\left(||e_{k+1}|| + ||e_k||\right). \end{aligned}$$

The following lemma, where the proof can be found in [1], p. 183, will be useful in the sequel.

Lemma 2. *Let $s \in \mathbb{R}^n$ be nonzero and let $E \in \mathbb{R}^{n\times n}$. Then*

$$\left\| E\left(I - \frac{ss^T}{s^T s}\right)\right\|_F \leq \|E\|_F - \frac{1}{2\|E\|_F}\left(\frac{||Es||}{||s||}\right)^2.$$

Using inequality (14) and Lemma 2 we derive

$$\begin{aligned} ||E_{k+1}||_F &\leq ||E_k||_F - \tfrac{||E_k s_k||^2}{2||E_k||_F ||s_k||^2} \\ &+ \tfrac{3}{4}\gamma||e_k|| + ||R||_F \\ &\leq ||E_k||_F - \tfrac{||E_k s_k||^2}{2||E_k||_F ||s_k||^2} \\ &+ \tfrac{3}{4}\left(\gamma + 2\alpha\sqrt{n}\right)||e_k||. \end{aligned}$$

This inequality is equivalent to

$$\frac{||E_k s_k||^2}{||s_k||^2} \leq 2||E_k||_F \left(||E_k||_F - ||E_{k+1}||_F + \frac{3}{4}(\gamma + 2\alpha\sqrt{n})||e_k||\right). \quad (17)$$

Using inequality (15) we show that

$$\sum_{k=0}^{+\infty} \frac{||E_k s_k||^2}{||s_k||^2} \leq 2c\left(||E_0||_F + \frac{3}{2}(\gamma + 2\alpha\sqrt{n})||e_0||\right),$$

where $c > 0$ is an upper bound of the sequence $\{E_k\}_k$. Hence, condition (16) is satisfied and the superlinear convergence is proved. □

3. Numerical results

We present now numerical tests by applying the proposed method to some classical test functions from the literature and we present a comparison of this method with the classical BRR method ($q = p-1$). The numerical experiments were carried out using the scientific computing software MATLAB. We use the following stopping criterion for our computer programs

$$||F(x_k)|| < \varepsilon_a + \varepsilon_r ||F(x_0)||,$$

where $\varepsilon_a = 10^{-15}$ and $\varepsilon_r = 10^{-15}$ (respectively, absolute and relative tolerances). For both BRR and DBRR methods most of the computational time is spent in evaluations of the function F and computation of the singular values decomposition of the update matrix.

Problem 1

Let us consider the trigonometric system

$$\begin{cases} F_1(x) &= \cos(x_1) - 9 + 3x_1 + 8\exp(x_2), \\ F_i(x) &= \cos(x_i) - 9 + 3x_i + 8\exp(x_{i-1}), \quad i = 2, \ldots, n-1, \\ F_n(x) &= \cos(x_i) - 1. \end{cases}$$

The size of this problem is $n = 1000000$, and the initial guess is given by $x_0 = (1.2, \ldots, 1.2)^T$. We plot in figure 1 the distribution of singular values of the update matrix for $p = 5, 8, 10$ and

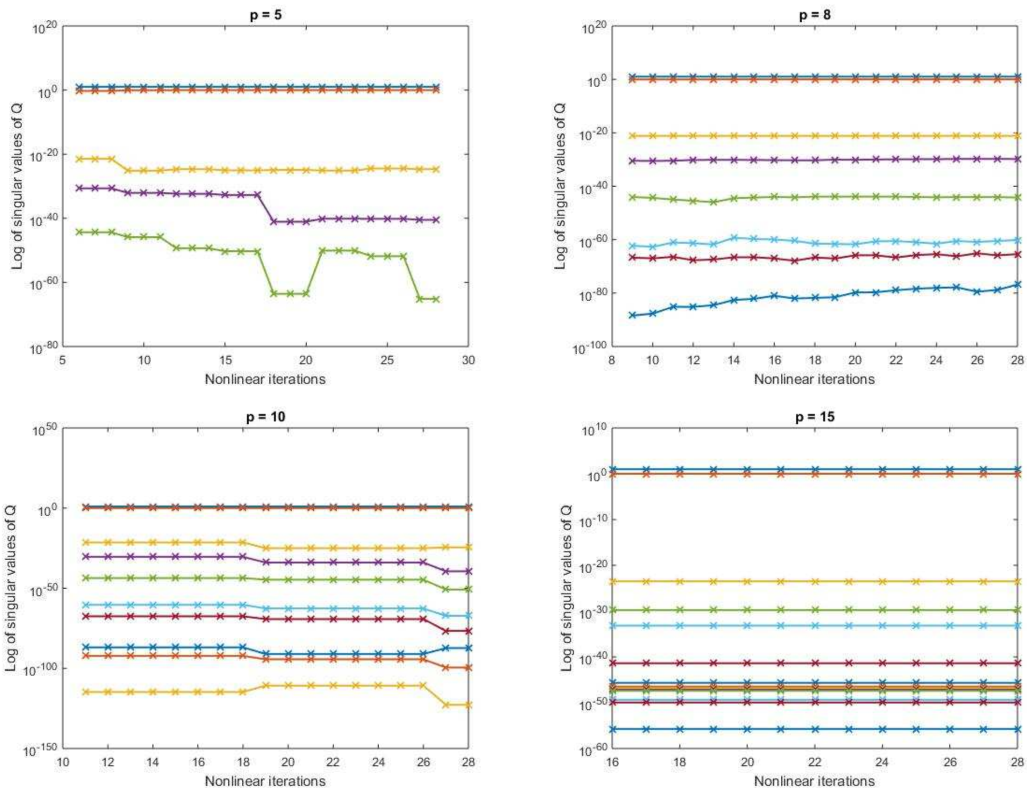

Figure 1. Singular values of the update matrix Q for $p = 5, 8, 10$ and $p = 15$ for Problem 1.

$p = 15$. For these values of p, the update matrix has rank two in all nonlinear iterations. Hence, the DBRR method requires less singular values decomposition calls. The size of this problem is $n = 1000000$, and the initial guess is given by $x_0 = (1.2, \ldots, 1.2)^T$. We plot in figure 1 the distribution of singular values of the update matrix for $p = 5, 8, 10$ and $p = 15$. For these values of p, the update matrix has rank two in all nonlinear iterations. Hence, the DBRR method requires less singular values decomposition calls.

For this example both BRR and DBRR do not converge for $p \leq 4$. Performances of DBBR and BRR methods, for different values of p, are presented in tables 1 and 2, respectively. For all p values, the choice of ε does not significantly affect the convergence rate and the computational time.

Problem 2

We consider now the so-called extended system of Byeong

$$F_i(x) = \cos(x_i^2 - 1) - 1, \quad i = 1, \ldots, n.$$

The size of this problem is $n = 1000000$, and the initial guess is given by $x_0 = (0.0087, \ldots, 0.0087)^T$. For this example, the update matrix has rank one during all nonlinear iterations, see figure 2.

So, whenever a reduction of the update matrix is needed, $(p - 1)$ singular values are removed freeing the memory to store new updates. For a given value of p, the choice of the parameter ε does not affect the performance of DBRR method as shown in table 3. A comparison of tables 3 and 4 shows the efficiency of the singular values thresholding process.

Problem 3

In this example, we compute the root of the so-called Spedicato function

$$F_i(x) = \begin{cases} 1 - x_i & \text{if} \quad i \quad \text{odd}, \\ 10(x_i - x_{i-1}^2) & \text{if} \quad i \quad \text{even}, \end{cases}$$

for $i = 1, \ldots, n$. The size of this problem is $n = 1000000$, and the initial guess is given by $x_0 = (-1.2, \ldots, -1.2)^T$. Both BRR and DBRR methods do not converge for $p \leq 4$. The rank of Q increases with the nonlinear iterations as shown in figure 3.

Performances of DBBR and BRR methods are presented in tables 5 and 6, respectively.

Problem 4

We consider the nonlinear convection-diffusion partial differential equation

Table 1. Performance of the DBRR method for Problem 1.

	$p=5$				$p=8$			
$\varepsilon =$	10^{-2}	10^{-4}	10^{-6}	10^{-10}	10^{-1}	10^{-3}	10^{-5}	10^{-10}
Iters	28	28	28	28	28	28	28	28
CPU time	10.865	11.104	12.011	11.021	10.380	12.417	12.879	11.505
SVD calls	8	8	8	8	3	4	4	4
SVD time	2.961	3.106	3.338	3.024	1.435	3.308	3.386	2.999
% SVD time	27.2	28.0	27.7	27.5	13.8	26.6	26.3	26.1
	$p=10$				$p=15$			
$\varepsilon =$	10^{-1}	10^{-3}	10^{-5}	10^{-10}	10^{-1}	10^{-3}	10^{-5}	10^{-10}
Iters	28	28	28	28	28	28	28	28
CPU time	10.989	13.712	13.235	12.897	14.436	13.227	13.224	13.269
SVD calls	2	3	3	3	1	1	1	1
SVD time	1.296	3.713	3.244	3.233	1.436	1.220	1.200	1.220
% SVD time	11.8	27.1	26.0	25.0	9.9	9.8	9.8	9.9

Table 2. Performance of the BRR method for Problem 1.

p	5	8	10	15
Iters	28	28	28	28
CPU time	18.315	26.526	36.235	34.971
SVD calls	23	20	18	13
SVD time	8.440	14.558	21.079	27.623
% SVD time	46.1	54.9	58.9	62.8

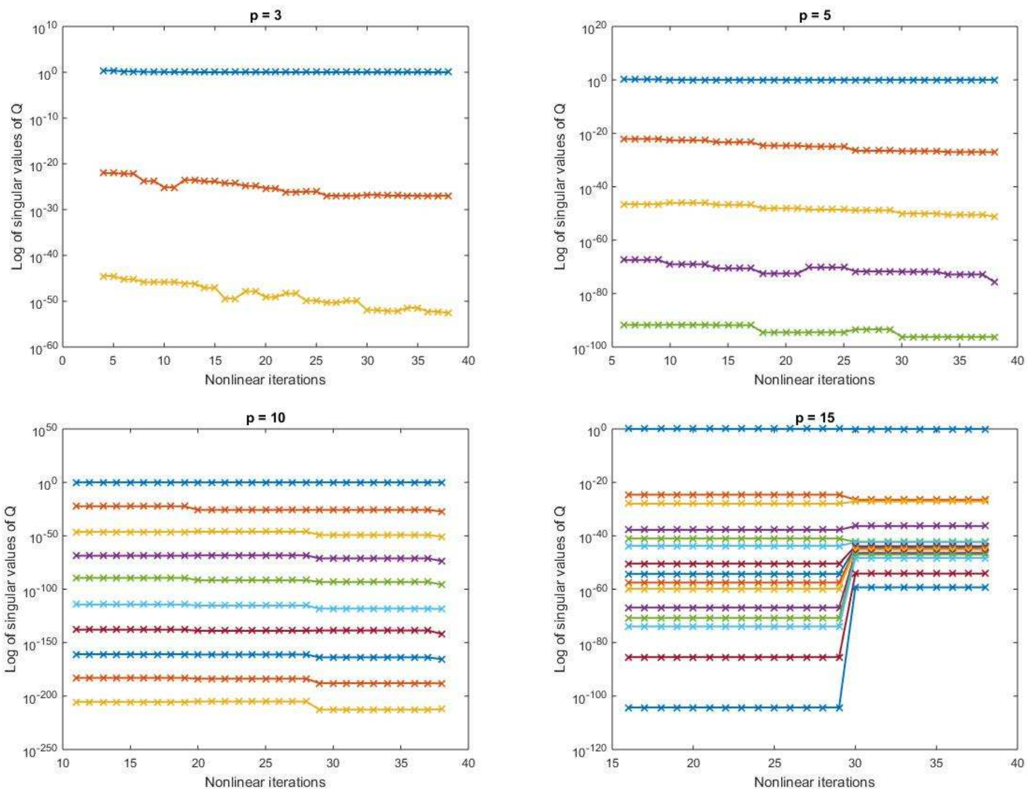

Figure 2. Singular values of the update matrix Q for $p = 3, 5, 10$ and $p = 15$ for Problem 2.

$$-\Delta u + Cu\left(\frac{\partial u}{\partial x} + \frac{\partial u}{\partial y}\right) = f \tag{18}$$

with homogeneous Dirichlet boundary conditions on the unit square $(0,1) \times (0,1)$. As in [2], the source f has been constructed so that the exact solution is

$$10xy(1-x)(1-y)\exp(x^{4.5}).$$

Table 3. Performance of the DBRR method for Problem 2.

	$p=3$				$p=5$			
$\varepsilon =$	10^{-1}	10^{-3}	10^{-5}	10^{-10}	10^{-1}	10^{-3}	10^{-5}	10^{-10}
Iters	38	38	38	38	38	38	38	38
CPU time	10.588	10.566	10.647	10.839	11.434	11.333	11.606	11.265
SVD calls	18	18	18	18	9	9	9	9
SVD time	3.399	3.340	3.310	3.381	3.507	3.446	3.461	3.428
% SVD time	32.1	31.6	31.1	32.2	30.7	30.4	29.9	30.5
	$p=10$				$p=15$			
$\varepsilon =$	10^{-1}	10^{-3}	10^{-5}	10^{-10}	10^{-1}	10^{-3}	10^{-5}	10^{-10}
Iters	38	38	38	38	38	38	38	38
CPU time	14.705	14.778	14.795	14.693	17.930	19.642	19.851	17.810
SVD calls	4	4	4	4	2	2	2	2
SVD time	4.505	4.462	4.490	4.500	5.244	6.257	4.260	5.224
% SVD time	30.7	30.2	30.4	30.7	29.2	31.8	29.6	29.39

Table 4. Performance of the BRR method for Problem 2.

p	3	5	10	15
Iters	38	38	38	38
CPU time	14.531	22.864	46.849	78.311
SVD calls	35	33	28	23
SVD time	6.225	12.021	29.772	3
% SVD time	46.1	54.9	58.9	62.8

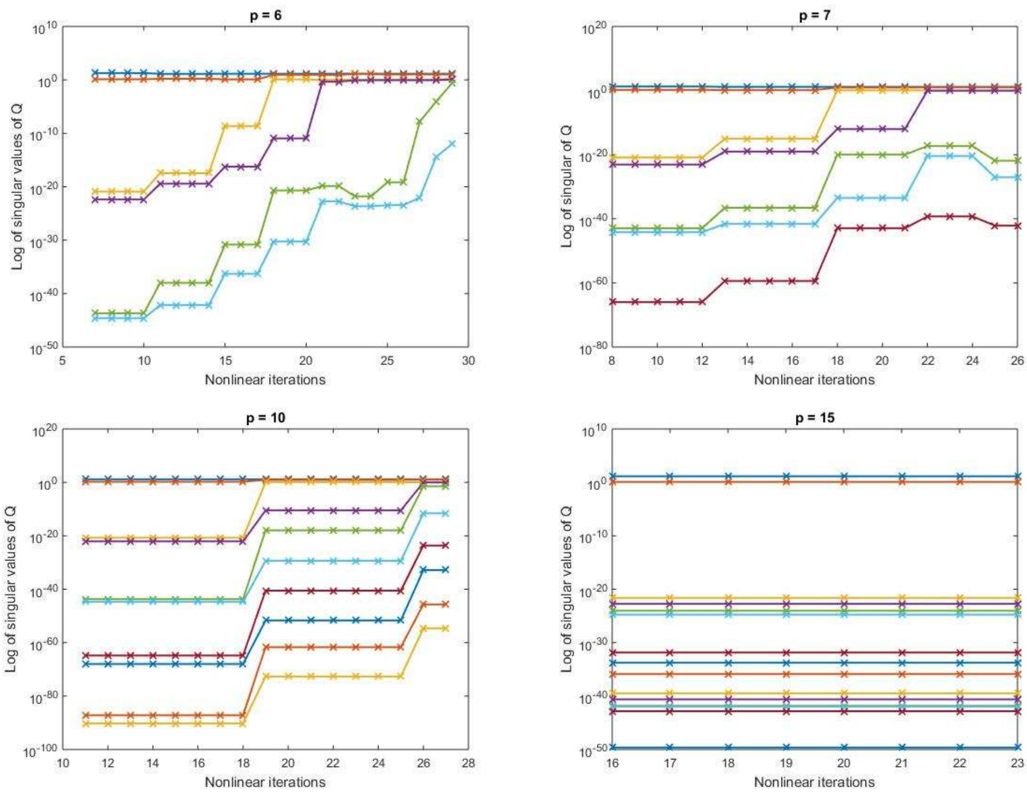

Figure 3. Singular values of the update matrix Q for $p = 6$, 7, 10 and $p = 15$ for Problem 3.

We set $C = 20$ and $u_0 = 0$. Equation (18) is discretized on a 500×500 grid using centered differences. Evolution of the sigular values of Q is displayed in figure 4 for different values of p.

For $p \leq 5$ the rank of Q is p, and only the p^{th} singular value is removed. In this case, BRR and DBRR methods behave similarly, see tables 7 and 8. For $p = 10$ the rank of Q is ten but condition (8) is satisfied in the first iterations for $\varepsilon = 10^{-1}$

Table 5. Performance of the DBRR method for Problem 3.

	$p=6$				$p=7$			
$\varepsilon =$	10^{-1}	10^{-3}	10^{-5}	10^{-10}	10^{-1}	10^{-3}	10^{-5}	10^{-10}
Iters	34	30	30	29	35	31	31	31
CPU time	64.624	59.187	48.712	62.041	62.158	60.539	53.024	56.152
SVD calls	7	10	10	10	6	7	7	8
SVD time	3.588	5.334	5.085	5.229	4.109	4.695	4.756	5.039
% SVD time	5.6	9.0	10.5	8.4	6.6	7.7	8.9	9.0
	$p=10$				$p=15$			
$\varepsilon =$	10^{-1}	10^{-3}	10^{-5}	10^{-10}	10^{-1}	10^{-3}	10^{-5}	10^{-10}
Iters	44	28	28	28	22	22	22	22
CPU time	88.144	50.620	57.985	47.654	39.766	47.879	48.934	40.140
SVD calls	5	3	3	3	1	1	1	1
SVD time	7.098	3.698	2.262	4.777	1.232	1.232	1.638	1.201
% SVD time	6.9	7.3	3.9	7.9	3.1	3.1	3.3	3

Table 6. Performance of the BRR method for Problem 3.

p	6	7	10	15
Iters	30	26	26	22
CPU time	66.512	64.398	74.920	55.834
SVD calls	24	19	16	17
SVD time	13.291	11.841	16.890	15.771
% SVD time	20.0	18.4	22.5	28.3

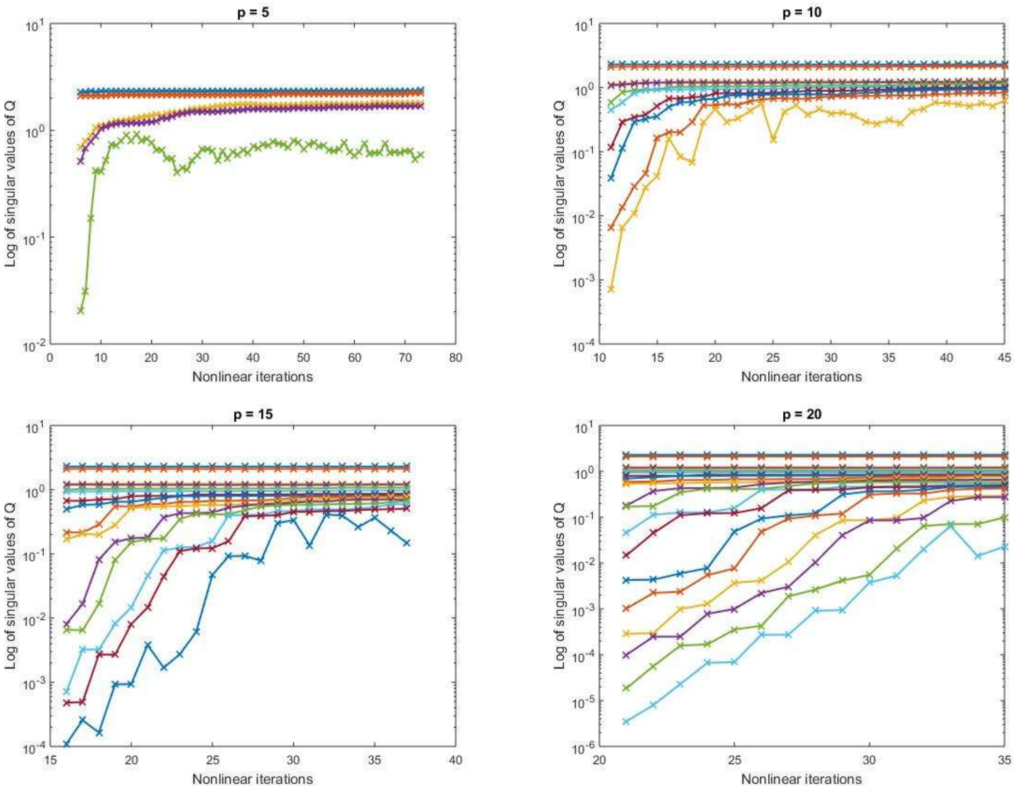

Figure 4. Singular values of the update matrix Q for $p = 5$, 10, 15 and $p = 20$ for Problem 4.

since, in this case, $q = 6$ at iteration 11 and $q = 8$ at both iterations 15 and 17. For $p = 20$ the rank of Q increases with nonlinear iterations, but condition (8) is satisfied for $\varepsilon = 10^{-1}, 10^{-3}, 10^{-5}$.

4. Conclusion

We have introduced a new Broyden rank reduction method to solve systems of nonlinear equations. The method is based on a thresholding

Table 7. Performance of the DBRR method for Problem 4.

	$p = 5$				$p = 10$			
$\varepsilon =$	10^{-1}	10^{-3}	10^{-5}	10^{-7}	10^{-1}	10^{-3}	10^{-5}	10^{-7}
Iters	73	73	73	73	45	45	45	45
CPU time	23.510	24.832	25.525	23.745	20.925	23.673	22.265	22.154
SVD calls	68	68	68	68	30	35	35	35
SVD time	5.945	6.283	6.406	5.960	7.608	9.508	9.083	8.976
% SVD time	25.3	25.7	25.1	25.1	36.8	40.1	40.8	40.5
	$p = 15$				$p = 20$			
$\varepsilon =$	10^{-1}	10^{-3}	10^{-5}	10^{-7}	10^{-1}	10^{-3}	10^{-5}	10^{-7}
Iters	36	38	37	37	36	35	35	35
CPU time	19.294	24.411	27.716	27.530	14.555	20.106	26.488	27.106
SVD calls	11	21	22	22	3	9	14	15
SVD time	6.797	10.992	13.067	12.661	2.979	8.078	12.978	13.575
% SVD time	35.4	45.1	47.2	46	20.5	40.2	49.0	50.1

Table 8. Performance of the BRR method for Problem 4.

p	5	10	15	20
Iters	73	45	37	35
CPU time	23.525	22.326	25.567	29.168
SVD calls	68	35	22	15
SVD time	5.825	9.002	12.045	14.646
% SVD time	24.8	41.0	47.1	50.9

process of the Broyden matrix singular values. All singular values of the update matrix that are smallest than a given threshold are removed. We have proved the local superlinear convergence and numerically tested the method on a variety of problems. As compared to classical Broyden rank reduction, our method induces a significant reduction of the execution time (CPU time) by reducing the number of calls of the singular values decomposition. As a perspective of this work is to combine the proposed method with that presented in [8].

Acknowledgements

This work has been partially supported by Hydrinv Euro-Mediterranean Project, LERMA, LIRIMA, IMIST and CNRST.

References

[1] Dennis, J. E. and Schnabel, R. B. (1983). Numerical methods for unconstrained optimization and nonlinear equations. Prentice-Hall.

[2] Kelley, C. T. (1995). Iterative methods for linear and nonlinear equations. Volume 16 of Frontiers in Applied Mathematics, SIAM, Philadelphia.

[3] Ortega, J. M. and Reinboldt, W. C. (2000). Iterative solution of nonlinear equations in several variables. SIAM, Philadelphia.

[4] Broyden, C. G. (1965). A class of methods for solving nonlinear simultaneous equations. *Mathematics of Computation*, (19), 577–593.

[5] Broyden, C. G., Dennis, J. E. and Moré, J. J. (1973). On the local and superlinear convergence of quasi-Newton methods. *IMA Journal of Applied Mathematics*, (12), 223–245.

[6] Byrd, R. H., Nocedal, J. and Schnabel, R. B. (1994). Representations of quasi-Newton matrices and their use in limited memory methods. *Mathematical Programming*, (63), 129–156.

[7] Van De Rotten, B. and Verduyn Lunel, S. M. (2003). A limited memory Broyden method to solve high dimensional systems of nonlinear equations. Technical Report MI 2003-06, Mathematical Institute, University of Leiden, The Netherlands.

[8] Ziani M. and Guyomarc'h F. (2008). An autoadaptative limited memory Broyden's method to solve systems of nonlinear equations. *Applied Mathematics and Computation*, (205), 202–211.

Mostafa Ouarit *is currently an Associate Professor and member of the Laboratory of Modelling, Analysis, Control and statistics at the Faculty of Sciences Ain Chock, Hassan II University Of Casablanca, Morocco. He received the PhD degree in Applied Mathematics at University of Technology of Compiégne, France. His research interests are in the areas of numerical analysis, optimization and optimal control.*

Ali Souissi *is Professor at the faculty of sciences, Mohammed V University, Rabat, Morocco. His main areas of interest are Scientific Computing, Optimal shape Design and Numerical Analysis of Partial Differential Equations. He received the PhD in Applied Mathematics from Laval University, Canada. He has publications in well-known journals and supervised many PhD theses.*

Mohammed Ziani *received his PhD in applied Mathematics at the University of Rennes (France) and Mohammed V University in Rabat (Morocco). He is professor of applied Mathematics at Faculty of sciences in Rabat. His research interests include issues related to solving large nonlinear systems of equations and partial differential equations based image processing.*

An International Journal of Optimization and Control: Theories & Applications (http://ijocta.balikesir.edu.tr)

An International Journal of Optimization and Control: Theories & Applications
ISSN: 2146-0957 eISSN: 2146-5703
Vol.9, No.2, pp.186-196 (2019)
https://doi.org/10.11121/ijocta.01.2019.00711

RESEARCH ARTICLE

A genetic algorithm for fuzzy order acceptance and scheduling problem

Esra Karakaş [a] *, Hakan Özpalamutçu [b]

[a] *Department of Business Administration, Adana Alparslan Türkeş Science and Technology University, Turkey*
[b] *Department of Industrial Engineering, Adana Alparslan Türkeş Science and Technology University, Turkey*
ekarakas@atu.edu.tr, hakan.ozpalamutcu@temsa.com

ARTICLE INFO

Article history:
Received: 19 September 2018
Accepted: 3 April 2019
Available Online: 23 April 2019

Keywords:
Fuzzy programming
Order acceptance and Scheduling
Signed distance
Integral value
Genetic algorithm

AMS Classification 2010:
90C70, 78M32

ABSTRACT

In light of the imprecise and fuzzy nature of real production environments, the order acceptance and scheduling (OAS) problem is associated with fuzzy processing times, fuzzy sequence dependent set up time and fuzzy due dates. In this study, a genetic algorithm (GA) which uses fuzzy ranking methods is proposed to solve the fuzzy OAS problem. The proposed algorithm is illustrated and analyzed using examples with different order sizes. As illustrative numerical examples, fuzzy OAS problems with 10, 15, 20, 25, 30 and 100 orders are considered. The feasibility and effectiveness of the proposed method are demonstrated. Due to the NP-hard nature of the problem, the developed GA has great importance to obtain a solution even for big scale fuzzy OAS problem. Also, the proposed GA can be utilized easily by all practitioners via the developed user interface.

1. Introduction

Make to Order (MTO) is a production strategy in which manufacturing starts once a customer's order is received. In a MTO production environment, manufacturers offer more customized products to appeal their potential customers. However, limitations on manufacturing capacity generally require manufacturers to make a selection among incoming customer orders. On top of this, while deciding which orders to accept, manufacturers have to simultaneously determine the schedule of these orders over a time frame that will make efficient use of their capacities. This problem, which involves the joint decision of order acceptance and order scheduling, is called the order acceptance and scheduling (OAS) problem [1]. The OAS problem arises from the limited the production capacity that is characteristic of MTO environment.

Based on Slotnick's detailed review and taxonomy of OAS problems [1], it is clear that numerous versions of OAS problems within various settings and with different objectives have been studied over the last decades. In this study, we concentrate on the OAS problem in a single machine environment. The single machine environment is one of the most commonly studied environments in scheduling literature [2]. Since many multi-machine environments generally have a bottleneck machine, which significantly affects the overall performance of the system, this machine can be isolated and considered as a single machine.

Some of the single machine problem studies take into account maximization of profit. Charnsirisaksul et al. [3] examined a mixed integer programming formulation in a preemptive environment with the goal of maximizing the producer's profit. Profit is defined as revenues obtained from all the accepted orders minus all the manufacturing, holding and tardiness costs. They later extended this study by including lead time flexibility into the model. They showed the benefits of lead-time flexibility through numerical analyses [4]. Slotnick and Morton [5] took into account the order acceptance decision with weighted lateness as the time-related penalty by calculating profit in single-machine OAS problem. Since the problem is NP-hard, an optimal branch and bound procedure and several heuristics that integrate the scheduling and acceptance decisions were proposed to solve the problem. Rom and Slotnick [6] presented a GA approach for OAS problem with customer weighted tardiness. They claimed that the proposed approach performed better than previous heuristics in terms of solution quality. Oguz et al. [7] incorporated sequence-dependent setup times in the OAS model. The proposed model maximized profit which is defined as revenues of accepted orders minus total weighted tardiness penalties. They also identified

*Corresponding author

two different due-dates: a preferred due-date after which a tardiness penalty is incurred, and the strict deadline after which the customer will not take the order. They assumed that the revenue gained from an accepted order decreases linearly with the order's tardiness until its deadline. A mixed integer linear programming (MILP) was formulated and solved optimally for small scale problems with 10 or 15 orders. In addition, they devised a simulated annealing (SA) algorithm and two constructive heuristics to solve larger scale problems. Nobibon and Leus [8] presented two branch and bound algorithms, along with heuristic algorithms, for the OAS problem, in which orders were characterized by deterministic processing time, delivery dates, revenues and the weight representing a penalty per unit time delay. Cesaret et al. [9] developed a tabu search (TS) algorithm that included a probabilistic local search procedure. The problem involved the sequence-dependent setup times, due dates and deadlines, and release dates for orders. The other meta-heuristic solution methodology was developed by Lin and Ying [10]. They suggested artificial bee colony (ABC) based algorithm to solve the single machine OAS problem with sequence-dependent setup times and release dates. The performance of the proposed algorithm was tested by a benchmark problem set containing test instances with up to 100 orders. Chen et al. [11] put forward an improved GA with a diversity controlling mechanism for the OAS problem with sequence dependent set up times, tardiness penalties and distinct release dates. They demonstrated that the developed diversity controlling mechanism was effective in improving solution quality in most of the used benchmark instances. Xie and Wang [12] formulated an OAS problem where each order has a known processing time, due date, revenue and set up time. The objective was to maximize the total revenue. To solve the problem, firstly they utilized basic ABC algorithm. Then taking into consideration the result of the first methodology, they developed an improved ABC algorithm by making some modifications. Zandieh and Roumani [13] proposed two meta-heuristic solutions: a biogeography-based optimization (BBO) algorithm and a GA for solving the OAS problem. They then compared the computational results of the algorithms and found that the BBO algorithm outperforms GA, especially for large size instances. Chaurasia and Singh [14] presented two hybrid metaheuristic algorithms, namely hybrid steady-state genetic algorithm (SSHGA) and hybrid evolutionary algorithm with guided mutation (EA/G). They defined the OAS problem the same as the study of Lin and Ying [10].

In the literature, there are also some studies with stochastic order arrivals. Wester et al. [15] presented a simulation model with Poisson order arrivals and limited capacity in a single machine environment. They developed three different order acceptance strategies and compare their performance via simulation experiments. De et al. [16] examined the OAS problem with random processing times and a random common due date. Stadje [17] presented scheduling and selecting procedures with random common due date and processing times to maximize the total expected reward by selecting and scheduling a predetermined number of orders. The machine was subjected to random breakdowns that cause processing to terminate. Two optimal procedures which involve myopic properties were presented. Rogers and Nandi [18] used simulation for the OAS with the objective of maximizing net profit, defined as revenue minus tardiness. Kate [19] compared various approaches to OAS problem with random arrivals via Simulation. Carr and Duenyas [20] took into account both make to stock (MTS) and MTO product classes, with random arrivals and processing times, and preemption. Their computational studies demonstrated that the performance of the policy that includes joint decision making in the OAS was superior to the other policy in which these decisions were made separately.

To the best of our knowledge, Koyuncu [21] was the first researcher to study the fuzzy OAS problem. In this study, fuzzy mixed integer linear programming model (fuzzy MILP) for a single machine OAS problem was proposed and the orders were defined by their fuzzy due dates, fuzzy processing times and fuzzy sequence dependent set up times. The proposed fuzzy MILP model was first converted into the equivalent crisp model using the signed distance method and then solved optimally via an appropriate package programme.

It is proved that the OAS problem is strongly NP-hard [9], so the fuzzy OAS problem is also strongly NP-hard. This means that an exact solution can be obtained only for small scale problems. In the light of above literature summary, there is not any meta-heuristic approach in the literature to solve the real-world complex fuzzy OAS problem. In the present study, a GA approach that uses ranking methods is developed to solve the fuzzy OAS problem. The proposed GA enables solving the fuzzy OAS problems with even hundreds of order. In addition, the fuzzy OAS problem is solved directly without transforming the model into the crisp equivalent.

The organization of this paper is as follows. In the next section, the problem description and formulation is presented. In Section 3, the proposed GA is illustrated. In Section 4, the computational results are discussed and in Section 5, the conclusions are presented.

2. Problem description and formulation

As mentioned in Section 1, there are various OAS problem formulations with different objective functions and different assumption settings in the literature. However, the parameters of the OAS problem in these studies are deterministic or stochastic except the study of Koyuncu [21]. Koyuncu [21] defined a fuzzy OAS problem and solved using a fuzzy MILP model. However, exact solutions can only be obtained for the small scale OAS problems using fuzzy MILP model. The aim of the present study is to develop a solution methodology based on a GA approach in order to solve the fuzzy OAS problem in any scale. Profit maximization is considered as the objective of the model and it is assumed that a set of incoming orders is available at the beginning. The schedule is non-preemptive, which means that when an order starts to be processed on the machine, the process cannot be interrupted before its completion.

In most production environments, scheduling frequently has inherent resource-related and/or job-related uncertainties [22]. Furthermore, poor reliability in the production process on account of issues such as machine hold-ups and man-made factors, may cause for example uncertainty in the processing and set up times. Thus, crisp processing and crisp sequence dependent set up times cannot reflect the real problem appropriately. As mentioned before, in the OAS literature, there are some stochastic OAS problems that represent uncertainties via stochastic modeling, where processing times and due dates are generally assumed to be random variables with a known probability distribution [17]. In real life situations, it may not be possible to obtain enough prior information to characterize the probability distribution of a random processing time. This is especially the case in MTO environments, where firms offer more customized and unique products that can be novel for them. Under such circumstances, it is extremely hard to get exact information or enough historical information to construct a probability distribution of processing and sequence dependent set up times. Taking this condition into account, a fuzzy OAS problem with profit maximization are defined in the present study.

In the presented fuzzy OAS problem, the fuzzy processing time of orders ($\breve{p}_i$), fuzzy sequence dependent set up time ($\check{S}_{ij}$) and fuzzy due date $\breve{d}_i$ are represented by a triangular fuzzy number (TFN). Fuzzy number $\widetilde{A}$, denoted by triplet (a_1, a_2, a_3) $where\ a_1 < a_2 < a_3$, is called a triangular fuzzy number if its membership function $\mu_{\widetilde{A}}$ is defined as;

$$\mu_{\tilde{A}} = \begin{cases} 0, x < a_1\ , x > a_3 \\ \frac{x-a_1}{a_2-a_1},\ \ a_1 < x < a_2 \\ \frac{a_3-x}{a_3-a_2}, a_2 < x < a_3 \\ 0, x > a_3 \end{cases} \tag{1}$$

The notations related to the formulation of the fuzzy OAS problem are as follows:

i: order index (i= 1,2,….n, i$\in SO$)

j: order index (j$= 0,1, \ldots . n+1,\ \ j \in SO$)

r_i: unit revenue of order i

$\tilde{s}_{ij}$: fuzzy sequence dependent set up times

$\tilde{p}_i$: fuzzy processing time of order i

$\tilde{d}_i$: fuzzy due date of order i

$\tilde{c}_i$: fuzzy completion time of order i

It is assumed that a set of independent orders (SO) is given at the beginning of the planning period. For each order i∈SO, data on fuzzy processing time $\tilde{p}_i$, fuzzy due date $\tilde{d}_i$, and fuzzy sequence dependent set up times $\tilde{s}_{ij}$ are available. Revenue of order i (r_i) denotes unit gain from order i. The manufacturer must complete order i until its fuzzy due date ($\tilde{d}_i$).

The objective is to find a processing sequence of all accepted orders on the single machine that maximizes the total revenue (TR), which can be formulated as:

$$\text{TR} = \text{Max} \sum_{i=1}^{n} r_i x_i \tag{2}$$

where,

x_i denotes a binary variable which equals to 1 if order i is accepted, or 0 otherwise.

For a given sequence of the order set, $\tilde{C}_j$ can be calculated as follows:

$\tilde{C}_i + (\tilde{s}_{ij} + \tilde{p}_j) = \check{C}_j$ (if order i is processed immediately before order j.) (3)

Then, the fuzzy completion time of order j can be compared with the fuzzy due date of order j. After the comparision, the acceptance decision of order j is made as in Eq. (4):

If $\check{C}_j \le \tilde{d}_j$ Accept Order j (4)

ELSE Reject Order j

If accepted, order j is scheduled after order i and the revenue gained from order j is added to the total revenue.

Comparison of fuzzy numbers can be made using various ranking methods. In this study, we employ the signed distance method and ranking based on the integral value method to make the acceptance decision in Eq.(4). Therefore, the proposed GA also includes the selected ranking method, which is explained in Section 3.

The other issue is the arithmetic of fuzzy numbers in the problem formulation. When two triangular fuzzy numbers are added or subtracted, the obtained fuzzy number will be a triangular fuzzy number. So, the calculation in Eq. (3) does not change the type of fuzzy number.

3. Proposed genetic algorithm

In the proposed formulation, there are fuzzy numbers in constraints, so the ranking methods are used to determine the feasibility of the constraints. This approach was proposed by Baykosoglu and Gocken [23] and is called the direct solution approach.

Two types of ranking methods are used in the solution approach. The first method is the signed distance method, and the second method is the integral value based method proposed by Liou and Wang [24].

3.1. Ranking fuzzy number using the signed distance method

The definition of signed distance for fuzzy numbers has some similar properties to those of the signed distance defined for the set of real numbers.

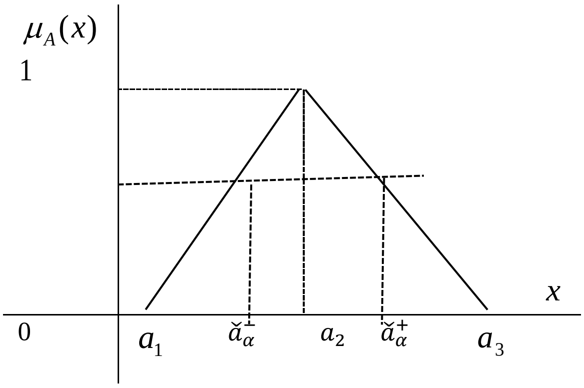

Figure 1. Triangular fuzzy number

The α level set of fuzzy triangular number $\widetilde{A}$, described in Figure 1, is defined as $\breve{a}_\alpha = \{x \backslash \mu_{\breve{a}}(x) \geq \alpha\}$ and can be represented by $\breve{a}_\alpha = [\breve{a}_\alpha^-, \breve{a}_\alpha^+]$ where $\breve{a}_\alpha^-$ and $\breve{a}_\alpha^+$ are the left and right end points, respectively. For the fuzzy number $\widetilde{A}$, $\breve{a}_\alpha^- = a_1 + (a_2 - a_1) \propto$ measures the signed distance of the left end point of the $\propto$ level set $[\breve{a}_\alpha^-, \breve{a}_\alpha^+]$ from the origin, and $\breve{a}_\alpha^+ = a_3 + (a_3 - a_2) \propto$ measures the signed distance of the right end point of the α-level set $[\breve{a}_\alpha^-, \breve{a}_\alpha^+]$ from the origin. Their average, $\frac{1}{2}(\breve{a}_\alpha^- + \breve{a}_\alpha^+)$, is taken as the signed distance of this α-level set from origin. The signed distance of $\breve{a}_\alpha$ from origin $d(\widetilde{a})$ is defined as the average of the signed distances of the α-level sets of $\widetilde{a}$ over $\alpha \in [0,1]$. It is calculated as [25]:

$$d(\breve{a}) = \int_0^1 \left[\frac{1}{2}(\breve{a}_\alpha^- + \breve{a}_\alpha^+)\right] d\alpha = \frac{1}{4}(2a_2 + a_1 + a_3) \quad (5)$$

Let $\widetilde{a}$ and $\widetilde{b}$ be two fuzzy numbers; their ranking relation is defined as:

$$\widetilde{a} \leq \widetilde{b} \leftrightarrow d(\breve{a}) \leq d(\breve{b}) \quad (6)$$

3.2. Ranking fuzzy number with integral value

Liou and Wang [24] develop an approach for ranking fuzzy numbers with integral value. This method takes into account the decision maker's degree of optimism $\alpha \in [0,1]$. The ranking method of Liou and Wang [24] is comparatively easy in computation, especially in ranking triangular and trapezoidal fuzzy numbers. This method can be used to rank more than two fuzzy numbers simultaneously. The definition of integral values for the triangular fuzzy number $\widetilde{A}$ is given as follows [26]:

$$I(\breve{A}) = \frac{1-\alpha}{2} a_1 + \frac{1}{2} a_2 + \frac{\alpha}{2} a_3 \quad (7)$$

where $0 \leq \alpha \leq 1$

3.3. Genetic algorithm for fuzzy OAS problem

Since the OAS problem has been proven to be NP-hard [7], no exact method can obtain an optimal solution in a reasonable computational time when the problem sizes are large. For this reason, some researchers use meta-heuristics to solve the OAS problem. In the present study, a GA approach with fuzzy ranking methods is proposed to solve the fuzzy OAS problem.

Genetic algorithms (Gas) are stochastic search techniques for approximating optimal solutions within complex search spaces. They are based on the process of natural selection. Before a GA can be run, a suitable encoding or representation for the solution of the problem must be developed. A fitness function is also needed. It assigns a value to each encoded solution to estimate the quality of the represented solution [27]. Starting with a randomly generated population of chromosomes, a GA performs a process of fitness based selection and recombination to produce the next generation. During the run, genetic operators (selection, crossover) are applied to parent chromosomes and their genetic materials are recombined to produce child chromosomes (offspring). As this process is iterated, the quality of the solutions in the current population increases and the algorithm converges on the best chromosomes, which represent the optimal or sub-optimal solution. The evolution of the process is terminated when a satisfying solution is achieved or when the predetermined run time is reached or when any other criterion or combination of criteria is satisfied [28].

The steps of the proposed GA are as follows:

Step 1. Population initialization

The adopted encoding scheme is based on random keys representation, which consists of random numbers between 0 and 1 [29]. For a problem with n orders, a sequence of n random numbers in (0, 1) is generated and then these random numbers are ordered in ascending order. For example, for n=5, the random numbers are generated as (0.17, 0.46, 0.25, 0.96, 0.34) and then reordered as (0.17, 0.25, 0.34, 0.46, 0.96). This random sequence represents the order sequence (1, 3, 5, 2, 4). This process is repeated until the desired number of chromosomes is generated for the initialized population. The same procedure was also used by Rom and Slotnick [6] and Chen et al. [11].

Step 2. Fitness Evaluation

The fitness function is the same as the objective function, which is total revenue. The fitness value of each chromosome is evaluated as follows:

2.1 Until the end of the order sequence in the chromosome, choose the next order to evaluate. When all orders are chosen to evaluate, go to step 2.4.

2.2. Calculate the start and completion time of the selected order.

$\breve{St}_i$: fuzzy start time of the order I

$\breve{C}_i$: fuzzy completion time of the order I

$\breve{st}_j = \tilde{C}_i + \tilde{s}_{ij}$ (if order I is processed immediately before order j.)

$\breve{C}_j = \breve{st}_j + \breve{p}_j$

2.3. Decide whether to accept or to reject the order.

$If\ \breve{C}_j \leq \breve{d}_j$ Accept order j (its sequence should also be saved)

$Else$ Reject order j

and return to step 2.1.

Fuzzy ranking methods are used to evaluate this fuzzy constraint.

2.4. When all the orders in the chromosome are evaluated (end of the order sequence), calculate the total revenue (TR) gained.

Step 3. Crossover

A variety of crossover methods are available in the literature. Rom and Slotnick [6] use a two-point crossover to generate offspring for the OAS problem. However, this method needs some correction operation if offspring are not feasible.

The same-site-copy-first crossover is applied in the present study to selected parent chromosomes to generate offspring. This approach was proposed by Wang and Wu [30] and later used by Chen et al. [11] in the proposed algorithm for OAS. The procedure can be described as follows:

3.1. Any gene-code that settles into the same position in both parents is assigned to the corresponding position in the offspring.

3.2. The remaining positions in the offspring are designated by the order of all gene-codes in Parent 1 within the sequence bounded by two randomly selected points.

3.3. The remaining unassigned positions are placed in the order of appearance in Parent 2.

An illustrative example of the crossover procedure is given in Figure 2.

				*		*			
Parent 1	3	9	7	8	2	4	1	6	5
Parent 2	5	9	7	4	2	1	8	3	6
Step 3.1.			7		2				
Step 3.2.			7	8	2	4	1		
Step 3.3.	5	9	7	8	2	4	1	3	6

Randomly selected points are represented by *

Figure 2. An illustrative example of the crossover procedure

We consider two different parent selection approaches for mating, namely random selection and selection based on the difference measurement proposed by Chen et al. [11]. To select parent chromosomes, firstly tournament selection was applied to select λ chromosomes from the population. The fittest of the λ chromosomes were selected to be the first parent and the chromosome that is most different from the first parent was selected as the second parent [11]. Chen et al. [11] suggested a distance measurement between two individuals based on the Hamming distance perspective. The new revised measurement takes into account the orders that are accepted. It can be defined as:

$$diff(u,v) = \frac{1}{n}\sum_{i=1}^{n} 1\ (u[i] \neq v[i])\ (x[u[i]] = 1)\ (x[v[i]] = 1) \tag{8}$$

Step 4. Mutation

Mutation operators are widely used in GAs to provide population diversity. There are many mutation operators for scheduling problems. In this study, shift-change mutation is performed, in which two positions are selected random and then one selected position is replaced with the other one. After that, all positions are shifted within the sequence bounded by the two selected positions [11].

Shift change mutation procedure is explained in Figure 3.

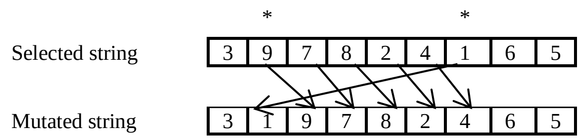

Randomly selected points are represented by *

Figure 3. Illustration of the mutation procedure

Step 5. Local Search

A local search procedure is useful in scheduling problems to improve the generated solutions. The most used local search method in OAS problems is performed in the present study. This procedure successively interchanges the positions of two immediate orders in the sequence. If any interchange improves the solution, it is kept as the new solution [6,11].

Flow chart of the proposed GA (Figure A1) is given in Appendix A.

4. Numerical examples and illustration

The proposed GA for the fuzzy OAS problem is implemented using the C++ programming language. Since there is no data related to the fuzzy OAS problem in the literature. The benchmark instances generated by Cesaret et al. [9], which are available at http://home.ku.edu.tr/~coguz/, are used to get fuzzy data. Crisp processing times, sequence dependent set up times, and due dates are revised as triangular fuzzy numbers. The data are revised using the developed user interface of the proposed program. The crispt number is taken as intermediate value (a_2), and then the value of a_2 is decreased at a random rate to get a_1 value; and increased at a random rate to obtain $a_3$value.

Since this is the first time that the fuzzy OAS problem has been studied, it is not possible to compare the current meta-heuristic algorithm of this study with other meta-heuristic algorithms in the literature. In this section, first, the results of the two ranking methods used in the algorithm are given and evaluated, then the effects of "diversity-based selection" and "local search" operators on solution quality are examined.

The developed user interface enables the practitioners to use the solution approach easily. Some illustration of interface screenshots related to entering data, parameter settings, solving the problem and displaying the solution are given in Figure A2, Figure A3, Figure A4, and Figure A5. The data of the problem can be transferred from any saved file and revised if needed after the “Select File” option is selected (Figure A2). The fuzzified problem data can be viewed by using the “Order Data” tab in the upper right-hand corner (Figure A3). The solution procedures start after selecting the “Initialize Population” and “Start Fuzzy Process” options. The other parameters of the algorithm can also be entered through the interface of the program.

Since the primary purpose of this study is to formulate the fuzzy OAS problem and to solve this problem efficiently, sophisticated parameter controlling strategies were not used. Some parameters of the GA algorithm are selected based on pretests conducted manually, while others are selected based on the study conducted by Chen et al. [11]. After testing, the best performance is achieved with a population size of 200. Crossover probability and mutation probability are set to 0.8 and 0.2, as in the study of Chen et al. [11] . When the maximum 5000 iterations are reached, the algorithms stop and return the best solutions. Since local search increases computation time, the search probability can be limited via “Local Search Probability” option. The local search is not limited for illustrative examples.

Six fuzzy OAS problems with 10, 15, 20, 25, 50 and 100 orders are solved to determine the performance of the proposed algorithm with different problem sizes. The data of the instances can be accessed at https://web.adanabtu.edu.tr/ekoyuncu/DuyuruList.

Table 1. The solutions obtained by signed distance and integral value with various α values.

Instances	Ranking Methods			
	Sign. Dist.	Int.Value (α =0,5)	Int.Value (α =0,7)	Int.Value (α =1)
Ins.1	119	119	116	116
Ins.2	134	134	131	127
Ins.3	194	194	188	183
Ins.4	285	287	269	260
Ins.5	456	458	433	428
Ins.6	886	891	869	826

The solutions for the integral value method for the α values of 0.5, 0.7 and 1 are given in the following table. For instances 1, 3 and 6, the same objective function values are acquired using integral value ranking with alpha value 0.5 and the signed distance ranking method. The objective function values of the other instances (Ins.2, Ins.4, Ins.5) are slightly higher when integral value ranking with alpha value 0.5 is implemented. The objective function values are generally smaller with integral value ranking, except when the alpha value is 0.5 (Table 1).

For some instances, alternative schedules that give the same objective function values can be obtained. The alternative schedules that gives the same profit can be monitored via the user interface. For example, there are two alternative schedules that give an objective function value of 196 for instance 3 using signed distance and integral value with alpha 0.5 (Figure A4 and Figure A5).

As can be seen in Figure A4 and Figure A5, both ranking methods yield the same revenue, but the accepted orders and schedules are different from each other. While, the schedule obtained by using integral value with alpha 0.5 is 8, 19, 5, 6, 7, 1, 15, 16, 20, 12, 4, 3, 17, 14, 18; the schedule obtained by using signed distance is 4, 5, 6, 14, 7, 1, 20, 13, 8, 12, 15, 3, 16, 2, 19, 18.

In order to determine the effect of “diversity-based selection” and “local search” on solution quality, the same instances are solved with the GA approach that uses only mutation and crossover operators (Table 2).

Table 2. The solutions obtained by GA without local search

Instances	Ranking Methods			
	Sign. Dist.	Int.Value (α =0,5)	Int.Value (α =0,7)	Int.Value (α =1)
Ins.1	119	119	116	116
Ins.2	134	136	131	127
Ins.3	196	196	190	186
Ins.4	288	289	275	262
Ins.5	461	464	448	425
Ins.6	892	849	862	849

After comparing the solutions in Table 1 and Table 2, we can conclude that diversity-based selection and local search operators seem to be effective at obtaining better solutions. This effect appears more clearly, especially as the size of the problem increases.

5. Conclusion

In this paper, a GA approach that employs fuzzy ranking methods is developed to solve the fuzzy OAS problem. There are many studies in the literature about OAS problem, many of which assume that all parameters and variables of the problem are crisp. Among these studies, a few model the problem as a stochastic OAS problem which represents uncertainties in processing times and due dates by a random variable with a known probability distribution. In most real production environments, it may not be possible to obtain enough prior information to characterize the probability distribution of a random processing time. It is even more difficult to obtain historical data, especially for MTO firms that offer more customized and unique products. To the best of our knowledge, only the study of Koyuncu [21] focused on the fuzzy nature of the problem and defined fuzzy OAS problem and presented a fuzzy MILP model to solve the small scale OAS problem Therefore, , a GA that employs two different fuzzy ranking methods is developed to solve this problem effectively.

Six instances with different numbers of orders are solved. The results obtained by using two different ranking methods are compared and show that the signed distance method and the integral value method with alpha value 0.5 give similar results. It can also be concluded that diversity-based selection and local search improves the solution, especially when the size of the problem increases.

In future studies, different meta-heuristic methods can be developed for solving the fuzzy OAS problem. These methods can then be compared with the proposed algorithm to demonstrate the performance of the methods. In addition, the effect of different ranking methods can be analyzed using more comprehensive statistical tests.

Acknowledgments

This work was supported by Unit of Scientific Research Project Coordination of Adana Alparslan Türkeş Science and Technology University. Project number: 16103008.

References

[1] Slotnick, S.A. (2011). Order acceptance and scheduling: a taxonomy and review. *European Journal of Operational Research*, 212, 1-11.

[2] Bilgintürk, Z. (2007). Order acceptance and scheduling decision in make to order systems. Master's Thesis. Koç University.

[3] Charnsirisakskul, K., Griffin, P.M., & Keskinocak, P. (2004). Order selection and scheduling with lead time flexibility. *IIE Transactions*, 36, 697–707.

[4] Charnsirisakskul, K., Griffin, P.M., & Keskinocak, P. (2006). Pricing and scheduling decisions with lead time flexibility. *European Journal of Operational Research*, 171, 153–169.

[5] Slotnick, S., & Morton T.E. (2007). Order acceptance with weighted tardiness. *Computers and Operations Research*, 34, 3029–3042.

[6] Rom, W.O., & Slotnick, S.A. (2009). Order acceptance using genetic algorithms. *Computers and Operations Research*, 36, 1758–1767.

[7] Oguz, C., Salman, F.S., & Yalcin, Z.B. (2010). Order acceptance and scheduling decisions in make-to-order systems. *International Journal of Production Economics*, 125 (1), 200–211.

[8] Nobibon, F.T., & Leus, R.. (2011). Exact algorithms for a generalization of the order acceptance and scheduling problem in a single-machine environment. *Computers and Operations Research*, 38, 367–378.

[9] Cesaret, B., Oguz, C., & Salman F.S. (2012). A tabu search algorithm for order acceptance and scheduling. *Computers and Operations Research*, 39, 1197–1205.

[10] Lin, S.W., & Ying, K.C. (2013). Increasing the total net revenue for single machine order acceptance and scheduling problems using an artificial bee colony algorithm. *Journal of the Operational Research Society*, 64, 293-311.

[11] Chen, C., Yang, Z., Tan, Y., & He, R. (2014). Diversity controlling genetic algorithm for order acceptance and scheduling problem. *Mathematical Problems in Engineering* doi: http://dx.doi.org/10.1155/2014/367152.

[12] Xie, X., & Wang, X. (2016). An enhanced ABC algorithm for single machine order acceptance and scheduling with class setups. *Applied Soft Comping*, 44, 255-566.

[13] Zandieh, M., & Roumani, M. A biogeography-based optimization algorithm for order acceptance and scheduling. *Journal of Industrial and Production Engineering*, 34(4), 312-321.

[14] Chaurasia, S.N., & Singh, A. (2017). Hybrid evolutionary approached for the single machine order acceptance and scheduling problem. *Applied Soft Comping*, 52, 725-747.

[15] Wester, F.A.W., Wijngaard J., & Zijm W.H.M. (1992). Order acceptance strategies in a production-to-order environment with setup times and due-dates. *International Journal of Production Research*, 30, 1313–1326.

[16] De, P., Ghosh, J.B., & Wells, C.E. (1993). Job selection and sequencing on a single machine in a random environment. *European Journal of Operational Research*, 70, 425–431.

[17] Stadje, W. (1995). Selecting jobs for scheduling on a machine subject to failure. *Discrete Applied Mathematics*, 63, 257–265.

[18] Rogers, P., & Nandi, A. (2007). Judicious order acceptance and order release in make-to-order manufacturing systems. *Production Planning and Control*, 18 (7), 610–625.

[19] Kate, H.A. (1994). Towards a better understanding of order acceptance. *International Journal of Production Economics*, 37, 139–152.

[20] Carr, S., & Duenyas, I. (2000). Optimal admission control and sequencing in a make-to-stock/ make-to-order production system. *Operations Research*, 48 (5), 709–720.

[21] Koyuncu, E. (2017). A fuzzy mathematical model for order acceptance and scheduling problem. *International Journal of Mathematical Computational, Physical, Electrical and Computer Engineering,* 11(4).

[22] Quelhadj, D., & Petrovic, S. (2009). A Survey of dynamic scheduling in manufacturing systems. *Journal of Scheduling*, 12(4), 417-431.

[23] Baykasoglu, A., & Gocken, T. (2012). A direct solution approach to fuzzy mathematical programs with fuzzy decision variables. *Expert System with Applications*, 39, 1972-1978.

[24] Liou, T.S., & Wang, M.J. (1992). Ranking fuzzy numbers with integral value. *Fuzzy Sets and Systems,* 50, 247–255.

[25] Zhou, W., & Gong, P. (2004). Economic effects of environmental concerns in forest management: an analysis of the cost of achieving environmental goals. *Journal of Forest Economics*, 10, 97-113.

[26] Liou, T.S., & Chen, C.W. (2006). Fuzzy decision analysis for alternative selection using a fuzzy annual worth criterion. *The Engineering Economist*, 51, 19-34.

[27] Goncalves, J.F., Mendes, J.M., & Resende, M.G.C. (2008). A genetic algorithm for the resource constrained multi-project scheduling problem. *European Journal of Operational Research*, 189, 1171–1190.

[28] Nicoara, E.S. (2015). Applying genetic algorithm to optimization problems in economics. *Economics Insights-Trends and Challenges*, 4(3), 125-132.

[29] Bean, J.C. (1994). Genetic algorithms and random keys for sequencing and optimization. *ORSA Journal on Computing*, 6(2), 154-160.

[30] Wang, H.F., & Wu, K.Y. (2004). Hybrid genetic algorithm for optimization problems with permutation property. *Computers and Operations Research,* 31(14), 2453–2471.

Esra Karakaş *received the Ph.D. degree in industrial engineering from the Çukurova University, Adana, Turkey, in 2011. She is an Assistant Professor with the Department of Business Administration, Adana Alparslan Türkeş Science and Technology University, Adana, Turkey. Her research interests are project scheduling, personnel scheduling, production scheduling, and fuzzy mathematical modeling. She has published papers in Journal of Medical Systems, International Journal of Production Research, and Computers & Industrial Engineering.*

Hakan Özpalamutçu *received his BS degree in computer engineering from Marmara University, İstanbul, Turkey, in 1998. He is a master student in Industrial Engineering Department in Adana Alparslan Türkeş Science and Technology University. He is also a software specialist in an automotive factory.*

APPENDIX

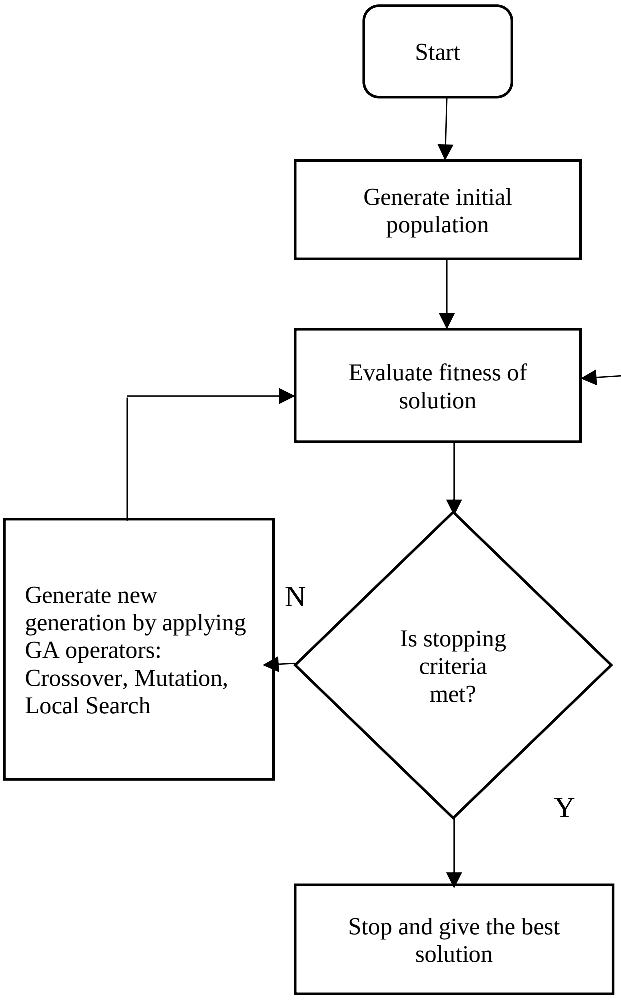

Figure A1. Flow chart of the proposed GA methodology for fuzzy OAS problem

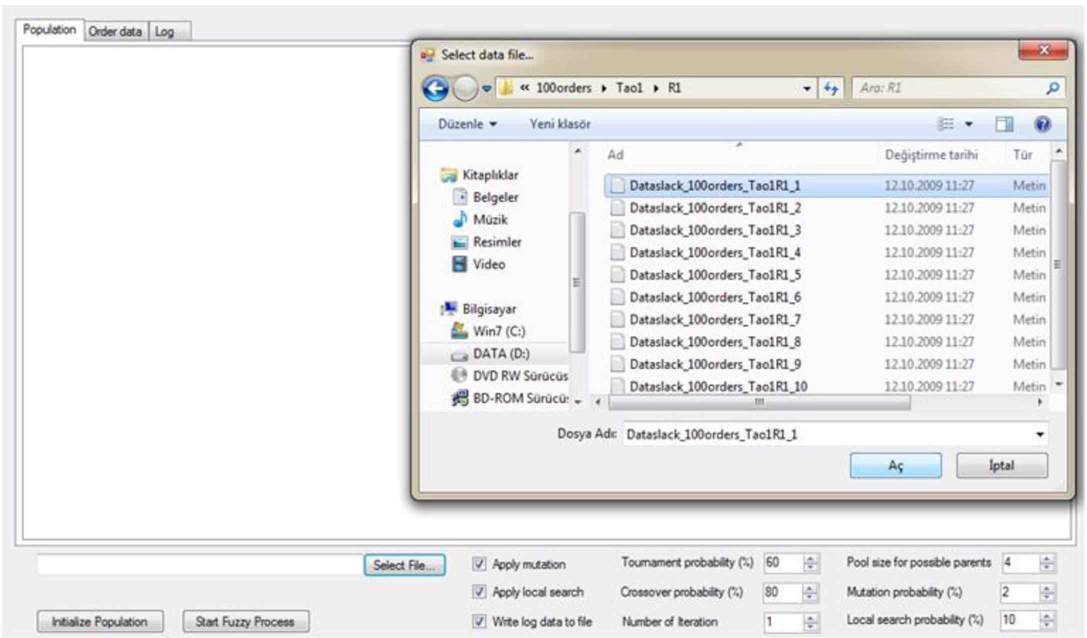

Figure A2. Transfer of the data to the program

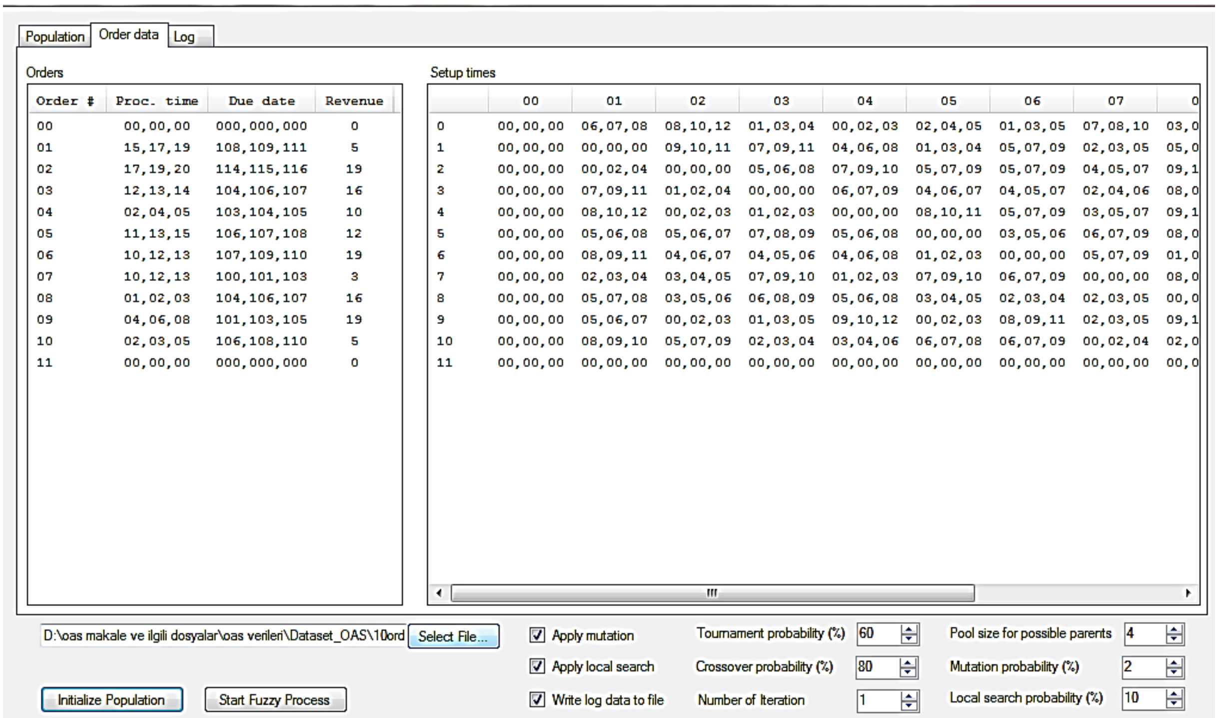

Figure A3. Data display screen

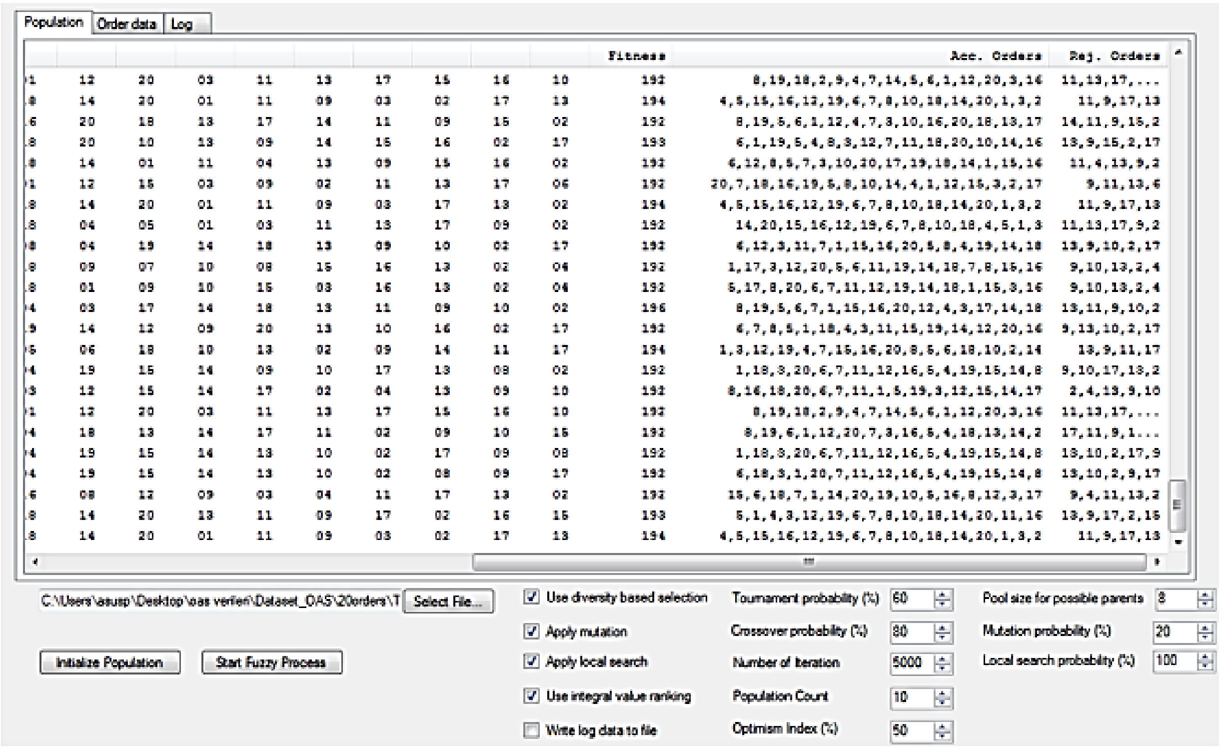

Figure A4. Solution screen with integral value method (α =0,5) for instance 3

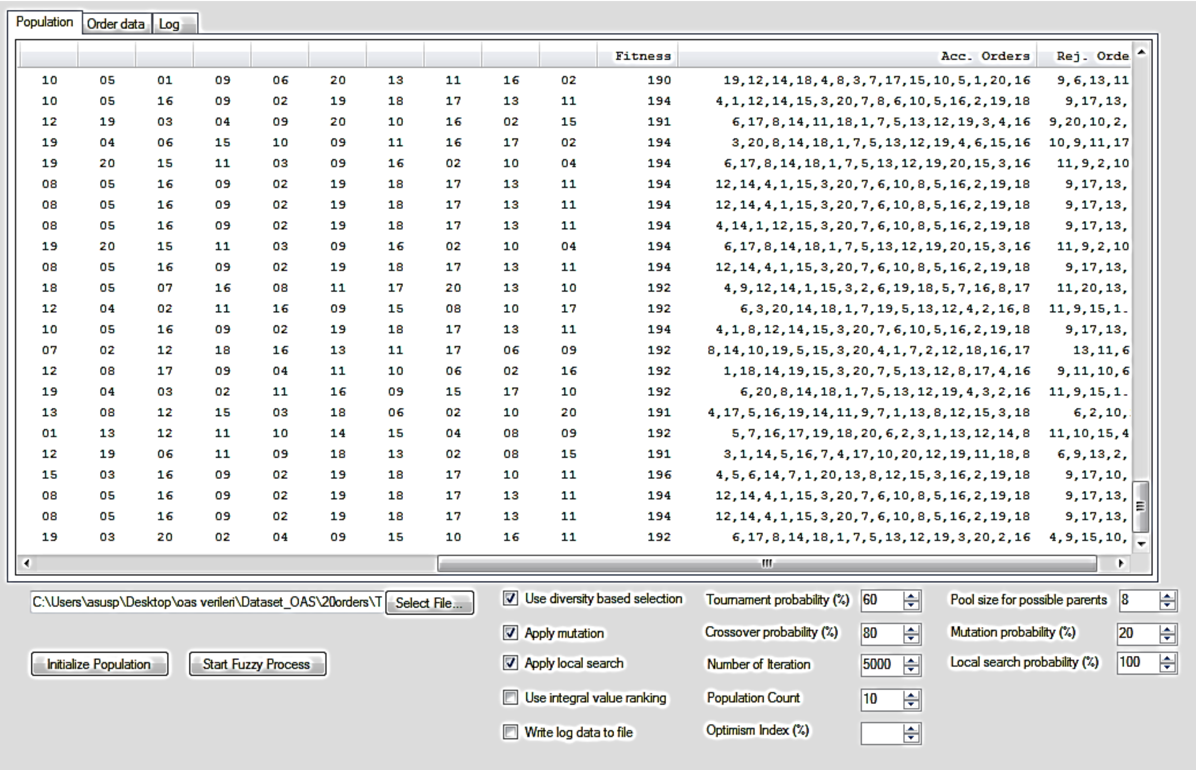

Figure A5. Solution screen with signed distance method for instance 3

An International Journal of Optimization and Control: Theories & Applications
ISSN: 2146-0957 eISSN: 2146-5703
Vol.9, No.2, pp.197-207 (2019)
https://doi.org/10.11121/ijocta.01.2019.00714

RESEARCH ARTICLE

Optimization of medical waste routing problem: The case of TRB1 region in Turkey

Suleyman Mete [a] *, Faruk Serin [b]

[a] *Department of Industrial Engineering, Munzur University, Turkey*
[b] *Department of Computer Engineering, Munzur University, Turkey*
suleymanmete@munzur.edu.tr, fserin@munzur.edu.tr

ARTICLE INFO

Article history:
Received: 24 September 2018
Accepted: 13 April 2019
Available Online: 29 April 2019

Keywords:
Medical waste
GIS
Routing
Case study

AMS Classification 2010:
90-08, 90B06, 90C10

ABSTRACT

A fundamental problem concerning medical waste disposal is the evaluation of the real and potential risks arising from waste with the focus on the risk of infection. Therefore, the optimization of medical waste routing from collection to disposal center can minimize the risk of infection. The routing of medical waste considers significant to determine potential routes and select the route with minimum distance. The management of the medical waste is important decision for environmental sustainability and includes the collection, transportation and disposal of these materials. In this paper, a geographic information system (GIS) solution approach is proposed to determine the best location of disposal center. Proposed approach is applied to medical waste transportation between 167 health institutions (collection centers) and predetermined 5 disposal centers through TRB1 region in Turkey, which consist of Malatya, Elazığ, Bingöl and Tunceli provinces. The results of case study are examined and suggestions for future research are provided.

1. Introduction

Medicine is one of the important sectors showing development throughout the world during recent decades. Thus, the industrial and technological advances in the medicine sector have created a large medical waste in the developed world. There are four types of waste generated by health institutions. They can be classified as municipal wastes, medical wastes, hazardous and radioactive wastes. The sub-groups of medical waste can be listed as infection wastes (used surgical operating clothes, infectious organ pieces, blood and blood products etc.), pathological wastes (organs, tissues, placenta etc.) and sharp objects (syringes, needles, blades, broken glass etc.). Besides, there are four interchangeable terms for entitled medical waste which are medical waste, hospital waste, infectious medical waste and regulated medical waste. The collection, transportation and disposal of the medical waste are serious processes that need to be considered [1].

Generated medical waste is increased day by day due to the increase in the number of health institutions and populations. Classification and appropriate segregation of medical waste are important processes for its transportation and disposal [2]. The medical waste materials have remarkable risks and to produce negative effect on human health and the environment during storage, handling, usage and transporting processes due to their naturel conditions. Awareness of environmental problems and living healthy have raised in modern societies in recent years. Therefore, plan and practices on transportation of medical waste should be applied to reduce the risks in addition to legal constraints. The selection of disposal center for the logistic operation of medical waste has a great importance due to potential negative effect of the medical waste over human health.

The locations of disposal center for medical waste have a significant impact on the feasible routing decisions and the total transportation risk and distance. It is important to consider the locations of medical waste disposal center and the routing plans simultaneously. Routing of vehicles that carry medical waste effects the costs, economic evaluation or environmental security and community issues. Therefore, alternative routes should be identified for these vehicles to choose the

*Corresponding author

route with minimum distance.

This study aims to present a solution for the routing problem of medical waste in TRB1 region of Turkey. The data is obtained using QGIS 3.0 Girona software and OpenStreetMap for four provinces as Malatya, Elazığ, Bingöl, and Tunceli. In the paper, QGIS 3.0 is employed as the GIS platform to support the analysis of routing problem. GIS-based solution approach is also applied for the determine the best location of disposal center. 167 collection centers of medical waste and predetermined 5 disposal centers are examined in the paper. The softwares used to solve the problem as travelling salesperson are QGIS 3.0, OpenStreetMap, PostgreSQL database, PostGIS, pgRouting, pgr_TSP routing function.

The rest of the paper is outlined as follows: in next section, we provide an overview and a summary of the related studies. In section 3, proposed approach to solve the problem are detailed. The case study is outlined and related data are given in section 4. Results of the case study are analyzed and discussed in section 5. Finally, evaluations are provided in the conclusion section.

2. Related studies

There are extensive literature related to routing problem. The problem is solved with different techniques such as mathematical modeling, meta-heuristics and geographic information system–based methods [3]. In this part literature is divided as three sub-section. Firstly, literature for the location-routing are analyzed then literature of hazardous material routing and medical waste collection are examined respectively.

A location-routing problem can be described as given a set of potential depots and a set of customers with known demand, define the optimal locations of the depots with vehicle routes from chosen depots to the customers simultaneously while minimizing the total system costs [4]. Exact solution and heuristic/ metaheuristic methods are developed for location-routing problem in the literature. The first exact solution approach for the general location-routing problem is proposed by Laporte and Nobert [5]. Later, Laporte et al. [6], Ghiani and Laporte [7], Averbakh and Berman [8], Labbe et al. [9], Alumur and Kara [10], Ponboon et al. [11] and Farham et al. [12] also propose exact methods to solve the problem with optimal manner. Heuristic and meta-heuristic approaches are also proposed to solve the problem since the complexity of the location-routing problem is NP-Hard nature [13]. Exact methods ensure important insights into problems, but they can tackle for small/medium instances due to the complexity of the problem [14]. Therefore, many researchers focus on the heuristic and metaheuristic approach to solve the problem such as simulated annealing algorithm [15], ant colony optimization [16], tabu search [17-18], hybrid heuristic algorithm approach [19] and memetic algorithm [20]. The reader is referred to the comprehensive surveys by Nagy and Salhi [14] for models and issues, models and methods of the location-routing problems, and they also develop a classification scheme for the location-routing studies.

There are extensive literature related to hazardous material routing problem. Different solution approaches are developed for hazardous material routing problem. Erkut and Verter [21] develop different risk models formulation to solve hazardous material shipment problem between a given origin-destination pair. Leonelli et al. [22] propose mathematical formulation to select the best route of the transportation of a hazardous substance. Androutsopoulos and Zografos [23] present model to solve the bicriterion routing and scheduling problem for hazardous material distribution. The concept of chaos theory based on dynamic risk definition and damage severity network is used by Mahmoudabadi and Seyedhosseini [24] to determine best route for transportation of hazardous material. On the other hand, meta-heuristics approaches are proposed to solve hazardous material routing problem. Zografos and Androutsopoulos [25] propose a heuristic algorithm integrated with GIS based decision support system to solve hazardous material distribution network. Huang et al. [26] integrate genetic algorithm with GIS based system to evaluate the risk of hazardous material transportation. Pamučar et al. [27] propose a new approach, which is based on adaptive neuro fuzzy inference system, artificial bee colony algorithm and Dijkstra's algorithm, for cost and risk assessment of hazardous material transportation on a network of city roads. Özceylan et al. [3] present a solution approach based on GIS for solving hazardous material routing with a case study. Hazardous waste has been investigated with consideration population and environmental impact by Yılmaz et al. [28]. The reader is referred to the comprehensive survey by Erkut et al. [29] for a recent coverage of the state of the art on models and solution algorithms.

We investigate the related problems in detail since our focus area is to solve problems of transportation and collection of medical waste. There are studied related medical waste routing and collection in the literature. Shih and Chang [30] use a computer program for the gathered of infectious medical waste. They propose a mathematical model and a two-phase periodic vehicle routing problem for scheduling and routing the gathered of medical waste. The proposed approach is also applied to 348 hospitals in the Tainan City/ Taiwan. Mourao and Almeida [31] define a capacitated arc routing problem to minimize total cost of a refuse collection in Lisbon. Therefore, two lower bounding method and a three-phase heuristic approach are developed for solving the problem. Alagöz and Kocasoy [2] use special software programs, which are called MapInfo and Roadnet, to solve the scheduling and route optimization for transportation health-care waste collection in Istanbul. Marinkovic et al. [32] introduce a combine approach based on a hierarchical structure from generation medical waste point to disposal center. The aim of proposed integrated approach points out probable solution for the management medical waste in Croatia. Abdulla et al. [33] investigate the medical waste management system, which is used in health institutions in northern Jordan. Therefore, they analyze a comprehensive inspection survey for all hospital located in the area, and they propose results of main findings of the study. Birpınar et al. [1] examine the present status of medical waste management in the light of the Medical Waste Control Regulation in Istanbul. Windfeld and Brooks [34] investigate medical waste management related studies including the common sources, governing legislation and handling and disposal methods. Alshraideh and Qdais [35] pay attention to stochastic medical waste collection problem in Jordan and proposed a route scheduling model for minimizing the total transportation cost and reduces emissions. Mmereki et al. [36] introduce an overview of the current generated waste from health institutions in Botswana. Hence, they analyze storage, collection, treatment and disposal system for the case in Botswana.

Scope of this study is to answer as follows questions: (i) how to route the produced medical waste from collection center to disposal center, (ii) which of the presented solutions are reasonable according to total distance. Therefore, a GIS-based solution approach is developed to solve routing of medical waste problem. The approach is applied to case study of TRB1 region in Turkey, which include Malatya, Elazığ, Bingöl and Tunceli provinces. Data related collection and disposal center are provided from QGIS 3.0 and OpenStreetMap.

3. The methodology

The mathematical model for routing is used in this paper to determine the best location for disposal center and routing. The model used in this study is proposed by Baldacci et al. [37]. The problem can be defined as capacitated vehicle routing problem. The mathematical model formulation is given as follows:

$$min \sum_{i,j\in E} d_{ij} X_{ij} \tag{1}$$

$$\sum_{i,j\in t(h)} X_{ij} = 2, \qquad \forall h \in V, \tag{2}$$

$$\sum_{i,j\in t(S)} X_{ij} \geq 2k(S), \qquad \forall S \in s, \tag{3}$$

$$\sum_{j\in V} X_{0j} = 2r, \tag{4}$$

$$X_{ij} \in \{0,1\}, \ \forall \ i,j \in E \setminus (0,j: j \in V) \tag{5}$$

$$X_{0j} \in 0,1,2, \qquad \forall \ 0,j, \quad j \in V, \tag{6}$$

$S = \{S: S \subseteq V, |S| \geq 2\}$, and $q(S) = \sum_{i\in S} q_i$ be the total produced of medical waste $S \in s$ and $k(S)$ minimum number of sub-routes that is equal to minimum number of vehicles with Q capacity for multi-vehicle routing problem, and r is the number of sub-route. Further, let $t(S) = \{\{i,j\} \in E: i \in S, \ j \notin S \ or \ i \notin S, \ j \in S\}$. $X_{i,j}$: a binary variable equal to 1 if and only if edge$(i;j)$ is chosen in the solution for all $\{i,j\} \in E \setminus \{\{0,j\}: j \in V\}$ and value $\{0,1,2,$ for all $\{0,j\}, j \in V$ with $X_{i,j} = 1$ when edge is traversed and $X_{0,j} = 2$ when a route $(0,j,0)$ in the solution.

The objective function (1) is to minimize total transportation distance between collection center and disposal center. Constraint (2) is degree restriction and it specifies the degree of each collection center. Constraint (3) are determined capacity restriction. Constraint (4) represent that a truck must leave and back to disposal center. Constraint (5 and 6) are integrality restriction.

The usage of GIS-based solution method for the medical waste routing problem presents several advantages. GIS offers database properties that can handle data qualification, and it allows the addition of relevant layers for using spatial analysis [38;40;41]. In this paper, a GIS-based routing problem for transporting medical waste between 167 collection centers and five different possible location for disposal centers is considered. Spatial data of collection and disposal centers were gathered on OpenStreetMap and stored to PostgreSQL database via QGIS 3.0 software. QGIS known as Quantum GIS is an open source and free software used for Geographic Information Systems. The gathered data were used as input for PostGIS an extension of PostgreSQL database. The results were obtained by using pgRouting, which is an extension of PostGIS for routing operation. A routing function of pgRouting, pgr_TSP, were used to solve the problem as travelling salesperson problem. Finally the route results were shown on the OpenStreetMap via QGIS.

4. The case study of TRB1 region in Turkey

In this paper, 167 collection centers and 5 predetermined disposal centers that are located in TRB1 region in Turkey are considered (see Figure 1). The following locations are selected as candidates for disposal center: (i) the four locations are predetermined in Malatya, Elazığ, Bingöl and Tunceli provinces respectively, (ii) one location is also predetermined between Elazığ, Bingöl and Tunceli provinces. In other words, we face a problem with 5 possible locations for disposal center, where we can choose only one of them.

Figure 1. Study area: TRB1 region of Turkey

Health institutions consist of state hospitals, special hospitals, health centers and university hospitals. The locations of health institutions (red nodes) and disposal centers (green nodes) are given in Figure 2. In addition, related data including coordinates, number of population and district for each locations of collection center are given in Table A1 as appendix.

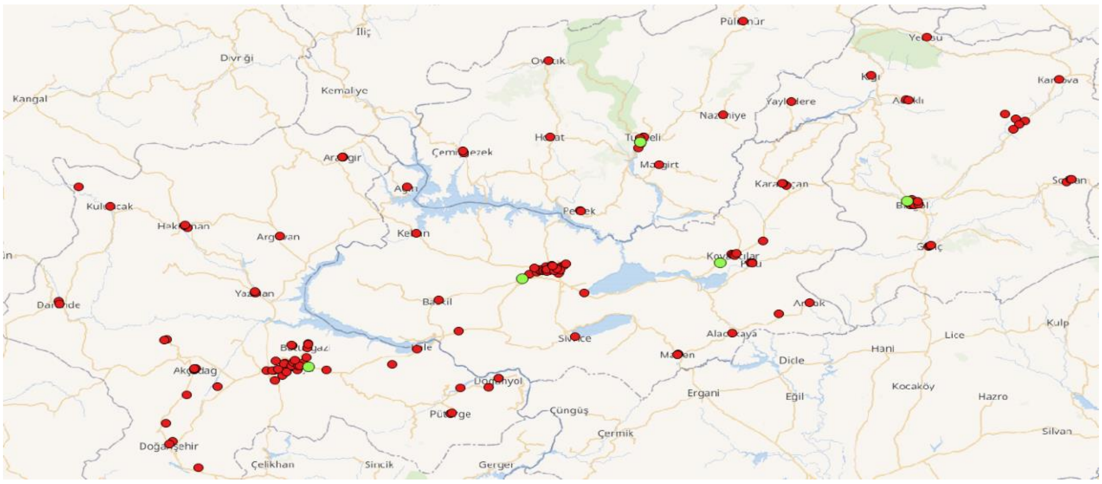

Figure 2. The locations of 167 collection centers (red nodes) and 5 disposal centers (green nodes)

Table1: Weekly produced medical waste according to the population of each collection center

Center	Medical Waste Produced (Kg)	Center	Medical Waste Produced (Kg)	Center	Medical Waste Produced (Kg)	Center	Medical Waste Produced (Kg)	Center	Medical Waste Produced (Kg)
1	120.462	35	99.116	69	45.938	103	183.490	137	63.261
2	120.462	36	99.116	70	45.938	104	183.490	138	98.164
3	120.462	37	79.829	71	45.938	105	183.490	139	98.164
4	120.462	38	79.829	72	45.938	106	183.490	140	142.760
5	120.462	39	98.999	73	45.938	107	183.490	141	1192.829
6	120.462	40	54.870	74	45.938	108	183.490	142	1192.829
7	72.953	41	37.448	75	27.225	109	183.490	143	1192.829
8	72.953	42	257.764	76	27.225	110	183.490	144	1192.829
9	136.758	43	257.764	77	27.225	111	183.490	145	1192.829
10	152.102	44	257.764	78	27.225	112	183.490	146	247.741
11	56.055	45	257.764	79	27.225	113	183.490	147	247.741
12	115.956	46	257.764	80	31.967	114	183.490	148	187.608
13	106.594	47	257.764	81	31.967	115	183.490	149	187.608
14	106.594	48	257.764	82	31.967	116	183.490	150	187.608
15	59.532	49	257.764	83	21.552	117	183.490	151	187.608
16	340.797	50	257.764	84	21.552	118	183.490	152	25.774
17	340.797	51	257.764	85	21.552	119	183.490	153	25.774
18	340.797	52	257.764	86	25.217	120	183.490	154	25.774
19	340.797	53	257.764	87	25.217	121	183.490	155	108.342
20	340.797	54	257.764	88	21.278	122	183.490	156	108.342
21	340.797	55	257.764	89	21.278	123	183.490	157	108.342
22	340.797	56	257.764	90	12.084	124	183.490	158	49.840
23	340.797	57	257.764	91	12.084	125	183.490	159	49.840
24	340.797	58	257.764	92	12.084	126	183.490	160	70.001
25	217.616	59	257.764	93	26.858	127	183.490	161	70.001
26	217.616	60	257.764	94	21.576	128	183.490	162	93.173
27	217.616	61	257.764	95	21.562	129	183.490	163	93.173
28	214.489	62	257.764	96	8.782	130	63.261	164	93.173
29	214.489	63	257.764	97	32.701	131	63.261	165	82.412
30	214.489	64	257.764	98	32.701	132	63.261	166	82.412
31	99.116	65	257.764	99	32.701	133	63.261	167	82.412
32	99.116	66	257.764	100	32.701	134	63.261		
33	99.116	67	257.764	101	32.701	135	63.261		
34	99.116	68	257.764	102	32.701	136	63.261		

The medical waste per person in Turkey is computed using the following formula: (Total generated medical waste for a year / total population). Hence, the annual produced medical waste per person is 8,1024,000 / 79,510,000=1.01 kg/person for the year 2016 according to Turkish Statistical Institute [39]. Total population of the TRB1 regions is approximately 1,726,199 people. Weekly produced medical waste according to the population of each health institutions (collection center) is given in Table 1. These values are calculated according to the population of each collection center. In other words, the generated medical waste in weekly for each collection center can be computed: (The total population of city x 1.01 / the number of collection center) / 52 week. For example, Tunceli province has six collection centers which are 1, 2, 3, 4, 5, 6, and each of them are produced approximately 120.462 kg/week medical waste with a population of 6,202 people (see Table 1).

Transportation cost of the medical waste is more than other waste since medical waste is shipped with special equipment and trucks. Therefore, distances between collection and disposal centers are used as a measure of cost. Thus, the cost of distance has a significant role to determine routing and disposal center. There is one type of truck that is used in this study to collect medical waste from collection center to disposal center, and it has 3,000 kg capacity. On a weekly basis, truck starts its trip from the disposal center, collects medical waste from the 167 collection centers, then drives back to the disposal center. When the truck reaches its capacity during trips, it back to disposal center to unload the medical waste, and then continues the trip. This trip is scheduled for every week.

In the study, single depot and single vehicle are considered for the problem. Euclidean distances between the identified collection points and the alternative locations were obtained by using QGIS 3.0 Girona software and OpenStreetMap, and the distances are calculated in meters. All runs are taken on a server with 2.4 GHz Intel® Core™ processor and 8 GB RAM, and the computation time required to solve the problem is less than 1 CPU second. Results for the routing problem of medical waste are analyzed in next section.

5. Results and Discussions

In this section, results of the five alternatives are analyzed, and the best of one is selected. A GIS-based solution approach is proposed to search feasible routes for shipping medical waste from 167 collection centers to one of the five alternative location (disposal centers). The objective is to minimize total distance which consist of total trip distance including loading and unloading distance. By this way, total risk of medical waste during shipping can be minimized.

Five different location areas are predefined for disposal center. These location areas are in Tunceli, Bingöl, Elazığ and Malatya provinces. Besides, one of the them is located between Tunceli, Bingöl and Elazığ provinces. Thus, we can determine the best location for disposal center among 5 different alternatives locations. Routes of these alternatives location for feasible routes between collection and disposal center are given in Figure 3. For example, if the disposal center locates in Tunceli province, total trip takes 6,558,215 meters and the truck will have to go through the disposal center 12 times during trip (see Figure 3a). Total trip takes 5,082,553 meters if disposal center locates in Malatya province (see Table 2). The results show that the opening of a disposal center in Malatya province seems to be a reasonable decision.

Total travel distance includes the distance from disposal center to first collection center, between sequential collection centers, and from last collection (where truck is full, or collections are finished) center to disposal center. Therefore, unloading number and amount of medical waste generated according to population is significant indicator to select location of disposal center. Thus, disposal center located in Malatya province is logical according to total population, amount of medical waste generated and distance.

Results of the feasible routes for location of disposal center in Malatya province are shown in Figure 4. There are 12 sub-routes (truck unloading number) for this solution.

Table 2. Total travel distance and truck unloading number according to disposal center

Location area	Total travel distance (m)	Unloading number
Tunceli	6,558,215	12
Bingöl	8,308,406	13
T-B-E*	6,126,680	13
Elazığ	5,237,900	13
Malatya	5,082,553	12

*Location area is between Tunceli, Bingöl and Elazığ provinces

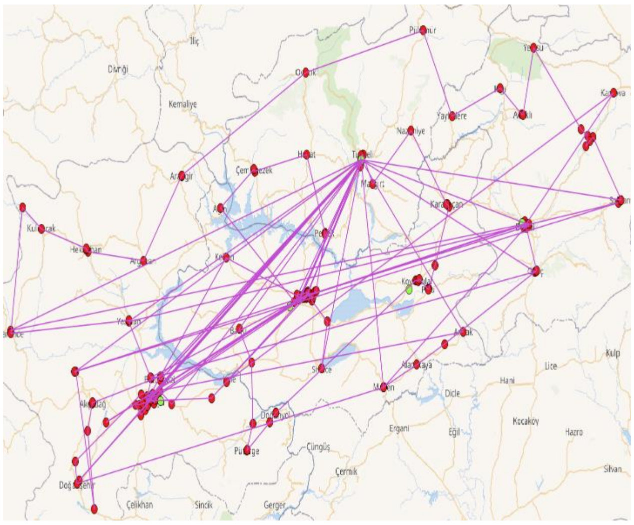

a

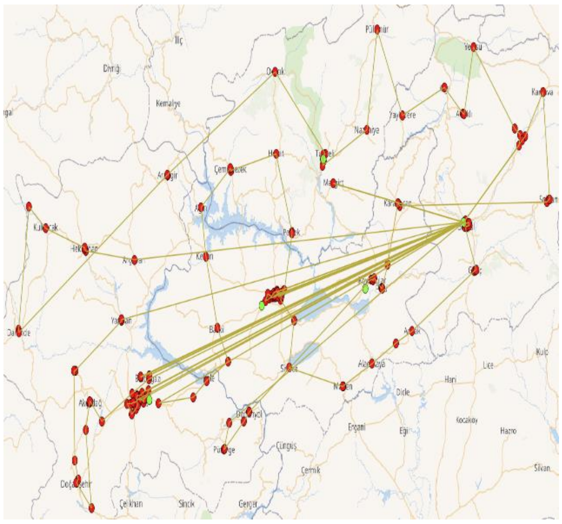

b

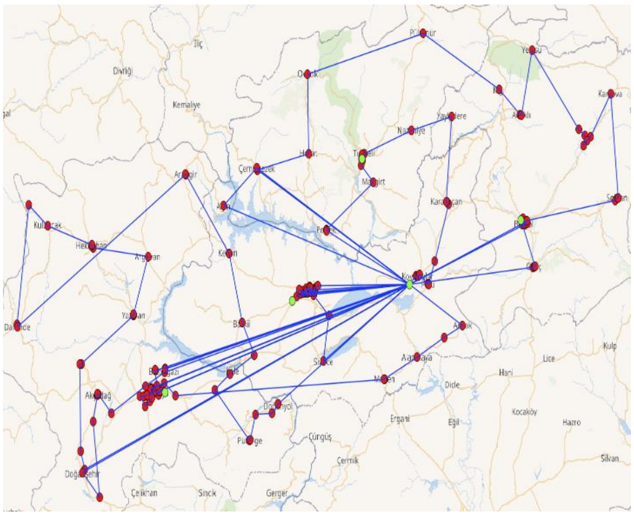

c

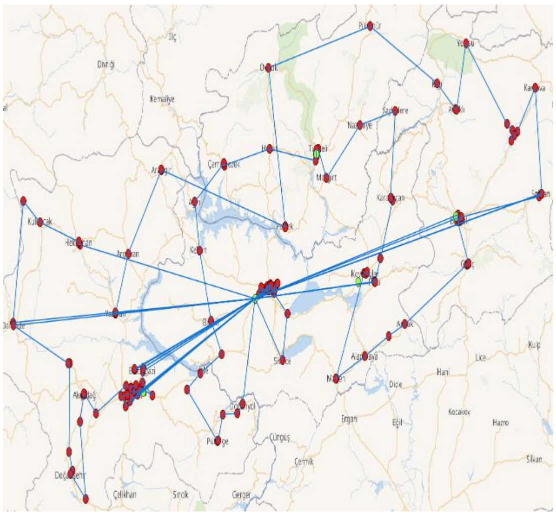

d

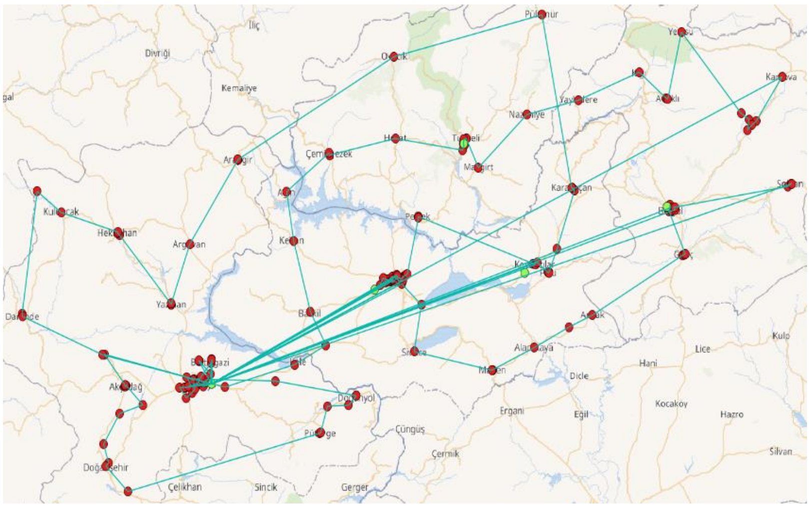

e

Figure 3. Feasible routes between collection and disposal center a) the disposal center located in Tunceli, b) the disposal center located in Bingöl, c) the disposal center located between Tunceli, Bingöl and Elazığ provinces, d) the disposal center located in Elazığ, e) the disposal center located in Malatya

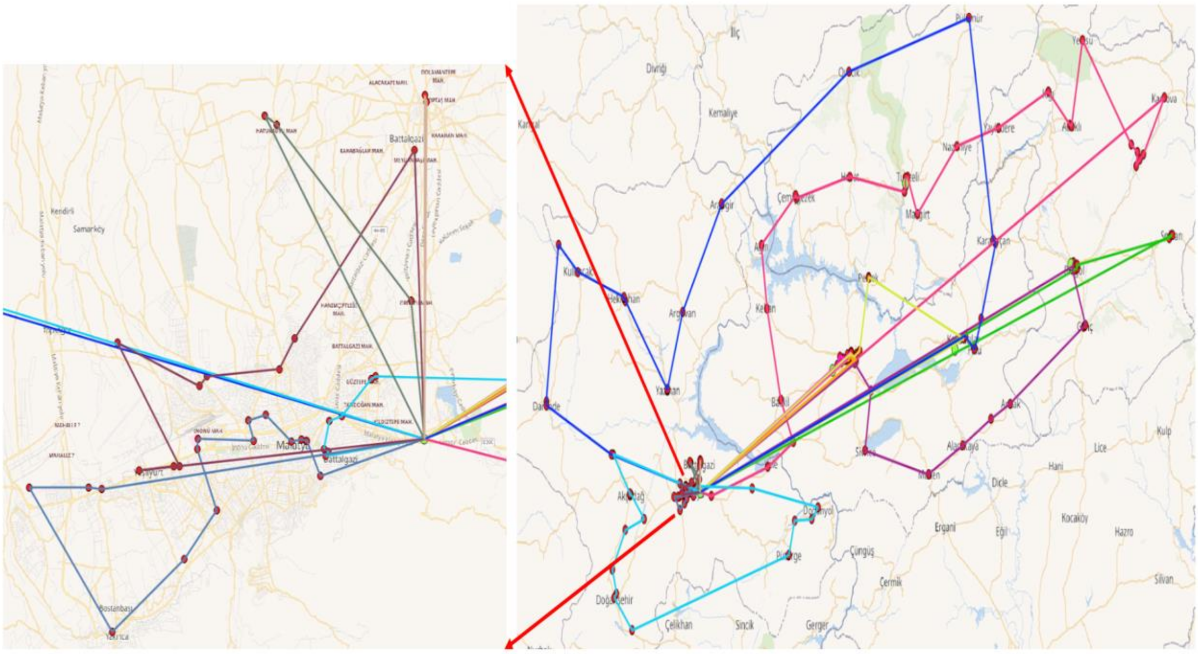

Figure 4. Disposal center located in Malatya province

Each of the sub-routes is painted with different colour (see Figure 5b). The route starts the disposal center and then collect medical waste from the first collection center and continue collecting waste from the other collection center until the route is terminated by truck capacity (see Figure 5a). When it reaches capacity, truck backs to disposal center to unload medical waste. For example, detail of a sub-route shown in Figure 5a, truck starts from disposal center located in Malatya then gather medical waste until it reaches its capacity after visit 25 collection center. Then, the truck returns back to disposal center with load of 2884.37 kg in order to unload waste (the sub-route 8 is given in Table 3).

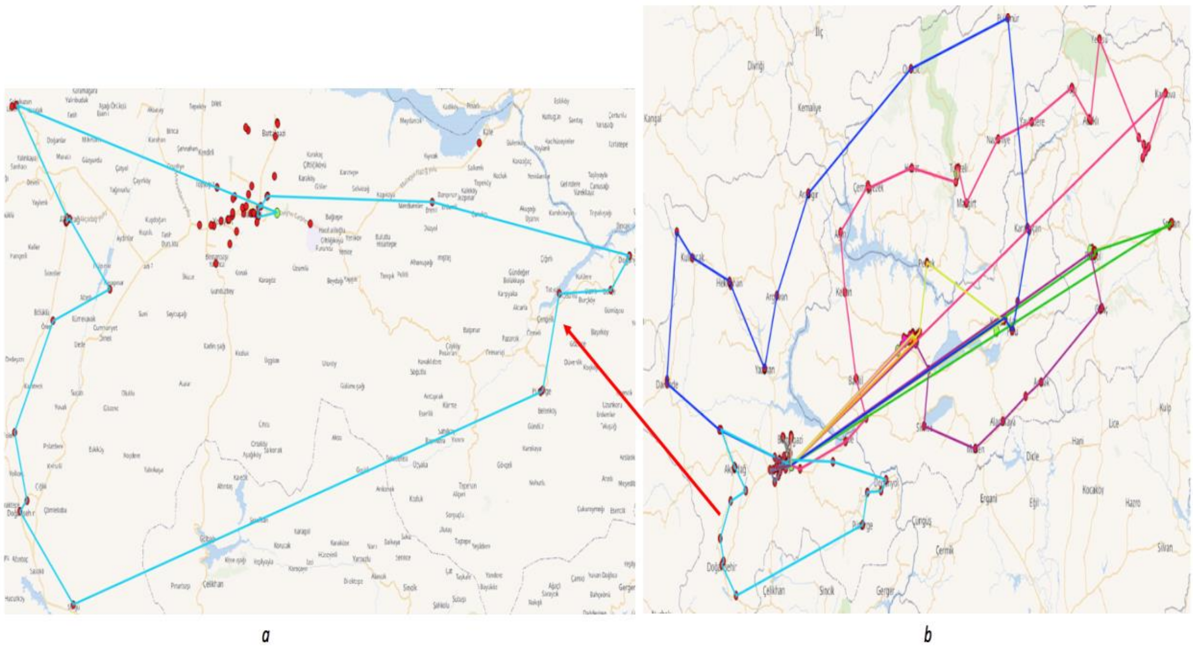

Figure 5. The best solution among 5 alternatives. a) Detail of one sub-route b) starting and finishing point for all sub-routes with different colour

All sub-routes of the best solution among the alternatives are given in Table 3. If the disposal center is opened in Malatya, the best solution is achieved according to total distance or total transportation cost. For example, if truck visits collection center 143 and 141 in the sub-route 11, it fills capacity with 2385.658

kg and returns to the disposal center. That is, these two health institutions are produced many waste, and they are in Malatya city center.

In this study, the weekly collection of medical waste from health institutions in TRB1 region of Turkey to the final disposal center are examined, and the best feasible (the most efficient) route among the alternatives is selected as disposal center with perspective of efficiency. Using the selected disposal center reduces risks to human health, cost arising from transportation and provides economic advantages

Table 3. Results of the best solution among all alternatives (disposal center in Malatya)

Sub-route	Trips	Waste (kg)
1	115-159-89-88-95-96-8-7-9-6-5-1-4-2-3-10-11-41-39-37-38-40-31-32-35-34-33-36	2801.644
2	30-29-28-24-17-16-23-22-21	2688.249
3	19-18-20-27-26-25-86-87-94-91-90-92-93-74-68	2948.947
4	70-69-50-49-48-47-44-46-43-65-64	2835.404
5	66-67-45-63-60-61-62-58-59-42-54	2835.404
6	72-73-53-52-51-71-55-56-57-14-13-75-76-77	2991.353
7	78-83-85-84-79-80-81-82-15-12-138-139-140-167-166-165-155-157-160-161-146-147-137	2992.009
8	136-133-130-132-131-134-135-151-148-149-150-162-163-164-154-152-153-158-113-114-127-126-110-111-112	2884.37
9	123-109-108-107-106-124-105-104-102-101-120-118-97-116-117-98	2935.84
10	119-99-100-122-121-103-125-128-142	2660.749
11	143-141	2385.658
12	145-144-129	2569.148

6. Conclusion

The medical waste routing is important problem among all logistic transportation. Therefore, nearly all societies have regulation and law for transportation waste to protect people and environment. Medical wastes are needed special regulations to transport them. Thus, the scope of this study is to answer as follows questions: (i) how to route the produced medical waste from collection center to disposal center, (ii) which of the presented solutions are reasonable according to total cost.

The TRB1 region of Turkey is the focus for this study. A GIS-based solution approach is applied the case study, which consist of Malatya, Elazığ, Bingöl, and Tunceli provinces, to determine the best location of disposal center and routing. The results show that the opening of a disposal center located in Malatya province seems to be a reasonable decision. The opening of disposal center near to Malatya province would be appropriate decision for planners or decision-makers due to number of collection center and generated amount of medical waste in Malatya.

Some of the limitations of this study is given as follows: we are focusing only TRB1 region of Turkey that makes the study a bit narrow scoped. The other region of Turkey can be considered for future research and different scenario can be analyzed. The values used in study are not real produced medical waste, these are taken based on the total population for each health institutions. Hence, the exact amount of medical waste generated per year can be determined from each health institution, and accordingly the real values can provide more rational decisions for future research. Lastly, we have used Euclidean distance between collection and disposal center, but in real life applications these distances must be real distances or rectilinear.

In this study, the problem is considered as single depot and single vehicle. However, the problem can be considered as multi-depot and single vehicle, single depot and multi-vehicle, or multi-depot and multi-vehicle in future works.

References

[1] Birpınar, M. E., Bilgili, M. S., & Erdoğan, T. (2009). Medical waste management in Turkey: A case study of Istanbul. Waste Management, 29(1), 445-448.

[2] Alagöz, A. Z., & Kocasoy, G. (2008). Improvement and modification of the routing system for the health-care waste collection and transportation in Istanbul. Waste Management, 28(8), 1461-1471.

[3] Özceylan, E., Erbaş, M., Çetinkaya, C., & Kabak, M. (2017). A GIS-based risk reduction approach for the hazardous materials routing problem in Gaziantep. Human and Ecological Risk Assessment: An International Journal, 23(6), 1437-1453.

[4] Wu, T. H., Low, C., & Bai, J. W. (2002). Heuristic solutions to multi-depot location-routing problems. Computers & Operations Research, 29(10), 1393-1415.

[5] Laporte, G., Nobert, Y., (1981). An exact algorithm for minimizing routing and operating costs in depot location. European Journal of Operational Research 6, 224–226.

[6] Laporte G, Nobert Y, Desrochers M (1985) Optimal routing under capacity and distance restrictions. Oper Res 33:1058–1073

[7] Ghiani, G., Laporte, G., (1999). Eulerian location problems. Networks 34, 291–302.

[8] Averbakh, I., Berman, O., (2002). Minmax p-traveling salesmen location problems on a tree. Annals of Operations Research, 110, 55–62.

[9] Labbé, M., Laporte, G., Martin, I. R., & González, J. J. S. (2005). Locating median cycles in networks. European Journal of Operational Research, 160(2), 457-470.

[10] Alumur, S., & Kara, B. Y. (2007). A new model for the hazardous waste location-routing problem. Computers & Operations Research, 34(5), 1406-1423.

[11] Ponboon, S., Qureshi, A. G., & Taniguchi, E. (2016). Branch-and-price algorithm for the location-routing problem with time windows. Transportation Research Part E: Logistics and Transportation Review, 86, 1-19.

[12] Farham, M. S., Süral, H., & Iyigun, C. (2018). A column generation approach for the location-routing problem with time windows. Computers & Operations Research, 90, 249-263.

[13] Perl, Jossef, and Mark S. Daskin (1985). A warehouse location-routing problem. Transportation Research Part B: Methodological,19(5): 381-396.

[14] Nagy, G., & Salhi, S. (2007). Location-routing: Issues, models and methods. European journal of operational research, 177(2), 649-672.

[15] Vincent, F. Y., Lin, S. W., Lee, W., & Ting, C. J. (2010). A simulated annealing heuristic for the capacitated location routing problem. Computers & Industrial Engineering, 58(2), 288-299.

[16] Ting, C. J., & Chen, C. H. (2013). A multiple ant colony optimization algorithm for the capacitated location routing problem. International Journal of Production Economics, 141(1), 34-44.

[17] Albareda-Sambola, M., Díaz, J. A., & Fernández, E. (2005). A compact model and tight bounds for a combined location-routing problem. Computers & Operations Research, 32(3), 407-428.

[18] Caballero, R., González, M., Guerrero, F. M., Molina, J., & Paralera, C. (2007). Solving a multiobjective location routing problem with a metaheuristic based on tabu search. Application to a real case in Andalusia. European Journal of Operational Research, 177(3), 1751-1763.

[19] Marinakis, Y., & Marinaki, M. (2008). A bilevel genetic algorithm for a real-life location routing problem. International Journal of Logistics: Research and Applications, 11(1), 49-65.

[20] Asgari, N., Rajabi, M., Jamshidi, M., Khatami, M., & Farahani, R. Z. (2017). A memetic algorithm for a multi-objective obnoxious waste location-routing problem: a case study. Annals of Operations Research, 250(2), 279-308.

[21] Erkut, E., & Verter, V. (1998). Modeling of transport risk for hazardous materials. Operations research, 46(5), 625-642.

[22] Leonelli, P., Bonvicini, S., & Spadoni, G. (2000). Hazardous materials transportation: a risk-analysis-based routing methodology. Journal of Hazardous Materials, 71(1-3), 283-300.

[23] Androutsopoulos, K. N., & Zografos, K. G. (2010). Solving the bicriterion routing and scheduling problem for hazardous materials distribution. Transportation Research Part C: Emerging Technologies, 18(5), 713-726.

[24] Mahmoudabadi, A., & Seyedhosseini, S. M. (2014). Solving Hazmat Routing Problem in chaotic damage severity network under emergency environment. Transport policy, 36, 34-45.

[25] Zografos, K. G., & Androutsopoulos, K. N. (2004). A heuristic algorithm for solving hazardous materials distribution problems. European Journal of Operational Research, 152(2), 507-519

[26] Huang, B., Cheu, R. L., & Liew, Y. S. (2004). GIS and genetic algorithms for HAZMAT route planning with security considerations. International Journal of Geographical Information Science, 18(8), 769-787.

[27] Pamučar, D., Ljubojević, S., Kostadinović, D., & Đorović, B. (2016). Cost and risk aggregation in multi-objective route planning for hazardous materials transportation—A neuro-fuzzy and artificial bee colony approach. Expert Systems with Applications, 65, 1-15.

[28] Yilmaz, O., Kara, B. Y., & Yetis, U. (2017). Hazardous waste management system design under population and environmental impact considerations. Journal of environmental management, 203, 720-731.

[29] Erkut, E., Tjandra, S. A., & Verter, V. (2007). Hazardous materials transportation. Handbooks in operations research and management science, 14, 539-621.

[30] Shih, L. H., & Chang, H. C. (2001). A routing and scheduling system for infectious waste collection. Environmental Modeling & Assessment, 6(4), 261-269.

[31] Mourao, M. C., & Almeida, M. T. (2000). Lower-bounding and heuristic methods for a refuse collection vehicle routing problem1. European Journal of operational research, 121(2), 420-434.

[32] Marinković, N., Vitale, K., Holcer, N. J., Džakula, A., & Pavić, T. (2008). Management of hazardous medical waste in Croatia. Waste management, 28(6), 1049-1056.

[33] Abdulla, F., Qdais, H. A., & Rabi, A. (2008). Site investigation on medical waste management practices in northern Jordan. Waste management, 28(2), 450-458.

[34] Windfeld, E. S., & Brooks, M. S. L. (2015). Medical waste management–A review. Journal of environmental management, 163, 98-108.

[35] Alshraideh, H., & Qdais, H. A. (2017). Stochastic modeling and optimization of medical waste collection in Northern Jordan. Journal of Material Cycles and Waste Management, 19(2), 743-753.

[36] Mmereki, D., Baldwin, A., Li, B., & Liu, M. (2017). Healthcare waste management in Botswana: storage, collection, treatment and disposal system. Journal of Material Cycles and Waste Management, 19(1), 351-365.

[37] Baldacci, R., Mingozzi, A., & Roberti, R. (2012). Recent exact algorithms for solving the vehicle routing problem under capacity and time window constraints. European Journal of Operational Research, 218(1), 1-6.

[38] Huang, B. (2006). GIS-based route planning for hazardous material transportation. Journal of Environmental Informatics, 8(1).

[39] TUIK (2016). Turkish Statistical Institute URL http://www.tuik.gov.tr/PreHaberBultenleri.do?id=24871 (accessed 08.03.2018)

[40] Koç, Ç., Erbaş, M., & Ozceylan, E. (2018). A rich vehicle routing problem arising in the replenishment of automated teller machines. An International Journal of Optimization and Control: Theories & Applications (IJOCTA), 8(2), 276-287.

[41] Özceylan, E., Uslu, A., Erbaş, M., Çetinkaya, C., & İşleyen, S. K. (2017). Optimizing the location-allocation problem of pharmacy warehouses: A case study in Gaziantep. An International Journal of Optimization and Control: Theories & Applications (IJOCTA), 7(1), 117-129.

***Suleyman Mete**, Ph.D., is an assistant professor employed at Industrial Engineering Department, Faculty of Engineering, Munzur University in Turkey. He received his Ph.D. from Gaziantep University Industrial Engineering in 2017. His research interests include optimization, assembly line balancing, disassembly line balancing, mathematical modelling, heuristics and supply chain network design.*

***Faruk Serin** Ph.D. is an assistant professor employed at Computer Engineering Department, Faculty of Engineering, Munzur University in Turkey. He received his Ph.D. from Inonu University Computer Engineering in 2017. His research interests include optimization, graph theory, medical image processing, software development and intelligent transportation.*

Appendix

Table A1. Details of each collection center (health institutions)

No	Coordinates of each collection center	Population	District	No	Coordinates of each collection center	Population	District
1	39.092656, 39.534555	6202	Tunceli	86	38.563042, 40.133517	7285	Arıcak
2	39.107586, 39.548470	6202	Tunceli	87	38.526074, 40.024725	7285	Arıcak
3	39.108177, 39.549838	6202	Tunceli	88	38.572833, 38.825329	6147	Baskil
4	39.105014, 39.537221	6202	Tunceli	89	38.469615, 38.897301	6147	Baskil
5	39.085395, 39.537456	6202	Tunceli	90	38.391986, 39.668712	3491	Maden
6	39.071738, 39.531108	6202	Tunceli	91	38.393291, 39.669636	3491	Maden
7	39.056797, 38.915608	3756	Çemişgezek	92	38.391711, 39.667650	3491	Maden
8	39.063197, 38.910971	3756	Çemişgezek	93	38.449708, 39.306255	7759	Sivrice
9	39.107788, 39.219301	7041	Hozat	94	38.461784, 39.862198	6233	Alacakaya
10	39.017486, 39.604064	7831	Mazgirt	95	38.791417, 38.747895	6229	Keban
11	39.181128, 39.828766	2886	Nazımiye	96	38.944260, 38.715064	2537	Ağın
12	39.358613, 39.213172	5970	Ovacık	97	38.306264, 38.249966	9447	Malatya
13	38.868046, 39.325471	5488	Pertek	98	38.338283, 38.246168	9447	Malatya
14	38.864925, 39.326670	5488	Pertek	99	38.343494, 38.272933	9447	Malatya
15	39.486677, 39.899012	3065	Pülümür	100	38.343520, 38.275126	9447	Malatya
16	38.893839, 40.512630	17546	Bingöl	101	38.347269, 38.281832	9447	Malatya
17	38.896886, 40.508926	17546	Bingöl	102	38.349641, 38.282068	9447	Malatya
18	38.903743, 40.493254	17546	Bingöl	103	38.363603, 38.285414	9447	Malatya
19	38.894091, 40.493612	17546	Bingöl	104	38.349209, 38.303028	9447	Malatya
20	38.884586, 40.488033	17546	Bingöl	105	38.353717, 38.300896	9447	Malatya
21	38.884425, 40.499017	17546	Bingöl	106	38.348958, 38.317117	9447	Malatya
22	38.885775, 40.503229	17546	Bingöl	107	38.349523, 38.320828	9447	Malatya
23	38.888507, 40.516567	17546	Bingöl	108	38.349181, 38.322555	9447	Malatya
24	38.896382, 40.515534	17546	Bingöl	109	38.349161, 38.322899	9447	Malatya
25	38.748457, 40.552280	11204	Genç	110	38.347355, 38.329214	9447	Malatya
26	38.750893, 40.559666	11204	Genç	111	38.346763, 38.330915	9447	Malatya
27	38.752232, 40.562885	11204	Genç	112	38.345762, 38.329923	9447	Malatya
28	38.960349, 41.039450	11043	Solhan	113	38.363641, 38.348608	9447	Malatya
29	38.968884, 41.054195	11043	Solhan	114	38.363067, 38.346979	9447	Malatya
30	38.968853, 41.057233	11043	Solhan	115	38.339852, 38.429746	9447	Malatya
31	39.184484, 40.822721	5103	Karlıova	116	38.338702, 38.218910	9447	Malatya
32	39.166470, 40.859766	5103	Karlıova	117	38.338702, 38.241226	9447	Malatya
33	39.160725, 40.892433	5103	Karlıova	118	38.322543, 38.276932	9447	Malatya
34	39.148974, 40.872563	5103	Karlıova	119	38.342497, 38.260033	9447	Malatya
35	39.133302, 40.851683	5103	Karlıova	120	38.333575, 38.289083	9447	Malatya
36	39.297461, 41.012747	5103	Karlıova	121	38.361435, 38.282608	9447	Malatya
37	39.231998, 40.474007	4110	Adaklı	122	38.371177, 38.251983	9447	Malatya

38	39.228551, 40.482647	4110	Adaklı	123	38.341261, 38.327933	9447	Malatya
39	39.311165, 40.350023	5097	Kığı	124	38.354986, 38.307458	9447	Malatya
40	39.434421, 40.545510	2825	Yedisu	125	38.365277, 38.312533	9447	Malatya
41	39.225182, 40.068196	1928	Yayladere	126	38.353613, 38.331258	9447	Malatya
42	38.665451, 39.176808	13271	Elazığ	127	38.354711, 38.335983	9447	Malatya
43	38.668440, 39.215796	13271	Elazığ	128	38.372137, 38.318308	9447	Malatya
44	38.675805, 39.218482	13271	Elazığ	129	38.380643, 38.361883	9447	Malatya
45	38.681706, 39.205488	13271	Elazığ	130	38.341398, 37.964915	3257	Akçadağ
46	38.675665, 39.218072	13271	Elazığ	131	38.344551, 37.971046	3257	Akçadağ
47	38.675526, 39.222176	13271	Elazığ	132	38.341889, 37.965867	3257	Akçadağ
48	38.675710, 39.224222	13271	Elazığ	133	38.345567, 37.966340	3257	Akçadağ
49	38.676096, 39.226041	13271	Elazığ	134	38.284262, 38.047939	3257	Akçadağ
50	38.676552, 39.226463	13271	Elazığ	135	38.257135, 37.939866	3257	Akçadağ
51	38.680583, 39.230025	13271	Elazığ	136	38.441390, 37.869899	3257	Akçadağ
52	38.682097, 39.226022	13271	Elazığ	137	38.439853, 37.860979	3257	Akçadağ
53	38.683806, 39.227159	13271	Elazığ	138	39.042819, 38.489391	5054	Arapgir
54	38.687404, 39.226380	13271	Elazığ	139	39.043341, 38.487801	5054	Arapgir
55	38.681304, 39.256234	13271	Elazığ	140	38.782882, 38.265986	7350	Arguvan
56	38.686995, 39.268710	13271	Elazığ	141	38.426661, 38.366989	61413	Battalgazi
57	38.690172, 39.274589	13271	Elazığ	142	38.414407, 38.363186	61413	Battalgazi
58	38.656429, 39.147293	13271	Elazığ	143	38.425235, 38.367706	61413	Battalgazi
59	38.663050, 39.171864	13271	Elazığ	144	38.420140, 38.311554	61413	Battalgazi
60	38.668174, 39.184377	13271	Elazığ	145	38.422173, 38.307073	61413	Battalgazi
61	38.672751, 39.181227	13271	Elazığ	146	38.567572, 37.488809	12755	Darende
62	38.677054, 39.162677	13271	Elazığ	147	38.558679, 37.490319	12755	Darende
63	38.667702, 39.196292	13271	Elazığ	148	38.103632, 37.889787	9659	Doğanşehir
64	38.668448, 39.204698	13271	Elazığ	149	38.094143, 37.876737	9659	Doğanşehir
65	38.666832, 39.209029	13271	Elazığ	150	38.014520, 37.978566	9659	Doğanşehir
66	38.672330, 39.208134	13271	Elazığ	151	38.162058, 37.866300	9659	Doğanşehir
67	38.672774, 39.208180	13271	Elazığ	152	38.312752, 39.038298	1327	Doğanyol
68	38.659779, 39.248515	13271	Elazığ	153	38.312919, 39.037713	1327	Doğanyol
69	38.669269, 39.234170	13271	Elazığ	154	38.283361, 39.002510	1327	Doğanyol
70	38.669867, 39.254512	13271	Elâzığ	155	38.809920, 37.940828	5578	Hekimhan
71	38.675446, 39.243989	13271	Elazığ	156	38.816863, 37.930921	5578	Hekimhan
72	38.684490, 39.227117	13271	Elazığ	157	38.819480, 37.932717	5578	Hekimhan
73	38.684306, 39.226773	13271	Elazığ	158	38.358658, 38.662539	2566	Kale
74	38.594938, 39.339688	13271	Elazığ	159	38.409407, 38.751558	2566	Kale
75	38.722280, 39.857082	7865	Kovancılar	160	38.879655, 37.670062	3604	Kuluncak
76	38.721591, 39.864926	7865	Kovancılar	161	38.945336, 37.558323	3604	Kuluncak
77	38.719497, 39.870589	7865	Kovancılar	162	38.196186, 38.869032	4797	Pütürge
78	38.726224, 39.877146	7865	Kovancılar	163	38.198197, 38.872848	4797	Pütürge
79	38.767172, 39.968681	7865	Kovancılar	164	38.280418, 38.904296	4797	Pütürge
80	38.948427, 40.050371	9235	Karakoçan	165	38.594554, 38.179979	4243	Yazıhan
81	38.955583, 40.040303	9235	Karakoçan	166	38.595805, 38.180568	4243	Yazıhan
82	38.955853, 40.036226	9235	Karakoçan	167	38.598539, 38.180332	4243	Yazıhan
83	38.695150, 39.926747	6226	Palu				
84	38.695564, 39.931961	6226	Palu				
85	38.693875, 39.930698	6226	Palu				

An International Journal of Optimization and Control: Theories & Applications
ISSN: 2146-0957 eISSN: 2146-5703
Vol.9, No.2, pp.208-215 (2019)
https://doi.org/10.11121/ijocta.01.2019.00631

RESEARCH ARTICLE

Credibility based chance constrained programming for project scheduling with fuzzy activity durations

Oğuzhan Ahmet Arık [a] *

[a] *Department of Industrial Engineering, Nuh Naci Yazgan University, Turkey*
oaarik@nny.edu.tr

ARTICLE INFO

Article history:
Received: 9 July 2018
Accepted: 29 March 2019
Available Online: 30 April 2019

Keywords:
Project scheduling
Fuzzy activity duration
Credibility
Chance constraint

AMS Classification 2010:
90C70, 65K05

ABSTRACT

This paper proposes a credibility based chance constrained programming approach for project scheduling problems with fuzzy activity durations where the objective is to minimize the fuzzy project completion time. This paper expresses the fuzzy events such as a project activity's duration or project completion time with fuzzy chance constraints and the chance of a fuzzy event is illustrated with fuzzy credibility distribution. Due to uncertainty in durations of a project, fuzzy sets and fuzzy numbers can be used in order to illustrate the uncertainty and find a solution space for the problem. Therefore, fuzzy credibility based chance constraint technique is investigated for project scheduling problems with fuzzy activity durations considering the uncertainty or chance of a fuzzy event within a closed interval. In this paper, a fuzzy mathematical model and its crisp equivalent by using credibility measure and chance-constrained programming are given for project scheduling problems with fuzzy activity durations.

1. Introduction

Activity durations in projects are mostly assumed as deterministic values but the real-life is full of uncertainty so determining each activity's duration in deterministic time periods may not be always possible. A decision maker or a project planner sometimes needs to express activity durations in a time interval in order to encode his/her biased judgment or experience for those activities. In order to express activity's durations in an interval or to encode the uncertainty in activity durations, fuzzy sets, and fuzzy numbers can be used. In this paper, fuzzy events such as a project activity's duration or project completion time is less than a certain real number are expressed with fuzzy chance constraints and the chance of a fuzzy event is illustrated with fuzzy credibility distribution. In order to express the uncertainty or chance of a fuzzy event within an interval, fuzzy credibility based chance constrained problem is investigated for project scheduling problems with fuzzy activity durations.

Fuzziness in project management and project scheduling has been investigated by researchers for more than 30 years. As far as findings from the literature search, the first study about fuzziness in project management was conducted by DePorter and Ellis [1]. Although they are not recent survey papers conducted by Bonnal et al. [2] and Herroelen and Leus [3], these papers can be a good guidance for readers. Hapke et al. [4] presented a fuzzy project scheduling decision support system which is applied to software project programming. There are two performance criteria for minimizing the project makespan and the maximum delay while allocating resources among the dependent activities in their study. Hapke and Slowinski [5] proposed generalizing the prioritized heuristic method to solve resource-constrained project planning problems with ambiguous time parameters. Wang and Fu [6] investigated fuzzy project planning in inflationary conditions. In their work, they dismissed four fuzzy timing models under inflationary conditions and solved their models by the α-cut method. Hapke et al. [7] investigated a multi-mode project planning problem under multi-categorized resource constraints with fuzzy activities. They presented a Simulated Annealing approach to creating a Pareto set for the problem. Özdamar and Alanya [8] investigated uncertainty modeling for software development projects and they presented a case study for their model. Wang [9] used possibility theory to encode uncertainty and he used a fuzzy beam search algorithm to minimize scheduling risk of a project for a new product development. Chanas et al. [10] analyzed the notion of necessary criticality with

*Corresponding author

respect to the path and to activities in a network with fuzzy activity durations. Chanas and Zieliński [11] presented complexity results for problems of evaluating the criticality of activities in planar networks with duration time intervals. They also showed that problems are in classes of NP-Hard and NP-Complete. Pan and Yeh [12] studied resource-constrained project scheduling problems with uncertain activity durations and they proposed a fuzzy genetic algorithm with a tabu mechanism to find an approximate solution. In another study of Pan and Yeh [13], they proposed a fuzzy simulated annealing approach to finding a solution for resource-constrained fuzzy project scheduling problem. Wang [14] developed a robust scheduling methodology for uncertain product development projects and proposed a genetic algorithm dependent on the possibility theory. Ke and Liu [15] studied project scheduling problems with fuzzy durations and total cost. With a hybrid intelligent algorithm that includes fuzzy simulation and genetic algorithms, they proposed fuzzy chance-constrained programming approach to solve the problem. Zieliński [16] demonstrated some polynomial solvable cases for the problems of calculating the interval between the latest starting times and the activity floats in networks with uncertain durations. Agarwal et al. [17] investigated resource-constrained project scheduling problems under fuzzy activity durations aimed at minimizing the time to complete the project and proposed the artificial immune system as a solution approach to the problem. Ke and Liu [18] investigated resource allocation in project scheduling problems with the mixed uncertainty of randomness and fuzziness for fuzzy activity durations. They proposed three types of random fuzzy models and presented a genetic algorithm with random fuzzy simulations as a solution approach. Long and Ohsato [19] proposed a fuzzy critical chain method for project scheduling problems with uncertainty and resource constraints. In their method, they developed a desired deterministic schedule with resource constraints and added a project buffer at the end of the calculations with fuzzy numbers. Huang et al. [20] proposed a hybrid intelligent algorithm, including genetic algorithm and random fuzzy simulation, to solve a project scheduling problem for software development with random fuzzy activity durations. Moradi et al. [21] investigated resource constrained project scheduling problem under uncertainty of resource availability and project durations. They also proposed some game theory methods for forming coalitions among subcontractors and they coded satisfactions of subcontractors with fuzzy set theory. Hu and Li [22] proposed an improved fuzzy critical path method for trapezoidal fuzzy numbers. Zhang et al. [23] proposed a novel solution approach for fuzzy programming model by proving lower and upper bounds of fuzzy objective values at a possibility level. Then, they applied their model to a project scheduling problem. Zhang et al. [24] investigated project selection and project scheduling problems under fuzzy environment. They proposed a multi objective nonlinear mathematical model and an algorithm for solving the problem. Some of the other recent papers in the literature are conducted by Castro-Lacouture et al. [25], Afshar and Fathi [26], Shi and Gong [27], Wang and Huang [28] , Bhaskar et al. [29], Ponz-Tienda et al. [30], Maravas and Pantouvakis [31], Xu and Zhang [32], Masmoudi and Haït [33], Huang et al. [34] , Chrysafis and Papadopoulos [35], Huang et al. [36], Yu et al. [37], Yousefli [38], Zohoori et al. [39], Habibi et al. [40] Alipouri et al. [41] and Birjandi and Mousavi [42].

As seen from the literature review of this paper, fuzzy project scheduling problems have been mostly investigated with fuzzy ranking methods, fuzzy simulation, and heuristic or metaheuristic. This paper investigates fuzzy scheduling problems with fuzzy chance-constrained programming approaches. For the readers, some scheduling papers (Toksarı and Arık [43], Arık and Toksarı [44], [45]) investigating fuzzy chance-constrained programming approach can be a good guidance for applicability and validity of the proposed method.

2. Basic definitions

This section presents some of basic definitions and notations of fuzzy numbers and measures of a fuzzy event such as credibility, possibility, and necessity for the readers.

If a fuzzy number $\tilde{A}$ with a membership function $\mu_{\tilde{A}}(x): R \rightarrow [0,1]$ is presented with three points on the real axis such that $\tilde{A} = (A^L, A^C, A^R)$, and this fuzzy number's membership function is as seen in Eq (1), then $\tilde{A}$ is defined as a triangular fuzzy number (TFN).

$$\mu_A^{(x)} = \begin{cases} \dfrac{x - A^L}{A^C - A^L}, & if\ A^C \geq x \geq A^L \\ \dfrac{A^R - x}{A^R - A^C}, & if\ A^C \geq x \geq A^R \\ 0, & otherwise \end{cases} \quad (1)$$

Possibility theory (Zadeh [46]) measures the chance of fuzzy event and its measure has a dual named Necessity measure. For a TFN $\tilde{A}$ with $\mu_{\tilde{A}}(x)$, Possibility and Necessity measures are calculated as follows:

$$\Pi_A(A \leq r) = \underset{x \leq r}{Sup}\ \mu_{\tilde{A}}^{(x)} = \begin{cases} 0, & r \leq A^L \\ \dfrac{r - A^L}{A^C - A^L}, & A^L \leq r \leq A^C \\ 1, & r \geq A^C \end{cases} \quad (2)$$

$$N_A(A \le r) = 1 - (\sup_{x>r} \mu_{\tilde{A}}^{(x)}) = \begin{cases} 0, & r \le A^C \\ \dfrac{r - A^C}{A^R - A^C}, & A^C \le r \le A^R \\ 1, & r \ge A^R \end{cases} \quad (3)$$

where r is a real number. These fuzzy measures are dual to each other, but they are not dual by their own. Credibility measure [47] is a self-dual fuzzy measure and it is average of Possibility and Necessity measures as follows:

$$Cr_A(A \le r) = \frac{1}{2}\left(\Pi_A(A \le r) + N_A(A \le r)\right) \quad (4)$$

The credibility distribution function $\Phi : R \to [0,1]$ (see [48]) of fuzzy number ξ can be shown in Eq. (5).

$$\Phi(x) = Cr_{\xi}(\theta \in \Theta | \xi(\theta) \le x) \quad (5)$$

The credibility distribution function $\Phi(x)$ is a strictly increasing function on the real axis and it has an inverse function $\Phi^{-1}(\alpha)$ that is unique for any α confidence level. $\Phi^{-1}(\alpha)$ is the inverse credibility distribution function and is a strictly increasing function as seen in Figure 1.

For a TFN Ã, the credibility distribution function and inverse credibility distribution function (see Figure 1) are calculated as follows:

$$\Phi(x) = Cr_A(A \le r) = \begin{cases} 0, & r \le A^L \\ \dfrac{r - A^L}{2(A^C - A^L)}, & A^L \le r \le A^C \\ \dfrac{A^R + r - 2A^C}{2(A^R - A^C)}, & A^C \le r \le A^R \\ 1, & r \ge A^R \end{cases} \quad (6)$$

$$\Phi^{-1}(\alpha) = \begin{cases} 2\alpha(A^C - A^L) + A^L, & 0 \le \alpha < 0.5 \\ A^R - (2 - 2\alpha)(A^R - A^C), & 0.5 \le \alpha \le 1 \end{cases} \quad (7)$$

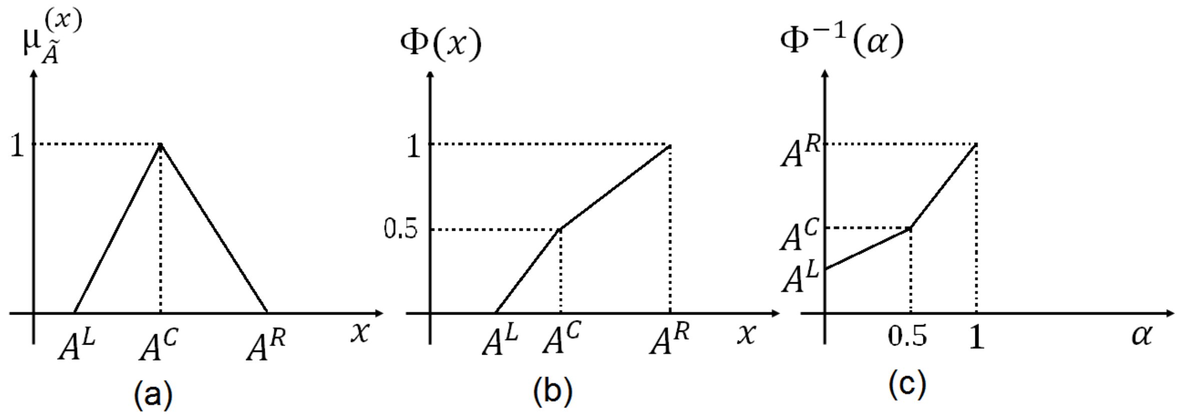

Figure 1. The membership function of a TFN (a), the credibility distribution function (b), the inverse credibility distribution function (c)

3. Fuzzy project scheduling mathematical model

In this chapter, the project scheduling problem with fuzzy activity durations where the objective is to minimize project completion time (makespan) is introduced. All activities are expressed with TFN because of the uncertainty in their existences. The proposed fuzzy model as follows:

<u>Indicies:</u>

i : index for activities,

<u>Parameters:</u>

$P_{i,j}$: precedence relationship between activity i and activity j ($i \neq j$). If activity i is a predecessor of activity j, then $P_{i,j} = 1$, otherwise it is zero.

$\tilde{t}_i$: fuzzy activity duration of activity i

<u>Decision variables:</u>

$\tilde{S}_i$: starting time of activity i

$\tilde{C}_i$: completion time of activity i

$\tilde{C}_{\max}$: completion time of the project (the makespan)

<u>Model:</u>

$$Min\ f = \tilde{C}_{max} \quad (8)$$

<u>s.t.:</u>

$$\tilde{C}_{max} \ge \tilde{C}_i \quad \forall i \quad (9)$$

$$\tilde{C}_i = \tilde{S}_i + \tilde{t}_i \quad \forall i \quad (10)$$

$$\tilde{S}_j \ge \tilde{C}_i P_{i,j} \quad \forall i, \forall j, P_{i,j} = 1 and\ i \ne j \quad (11)$$

$$\tilde{C}_i, \tilde{S}_i \ge 0 \quad (12)$$

$$\tilde{C}_{\max} \ge 0 \quad (13)$$

The objective function (8) is to minimize fuzzy makespan of the project. Constraint (9) guarantees that the fuzzy makespan is the maximum completion time of all fuzzy activities. Constraint (10) shows that completion time of an activity is equal to the sum of its start time and duration. Constraint (11) assures that the starting time of activity j must be greater than or equal to the completion time of activity i, if there is a precedence relation from activity i to activity j. Constraints (12-13) show necessary domains of all decision variables.

4. Fuzzy chance constrained programming model

For stochastic optimization problems, Charnes and Cooper [49] introduced the chance-constrained programming method. Liu and Iwamura [50] modified Charnes and Cooper's [49] proposed method for the fuzzy environment and they presented an auxiliary crisp model for solving problems with fuzzy parameters and decision variables. Their auxiliary crisp model is as follows:

$$\max \quad f(x)$$

$$s.t.: \quad Cr\left\{\xi | g_i(x,\xi) \le 0, i = 1,2,\dots,p\right\} \ge \alpha_i \; \forall i,$$

In order to convert chance constraints with credibility measures to crisp equivalents, the inverse credibility distributions (see Eq. (7)) of fuzzy events are used. For any predetermined confidence level α_i, there is an unique $\Phi^{-1}(\alpha_i \mid K_{\alpha_i} \le \xi_i)$ value where $Cr\left\{\xi_i | K_{\alpha_i} \le \xi_i\right\} = \alpha_i$. With help of Eq. (7), credibility based chance constrained mathematical model of project scheduling problem can be seen as follows:

$$\min f = \Phi^{-1}_{C_{\max}}(\alpha) \tag{14}$$

<u>*s.t.:*</u>

$$\Phi^{-1}_{C_{max}}(\alpha) \ge \Phi^{-1}_{C_i}(\alpha) \; \forall i \tag{15}$$

$$\Phi^{-1}_{C_i}(\alpha) = \Phi^{-1}_{S_i}(\alpha) + \Phi^{-1}_{t_i}(\alpha) \forall i \tag{16}$$

$$\Phi^{-1}_{S_j}(\alpha) \ge \Phi^{-1}_{C_i}(\alpha) P_{i,j} \; \forall i, \quad \forall j \; P_{i,j} = 1 and\, i \ne j \tag{17}$$

$$\Phi^{-1}_{S_i}(\alpha), \Phi^{-1}_{C_i}(\alpha), \Phi^{-1}_{t_i}(\alpha) \ge 0 \tag{18}$$

$$\Phi^{-1}_{C_{max}}(\alpha) \ge 0 \tag{19}$$

$$\Phi^{-1}_{t_i}(\alpha) = \begin{cases} 2\alpha\left(t^C - t^L\right) + t^L, & if\; 0 \le \alpha < 0.5 \\ t^R - (2-2\alpha)\left(t^R - t^C\right), & if\; 0.5 \le \alpha \le 1 \end{cases} \forall i \tag{20}$$

The objective function (14) is to minimize the equivalent makespan value of the inverse credibility distribution function for makespan values for a given confidence level $\alpha \in [0,1]$. The others constraints (15-19) have same missions with constraints (9-13). Constraint (20) transforms the fuzzy activity duration $\tilde{t}_i = (t^L, t^C, t^R)$ to the equivalent of that activity's duration of the inverse function of credibility distribution for a given confidence level α.

5. Numerical example

In this section of the paper, a numerical example is presented for the proposed solution approach. Let us have a project including ten activities. The durations of these activities are expressed with TFNs as seen in Table 1. For a given confidence level α, the mathematical model in Eqs. (14-20) can be used to find the project completion time's equivalent considering all fuzzy activity durations at the same confidence level α. Table 2 shows the solution space of the problem having activities in Table 1 for different confidence levels from 0 to 1 with increment 0.05.

Table 1. Comparison of the mean-field predictions

i	**Activity Code**	$\tilde{t}_i = (t_i^L, t_i^C, t_i^R)$ **in weeks**	**Predecessors**
1	A	(5,7,9)	-
2	B	(6,8,10)	-
3	C	(3,4,7)	B
4	D	(13,15,19)	A
5	E	(9,28,35)	C,D
6	F	(2,5,6)	D
7	G	(11,17,19)	F
8	H	(9,13,15)	E,G
9	I	(7,8,9)	K
10	J	(2,3,4)	L

The precedence relations of the project in Table 1 can be seen in Figure 2.

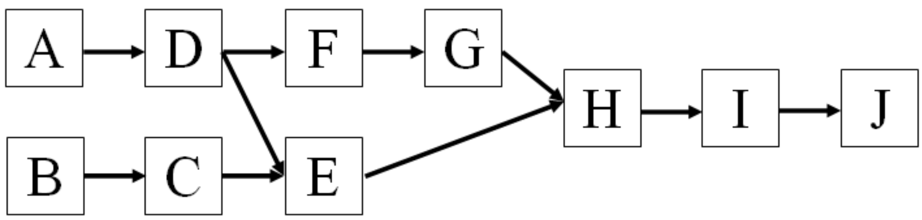

Figure 2. Activity-on-Node diagram of the project

Table 2. Project completion times for different confidence levels

Confidence level α	Project completion time (in weeks)	Critical path
0.00	49.0	Path#1
0.05	50.9	Path#1
0.10	52.8	Path#1
0.15	54.7	Path#1
0.20	56.6	Path#1 or Path#2
0.25	59.5	Path#2
0.30	62.4	Path#2
0.35	65.3	Path#2
0.40	68.2	Path#2
0.45	71.1	Path#2
0.50	74.0	Path#2
0.55	76.9	Path#2
0.60	79.8	Path#2
0.65	82.7	Path#2
0.70	85.6	Path#2
0.75	88.5	Path#2
0.80	91.4	Path#2
0.85	94.3	Path#2
0.90	97.2	Path#2
0.95	101.1	Path#2
1.00	103.0	Path#2

***Path#1** = A / D / F / G / H / I / J ***Path#2** = A / D / E / H / I / J

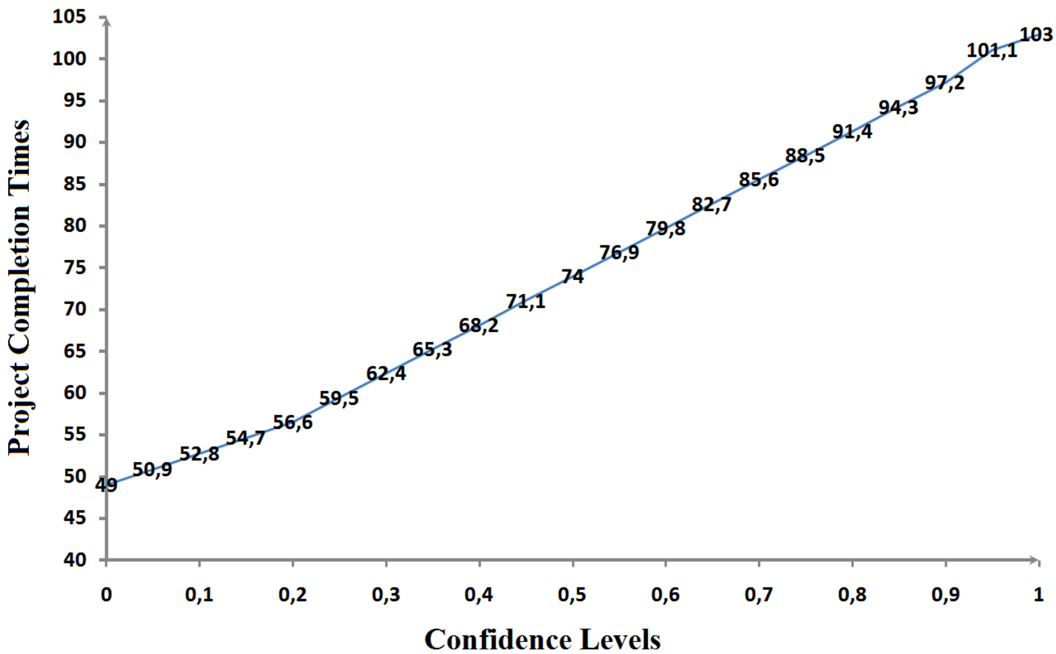

Figure 3. The relationship between completion times and confidence levels

As seen in Figure 3 and Table 2, difference confidence levels produce different project completion times and activities on the critical path. While confidence level is increasing, the project completion time is also increasing and critical activities may change. The results in Table 2 are obtained with GAMS software. This proposed model can be considered to produce the solution space of a fuzzy problem. The solution space of project completion time is on the interval of [49].

6. Conclusion

This paper investigates a project scheduling problem with fuzzy activity durations where the objective is to minimize fuzzy project completion time. Fuzzy credibility based chance constraint technique is investigated for project scheduling problems with fuzzy activity durations considering the uncertainty or chance of a fuzzy event within a closed interval. In this paper, a fuzzy mathematical model and its crisp equivalent by using credibility measure and chance-constrained programming are given for project scheduling problems with fuzzy activity durations. A numerical example is illustrated and it is shown that how the critical path of a project can be changed by using different levels of uncertainty predetermined with given confidence levels. For future researches, credibility based chance constrained programming approach can be investigated with other fuzzy project scheduling problems where other parameters such as precedence relations are expressed in fuzzy sets with resource constraints, resource allocation, resource ability constraints.

Acknowledgments

The authors would like to thank the anonymous reviewers for their valuable comments.

References

[1] DePorter, E. L., & Ellis, K. P. (1990). Optimization of project networks with goal programming and fuzzy linear programming. Computers and Industrial Engineering, 19(1–4), 500–504.

[2] Bonnal, P., Gourc, D., & Lacoste, G. (2004). Where do we stand with fuzzy project scheduling? Journal of Construction Engineering and Management, 130(1), 114–123.

[3] Herroelen, W., & Leus, R. (2005). Project scheduling under uncertainty: Survey and research potentials. European Journal of Operational Research, 165(2), 289–306.

[4] Hapke, M., Jaszkiewicz, A., & Slowinski, R. (1994). Fuzzy project scheduling system for software development. Fuzzy Sets and Systems, 67(1), 101–117.

[5] Hapke, M., & Slowinski, R. (1996). Fuzzy priority heuristics for project scheduling. Fuzzy Sets and Systems, 83(3), 291–299.

[6] Wang, H.-F., & Fu, C.-C. (1996). Fuzzy project scheduling models under inflation condition. International Journal of Uncertainty, Fuzziness and Knowlege-Based Systems, 4(6), 497–514.

[7] Hapke, M., Jaszkiewicz, A., & Slowinski, R. (1997). Fuzzy project scheduling with multiple criteria. In IEEE International Conference on Fuzzy Systems, 3, 1277–1282.

[8] Özdamar, L., & Alanya, E. (2001). Uncertainty Modelling in Software Development Projects (With Case Study). Annals of Operations Research, 102(1–4), 157–178.

[9] Wang, J. (2002). A fuzzy project scheduling approach to minimize schedule risk for product development. Fuzzy Sets and Systems, 127(2), 99–116.

[10] Chanas, S., Dubois, D., & Zieliński, P. (2002). On the sure criticality of tasks in activity networks with imprecise durations. IEEE Transactions on Systems, Man, and Cybernetics, Part B: Cybernetics, 32(4), 393–407.

[11] Chanas, S., & Zieliński, P. (2003). On the hardness of evaluating criticality of activities in a planar network with duration intervals. Operations Research Letters, 31(1), 53–59.

[12] Pan, H., & Yeh, C.-H. (2003). Fuzzy project scheduling. In IEEE International Conference on Fuzzy Systems, 1, 755–760.

[13] Pan, H., & Yeh, C.-H. (2003). A metaheuristic approach to fuzzy project scheduling. In Lecture Notes in Artificial Intelligence (Subseries of Lecture Notes in Computer Science), 2773 PART, 1081–1087.

[14] Wang, J. (2004). A fuzzy robust scheduling approach for product development projects. European Journal of Operational Research, 152(1), 180–194.

[15] Ke, H., & Liu, B. (2004). Project scheduling problem with fuzzy activity duration times. In IEEE International Conference on Fuzzy Systems, 2, 819–823.

[16] Zieliński, P. (2005). On computing the latest starting times and floats of activities in a network with imprecise durations. Fuzzy Sets and Systems, 150(1), 53–76.

[17] Agarwal, R., Tiwari, M. K., & Mukherjee, S. K. (2007). Artificial immune system based approach for solving resource constraint project scheduling problem. International Journal of Advanced Manufacturing Technology, 34(5–6), 584–593.

[18] Ke, H., & Liu, B. (2007). Project scheduling problem with mixed uncertainty of randomness and fuzziness. European Journal of Operational Research, 183(1), 135–147.

[19] Long, L. D., & Ohsato, A. (2008). Fuzzy critical chain method for project scheduling under resource constraints and uncertainty. International Journal of Project Management, 26(6), 688–698.

[20] Huang, W., Ding, L., Wen, B., & Cao, B. (2009). Project scheduling problem for software development with random fuzzy activity duration times. Lecture Notes in Computer Science (including subseries Lecture Notes in Artificial Intelligence and Lecture Notes in Bioinformatics), Vol. 5552.

[21] Moradi, M., Hafezalkotob, A., & Ghezavati, V. (2018). Sustainability in fuzzy resource constraint project scheduling in a cooperative environment under uncertainty: Iran's Chitgar lake case study. Journal of Intelligent and Fuzzy Systems, 35(6), 6255–6267.

[22] Hu, C., & Liu, D. (2018). Improved Critical Path Method with Trapezoidal Fuzzy Activity Durations. Journal of Construction Engineering and Management, 144(9).

[23] Zhang, Q., Zhou, J., Wang, K., & Pantelous, A. A. (2018). An Effective Solution Approach to Fuzzy Programming with Application to Project Scheduling. International Journal of Fuzzy Systems, 20(8), 2383–2398.

[24] Zhang, X., Hipel, K. W., & Tan, Y. (2019). Project portfolio selection and scheduling under a fuzzy environment. Memetic Computing.

[25] Castro-Lacouture, D., Süer, G. A., Gonzalez-Joaqui, J., & Yates, J. K. (2009). Construction project scheduling with time, cost, and material restrictions using fuzzy mathematical models and critical path method. Journal of Construction Engineering and Management, 135(10), 1096–1104.

[26] Afshar, A., & Fathi, H. (2009). Fuzzy multi-objective optimization of finance-based scheduling for construction projects with uncertainties in cost. Engineering Optimization, 41(11), 1063–1080.

[27] Shi, Q., & Gong, T. (2009). An improved project buffer sizing approach to critical chain management under resources constraints and fuzzy uncertainty. In 2009 International Conference on Artificial Intelligence and Computational Intelligence, AICI 2009, 1, 486–490.

[28] Wang, X., & Huang, W. (2010). Fuzzy resource-constrained project scheduling problem for software development. Wuhan University Journal of Natural Sciences, 15(1), 25–30.

[29] Bhaskar, T., Pal, M. N., & Pal, A. K. (2011). A heuristic method for RCPSP with fuzzy activity times. European Journal of Operational Research, 208(1), 57–66.

[30] Ponz-Tienda, J. L., Pellicer, E., & Yepes, V. (2012). Complete fuzzy scheduling and fuzzy earned value management in construction projects. Journal of Zhejiang University: Science A, 13(1), 56–68.

[31] Maravas, A., & Pantouvakis, J.-P. (2012). Project cash flow analysis in the presence of uncertainty in activity duration and cost. International Journal of Project Management, 30(3), 374–384.

[32] Xu, J., & Zhang, Z. (2012). A fuzzy random resource-constrained scheduling model with multiple projects and its application to a working procedure in a large-scale water conservancy and hydropower construction project. Journal of Scheduling, 15(2), 253–272.

[33] Masmoudi, M., & Haït, A. (2013). Project scheduling under uncertainty using fuzzy modelling and solving techniques. Engineering Applications of Artificial Intelligence, 26(1), 135–149.

[34] Huang, W., Oh, S.-K., & Pedrycz, W. (2013). A fuzzy time-dependent project scheduling problem. Information Sciences, 246, 100–114.

[35] Chrysafis, K. A., & Papadopoulos, B. K. (2015). Possibilistic moments for the task duration in fuzzy PERT. Journal of Management in Engineering, 31(5).

[36] Huang, X., Dai, W., & Du, B. (2016). Resource-constrained project scheduling problem for large complex equipment: A hybrid approach using pareto genetic algorithm and interval-valued intuitionistic fuzzy sets. Academic Journal of Manufacturing Engineering, 14(1), 12–21.

[37] Yu, M.-C., Dang, V.-L., & Yeh, H.-C. (2017). Measuring cash flow and overdraft for fuzzy project networks with overlapping activities. Journal of Civil Engineering and Management, 23(4), 487–498.

[38] Yousefli, A. (2017). A fuzzy ant colony approach to fully fuzzy resource constrained project scheduling problem. Industrial Engineering and Management Systems, 16(3), 307–315.

[39] Zohoori, B., Verbraeck, A., Bagherpour, M., & Khakdaman, M. (2019). Monitoring production time and cost performance by combining earned value analysis and adaptive fuzzy control. Computers and Industrial Engineering, 127, 805–821.

[40] Habibi, F., Barzinpour, F., & Sadjadi, S. J. (2019). A mathematical model for project scheduling and material ordering problem with sustainability considerations: A case study in Iran. Computers and Industrial Engineering, 128, 690–710.

[41] Alipouri, Y., Sebt, M. H., Ardeshir, A., & Chan, W. T. (2019). Solving the FS-RCPSP with hyper-heuristics: A policy-driven approach. Journal of the Operational Research Society, 70(3), 403–419.

[42] Birjandi, A., & Mousavi, S. M. (2019). Fuzzy resource-constrained project scheduling with

multiple routes: A heuristic solution. Automation in Construction, 100, 84–102.

[43] Toksarı, M. D., & Arık, O. A. (2017). Single machine scheduling problems under position-dependent fuzzy learning effect with fuzzy processing times. Journal of Manufacturing Systems, 45, 159–179.

[44] Arık, O. A., & Toksarı, M. D. (2018). Multi-objective fuzzy parallel machine scheduling problems under fuzzy job deterioration and learning effects. International Journal of Production Research, 56(7), 2488–2505.

[45] Arık, O. A., & Toksarı, M. D. (2018). Fuzzy chance constrained programming technique for single machine earliness/tardiness scheduling problem under effects of fuzzy learning and deterioration. Sakarya University Journal of Science, 22(2), 1–1.

[46] Zadeh, L. A. (1978). Fuzzy sets as a basis for a theory of possibility. Fuzzy Sets and Systems, 1(1), 3–28.

[47] Liu, B., & Liu, Y. (2002). Expected value of fuzzy variable and fuzzy expected value models. IEEE Transactions on Fuzzy Systems, 10(4), 445–450.

[48] Liu, B. (2002). Theory and Practice ofUncertain Programming (2nd ed.). Heidelberg: Springer-Verlag Berlin.

[49] Charnes, A., & Cooper, W. W. (1959). Chance-Constrained Programming. Management Science, 6(1), 73–79.

[50] Liu, B., & Iwamura, K. (1998). Chance constrained programming with fuzzy parameters. Fuzzy Sets and Systems, 94(2), 227–237.

Oğuzhan Ahmet Arık *obtained his B.S. degree from Industrial Engineering Department of Bahcesehir University in Turkey in 2009. He obtained his M.S. and Ph.D. in Industrial Engineering Department of Erciyes University in 2014 and 2017 respectively. He has worked as Asst. Prof. Dr. in Industrial Engineering Department of Nuh Naci Yazgan University since 2017. His research area lies in scheduling, project management, heuristics and fuzzy sets.*

An International Journal of Optimization and Control: Theories & Applications
ISSN:2146-0957 eISSN:2146-5703
Vol.9, No.2, pp.216-222 (2019)
http://doi.org/10.11121/ijocta.01.2019.00738

RESEARCH ARTICLE

Some integral inequalities for multiplicatively geometrically P-functions

Huriye Kadakal

Ministry of Education, Bulancak Bahçelievler Anatolian High School, Giresun, Turkey
huriyekadakal@hotmail.com

ARTICLE INFO

Article History:
Received 24 October 2018
Accepted 15 March 2019
Available 31 July 2019

Keywords:
Multiplicatively P-functions
Multiplicatively geometrically P-function

AMS Classification 2010:
26A51; 26D15

ABSTRACT

In this manuscript, by using a general identity for differentiable functions we can obtain new estimates on a generalization of Hadamard, Ostrowski and Simpson type inequalities for functions whose derivatives in absolute value at certain power are multiplicatively geometrically P-functions. Some applications to special means of real numbers are also given.

1. Preliminaries

Let function $\psi : I \subseteq \mathbb{R} \to \mathbb{R}$ be a convex defined on an interval I of real numbers and $\zeta, \eta \in I$ with $\zeta < \eta$. The following

$$\psi\left(\frac{\zeta+\eta}{2}\right) \leq \frac{1}{\eta-\zeta}\int_{\zeta}^{\eta} \psi(u)du \leq \frac{\psi(\zeta)+\psi(\eta)}{2}. \tag{1}$$

holds. This double inequality is known in the literature as Hermite-Hadamard integral inequality for convex functions [1]. Both inequalities hold in the reversed direction if the function ψ is concave.

Let $\psi : I \subseteq \mathbb{R} \to \mathbb{R}$ be a mapping differentiable in I°, the interior of I, and let $\zeta, \eta \in I^{\circ}$ with $\zeta < \eta$. If $|\psi'(x)| \leq M$ for all $x \in [\zeta, \eta]$, then we hold the following inequality

$$\left|\psi(x) - \frac{1}{\eta-\zeta}\int_{\zeta}^{\eta} \psi(t)dt\right| \leq \frac{M}{\eta-\zeta}\left[\frac{(x-\zeta)^2+(\eta-x)^2}{2}\right]$$

for all $x \in [\zeta, \eta]$. This inequality is known as the Ostrowski inequality [2].

The following inequality is well known as Simpson's inequality .

Let $\psi : [\zeta, \eta] \to \mathbb{R}$ be a four-times continuously differentiable mapping on (ζ, η) and $\left\|\psi^{(4)}\right\|_{\infty} = \sup_{x\in(\zeta,\eta)} \left|\psi^{(4)}(x)\right| < \infty$. Then the following inequality

$$\left|\frac{1}{3}\left[\frac{\psi(\zeta)+\psi(\eta)}{2} + 2\psi\left(\frac{\zeta+\eta}{2}\right)\right] - \frac{1}{\eta-\zeta}\int_{\zeta}^{\eta} \psi(u)du\right| \leq \frac{1}{2880}\left\|\psi^{(4)}\right\|_{\infty}(\eta-\zeta)^4.$$

holds.

Definition 1. *A nonnegative function $\psi : I \subseteq \mathbb{R} \to \mathbb{R}$ is called P-function if*

$$\psi(t\zeta + (1-t)\eta) \leq \psi(\zeta) + \psi(\eta)$$

holds for all $\zeta, \eta \in I$ and $t \in (0,1)$.

We will denote by $P(I)$ the set of P-function on the interval I. Note that $P(I)$ contains all non-negative convex and quasi-convex functions.

In [3], Dragomir et al. proved the following inequality of Hadamard type for class of P-functions.

Theorem 1. *Let $\psi \in P(I)$, $\zeta, \eta \in I$ with $\zeta < \eta$ and $\psi \in L[\zeta, \eta]$. Then*

$$\psi\left(\frac{\zeta+\eta}{2}\right) \le \frac{2}{\eta-\zeta}\int_{\zeta}^{\eta}\psi(u)du \le 2\left[\psi(\zeta)+\psi(\eta)\right].$$

Definition 2 ([4]). *Let $I \neq \emptyset$. The function $\psi : I \to [0,\infty)$ is called multiplicatively P-function (or* log-*P-function), if the inequality*

$$\psi\left(t\zeta+(1-t)\eta\right) \le \psi(\zeta)\psi(\eta)$$

holds for all $\zeta, \eta \in I$ and $t \in [0,1]$.

We will denote by $MP(I)$ the class of all multiplicatively P-convex functions on interval I. Clearly, $\psi : I \to [0,\infty)$ is multiplicatively P-function if and only if $\log\psi$ is P-function. We state that the range of the multiplicatively P-functions is greater than or equal to 1. In recent years many authors have studied P-functions and multiplicatively P-function, see [3, 5–8] and therein.

In [4], Kadakal proved the following inequalities of Hermite-Hadamard type integral inequalities for class of multiplicatively P-functions.

Theorem 2. *Let the function $\psi : I \to [1,\infty)$ be a multiplicatively P-function. If $\psi \in L[\zeta,\eta]$, then the following inequalities hold:*

$$\begin{aligned} &i)\quad \psi\left(\frac{\zeta+\eta}{2}\right)\\ \le\ & \frac{1}{\eta-\zeta}\int_{\zeta}^{\eta}\psi(u)\psi(\zeta+\eta-u)\,du \le \left[\psi(\zeta)\psi(\eta)\right]^2\\ &ii)\quad \psi\left(\frac{\zeta+\eta}{2}\right)\\ \le\ & \psi(\zeta)\psi(\eta)\frac{1}{\eta-\zeta}\int_{\zeta}^{\eta}\psi(u)du \le \left[\psi(\zeta)\psi(\eta)\right]^2 \end{aligned}$$

In [9], Kadakal et al. gave the following definition in the literature.

Definition 3. *Let $I \neq \emptyset$ be an interval in $(0,\infty) \subseteq \mathbb{R}$. The function $\psi : I \subseteq (0,\infty) \to [0,\infty)$ is said to be multiplicatively geometrically P-function, if the following inequality*

$$\psi\left(\zeta^t\eta^{1-t}\right) \le \psi(\zeta)\psi(\eta)$$

holds for all $\zeta, \eta \in I$ and $t \in [0,1]$.

We will denote by $MGP(I)$ the class of all multiplicatively geometrically P-convex functions on interval I. Clearly, $\psi : I \subseteq (0,\infty) \to [0,\infty)$ is multiplicatively geometrically P-function if and only if $log\psi$ is P-GA-function. The range of the multiplicatively geometrically P-functions is greater than or equal to 1.

Lemma 1 ([10]). *Let $\psi : I \subseteq \mathbb{R} \to \mathbb{R}$ be a differentiable mapping on I° and $\zeta, \eta \in I$ with $\zeta < \eta$. If $\psi' \in L[\zeta,\eta]$, then*

$$\begin{aligned} &\psi\left(\sqrt{\zeta\eta}\right) - \frac{1}{\ln\eta-\ln\zeta}\int_{\zeta}^{\eta}\frac{\psi(u)}{u}du\\ =\ & \frac{\ln\eta-\ln\zeta}{4}\left[\zeta\int_0^1 t\left(\frac{\eta}{\zeta}\right)^{\frac{t}{2}} f'\left(\zeta^{1-t}(\zeta\eta)^{\frac{t}{2}}\right)dt\right.\\ &\left.-\eta\int_0^1 t\left(\frac{\zeta}{\eta}\right)^{\frac{t}{2}} f'\left(\eta^{1-t}(\eta)^{\frac{t}{2}}\right)dt\right] \end{aligned}$$

and

$$\begin{aligned} &\frac{\psi(\zeta)+\psi(\eta)}{2} - \frac{1}{\ln\eta-\ln\zeta}\int_{\zeta}^{\eta}\frac{\psi(u)}{u}du\\ =\ & \frac{\ln\eta-\ln\zeta}{2}\left[\zeta\int_0^1 t\left(\frac{\eta}{\zeta}\right)^{t} f'\left(\zeta^{1-t}\eta^t\right)dt\right.\\ &\left.-\eta\int_0^1 t\left(\frac{\zeta}{\eta}\right)^{t} f'\left(\eta^{1-t}\zeta^t\right)dt\right]\\ =\ & \zeta\frac{\ln\eta-\ln\zeta}{2}\int_0^1 (2t-1)\left(\frac{\eta}{\zeta}\right)^{t} f'\left(\zeta^{1-t}\eta^t\right)dt. \end{aligned}$$

The aim of this paper is to obtain the general integral inequalities giving the Hermite-Hadamard, Ostrowsky and Simpson type inequalities for the multiplicatively geometrically P-function in the special case using the above lemma.

2. Main results for the Lemma

Theorem 3. *Let the function $\psi : I \subseteq [1,\infty) \to \mathbb{R}$ be a differentiable mapping on I° such that $\psi' \in L[\zeta,\eta]$, where $\zeta, \eta \in I^\circ$ with $\zeta < \eta$ and $\theta, \lambda \in [0,1]$. If $|\psi'|^q$ is multiplicatively P-function on $[\zeta,\eta]$, $q \ge 1$, then following holds:*

$$
\begin{aligned}
&\left|(1-\theta)\left(\lambda\psi(\zeta)+(1-\lambda)\psi(\eta)\right)\right. \\
&\left.+\theta\psi((1-\lambda)\zeta+\lambda\eta)-\frac{1}{\eta-\zeta}\int_{\zeta}^{\eta}\psi(u)du\right| \\
\leq\; & (\eta-\zeta)A_1(\theta)\left|\psi'(A_\lambda)\right| \\
&\times\left(\lambda^2\left|\psi'(\zeta)\right|+(1-\lambda)^2\left|\psi'(\eta)\right|\right) \qquad (2)
\end{aligned}
$$

where

$$A_1(\theta)=\theta^2-\theta+\frac{1}{2}$$

and $A_\lambda=(1-\lambda)\zeta+\lambda\eta$.

Proof. Let $q\geq 1$ and $A_\lambda=(1-\lambda)\zeta+\lambda\eta$. Using the Lemma 1 and power-mean integral inequality,

$$
\begin{aligned}
&\left|(1-\theta)\left(\lambda\psi(\zeta)+(1-\lambda)\psi(\eta)\right)+\theta\psi(A_\lambda)\right. \\
&\left.-\frac{1}{\eta-\zeta}\int_{\zeta}^{\eta}\psi(u)du\right| \\
\leq\; & (\eta-\zeta)\left|\lambda^2\int_0^1|t-\theta|\left|\psi'(t\zeta+(1-t)A_\lambda)\right|dt\right. \\
&\left.+(1-\lambda)^2\int_0^1|t-\theta|\left|\psi'(t\eta+(1-t)A_\lambda)\right|dt\right| \\
\leq\; & (\eta-\zeta)\left\{\lambda^2\left(\int_0^1|t-\theta|\,dt\right)^{1-\frac{1}{q}}\right. \\
&\left(\int_0^1|t-\theta|\left|\psi'(\zeta+(1-t)A_\lambda)\right|^q dt\right)^{\frac{1}{q}} \\
&+(1-\lambda)^2\left(\int_0^1|t-\theta|\,dt\right)^{1-\frac{1}{q}} \\
&\left.\left(\int_0^1|t-\theta|\left|\psi'(t\eta+(1-t)A_\lambda)\right|^q dt\right)^{\frac{1}{q}}\right\} \qquad (3)
\end{aligned}
$$

is obtain. Since $|\psi'|^q$ is multiplicatively P-function on $[\zeta,\eta]$, we know that for $t\in[0,1]$

$$\left|\psi'(t\zeta+A_\lambda(1-t))\right|^q\leq\left|\psi'(\zeta)\right|^q\left|\psi'(A_\lambda)\right|^q \qquad (4)$$

and

$$\left|\psi'(t\eta+A_\lambda(1-t))\right|^q\leq\left|\psi'(\eta)\right|^q\left|\psi'(A_\lambda)\right|^q. \qquad (5)$$

By simple computation

$$
\begin{aligned}
&\int_0^1|t-\theta|\left|\psi'(t\zeta+(1-t)A_\lambda)\right|^q dt \\
\leq\; & \int_0^1|t-\theta|\left|\psi'(\zeta)\right|^q\left|f'(A_\lambda)\right|^q dt \\
=\; & \left|\psi'(\zeta)\right|^q\left|\psi'(A_\lambda)\right|^q\int_0^1|t-\theta|\,dt \\
=\; & \left|\psi'(\zeta)\right|^q\left|\psi'(A_\lambda)\right|^q\int_0^1|t-\theta|\,dt \qquad (6)
\end{aligned}
$$

and similarly

$$
\begin{aligned}
&\int_0^1|t-\theta|\left|\psi'(t\eta+(1-t)A_\lambda)\right|^q dt \qquad (7) \\
\leq\; & \left|\psi'(\eta)\right|^q\left|\psi'(A_\lambda)\right|^q\left[\theta^2-\theta+\frac{1}{2}\right]
\end{aligned}
$$

and

$$\int_0^1|t-\theta|\,dt=\theta^2-\theta+\frac{1}{2}. \qquad (8)$$

Thus, using (6-8) in (3), we get the inequality (2). □

Corollary 1. *Using the conditions of Theorem 3 for* $\theta=1$, *then the following generalized midpoint type inequality is obtained:*

$$
\begin{aligned}
&\left|\psi((1-\lambda)\zeta+\lambda\eta)-\frac{1}{\eta-\zeta}\int_{\zeta}^{\eta}\psi(u)du\right| \\
\leq\; & \frac{\eta-\zeta}{2}\left|\psi'(A_\lambda)\right|\left(\lambda^2\left|\psi'(\zeta)\right|+(1-\lambda)^2\left|\psi'(\eta)\right|\right).
\end{aligned}
$$

Corollary 2. *Using the conditions of Theorem 3 for* $\theta=1$, *if* $|\psi'(x)|\leq M$, $x\in[\zeta,\eta]$, *then the following Ostrowski type inequality is obtained*

$$
\begin{aligned}
&\left|\psi(x)-\frac{1}{\eta-\zeta}\int_{\zeta}^{\eta}\psi(u)du\right| \qquad (9) \\
\leq\; & M^2\left[\frac{(x-\zeta)^2+(\eta-x)^2}{2(\eta-\zeta)}\right]
\end{aligned}
$$

for each $x\in[\zeta,\eta]$.

Proof. For each $x \in [\zeta, \eta]$, there exist $\lambda_x \in [0,1]$ such that $x = (1-\lambda_x)\zeta + \lambda_x \eta$. Hence, we have $\lambda_x = \frac{x-\zeta}{\eta-\zeta}$ and $1-\lambda_x = \frac{\eta-x}{\eta-\zeta}$. Therefore for each $x \in [\zeta, \eta]$, from the inequality (2), (9) is obtained. □

Corollary 3. *Using the conditions of Theorem 3 for $\theta = 0$, then the following generalized trapezoid type inequality is obtained:*

$$\begin{aligned} &\left|\lambda\psi(\zeta) + (1-\lambda)\psi(\eta) - \frac{1}{\eta-\zeta}\int_\zeta^\eta \psi(u)du\right| \\ \leq\ & \frac{\eta-\zeta}{2}\left|\psi'(A_\lambda)\right|\left(\lambda^2\left|\psi'(\zeta)\right| + (1-\lambda)^2\left|\psi'(\eta)\right|\right). \end{aligned}$$

Corollary 4. *Using the conditions of Theorem 3 for $\lambda = \frac{1}{2}$ and $\theta = \frac{2}{3}$, then the following Simpson type inequality is obtained*

$$\begin{aligned} &\left|\frac{1}{6}\left[\psi(\zeta) + 4\psi\left(\frac{\zeta+\eta}{2}\right) + \psi(\eta)\right] - \frac{1}{\eta-\zeta}\int_\zeta^\eta \psi(u)du\right| \\ \leq\ & \frac{5}{36}(\eta-\zeta)\left|\psi'\left(\frac{\zeta+\eta}{2}\right)\right| A\left(\left|\psi'(\zeta)\right|, \left|\psi'(\eta)\right|\right), \end{aligned}$$

where A is arithmetic mean.

Corollary 5. *Using the conditions of Theorem 3 for $\lambda = \frac{1}{2}$ and $\theta = 1$, then the following midpoint type inequality is obtained*

$$\begin{aligned} &\left|\psi\left(\frac{\zeta+\eta}{2}\right) - \frac{1}{\eta-\zeta}\int_\zeta^\eta \psi(u)du\right| \\ \leq\ & \frac{\eta-\zeta}{4}\left|\psi'\left(\frac{\zeta+\eta}{2}\right)\right| A\left(\left|\psi'(\zeta)\right|, \left|\psi'(\eta)\right|\right), \end{aligned}$$

where A is arithmetic mean.

Corollary 6. *Using the conditions of Theorem 3 for $\lambda = \frac{1}{2}$, and $\theta = 0$, then the following trapezoid type inequality is obtained*

$$\begin{aligned} &\left|\frac{\psi(\zeta) + \psi(\eta)}{2} - \frac{1}{\eta-\zeta}\int_\zeta^\eta \psi(u)du\right| \\ \leq\ & \frac{\eta-\zeta}{4}\left|\psi'\left(\frac{\zeta+\eta}{2}\right)\right| A\left(\left|\psi'(\zeta)\right|, \left|\psi'(\eta)\right|\right), \end{aligned}$$

where A is arithmetic mean.

We will give another result for the considered multiplicatively P-functions as follows using Lemma 1

Theorem 4. *Let $\psi : I \subseteq [1,\infty) \to \mathbb{R}$ be a differentiable mapping on I° such that $\psi' \in L[\zeta, \eta]$, where $\zeta, \eta \in I^\circ$ with $\zeta < \eta$ and $\theta, \lambda \in [0,1]$. If $|\psi'|^q$ is multiplicatively P-function on $[\zeta, \eta]$, $q > 1$, then*

$$\begin{aligned} &|(1-\theta)(\lambda\psi(\zeta) + (1-\lambda)\psi(\eta)) \\ &\left. +\theta\psi((1-\lambda)\zeta + \lambda\eta) - \frac{1}{\eta-\zeta}\int_\zeta^\eta \psi(u)du\right| \\ \leq\ & (\eta-\zeta)\left(\frac{\theta^{p+1} + (1-\theta)^{p+1}}{p+1}\right)^{\frac{1}{p}}\left|\psi'(A_\lambda)\right| \\ &\left[\lambda^2\left|\psi'(\zeta)\right| + (1-\lambda)^2\left|\psi'(\eta)\right|\right]. \qquad (10) \end{aligned}$$

holds, where $A_\lambda = (1-\lambda)\zeta + \lambda\eta$ and $\frac{1}{p} + \frac{1}{q} = 1$.

Proof. Let $A_\lambda = (1-\lambda)\zeta + \lambda\eta$. From Lemma 1 and by Hölder's inequality, we obtain

$$\begin{aligned} &[(1-\theta)(\lambda\psi(\zeta) + (1-\lambda)\psi(\eta)) \\ &\left. +\theta\psi(A_\lambda) - \frac{1}{\eta-\zeta}\int_\zeta^\eta \psi(u)du\right| \\ &\leq (\eta-\zeta)\left[\lambda^2\int_0^1 |t-\theta|\left|\psi'(t\zeta + (1-t)A_\lambda)\right|dt\right. \\ &\left. +(1-\lambda)^2\int_0^1 |t-\theta|\left|\psi'(t\eta + (1-t)A_\lambda)\right|dt\right] \\ \leq\ & (b-a)\left\{\lambda^2\left(\int_0^1 |t-\theta|^p dt\right)^{\frac{1}{p}}\right. \\ &\left(\int_0^1 \left|\psi'(t\zeta + (1-t)A_\lambda)\right|^q dt\right)^{\frac{1}{q}} \\ &+(1-\lambda)^2\left(\int_0^1 |t-\theta|^p dt\right)^{\frac{1}{p}} \\ &\left.\left(\int_0^1 \left|\psi'(t\eta + (1-t)A_\lambda)\right|^q dt\right)^{\frac{1}{q}}\right\}. \qquad (11) \end{aligned}$$

Because $|\psi'|^q$ is multiplicatively P-function on $[\zeta, \eta]$, the inequalities (4) and (5) holds. Hence, by simple computation

$$\int_0^1 \left|\psi'\left(t\zeta+(1-t)A_\lambda\right)\right|^q dt \le \left|\psi'(\zeta)\right|^q \left|\psi'(A_\lambda)\right|^q \tag{12}$$

$$\int_0^1 \left|\psi'\left(t\eta+(1-t)A_\lambda\right)\right|^q dt \le \left|\psi'(\eta)\right|^q \left|\psi'(A_\lambda)\right|^q \tag{13}$$

and

$$\int_0^1 |t-\theta|^p\, dt = \frac{\theta^{p+1}+(1-\theta)^{p+1}}{p+1} \tag{14}$$

thus, using (12)-(14) in (11), (10) is obtained. □

Corollary 7. *Using the conditions of Theorem 4 with $\theta = 1$, then the following generalized midpoint type inequality is obtained*

$$\begin{aligned}&\left|\psi((1-\lambda)\zeta+\lambda\eta)-\frac{1}{\eta-\zeta}\int_\zeta^\eta \psi(u)du\right| \\ \le\ & (\eta-\zeta)\left(\frac{1}{p+1}\right)^{\frac{1}{p}}\left|\psi'(A_\lambda)\right| \\ &\times\left[\lambda^2\left|\psi'(\zeta)\right|+(1-\lambda)^2\left|\psi'(\eta)\right|\right].\end{aligned}$$

where $A_\lambda = (1-\lambda)\zeta+\lambda\eta$ and $\frac{1}{p}+\frac{1}{q}=1$.

Corollary 8. *Using the conditions of Theorem 4 for $\theta = 0$, then the following generalized trapezoid type inequality is obtained*

$$\begin{aligned}&\left|\lambda\psi(\zeta)+(1-\lambda)\psi(\eta)-\frac{1}{\eta-\zeta}\int_\zeta^\eta \psi(u)du\right| \\ \le\ & \frac{(\eta-\zeta)}{(p+1)^{\frac{1}{p}}}\left|\psi'(A_\lambda)\right| \\ &\times\left[\lambda^2\left|\psi'(\zeta)\right|+(1-\lambda)^2\left|\psi'(\eta)\right|\right],\end{aligned}$$

where $A_\lambda = (1-\lambda)\zeta+\lambda\eta$ and $\frac{1}{p}+\frac{1}{q}=1$.

Corollary 9. *Using the conditions of Theorem 4 for $\theta = 1$, if $|\psi'(x)| \le M$, $x\in[\zeta,\eta]$, then the following Ostrowski type inequality is obtained*

$$\begin{aligned}&\left|\psi(x)-\frac{1}{\eta-\zeta}\int_\zeta^\eta \psi(u)du\right| \\ \le\ & \frac{M^2}{(p+1)^{\frac{1}{p}}}\left[\frac{(x-\zeta)^2+(\eta-x)^2}{\eta-\zeta}\right]\end{aligned} \tag{15}$$

for each $x\in[\zeta,\eta]$.

Proof. For each $x\in[\zeta,\eta]$, there exist $\lambda_x\in[0,1]$ such that $x=(1-\lambda_x)\zeta+\lambda_x\eta$. Hence we have $\lambda_x=\frac{x-\zeta}{\eta-\zeta}$ and $1-\lambda_x=\frac{\eta-x}{\eta-\zeta}$. Therefore, for each $x\in[\zeta,\eta]$, from the inequality (10), the inequality (15) is obtained. □

Corollary 10. *Using the conditions of Theorem 4 for $\lambda=\frac{1}{2}$ and $\theta=\frac{2}{3}$, then the following Simpson type inequality*

$$\begin{aligned}&\left|\frac{1}{6}\left[\psi(\zeta)+4\psi\left(\frac{\zeta+\eta}{2}\right)+\psi(b)\right]\right. \\ &\left.-\frac{1}{\eta-\zeta}\int_\zeta^\eta \psi(u)du\right| \le \frac{\eta-\zeta}{6}\left(\frac{1+2^{p+1}}{3(p+1)}\right)^{\frac{1}{p}} \\ &\times\left|\psi'\left(\frac{\zeta+\eta}{2}\right)\right| A\left(\left|\psi'(\zeta)\right|,\left|\psi'(\eta)\right|\right),\end{aligned}$$

is obtained, where A is the arithmetic mean.

Corollary 11. *Using the conditions of Theorem 4 for $\lambda=\frac{1}{2}$ and $\theta=1$, then the following midpoint type inequality*

$$\begin{aligned}&\left|\psi\left(\frac{\zeta+\eta}{2}\right)-\frac{1}{\eta-\zeta}\int_\zeta^\eta \psi(u)du\right| \\ \le\ & \frac{\eta-\zeta}{2}\left(\frac{1}{p+1}\right)^{\frac{1}{p}}\left|\psi'\left(\frac{\zeta+\eta}{2}\right)\right| \\ &\times A\left(\left|\psi'(\zeta)\right|,\left|\psi'(\eta)\right|\right),\end{aligned}$$

is obtained, where A is the arithmetic mean.

Corollary 12. *Using the conditions of Theorem 4 for $\lambda=\frac{1}{2}$ and $\theta=0$, then the following trapezoid type inequality*

$$\begin{aligned}&\left|\frac{\psi(\zeta)+\psi(\eta)}{2}-\frac{1}{\eta-\zeta}\int_\zeta^\eta \psi(u)du\right| \\ \le\ & \frac{\eta-\zeta}{2}\left(\frac{1}{p+1}\right)^{\frac{1}{p}}\left|\psi'\left(\frac{\zeta+\eta}{2}\right)\right| \\ &\times A\left(\left|\psi'(\zeta)\right|,\left|\psi'(\eta)\right|\right),\end{aligned}$$

is obtained, where A is the arithmetic mean.

3. Some applications for special means

(1) The weighted arithmetic mean

$$A_{\alpha}(\zeta,\eta) \; : \; = \alpha\zeta + (1-\alpha)\eta, \quad \alpha \in [0,1], \; \zeta,\eta \in \mathbb{R}.$$

(2) The weighted geometric mean

$$G_{\alpha}(\zeta,\eta) := \zeta^{\alpha}\eta^{1-\alpha}, \quad \zeta,\eta > 0.$$

(3) The Logarithmic mean

$$L(\zeta,\eta) := \frac{\eta-\zeta}{\ln\eta - \ln\zeta}, \quad \zeta \neq \eta, \quad \zeta,\eta > 0.$$

Considering the results in Section 2, some inequalities can be obtained for the means given above.

Proposition 1. *Let $\zeta,\eta \in \mathbb{R}$ with $0<\zeta<\eta$ and $\lambda,\theta \in [0,1]$ we have the following inequality:*

$$\left|(1-\theta)A_{\lambda}\left(e^{\zeta},e^{\eta}\right) + \theta G_{\lambda}\left(e^{\zeta},e^{\eta}\right) - L\left(e^{\zeta},e^{\eta}\right)\right|$$

$$\leq (\eta-\zeta)A_1(\theta)e^{A_{\lambda}(\zeta,\eta)}\left(\lambda^2 e^{\zeta} + (1-\lambda)^2 e^{\eta}\right)$$

where $A_1(\theta)$ is defined as in Theorem 3.

Proof. Using the Theorem 3 for the function $\psi(t) = e^t$, $t \in [0,\infty)$, the assertion is easily seen. □

Proposition 2. *Let $\zeta,\eta \in \mathbb{R}$ with $0<\zeta<\eta$, $p,q>1$, $\frac{1}{p}+\frac{1}{q}=1$ and $\lambda,\theta\in[0,1]$, following inequality*

$$\left|(1-\theta)A_{\lambda}\left(e^{\zeta},e^{\eta}\right) + \theta G_{\lambda}\left(e^{\zeta},e^{\eta}\right) - L\left(e^{\zeta},e^{\eta}\right)\right|$$

$$\leq (b-a)\left(\frac{\theta^{p+1}+(1-\theta)^{p+1}}{p+1}\right)^{\frac{1}{p}} \times e^{A_{\lambda}(\zeta,\eta)}\left(\lambda^2 e^{\zeta} + (1-\lambda)^2 e^{\eta}\right)$$

is obtained, where $\frac{1}{p}+\frac{1}{q}=1$.

Proof. Using the Theorem 4 for the function $\psi(t) = e^t$, $t \in [0,\infty)$, the assertion is easily seen. □

References

[1] Dragomir, S.S. and Pearce, C.E.M. (2000). Selected Topics on Hermite-Hadamard Inequalities and Applications, RGMIA Monographs, Victoria University, 2000.

[2] Dragomir, S.S. and Rassias, Th. M. (2002). *Ostrowski type inequalities and applications in numerical integration.* Kluwer Academic Publishers, Dordrecht, Boston, London.

[3] Dragomir, S.S. Pečarić, J. and Persson, L.E. (1995). Some inequalities of Hadamard type. *Soochow Journal of Mathematics*, 21(3), 335-341.

[4] Kadakal, H. (2018). Multiplicatively P-functions and some new inequalities. *New Trends in Mathematical Sciences*, 6(4), 111-118.

[5] İşcan, İ., Numan, S. and Bekar, K. (2014). Hermite-Hadamard and Simpson type inequalities for differentiable harmonically P-functions. *British Journal of Mathematics & Computer Science*, 4(14), 1908-1920.

[6] Kadakal, H., Maden, S., Kadakal M. and İşcan, İ. (2017). Some new integral inequalities for n-times differentiable P-functions. *International Conference on Advances in Natural and Applied Sciences*, Antalya, Turkey, 18-21 April 2017.

[7] Kadakal, M., Turhan, S. Maden S. and İşcan, İ. (2018). Midpoint type inequalities for the multiplicatively P-functions. International Conference on Mathematics and Mathematics Education, ICMME-2018, Ordu University, Ordu, 27-29 June 2018.

[8] Pearce, C.E.M. and Rubinov, A.M. (1999). P-functions, quasi-convex functions and Hadamard-type inequalities. Journal of Mathematical Analysis and Applications, 240, 92–104.

[9] Kadakal, M., Karaca, H. and İşcan, İ. (2018). Hermite-Hadamard type inequalities for multiplicatively geometrically P-functions. *Poincare Journal of Analysis & Applications*, 2018(2(I)), 77-85.

[10] İşcan, İ. (2014). Hermite-Hadamard type inequalities for GA-s-convex functions, Le Matematiche, Vol. LXIX-Fasc. II, 129–146.

Huriye Kadakal *is a mathematics teacher in the Ministry of National Education. She received his B. Sc. (1993) degree from Department of Mathematics Teaching, Faculty of Education, Ondokuz Mayıs University and M. Sc. (2011) degree from Ahi Evran University and Ph.D (2018) from Ordu University, Turkey. She has research papers about the Theory of inequalities and convexity.*

An International Journal of Optimization and Control: Theories & Applications (http://ijocta.balikesir.edu.tr)

An International Journal of Optimization and Control: Theories & Applications
ISSN:2146-0957 eISSN:2146-5703
Vol.9, No.2, pp.223-235 (2019)
http://doi.org/10.11121/ijocta.01.2019.00709

RESEARCH ARTICLE

A mixed method approach to Schrödinger equation: Finite difference method and quartic B-spline based differential quadrature method

Ali Başhan[a]

Department of Mathematics, University of Zonguldak Bulent Ecevit, Turkey
alibashan@gmail.com

ARTICLE INFO

Article History:
Received 12 September 2018
Accepted 16 May 2019
*Available ** July 2019*

Keywords:
Differential quadrature method
Finite difference method
Quartic B-Splines
Nonlinear Schrödinger equation

AMS Classification 2010:
65M99; 65D07; 15A30

ABSTRACT

The present manuscript includes finite difference method and quartic B-spline based differential quadrature method (FDM-DQM) for getting the numerical solutions for the nonlinear Schrödinger (NLS) equation. To solve complex NLS equation firstly we have separated NLS equation into the two real value partial differential equations. After that they are discretized in time using special type of classical finite difference method namely, Crank-Nicolson scheme. Then, for space integration differential quadrature method has been implemented. So, partial differential equation turn into simple a system of algebraic equations. To display the accuracy of the present hybrid method, the error norms L_2 and L_∞ and two lowest invariants I_1 and I_2 and relative changes of invariants have been calculated. As a last step, the numerical result already obtained have been compared with earlier studies by using same parameters. The comparison has clearly indicated that the presently used method, namely FDM-DQM, is an appropriate and accurate numerical scheme and allowed us to present for solving a wide class of partial differential equations.

1. Introduction

In recent years, studies on findings numerical solutions of differential equations have took attention of researchers throughout over the world [1–6]. In nature, several physical phenomena can easily be defined by NLS equation such as propagation of optical pulses, waves in water, waves in plasmas, and self focusing in laser pulses. Because of this, among others, several authors have tried hard to present analytical solutions of NLS [7–9] and numerical solutions have been studied [10–18]. NLS equation has a nature of attracting the attention of a lot of researchers for illustrate the efficiency of the numerical methods. Therefore, recently, many studies of different methods such as quadratic FEM [19], radial based collocation method [20], Taylor collocation method based on cubic B-spline [21], quintic B-spline based FEM [22] for the NLS equation may be encountered.

Firstly, we will handle the NLS equation given in the following form

$$iz_t + z_{xx} + \gamma |z|^2 z = 0 \quad a \le x \le b, \quad t \in [0, T] \tag{1}$$

together having the boundary conditions

$$z(a,t) = z(b,t) = 0$$

where $i = \sqrt{-1}$, γ is a real parameter. Meanwhile the subscripts t and x describe partial derivatives with respect to time and space, respectively.

For being capable of computing the complex function z, we have to separate it into the two real value functions by rewriting

$$z(x,t) = u(x,t) + iv(x,t), \tag{2}$$

in which both $u(x,t)$ and $v(x,t)$ are real functions. Upon substituting (2) into the Eq.(1) it results in coupled real value partial differential equation system

$$\begin{aligned} u_t + v_{xx} + \gamma\left[u^2 v + v^3\right] &= 0, \\ v_t - u_{xx} - \gamma\left[v^2 u + u^3\right] &= 0. \end{aligned} \tag{3}$$

After applying the boundary conditions to (2) newly obtained boundary conditions may be stated in the following form

$$\begin{aligned} u(a,t) &= u(b,t) = 0, \\ v(a,t) &= v(b,t) = 0. \end{aligned} \tag{4}$$

DQM, first introduced by Bellman *et al.* [24] in 1972, has had wide application areas due to its considerably less number of mesh points usage. When one search the literature, it can be seen that many scientists have improved different types of DQM using various base functions [24–35]. In this study, fourth order quartic B-spline based FDM-DQM will be used to obtain numerical solutions of the NLS equation.

2. Fourth order quartic B-spline based DQM

Let us take the grid distribution $a = x_1 < x_2 < \cdots < x_N = b$ of a finite interval $[a,b]$ into consideration. Under the condition that a function $U(x)$ is enough smooth over the solution domain, its derivatives with respect to x at a grid point x_i can be approximated by a linear combination of all the functional values over the solution domain of the problem, that is,

$$\begin{aligned} \frac{d^{(r)}U}{dx^{(r)}} \mid_{x_i} &= \sum_{j=1}^{N} w_{ij}^{(r)} U(x_j), \\ i &= 1,2,...,N, \quad r = 1,2,...,N-1 \end{aligned} \tag{5}$$

where r represents the order of the derivative, $w_{ij}^{(r)}$ denote the weighting coefficients of the r^{th} order derivative approximation and N denotes the number of mesh points in the solution domain. Here, the index j emphasizes the fact that $w_{ij}^{(r)}$ is the corresponding weighting coefficient of the functional value $U(x_j)$.

In this study, we need the first order and the second order derivative of the function $U(x)$. So, firstly we will find value of the equation (5) for the $r = 1$.

Let $Q_s(x)$, be the quartic B-splines having nodes at the points x_i where the uniformly distributed N nodal points are taken into consideration as $a = x_1 < x_2 < \cdots < x_N = b$ on the ordinary real axis. Then, the B-splines $\{Q_{-1}, Q_0, \ldots, Q_{N+1}\}$ constitute a basis for functions defined over $[a,b]$. The quartic B-splines $Q_s(x)$ are described by the relationships:

$$Q_s(x) = \frac{1}{h^4}\begin{cases} q_1, & x \in [x_{s-2}, x_{s-1}], \\ q_1 - 5q_2, & x \in [x_{s-1}, x_s], \\ q_1 - 5q_2 + 10q_3, & x \in [x_s, x_{s+1}], \\ q_4 - 5q_5, & x \in [x_{s+1}, x_{s+2}], \\ q_4, & x \in [x_{s+2}, x_{s+3}], \\ 0, & otherwise. \end{cases}$$

where $q_1 = (x - x_{s-2})^4$, $q_2 = (x - x_{s-1})^4$, $q_3 = (x - x_s)^4$, $q_4 = (x_{s+3} - x)^4$ $q_5 = (x_{s+2} - x)^4$, $h = x_s - x_{s-1}$ for all s.

Table 1. Quartic B-splines and their corresponding derivatives at the nodal points.

x	x_{s-2}	x_{s-1}	x_s	x_{s+1}	x_{s+2}	x_{s+3}
Q	0	1	11	11	1	0
hQ'	0	4	12	−12	−4	0
h^2Q''	0	12	−12	−12	12	0
h^3Q'''	0	24	−72	72	−24	0

Using the quartic B-splines as trial functions in the fundamental DQM equation (5) results in to the equation

$$\begin{aligned} \frac{d^{(r)}Q_s(x_i)}{dx^{(r)}} &= \sum_{j=s-1}^{s+2} w_{i,j}^{(r)} Q_s(x_j), \\ s &= -1, 0, \ldots, N+1, \ i = 1,2,...,N. \end{aligned} \tag{6}$$

2.1. *The 1st* order *weighting coefficients*

When DQM methodology is applied, the fundamental equality for determining the corresponding weighting coefficients of the first order derivative approximation is obtained as Korkmaz used [29]:

$$\begin{aligned} \frac{dQ_s(x_i)}{dx} &= \sum_{j=s-1}^{s+2} w_{i,j}^{(1)} Q_s(x_j), \\ s &= -1, 0, \ldots, N+1, \ i = 1,2,...,N. \end{aligned} \tag{7}$$

In the process, the initial step for finding out the corresponding weighting coefficients $w_{i,j}^{(1)}$, $j = -2, -1, \ldots, N+3$ of the first grid point x_1 is to apply the test functions Q_s, $s = -1, 0, \ldots, N+1$ at the grid point x_1. After all the Q_s trial functions are applied, we obtain the following algebraic equation system:

$$A_1 . \begin{bmatrix} w_{1,-2}^{(1)} \\ w_{1,-1}^{(1)} \\ w_{1,0}^{(1)} \\ w_{1,1}^{(1)} \\ w_{1,2}^{(1)} \\ \vdots \\ w_{1,N+2}^{(1)} \\ w_{1,N+3}^{(1)} \end{bmatrix} = \begin{bmatrix} -\frac{4}{h} \\ -\frac{12}{h} \\ \frac{12}{h} \\ \frac{4}{h} \\ 0 \\ \vdots \\ 0 \\ 0 \end{bmatrix} \tag{8}$$

where

$$A_1 = \begin{bmatrix} 1 & 11 & 11 & 1 & & & & \\ & 1 & 11 & 11 & 1 & & & \\ & & \ddots & \ddots & \ddots & \ddots & & \\ & & & & & & & \\ & & & & & & & \\ & & & 1 & 11 & 11 & 1 & \\ & & & & 1 & 11 & 11 & 1 \end{bmatrix}$$

The weighting coefficients $w_{1,j}^{(1)}$ related to the first grid point are determined by solving equation system (8). The equation system (8) composed of $N+6$ unknowns and $N+3$ equations. To have a distinct solution, it is required to add three additional equations to the system. By the derivations of the equations

$$\frac{d^2 Q_{-1}(x_1)}{dx^2} = \sum_{j=-2}^{1} w_{1,j}^{(1)} Q'_{-1}(x_j) \tag{9}$$

$$\frac{d^2 Q_N(x_1)}{dx^2} = \sum_{j=N-1}^{N+2} w_{1,j}^{(1)} Q'_N(x_j) \tag{10}$$

$$\frac{d^2 Q_{N+1}(x_1)}{dx^2} = \sum_{j=N}^{N+3} w_{1,j}^{(1)} Q'_{N+1}(x_j) \tag{11}$$

is obtained. By using the equations (9), (10) and (11) which we obtained by derivations, three unknown terms will be eliminate from equation system.

$$A_2 . \begin{bmatrix} w_{1,-1}^{(1)} \\ w_{1,0}^{(1)} \\ w_{1,1}^{(1)} \\ w_{1,2}^{(1)} \\ w_{1,3}^{(1)} \\ \vdots \\ w_{1,N}^{(1)} \\ w_{1,N+1}^{(1)} \end{bmatrix} = \begin{bmatrix} -\frac{7}{h} \\ -\frac{12}{h} \\ \frac{12}{h} \\ \frac{4}{h} \\ 0 \\ \vdots \\ 0 \\ 0 \end{bmatrix} \tag{12}$$

where

$$A_2 = \begin{bmatrix} 8 & 14 & 2 & & & & \\ 1 & 11 & 11 & 1 & & & \\ & \ddots & \ddots & \ddots & \ddots & & \\ & & & & & & \\ & & & 1 & 11 & 11 & 1 \\ & & & & 2 & 14 & 8 \\ & & & & & 30 & 42 \end{bmatrix}$$

So, the number of algebraic equations and the unknowns will be equal and the equation system will be solved with Thomas algorithm. The new matrix system(12) contains $N+3$ equations and $N+3$ unknowns. By the same idea, for the determine weighting coefficients $w_{k,j}^{(1)}$, $j=-1,0,\ldots,N+1$ at grid points x_k, $2 \le k \le N-1$ we got the algebraic equation system:

$$A_2 . \begin{bmatrix} w_{k,-1}^{(1)} \\ \vdots \\ w_{k,k-3}^{(1)} \\ w_{k,k-2}^{(1)} \\ w_{k,k-1}^{(1)} \\ w_{k,k}^{(1)} \\ w_{k,k+1}^{(1)} \\ w_{k,k+2}^{(1)} \\ \vdots \\ w_{k,N+1}^{(1)} \end{bmatrix} = \begin{bmatrix} 0 \\ \vdots \\ 0 \\ \frac{-4}{h} \\ \frac{-12}{h} \\ \frac{12}{h} \\ \frac{4}{h} \\ 0 \\ \vdots \\ 0 \end{bmatrix} \tag{13}$$

For the last grid point of the domain x_N with same idea, determine weighting coefficients $w_{N,j}^{(1)}$, $\quad j=-1,0,\ldots,N+1$ we got the algebraic equation system:

$$A_2 . \begin{bmatrix} w_{N,-1}^{(1)} \\ w_{N,0}^{(1)} \\ \vdots \\ w_{N,N-3}^{(1)} \\ w_{N,N-2}^{(1)} \\ w_{N,N-1}^{(1)} \\ w_{N,N}^{(1)} \\ w_{N,N+1}^{(1)} \end{bmatrix} = \begin{bmatrix} 0 \\ 0 \\ \vdots \\ 0 \\ \frac{-4}{h} \\ \frac{-12}{h} \\ \frac{9}{h} \\ \frac{53}{h} \end{bmatrix} \tag{14}$$

2.2. *The 2^{nd}* **order** *weighting coefficients*

If we use matrix multiplication approach, then all the corresponding weighting coefficients can be found out. The present method is based on the first order weighting coefficients to obtain the weighting coefficients of the second order derivatives. When one uses matrix multiplication procedure, the second order weighting coefficients are determined as below [23]:

$$\left[A^{(2)}\right] = \left[A^{(1)}\right]\left[A^{(1)}\right], \tag{15}$$

where $\left[A^{(1)}\right], \left[A^{(2)}\right]$ are the weighting coefficients matrices of the first- and the second-order derivatives, respectively [23].

3. Discretization of the mixed method

The Eq. system (3) is given of the form

$$\begin{aligned} u_t + v_{xx} + \gamma\left[u^2 v + v^3\right] &= 0, \quad (16)\\ v_t - u_{xx} - \gamma\left[v^2 u + u^3\right] &= 0. \quad (17)\end{aligned}$$

One can implement Crank-Nicolson scheme to Eq. (16) and easily obtain

$$\begin{aligned} &\frac{u^{n+1}-u^n}{\Delta t} + \frac{v_{xx}^{n+1}+v_{xx}^n}{2} + \\ &\gamma\left[\frac{\left(v^3\right)^{n+1}+\left(v^3\right)^n}{2}\right] + \\ &\gamma\left[\frac{\left(u^2 v\right)^{n+1}+\left(u^2 v\right)^n}{2}\right] \\ =\ & 0. \end{aligned} \tag{18}$$

After that, the rearrangement of Eq. (18) yields the following form

$$\begin{aligned} & 2u^{n+1} + \Delta t\left[v_{xx}^{n+1} + \gamma\left(\left(v^3\right)^{n+1} + \left(u^2 v\right)^{n+1}\right)\right] \\ =\ & 2u^n - \Delta t\left[v_{xx}^n + \gamma\left(\left(v^3\right)^n + \left(u^2 v\right)^n\right)\right]. \end{aligned} \tag{19}$$

If we use the Rubin and Graves linearization techniques [36] in Eq. (19) to vanish the nonlinear terms, thus one obtains the linear equation

$$\begin{aligned} & 2u^{n+1} + \Delta t\begin{bmatrix} v_{xx}^{n+1} + 3\gamma\left(v^2\right)^n v^{n+1} + \\ \gamma\left(u^2\right)^n v^{n+1} + 2\gamma u^n v^n u^{n+1} \end{bmatrix} \\ =\ & 2u^n + \Delta t\left[-v_{xx}^n + \gamma\left(v^3\right)^n + \gamma\left(u^2 v\right)^n\right]. \end{aligned} \tag{20}$$

Some simple organizations for Eq. (20) and definitions as stated below are made

$$\begin{aligned} A_i^n &= \sum_{j=1}^{N} w_{i,j}^{(2)} U_j^n = U_{xx_i}^n, \\ B_i^n &= \sum_{j=1}^{N} w_{i,j}^{(2)} V_j^n = V_{xx_i}^n, \\ U_{xx_i}^{n+1} &= \sum_{j=1}^{N} w_{i,j}^{(2)} U_j^{n+1},\ V_{xx_i}^{n+1} = \sum_{j=1}^{N} w_{i,j}^{(2)} V_j^{n+1} \\ \Phi_i^n &= 2U_i^n + \\ & \quad \Delta t\left[-B_i^n + \gamma\left(V_i^n\right)^3 + \gamma\left(U_i^n\right)^2 V_i^n\right] \\ \Psi_i^n &= 2V_i^n + \\ & \quad \Delta t\left[A_i^n - \gamma\left(U_i^n\right)^3 - \gamma\left(V_i^n\right)^2 U_i^n\right] \end{aligned} \tag{21}$$

for $i = 1\,(1)\,N$. When substituted Eq. (21) into Eq. (20) one can obtain

$$\begin{aligned} & 2U_i^{n+1} + \\ & \Delta t\left[\gamma\begin{pmatrix} \sum_{j=1}^{N} w_{i,j}^{(2)} V_j^{n+1} + \\ 3\left(V_i^n\right)^2 V_i^{n+1} + \\ \left(U_i^n\right)^2 V_i^{n+1} + 2U_i^n V_i^n U_i^{n+1} \end{pmatrix}\right] \\ =\ & \Phi_i^n. \end{aligned} \tag{22}$$

When we make some arrangements in Eq. (22), we obtain the following equation

$$\begin{aligned} & \left[2 + 2\gamma\Delta t U_i^n V_i^n\right] U_i^{n+1} + \\ & \left[\Delta t\left(w_{i,i}^{(2)} + \gamma\left(3\left(V_i^n\right)^2 + \left(U_i^n\right)^2\right)\right)\right] V_i^{n+1} \\ & + \sum_{j=1, i\neq j}^{N}\left(\Delta t w_{i,j}^{(2)}\right) V_j^{n+1} \\ =\ & \Phi_i^n\ . \end{aligned} \tag{23}$$

Using the same procedure the same process now for Eq. (17), the following equation is obtained

$$\begin{aligned} & \left[-\Delta t\left(w_{i,i}^{(2)} + \gamma\left(3\left(U_i^n\right)^2 + \left(V_i^n\right)^2\right)\right)\right] U_i^{n+1} \\ & + \sum_{j=1, i\neq j}^{N}\left(-\Delta t w_{i,j}^{(2)}\right) U_j^{n+1} + \\ & \left[2 - 2\gamma\Delta t U_i^n V_i^n\right] V_i^{n+1} \\ =\ & \Psi_i^n\ . \end{aligned} \tag{24}$$

When the boundary conditions in Eq. (4), are used the algebraic equation system in the form of $(2N-4)\times(2N-4)$ matrix is obtained and solved by Gauss elimination.

4. Numerical studies

In this part, four famous problems namely single soliton, double solitons, standing soliton and mobile soliton have been searched. The efficiency of the proposed newly scheme is checked using the two error norms L_2 and L_∞, respectively:

$$\begin{aligned} L_2 &= \|u-U\|_2 \simeq \sqrt{h\sum_{j=1}^{N}\left|u_j^{exact}-(U_N)_j\right|^2}, \\ L_\infty &= \|u-U\|_\infty \simeq \max_j \left|u_j^{exact}-(U_N)_j\right|, \\ j &= 1\,(1)\,N. \end{aligned}$$

Besides error norms L_2 and L_∞, the lowest two invariants, of which formulae are presented below, are computed

$$\begin{aligned} &I_1 = \int_a^b |u|^2 dx \\ &\approx h\sum_{j=0}^{N}\left|U_j^n\right|^2, \\ &I_2 = \int_a^b \left[|u_x|^2 - \tfrac{\gamma}{2}|u|^4\right] dx \\ &\approx h\sum_{j=0}^{N}\left[|\left(U_x\right)_j^n|^2 - \tfrac{\gamma}{2}|U_j^n|^4\right]. \end{aligned}$$

Relative changes of invariants described by $\widehat{I_j} = \frac{I_j^{final}-I_j^{initial}}{I_j^{initial}}$, $j=1,2$ have been checked.

4.1. Single Soliton

The first example has been taken into consideration as the motion of single soliton of which exact solution is presented of the form

$$\begin{aligned} z(x,t) &= \alpha\sqrt{\frac{2}{\gamma}}. \\ &\exp i\left\{\frac{2\sigma x-\left(\sigma^2-\alpha^2\right)t}{4}\right\}. \\ &\operatorname{sech}\alpha\left(x-\sigma t\right) \end{aligned} \tag{25}$$

where σ represents the velocity of the single soliton of which amplitude depends on α. We have selected the values of $\gamma=2, \sigma=4, \alpha=1$ and $\alpha=2$ at the solution domain $-20\le x\le 20$ just capable of comparing with earlier studies. When $\alpha=1$ is taken the envelop soliton

$$|z| = \operatorname{sech}\ (x-4t)$$

moves toward the right with unchanged characteristics such as speed $\sigma=4$, shape, and amplitude $\alpha=1$. For visual representation, the simulations of single soliton for values of $\Delta t=0.005$, $N=291$at various times from $t=0$ to $t=4$ are plotted in Figure 1. As it is seen obviously from Figure 1, the real and imaginary parts of the z separately and the module $|z|$ is given.

To compare the results, the values of the error norms L_2 and L_∞, and the two lowest invariants I_1 and I_2, and relative changes of invariants are illustrated in comparison with quadratic B-spline based finite element method [19] for values of $\Delta t=0.005$ and $N=291$ at several times in Table 2. As one can see clearly from Table 2, by using the same parameters and less number of the nodal points than earlier work [19] the new results are better than quadratic B-spline based finite element method [19] solutions.

A deeper comparison of numerical results, for amplitude $\alpha=1$, at time $t=1$ is given in Table 3. It can be obviously seen from Table 3 that by decreasing the time increments, the error norm L_∞ of FDM-DQM get decreased to the 1.5×10^{-4}. Those are the best results in the presented results.

One can see the comparison of numerical results with another studies that Gaussian, Multiquadric, Inverse Multiquadric and Inverse Quadric radial based collocation method [20] , for amplitude $\alpha=1$, at time $t=2.5$ in Table 4. The error norms L_2 and L_∞ of FDM-DQM are the best results among all given results except the Gaussian radial based collocation method.

Similar to the solutions of amplitude $\alpha=1$, for the bigger amplitude $\alpha=2$, results have been illustrated with comparison of earlier studies at time $t=1$ at Table 5. One more time, by decreasing the time steps the error norm L_∞ of FDM-DQM decrease to the 2.5×10^{-4} which is the best result for NLS equation in the all given studies.

4.2. Double solitons

In our second trial example, the initial condition of collision of double solitons is taken as follows [10]:

$$z(x,0)=\sum_{k=1}^{2} z_k(x,0) \tag{26}$$

where

$$\begin{aligned} z_k(x,0) &= \alpha_k\sqrt{\frac{2}{\gamma}}. \\ &\exp i\left\{\frac{\sigma_k}{2}\left(x-x_k\right)\right\}. \\ &\operatorname{sech}\alpha_k\left(x-x_k\right), \qquad (27) \\ k &= 1,2. \end{aligned}$$

We have chosen the values of $\gamma=2$, $\alpha_1=\alpha_2=1$, $\sigma_1=-4$, $\sigma_2=4$, $x_1=10$, and $x_2=-10$ over the region $-20\le x\le 20$. These simulations show the

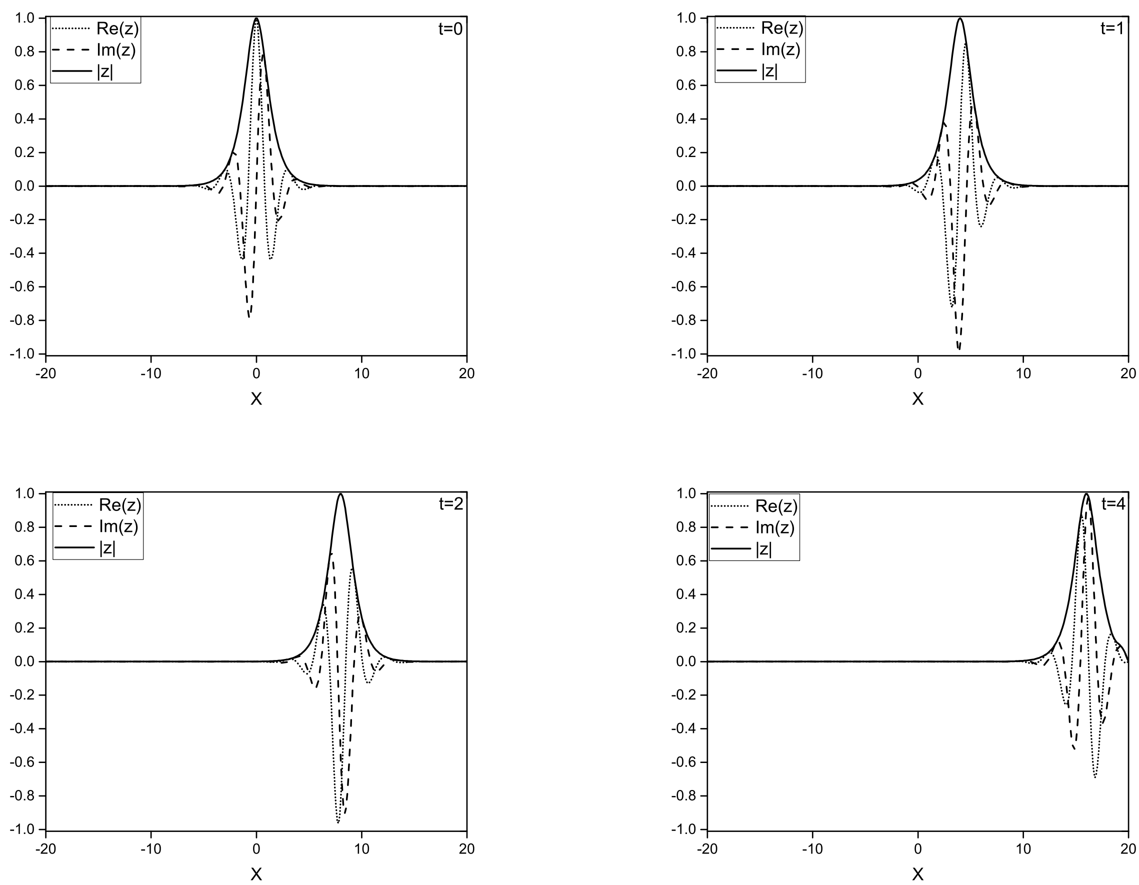

Figure 1. Simulation of single soliton $\Delta t = 0.005, N = 291$.

Table 2. Error norms, invariants and relative changes of invariants: $\Delta t = 0.005$.

	Present (FDM-DQM) N=291						Quad. FEM [19] N=800			
t	I_1	I_2	$\widehat{I_1}$	$\widehat{I_2}$	L_2	L_∞	I_1	I_2	L_2	L_∞
0.0	2.00000	7.33370	-	-	0.00000	0.00000	2.0	7.3537736	0.0000	0.0000
0.5	2.00000	7.33371	1.0×10^{-6}	8.2×10^{-7}	0.00012	0.00008	2.0	7.3537756	0.0002	0.0002
1.0	2.00001	7.33373	4.0×10^{-6}	3.7×10^{-6}	0.00023	0.00015	2.0	7.3537778	0.0004	0.0003
1.5	2.00001	7.33374	5.5×10^{-6}	4.4×10^{-6}	0.00032	0.00021	2.0	7.3537793	0.0007	0.0004
2.0	2.00001	7.33375	6.0×10^{-6}	6.1×10^{-6}	0.00040	0.00026	2.0	7.3537802	0.0008	0.0005
2.5	2.00001	7.33377	6.5×10^{-6}	9.4×10^{-6}	0.00047	0.00029	2.0	7.3537803	0.0009	0.0006

collision of two solitons at the different positions which are $x_1 = 10$, and $x_2 = -10$ in the opposite ways with same amplitudes, $\alpha_1 = \alpha_2 = 1$, and same speeds, $\sigma_1 = \sigma_2 = 4$. Due to characteristics of solitons, after the collision finished double solitons conserve their properties such as shape, speed and amplitudes, which can be seen at the simulations of double solitons shown in Figure 2. The simulations are run up to the time $t = 5.5$. As time increases, collision begins close to $t = 2$ and height of the amplitudes nearly $\alpha = 2$ observed at time $t = 2.5$. At the time interaction ends at time $t = 5.5$, two solitons preserve their originally properties like the initial position.

Two lowest invariants of the this method is presented with comparison of earlier works, in Table 6. Particularly at interaction typical observed at time $t = 2.5$ changes of two invariants I_1 and I_2 have more importance for efficiency of the implemented methods. As it is seen in Table 6 that relative changes of the invariants I_1 and I_2 at collision time $t = 2.5$ are -1.0×10^{-6} and -3.4×10^{-6}, respectively and in the end of the simulations this changes are 2.5×10^{-7} and -6.8×10^{-7}, respectively.

The obtained new results are presented and compared with earlier studies in Table 6. Numerical results are clearly shows that more particularly at

Table 3. L_∞ error norm and relative changes of invariants of single soliton: *amp.* $= 1, t = 1$.

Method	N	h	Δt	L_∞	$\widehat{I_1}$	$\widehat{I_2}$
FDM-DQM	152	0.26	0.02	0.00254	1.9×10^{-4}	2.2×10^{-4}
(Present)	291	0.14	0.005	0.00015	4.0×10^{-6}	3.7×10^{-6}
Quad.Gal. [19]		0.3125	0.02	0.002	0.0000066	-0.0003417
		0.05	0.005	0.0003	0.0000000	0.0000006
Quin. Coll. [22]		0.3125	0.02	0.002	0.0000000	0.0000063
		0.05	0.005	0.0003	0.0000000	0.0000000
Tay.Coll. [21]		0.3125	0.02	0.00176	0.0000019	0.000016
		0.05	0.005	0.00026	-0.00000002	-0.00000003
Cub. Coll. [15]		0.05	0.005	0.008	0.00000	0.00000
		0.03	0.005	0.002	0.00000	0.00000
Explicit [11]		0.05	0.000625	0.00564	0.00000	-0.00556
Implicit/Explicit [11]		0.05	0.001	0.00577	-0.00393	-0.01205
Implicit Cr-Ni. [11]		0.05	0.005	0.00585	-0.00001	-0.00557
Hopscotch [11]		0.08	0.002	0.00538	0.00003	-0.01407
Split step Four. [11]		0.3125	0.02	0.00466	0.00000	0.00005
A-L Local [11]		0.06	0.0165	0.00580	0.00004	-0.00797
A-L Global [11]		0.05	0.04	0.00561	0.00003	0.00550
Pseudospectral [11]		0.3125	0.0026	0.00513	0.00001	-0.00003

Table 4. L_2 and L_∞ error norms and invariants of single soliton: *amp.* $= 1, t = 2.5$.

Method	N	h	Δt	L_2	L_∞	I_1	I_2
FDM-DQM	291	0.14	0.005	0.000226	0.000153	2.000008	7.333730
G [20]		0.3125	0.001	0.000046	0.000028	1.999908	7.333177
MQ [20]		0.3125	0.001	0.004434	0.002165	1.999472	7.331960
IMQ [20]		0.3125	0.001	0.000668	0.000486	1.999137	7.329795
IQ [20]		0.3125	0.001	0.005652	0.002037	1.999812	7.329801

Table 5. L_∞ error norm and relative changes of invariants of single soliton, *amp.* $= 2, t = 1$.

Method	N	h	Δt	L_∞	$\widehat{I_1}$	$\widehat{I_2}$
FDM-DQM	386	0.1	0.005	0.00031	0.0×10^{-13}	4.5×10^{-5}
(Present)	391	0.1	0.0048	0.00028	-5.0×10^{-7}	3.8×10^{-5}
	491	0.08	0.0025	0.00025	-2.5×10^{-6}	1.4×10^{-5}
Quad.Gal. [19]		0.1	0.005	0.0004	0.00000001	-0.000008
		0.1563	0.0048	0.004	0.0000095	-0.000276
Quin. Coll. [22]		0.015	0.005	0.001	0.0000000	0.0000001
		0.1	0.005	0.0007	0.0000000	0.0000000
		0.1563	0.0048	0.002	0.0000000	0.0000026
		0.02	0.0025	0.0003	0.0000000	0.0000000
Tay.Coll. [21]		0.05	0.005	0.00104	0.00000002	-0.00000017
		0.1	0.005	0.00076	0.00000006	0.00000003
		0.1563	0.0048	0.00207	0.00000034	0.00000358
Cub. Coll. [15]		0.015	0.005	0.008	0.00000	0.00025
		0.02	0.0025	0.011	0.00000	0.00004
Explicit [11]		0.02	0.0001	0.00931	-0.00437	-0.00284
Implicit/Explicit [11]		0.03	0.00022	0.00759	0.00003	-0.02243
Implicit Cr-Ni. [11]		0.02	0.011	0.00971	0.00000	-0.00273
Hopscotch [11]		0.02	0.0004	0.00963	0.00002	-0.00284
Split step Four. [11]		0.1563	0.0048	0.00464	0.00000	0.00034
A-L Local [11]		0.06	0.03	0.00695	-0.00001	-0.02526
A-L Global [11]		0.07	0.012	0.00937	-0.00004	-0.03324
Pseudospectral [11]		0.1563	0.0011	0.00840	0.00000	0.00005

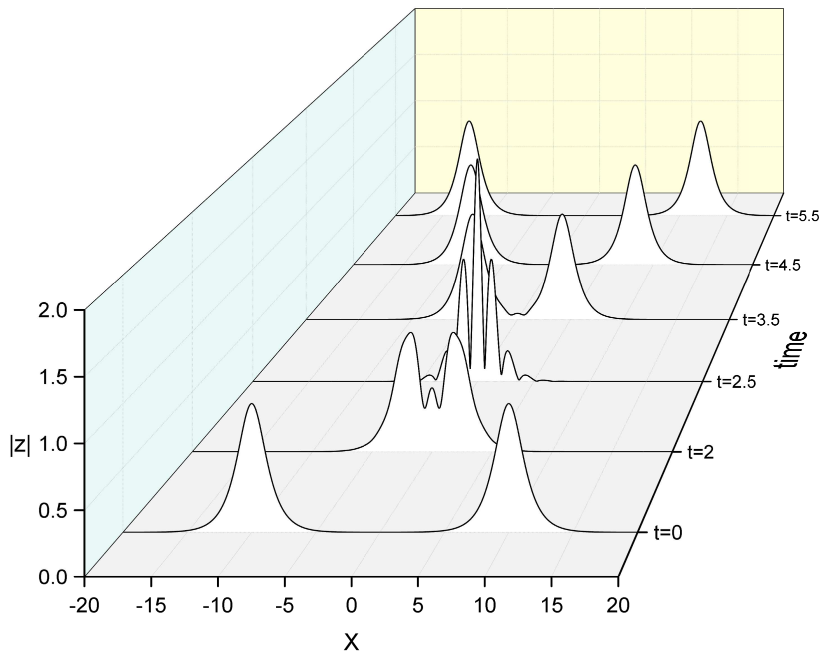

Figure 2. Double solitons $\alpha_1 = \alpha_2 = 1$.

Table 6. Invariants and relative changes of invariants of double solitons:$\alpha_1 = \alpha_2 = 1$

	Present (FDM-DQM)				Cub. Coll. [15]		Quad.Gal. [19]	
t	I_1	I_2	$\widehat{I_1}$	$\widehat{I_2}$	I_1	I_2	I_1	I_2
0.0	3.999998	14.66677	-	-	3.99998	14.66596	3.99999	14.83143
0.5	3.999996	14.66668	-5.0×10^{-7}	-6.1×10^{-6}	3.99998	14.66644	3.99999	14.83150
1.0	3.999999	14.66668	2.5×10^{-7}	-6.1×10^{-6}	3.99998	14.66706	3.99999	14.83157
1.5	4.000000	14.66667	5.0×10^{-7}	-6.8×10^{-6}	3.99999	14.66753	3.99999	14.83161
2.0	3.999998	14.66668	0.0×10^{-13}	-6.1×10^{-6}	3.99999	14.66693	3.99999	14.83261
2.5	3.999994	14.66672	-1.0×10^{-6}	-3.4×10^{-6}	3.99998	14.61440	3.99999	14.95380
3.0	3.999998	14.66667	0.0×10^{-13}	-6.8×10^{-6}	3.99998	14.66789	3.99999	-
3.5	3.999999	14.66668	2.5×10^{-7}	-6.1×10^{-6}	3.99999	14.66781	3.99999	14.83161
4.0	3.999996	14.66668	-5.0×10^{-7}	-6.1×10^{-6}	3.99998	14.66746	3.99999	14.83158
4.5	3.999997	14.66669	0.0×10^{-13}	-5.5×10^{-6}	3.99999	14.66613	3.99999	14.83156
5.0	3.999997	14.66667	-2.5×10^{-7}	-6.8×10^{-6}	3.99999	14.66684	3.99999	14.83153
5.5	3.999999	14.66676	2.5×10^{-7}	-6.8×10^{-7}	3.99999	14.66669	4.00000	14.83153

the critical time of collision $t = 2.5$ FDM-DQM solutions are better than cubic B-spline based FEM [15] and quadratic B-spline based FEM [19].

4.3. The standing soliton

Our next problem, having an initial condition $z(x, 0)$, a soliton is taken. The theory says that if

$$I = \int_{-\infty}^{\infty} z(x, 0)dx \geq \pi$$

then a soliton will appear with time, otherwise the soliton declines away [14]. To compare the newly results with earlier studies, we have selected Maxwellian initial condition

$$z(x, 0) = A \exp\left(-x^2\right) \tag{28}$$

along the region $-45 \leq x \leq 45$. By using Maxwellian initial condition $I = A\sqrt{\pi}$ obtained so that if $A > \sqrt{\pi} = 1.7725$ use a soliton will appear.

The characteristics of solutions for value of $A = 1$ and $A = 1.78$ time running up from $t = 0$ to $t = 6$ are given in Figure 3. As it is seen from Figure 3, the approximate solution of $|z|$ decay as time increases for value of $A = 1$ unless for the value of $A = 1.78$ soliton's amplitude, shape and speed are preserved. At the same time the position of soliton do not change for both values of $A = 1$ and $A = 1.78$. Numerical results for $A = 1$ with values of $\Delta t = 0.01$ and $N = 611$ are calculated,

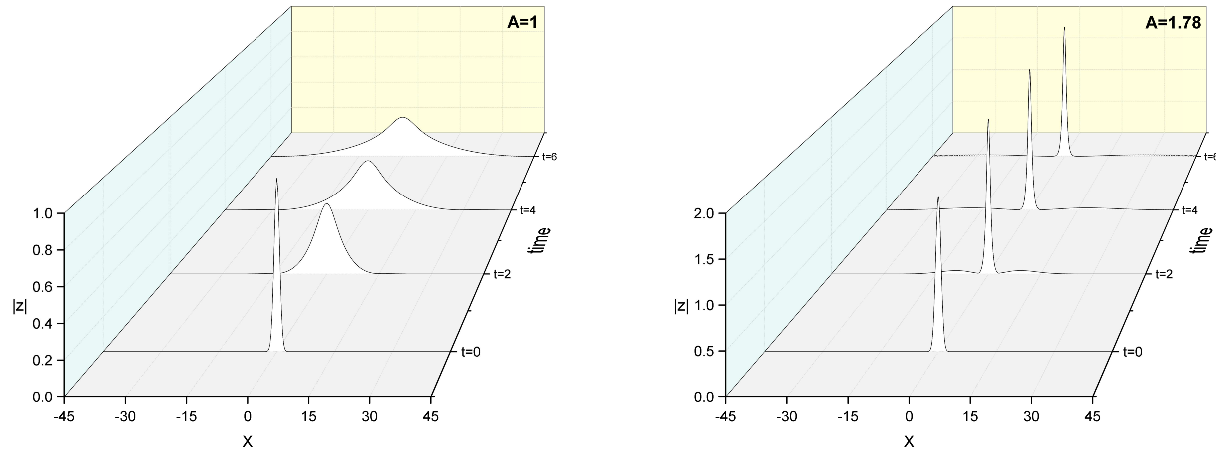

Figure 3. The standing soliton: $A = 1, A = 1.78$.

Table 7. Invariants and relative change of invariants of formation of standing soliton: A=1.

	FDM-DQM			
t	I_1	I_2	$\widehat{I}_1$	$\widehat{I}_2$
0.0	1.25331	0.36711	-	-
0.5	1.25331	0.36712	-8.0×10^{-7}	9.5×10^{-6}
1.0	1.25331	0.36712	-3.9×10^{-6}	1.9×10^{-5}
1.5	1.25331	0.36712	-4.8×10^{-6}	2.6×10^{-5}
2.0	1.25331	0.36712	-6.4×10^{-6}	3.1×10^{-5}
2.5	1.25331	0.36712	-4.8×10^{-6}	2.9×10^{-5}
3.0	1.25330	0.36712	-8.8×10^{-6}	1.4×10^{-5}
3.5	1.25330	0.36711	-1.0×10^{-5}	-3.8×10^{-6}
4.0	1.25330	0.36713	-7.9×10^{-6}	4.0×10^{-5}
4.5	1.25330	0.36714	-1.2×10^{-5}	6.6×10^{-5}
5.0	1.25330	0.36714	-1.4×10^{-5}	7.7×10^{-5}
5.5	1.25330	0.36715	-1.4×10^{-5}	8.7×10^{-5}
6.0	1.25329	0.36713	-1.9×10^{-5}	5.8×10^{-5}

Table 8. Two lowest invariants of the standing soliton: A=1.78

	FDM-DQM		Tay.Coll. [21]		Cub. Coll. [15]		Quad.Gal. [19]		Quin. Coll. [22]	
t	I_1	I_2	I_1	I_2	I_1	I_2	I_1	I_2	I_1	I_2
0.0	3.97100	-4.92558	3.971000	-4.925617	3.97100	-4.9387	3.97100	-4.90562	3.97100	-4.92562
0.5	3.97105	-4.92610	3.965336	-4.911705						
1.0	3.97098	-4.92566	3.967435	-4.925296			3.97099	-4.88626	3.97100	-4.93240
1.5	3.97096	-4.92554	3.967038	-4.910169						
2.0	3.97093	-4.92539	3.966703	-4.908872			3.97099	-4.88421	3.97100	-4.93377
2.5	3.97088	-4.92514	3.967008	-4.910052						
3.0	3.97085	-4.92496	3.967031	-4.910143	3.97095	-4.9387	3.97099	-4.88477	3.97100	-4.93326
3.5	3.97084	-4.92469	3.966839	-4.909396	3.97095	-4.9389				
4.0	3.97080	-4.92446	3.966927	-4.909737	3.97095	-4.9387	3.97099	-4.88472	3.97100	-4.93335
4.5	3.97076	-4.92420	3.967020	-4.910098	3.97095	-4.9386				
5.0	3.97074	-4.92385	3.966900	-4.909633	3.97093	-4.9390	3.97099	-4.88456	3.97100	-4.93346
5.5	3.97072	-4.92335	3.966890	-4.909550	3.97093	-4.9400				
6.0	3.97070	-4.92271	3.966994	-4.909682	3.97094	-4.9416	3.97099	-4.88157	3.97100	-4.93298

and reported in Table 7. As it is seen undoubtedly from Table 7 that FDM-DQM results in two invariants I_1 and I_2 which are nearly constant and acceptable good. Numerical results for $A = 1.78$ with values of $\Delta t = 0.005$ and $N = 721$ are computed and illustrated in Table 8. One can easily see from Table 8 that FDM-DQM produces two invariants I_1 and I_2 which are nearly constant and acceptable good.

4.4. The mobile soliton

As the fourth and the last test problem, the mobile soliton is used with the following initial condition

$$z(x,0) = A\exp\left(-x^2 + 2ix\right) \tag{29}$$

along the domain $-45 \leq x \leq 45$.

The characteristics of solutions for values of $A = 1$ and $A = 1.78$ from time $t = 0$ to $t = 6$ are illustrated in Figure 4. As one can see from Figure 4, the approximate solution of $|z|$ decay as time increases for value of $A = 1$ unless the value of $A = 1.78$ soliton's amplitude, shape and speed are preserved. Numerical results for $A = 1$ with values of $\Delta t = 0.01$ and $N = 581$ are computed and illustrated in Table 9. As one can see obviously from Table 9, FDM-DQM results in two invariants I_1 and I_2 which are almost constant and acceptable good. Numerical results for $A = 1.78$ with values of $\Delta t = 0.005$ and $N = 691$ are computed and tabulated in Table 10. As one can see obviously from Table 10, FDM-DQM yields the two invariants I_1 and I_2 which are nearly constant and acceptable good.

5. Conclusion

In this manuscript, we have applied quartic B-spline based FDM-DQM to obtain the numerical solution of NLS equation. During the solution procedure, to be able to calculate the complex value of function z, we have converted it into the coupled real value functions. For obtaining the second order derivative approximation, differential quadrature method based on fourth order quartic B-spline is used. After that, four famous trial problems have been solved. Simulation of the all of the test problems namely single soliton, double solitons, the standing soliton and mobile soliton given in the Figure 1−Figure 4. As it seen at the Figure 1−Figure 4 that properties of the solitons observed clearly. The efficiency of the method has been tested by calculating the error norms L_2 and L_∞, and two lowest invariants I_1 and I_2 and their relative changes given in the Table 2−Table 10. As one can see from the comparison of the the error norms of the newly method and earlier studies, FDM-DQM results are obviously the best one except for the single soliton at time $t = 2.5$ obtained by Gaussian radial basis collocation method [20]. The already found results clearly indicate that FDM-DQM can also be utilized to obtain numerical results of the NLS equation with high efficiency.

References

[1] Demir, H., & Şahin, S. (2016). Numerical investigation of a steady flow of an incompressible fluid in a lid driven cavity. *Turkish Journal of Mathematics and Computer Science*, 1, 14-23.

[2] Yokus, A., Baskonus, H.M., Sulaiman, T.A., & Bulut, H. (2018). Numerical simulation and solutions of the two-component second order KdV evolutionary system. *Numerical Methods for Partial Differential Equations*, 34, 211-227.

[3] Demir, H., & Süngü, İ. Ç. (2009). Numerical solution of a class of nonlinear Emden-Fowler equations by using differential transform method. *Cankaya University Journal Science and Engineering*, 12, 75-81.

[4] Demir, H., & Baltürk, Y. (2017). On numerical solution of fractional order boundary value problem with shooting method. *ITM Web of Conferences*, 13, 01032.

[5] Demir, H., & Ertürk, V.S. (2001). A numerical study of wall driven flow of a viscoelastic fluid in rectangular cavities. *Indian Journal of Pure and Applied Mathematics*, 32(10), 1581-1590.

[6] Yokus, A., Sulaiman, T.A., Baskonus, H.M., & Atmaca, S.P. (2018). On the exact and numerical solutions to a nonlinear model arising in mathematical biology. *ITM Web of Conferences*, 22, 01061.

[7] Karpman, V.I., & Krushkal, E.M. (1969). Modulated waves in non-linear dispersive media. *Soviet Physics—JETP*, 28, 277.

[8] Scott, A.C., Chu, F.Y.F., & Mclaughlin, D.W. (1973). The soliton: A new concept in applied science, *Proceedings of the IEEE*, 61(10),1443-1483.

[9] Zakharov, V.E., & Shabat, A.B. (1972). Exact theory of two dimensional self focusing and one dimensional self waves in non-linear media. *Soviet Journal of Experimental and Theoretical Physics*, 34,62.

[10] Delfour, M., Fortin, M., & Payre, G. (1981). Finite-difference solutions of a non-linear Schrödinger equation. Journal of Computational Physics, 44, 277-288.

[11] Thab, T.R., & Ablowitz, M.J. (1984). Analytical and numerical aspects of certain nonlinear evolution equations. II, Numerical, nonlinear Schrödinger equations. *Journal of Computational Physics*, 55, 203-230.

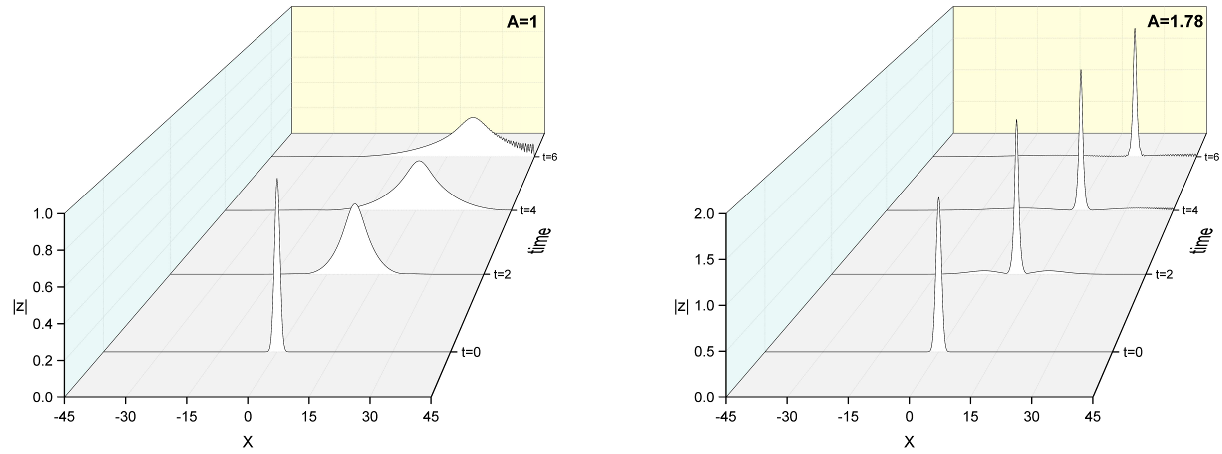

Figure 4. The mobile soliton: $A = 1, A = 1.78$.

Table 9. Invariants of mobile soliton:A=1.

	FDM-DQM			
t	I_1	I_2	$\widehat{I_1}$	$\widehat{I_2}$
0	1.25331	5.38148	-	-
1	1.25324	5.37853	-5.9$\times10^{-5}$	-5.5$\times10^{-4}$
2	1.25324	5.37795	-6.1$\times10^{-5}$	-6.6$\times10^{-4}$
3	1.25323	5.37768	-6.5$\times10^{-5}$	-7.1$\times10^{-4}$
4	1.25324	5.37761	-6.2$\times10^{-5}$	-7.2$\times10^{-4}$
5	1.25325	5.37758	-5.5$\times10^{-5}$	-7.3$\times10^{-4}$
6	1.25328	5.37752	-2.9$\times10^{-5}$	-7.4$\times10^{-4}$

Table 10. Invariants of mobile soliton:A=1.78

	FDM-DQM		Quin. Coll. [22]		Cub. Coll. [15]		Quad.Gal. [19]		Tay.Coll. [21]	
t	I_1	I_2	I_1	I_2	I_1	I_2	I_1	I_2	I_1	I_2
0	3.97100	10.96012	3.97100	10.95837	3.97100	10.9583	-	-	-	-
1	3.97111	10.96130	3.97100	10.97104	3.97101	10.2915	3.97096	11.34136	3.96377	10.93552
2	3.97114	10.96184	3.97100	10.97294			3.97095	11.36011	3.96199	10.93271
3	3.97114	10.96234	3.97100	10.97289			3.97095	11.35076	3.96292	10.93364
4	3.97114	10.96272	3.97100	10.97336	3.97100	8.50	3.97095	11.35546	3.96250	10.93377
5	3.97112	10.96289	3.97100	10.97374	3.97101	8.05	3.97095	11.35412	3.96255	10.93385
6	3.97107	10.96299	3.97100	10.97592			3.97123	11.38259	3.96276	10.93627

[12] Argyris, J., & Haase, M. (1987). An engineer's guide to soliton phenomena: Application of the finite element method. *Computer Methods in Applied Mechanics and Engineering*, 61, 71-122.

[13] Twizell, E.H., Bratsos, A.G., & Newby, J.C. (1997). A finite-difference method for solving the cubic Schrödinger equation. *Mathematics and Computers in Simulation*, 43,67-75.

[14] Gardner, L.R.T., Gardner, G.A., Zaki, S.I., & El Sharawi, Z.(1993). A leapfrog algorithm and stability studies for the non-linear Schrödinger equation. *Arabian Journal for Science and Engineering*, 18(1), 23-32.

[15] Gardner, L.R.T., Gardner, G.A., Zaki, S.I., & El Sharawi, Z.(1993). B-spline finite element studies of the non-linear Schrödinger equation. *Computer Methods in Applied Mechanics and Engineering*, 108, 303-318.

[16] Herbst, B.M., Morris, J. Ll. & Mitchell, A.R. (1985). Numerical experience with the nonlinear Schrödinger equation. *Journal of Computational Physics*, 60, 282-305.

[17] Robinson, M.P., & Fairweather, G. (1994). Orthogonal spline collocation methods for Schrödinger-type equation in one space variable. *Numerische Mathematik*, 68(3), 303-318.

[18] Robinson, M.P. (1997). The solution of nonlinear Schrödinger equations using orthogonal spline collacation. *Computers & Mathematics with Applications*, 33(7), 39-57.

[19] Dağ, I. (1999). A quadratic b-spline finite element method for solving the nonlinear Schrödinger equation. *Computer Methods in Applied Mechanics and Engineering*, 174, 247-258.

[20] Dereli, Y., Irk, D., & Dag, I. (2009). Soliton solutions for NLS equation using radial basis functions. *Chaos, Solitons and Fractals*, 42, 1227-1233.

[21] Aksoy, A.M., Irk, D., & Dag, I. (2012). Taylor collocation method for the numerical solution of the nonlinear Schrödinger equation using quintic b-spline basis. *Physics of Wave Phenomena*, 20(1), 67-79.

[22] Saka, B. (2012). A quintic B-spline finite-element method for solving the nonlinear Schrödinger equation. *Physics of Wave Phenomena*, 20(2), 107-117.

[23] Shu, C. (2000). *Differential quadrature and its application in engineering*. Springer-Verlag, London.

[24] Bellman, R., Kashef, B.G., & Casti, J. (1972). Differential quadrature: a tecnique for the rapid solution of nonlinear differential equations. *Journal of Computational Physics*, 10, 40-52.

[25] Zhong, H. (2004). Spline-based differential quadrature for fourth order equations and its application to Kirchhoff plates. *Applied Mathematical Modelling,* 28, 353-366.

[26] Shu, C., & Xue, H. (1997). Explicit computation of weighting coefficients in the harmonic differential quadrature. *Journal of Sound and Vibration,* 204(3), 549-555.

[27] Cheng, J., Wang, B., & Du, S. (2005). A theoretical analysis of piezoelectric/composite laminate with larger-amplitude deflection effect, Part II: hermite differential quadrature method and application. *International Journal of Solids and Structures*, 42, 6181-6201.

[28] Shu, C. & Wu, Y.L. (2007). Integrated radial basis functions-based differential quadrature method and its performance. *International Journal for Numerical Methods in Fluids*, 53, 969-984.

[29] Korkmaz, A., Aksoy, A.M., & Dağ, I. (2011). Quartic b-spline differential quadrature method. *International Journal of Nonlinear Science*, 11(4), 403-411.

[30] Başhan, A., Yağmurlu, N.M., Uçar, Y., & Esen, A. (2018). A new perspective for the numerical solutions of the cmKdV equation via modified cubic B-spline differential quadrature method. International *Journal of Modern Physics C*, 29(06), 1850043.

[31] Karakoc, S.B.G., Başhan A., & Geyikli, T. (2014).Two different methods for numerical solution of the modified burgers' equation. *The Scientific World Journal*,2014, Article ID 780269, 13 pages, http://dx.doi.org/10.1155/2014/780269

[32] Başhan, A., Karakoç, S.B.G., & Geyikli, T. (2015). Approximation of the KdVB equation by the quintic B-spline differential quadrature method. *Kuwait Journal of Science*, 42(2), 67-92.

[33] Başhan, A., Karakoç, S.B.G., & Geyikli, T. (2015). B-spline differential quadrature method for the modified burgers' equation. *Çankaya University Journal of Science and Engineering*, 12(1), 001-013.

[34] Başhan, A., Uçar, Y., Yağmurlu, N.M., & Esen, A. (2016). Numerical solution of the complex modified Korteweg-de Vries equation by DQM. *Journal of Physics: Conference Series* 766, 012028 doi:10.1088/1742-6596/766/1/012028

[35] Başhan, A., (2018). An effective application of differential quadrature method based on modified cubic B-splines to numerical solutions of KdV equation. *Turkish Journal of Mathematics*, 42, 373-394. DOI: 10.3906/mat-1609-69.

[36] Rubin, S.G., & Graves, R.A. (1975). A cubic spline approximation for problems in fluid mechanics. NASA technical report, NASA TR R-436.

[37] Prenter, P.M. (1975). *Splines and Variational Methods*. John Wiley, New York.

Ali Başhan *received his undergraduate degree in mathematics education from the Marmara University in 2003. He has completed his M.Sc. at Fırat University and Ph.D. degree at Inonu University in applied mathematics. He is currently studying about the numerical solutions of the partial differential equations. His research interests include finite difference methods and differential quadrature methods.*

An International Journal of Optimization and Control: Theories & Applications
ISSN:2146-0957 eISSN:2146-5703
Vol.9, No.2, pp.236-252 (2019)
http://doi.org/10.11121/ijocta.01.2019.00611

RESEARCH ARTICLE

Robust reformulations of ambiguous chance constraints with discrete probability distributions

İhsan Yanıkoğlu

Department of Industrial Engineering, Özyegin University, İstanbul, Turkey
ihsan.yanikoglu@ozyegin.edu.tr

ARTICLE INFO

Article History:
Received 04 May 2018
Accepted 06 May 2019
Available 31 July 2019

Keywords:
Robust optimization
Chance constraint
Ambiguous chance constraint

AMS Classification 2010:
90C11; 90C15; 90C35

ABSTRACT

This paper proposes robust reformulations of ambiguous chance constraints when the underlying family of distributions is discrete and supported in a so-called "p-box" or "p-ellipsoidal" uncertainty set. Using the robust optimization paradigm, the deterministic counterparts of the ambiguous chance constraints are reformulated as mixed-integer programming problems which can be tackled by commercial solvers for moderate sized instances. For larger sized instances, we propose a safe approximation algorithm that is computationally efficient and yields high quality solutions. The associated approach and the algorithm can be easily extended to joint chance constraints, nonlinear inequalities, and dependent data without introducing additional mathematical optimization complexity to that of the original robust reformulation. In numerical experiments, we first present our approach over a toy-sized chance constrained knapsack problem. Then, we compare optimality and computational performances of the safe approximation algorithm with those of the exact and the randomized approaches for larger sized instances via Monte Carlo simulation.

1. Introduction

Chance constrained optimization is introduced by [1] (also see, [2–4]) and it ensures that the probability of satisfying an uncertain constraint is greater than or equal to a certain threshold while minimizing or maximizing a given objective function. A *chance constraint* is given by

$$\Pr_{\boldsymbol{\zeta}\sim\mathbb{P}}\{\boldsymbol{\zeta} : f(\boldsymbol{x},\boldsymbol{\zeta}) \le 0\} \ge 1-\epsilon, \qquad (1)$$

where $f(\boldsymbol{x},\boldsymbol{\zeta})$ denotes a function of a decision vector $\boldsymbol{x} \in \boldsymbol{X} \subseteq \mathbb{R}^n$ ($\boldsymbol{X}$ is the set of feasible decisions) and a vector of uncertainty parameters $\boldsymbol{\zeta} \in \mathbb{R}^L$, $\epsilon \in [0,1]$ is the predetermined probability threshold, and $\mathbb{P}$ is the known probability distribution of $\boldsymbol{\zeta}$. It can be shown that the feasible set of (1) is convex when $\boldsymbol{\zeta}$ follows a Gaussian distribution and $f(\boldsymbol{x},\boldsymbol{\zeta})$ is linear in $\boldsymbol{x}$ and $\boldsymbol{\zeta}$; see [5–7]. Additional convexity results for (1) can be shown when $f(\boldsymbol{x},\boldsymbol{\zeta})$ is additively separable and $\boldsymbol{\zeta}$ follows a log-concave distribution ([8, 9]). Even though the chance constraint is tractable for the above mentioned problem classes, it is generally computationally intractable because the feasible set of the chance constraint is non-convex or it is computationally intractable to compute the left-hand side (LHS) of the constraint even when the feasible set is convex. In the latter case, one may use a Monte Carlo simulation to check the feasibility of the chance constraint, nevertheless, the simulation approach can also be too costly at high accuracies.

The chance constraint approach can be extended to multiple constraints, i.e., referred to as the joint chance constraint:

$$\Pr_{\boldsymbol{\zeta}\sim\mathbb{P}}\{\boldsymbol{\zeta} : f_k(\boldsymbol{x},\boldsymbol{\zeta}) \le 0 \quad \forall k \in K\} \ge 1-\epsilon. \qquad (2)$$

Notice that (2) is at least as computationally challenging as (1).

Computationally tractable safe approximations of the chance constraint have been proposed to overcome the difficulties that are mentioned above. A safe approximation method replaces the chance constraint with a set of constraints that yields a solution set that is a subset of the feasible set of the chance constraint. Nemirovski and Shapiro [10] propose a computationally tractable approximation of a chance constrained problem where constraints are affine in the uncertainty parameters that are independent with known support. Ben-Tal and Nemirovski [11] translate the existing stochastic uncertainties to 'uncertain-but-bounded' sets under mild assumptions. Namely, a feasible solution $\boldsymbol{x} \in \boldsymbol{X}$ for the tractable reformulation of the safe approximation

$$f(\boldsymbol{x}, \boldsymbol{\zeta}) \leq 0 \quad \forall \boldsymbol{\zeta} \in \mathcal{Z} \tag{3}$$

satisfies the chance constraint (1) with at least $1 - \epsilon$ probability where $\mathcal{Z}$ denotes a 'bounded' uncertainty set.

The accuracies of the obtained approximations in [10, 11] are good when the number of uncertainty parameters is high. Associated approximations are famous because they yield tractable robust reformulations for (1) using modern *robust optimization* (RO) techniques. We shall delve into details of these RO methods in the next section.

Chen et al. [12] propose a conservative approximation of a joint chance constraint in terms of a worst-case conditional value-at-risk (CVaR) constraint. The resulting approximation outperforms the Bonferroni approximation that is known to be pessimistic ([10, 12–14]). Zymler et al. [14] propose a method for approximating joint chance constraints when the first- and second-order moments together with the support of the uncertainty parameter are known. Similar to the safe approximations methods that are mentioned above, extension of our approach to the joint chance constraint is also straightforward; later in §3, the associated extension shall be mentioned. Calafiore and Campi [15] and Campi and Garatti [16] substitute the chance constraint with a finite number of constraints which are randomly sampled from the original constraint according to the known distribution of the uncertainty parameter. The authors show that the resulting solution that comes out of the randomized approach fails to satisfy the chance constraint with the given confidence level provided that a sufficient number of samples is drawn.

In practice, we usually have partial or no information on the probability distribution $\mathbb{P}$, since it needs to be estimated from historical data. This is why it makes sense to pass to *ambiguous* chance constraint. The term 'ambiguous' stands for the uncertainty in the probability distribution. In other words, the distribution of the uncertainty parameters is itself uncertain ([25]). The ambiguous chance constraint can be formulated as follows

$$\Pr_{\boldsymbol{\zeta} \sim \mathbb{P}} \{\boldsymbol{\zeta} : f(\boldsymbol{x}, \boldsymbol{\zeta}) \leq 0\} \geq 1 - \epsilon \quad \forall \mathbb{P} \in \mathcal{P}, \tag{4}$$

where $\mathbb{P}$ belongs to a family $\mathcal{P}$ of distributions and the chance constraint is satisfied for all ($\forall$) probability distributions in $\mathcal{P}$. This introduces an additional computational complexity in solving the problem aside from the existing difficulties that are mentioned above. To the best of our knowledge, there is no systematic and exact way of solving ambiguous chance constraint problems for general family classes with continuous distributions. Formulating ambiguity in the probability distribution has taken attention of scholars from different fields. In the absence of full information on the probability distribution or when only a set of possible distributions $\mathcal{P}$ is known, it is natural to optimize the expectation function corresponding to the worst-case probability distribution in $\mathcal{P}$. This lead to the following formulation: $[\min_{\boldsymbol{x} \in \boldsymbol{X}} \sup_{\mathbb{P} \in \mathcal{P}} \mathbb{E}_{\mathbb{P}}[f(\boldsymbol{x}, \boldsymbol{\zeta})]]$. For more details, we refer to [17–20]. Moreover, ambiguity in the probability distribution is also addressed by [21–23] in economics.

Ambiguity in the context of the chance constrained optimization has been studied by [10, 24, 25]. It is important to point out that the ambiguous chance constraint is 'severely' intractable compared to the regular chance constraint. Good news is that, as it is pointed out by [26, 27], robust reformulation methods for chance constraints can be straightforwardly extended to the ambiguous chance constraints and this is why the adjective 'ambiguous' is generally skipped. Erdoğan and Iyengar [24] define the distribution family $\mathcal{P}$ in (4) using the Prohorov metric. The authors propose a robust sampled problem that is a good approximation for the associated ambiguous chance constrained problem with high probability. Yanıkoğlu et al. [25] propose an iterative algorithm that constructs the uncertainty set yielding a tractable robust counterpart that safely approximates the ambiguous chance constraint; the authors use the ϕ-divergence metric and historical data on the uncertainty parameters to define the distribution family $\mathcal{P}$. For further details on such approximations, we refer reader to [25–27].

In this paper, we focus on robust reformulations of ambiguous chances constraints with discrete probability distributions. More precisely, $\mathbb{P}$ corresponds to a discrete probability distribution, i.e., we have a finite set of scenarios for uncertainty realizations $\{\boldsymbol{\zeta}^1, \boldsymbol{\zeta}^2, \ldots, \boldsymbol{\zeta}^{|S|}\}$ where each scenario

$s \in S$ or realization $\boldsymbol{\zeta}^s$ has an individual probability $p_s \geq 0$ of being realized; needless to say all probabilities are summed to 1, i.e.,$\sum_{s\in S} p_s = 1$. Finite supports are often faced in practice when data at hand is discrete, some examples are, demand, the number of customers in a queue, the amount of inventory in a production facility, the time and quantity of returning products in a reverse logistics network, the number of quality grades in remanufacturing and so on. On the other hand, empirical distributions are often used when the data at hand is scarce so that no continuous distribution can be fitted; or when the information is based on an expert opinion. Last but not least, continuous supports may be reduced to finite ones in order to yield computational tractability for the problem at hand (e.g., see [28]).

When $\boldsymbol{\zeta}$ follows a discrete probability distribution, the chance constraint (1) can be *equivalently* reformulated as

$$\begin{aligned} & f(\boldsymbol{x}, \boldsymbol{\zeta}^s) \leq M(1 - y_s) \qquad \forall s \in S \\ & \sum_{s\in S} p_s y_s \geq 1 - \epsilon, \end{aligned}$$

where binary variable $y_s \in \{0, 1\}$ is 1 if solution $\boldsymbol{x} \in \boldsymbol{X}$ satisfies the constraint $[f(\boldsymbol{x}, \boldsymbol{\zeta}^s) \leq 0]$ for realization $\boldsymbol{\zeta}^s$ or 0 otherwise, and M denotes a large constant; also see [29,30] that adopt the associated big-M reformulation technique and propose branch-and-bound/cut solution approach to chance constrained problems under finite support.

As it is pointed out above, the probability distribution $\mathbb{P}$ that has to be known is often not (exactly) known in practice; the probability vector $\boldsymbol{p} \in [0, 1]^{|S|}$ of the discrete uncertainty parameter $\boldsymbol{\zeta} \in \mathbb{R}^L$ often comes from an expert opinion or a forecast, i.e., the probability vector that determines the structure of the uncertainty is in itself uncertain. This is why, working with so-called a nominal probability vector may cause a lot of problems if the associated ambiguity in the discrete probability distribution is not taken into account. The ambiguous chance constraint (4) can be equivalently reformulated as the following semi-infinite mixed-integer problem when $\mathbb{P}$ follows a discrete probability distribution.

$$\begin{aligned} & f(\boldsymbol{x}, \boldsymbol{\zeta}^s) \leq M(1 - y_s) \qquad \forall s \in S \\ & \sum_{s\in S} p_s y_s \geq 1 - \epsilon \qquad \forall \boldsymbol{p} \in \mathcal{U}, \end{aligned} \tag{5}$$

where $\mathcal{U}$ denotes the ambiguity (or uncertainty) set that supports the family of distributions $\mathcal{P}$ in the ambiguous chance constraint. As pointed out above, (5) is a semi-infinite optimization problem, i.e., it has finitely many decision variables and infinitely many constraints (see, $\forall \boldsymbol{p} \in \mathcal{U}$) that is intractable in its current form. Using the robust optimization paradigm, the tractable reformulations of (5) shall be proposed in this paper. The associated approach is exact, i.e., it equivalently reformulates the ambiguous chance constraint by exploiting the deterministic structure of the distribution, when the random perturbation in $\boldsymbol{p}$ is independent; and we propose safe approximations when $\boldsymbol{p}$ is dependent.

Hanasusanto et al. [31] derive explicit conic representations of ambiguous chance constraints for tractable classes and efficiently solvable conservative approximations for the intractable ones using tools from *distributionally robust optimization* (DRO). The authors, derive tractable reformulations of the ambiguous individual chance constraint when the ambiguity set is Markov. For the joint case, the tractability is obtained only for conic moment ambiguity sets. The authors propose a conservative approximation algorithm for the intractable cases which is based on improving the fixed decision at each stage of the algorithm. Hanasusanto et al. [32] study conic representable reformulations of ambiguous joint chance constraints when the mean and the support, and the upper bound on the dispersion of the uncertainty parameters are known. The authors also provide the conic representable reformulation of the optimistic chance constraint for specific classes. Jiang and Guan [33] study distributionally robust chance constraints when the family of distributions is based on a phi-divergence measure. The problems are efficiently solvable by using strong cutting planes and hence a branch-and-cut algorithm. Chen et al. [34] propose distributionally robust reformulations of data-driven chance constraints using the Wasserstein ball uncertainty set that is often used in DRO framework. The resulting RC is mixed-integer linear program that can be solved for moderate sized instances. The method can also be extended to joint chance constraints when the uncertainty is in the right-hand side (RHS). Similarly, Ji and Lejeune [35] study distributionally robust chance-constrained programming with data-driven Wasserstein ambiguity sets. They strengthen the formulations by adopting valid inequalities. The resulting RC is a mixed-integer second-order cone programing (MISOCP) reformulation for the exact model with RHS uncertainty. The authors also propose a MISOCP relaxation for models with random technology vector. Zhang et al. [36] study distributionally robust reformulation of chance-constrained bin packing problem. Using two moments of the uncertainty, they construct the ambiguity set and the resulting robust reformulation of the problem. To strengthen second-order RC formulation, the authors adopt valid polymatroid inequalities that improves the computational performance the off-the-self solvers such as GUROBI and CPLEX for the given test instances. Cheng et al. [37] consider distributionally robust version of the quadratic knapsack problem where the knapsack constraint coincides with an ambiguous chance constraint such that the two moments of the distributions in the ambiguity sets are partly known. The resulting RC is a semi-definite programming (SDP) relaxation reformulation. The joint case is more challenging and the authors propose two tractable methods to find upper and lower bounds for the SDP relaxation. Hu and Hong [38] propose a DRO framework that adopts the Kullback-Leibler phi-diverge measure to model the ambiguity set of the unknown probability distribution. The authors show that the associated approach can also be used to reformulate ambiguous chances constraints when the confidence level of the phi-divergence measure is set to the probability threshold of the chance constraint. Xie and Ahmed [39] propose robust reformulations of ambiguous chance constrained problems when the ambiguity set is specified by convex moment constraints. They show that distributionally robust chance constrained problem can be modeled as a convex optimization problem under certain conditions. Xie et al. [40] propose a Bonferronni approximation approach to solve distributionally robust joint chance constrained programs. The author shows that the associated approximation is convex and tractable when the family of distributions is specified by moments or by marginal distributions. Xie [41] studies exact and approximate reformulations of distributionally robust chance constrained problems where the ambiguity set is determined by Wasserstein metric. The author adopts a branch and cut algorithm to solve the resulting reformulations.

Finite dimensional uncertainty parameters are often faced in regression analysis and worst-case expectation problems with Wasserstein ambiguity sets often yield efficient second-order conic formulation; we refer reader to [42] for distributionally robust regression. Similarly, Özmen et al. [43] robustify an extension of multivariate adaptive regression splines (MARS) under polyhedral uncertainty (i.e., so-called RCMARS) by adopting RO; we refer reader to [44] for MARS and to [45] for its deterministic extension, i.e., so-called CMARS. For robust reformulations of various risk measures that are often used in financial optimization, we refer to [12, 46–48], and references therein.

The remainder of the paper is organized as follows. In §2, we first give a brief introduction to the RO paradigm (§2.1), then we propose the robust reformulations of the ambiguous chance constraints with discrete probability distributions (§2.2). In §2.3, we propose a safe approximation algorithm for the robust reformulations. In §3, we present extensions of our approach. In §4, we present numerical experiments. Finally, we give our concluding remarks and future research directions in §5.

Notation. Bold-face, lower-case letters and numbers represent vectors, e.g., $\mathbf{0}$ denotes a vector of zeros and $\boldsymbol{e}$ is the all-one vector. Bold-face, upper-case letters represent matrices. The dimensions of the vectors and matrices will usually be clear from the context. Lower-case letters refer to vector elements, e.g., p_s denotes the s^{th} element of vector $\boldsymbol{p}$. A vector or matrix superscript indicates either the transpose ($\top$) or the element-wise power of a given vector or matrix, e.g., $\boldsymbol{q}^{-2}$ and $\boldsymbol{Q}^2$; only exceptions are indexes of probability vectors ($\boldsymbol{p}^0$, $\boldsymbol{p}^{(j)}$) and uncertainty parameter realizations ($\boldsymbol{\zeta}^s$). $\mathbb{P}$ denotes a probability distribution and $\mathcal{P}$ denotes a family of distributions. The uncertainty set is given by $\mathcal{Z}$ where $\boldsymbol{\zeta} \in \mathcal{Z} \subseteq \mathbb{R}^L$ denotes the uncertainty parameter and L is the number of uncertain parameters. The ambiguity set is given by $\mathcal{U}$ where $\boldsymbol{\xi} \in \mathcal{U} \subseteq \mathbb{R}^{|S|}$ denotes the perturbation vector of the probability vector $\boldsymbol{p} \in [0,1]^{|S|}$ and S denotes the set of indexes for the uncertainty parameter realizations, i.e., the components of the probability vector. The subscripts B and E for the ambiguity set denote the specific properties of the set, namely, p-box ($\mathcal{U}_B$) and p-ellipsoidal ($\mathcal{U}_E$). Finally, "..." denotes that the remainder of an expression shall continue in the next line.

2. Methodology

In this section, we first present the three core steps of the RO paradigm. Later we adopt RO to ambiguous chance constraints with discrete probability distributions and we to derive the tractable robust reformulations of the ambiguous chance constraints.

2.1. Introduction to robust optimization

For the sake of simplicity, we assume that LHS of the constraint $[f(\boldsymbol{x}, \boldsymbol{\zeta}) \leq 0]$ is a simple linear function $[f(\boldsymbol{x}, \boldsymbol{\zeta}) = (\boldsymbol{a} + \boldsymbol{B}\boldsymbol{\zeta})^\top \boldsymbol{x}]$ and the uncertainty parameter $\boldsymbol{\zeta}$ resides in a polyhedral uncertainty set $[\mathcal{U} = \boldsymbol{D}\boldsymbol{\zeta} + \boldsymbol{d} \geq 0]$, i.e., the constraint can be formulated as follows:

$$(\boldsymbol{a}+\boldsymbol{B\zeta})^\top \boldsymbol{x} \le 0 \qquad \forall \boldsymbol{\zeta} \ : \ \boldsymbol{D\zeta}+\boldsymbol{d} \ge \boldsymbol{0}, \quad (6)$$

where $\boldsymbol{x} \in \mathbb{R}^n$, $\boldsymbol{a} \in \mathbb{R}^n$, $\boldsymbol{B} \in \mathbb{R}^{n\times L}$, $\boldsymbol{D} \in \mathbb{R}^{m\times L}$, $\boldsymbol{d} \in \mathbb{R}^m$. Next, we present a three step procedure to remove the universal quantifier ($\forall$) in (6); the resulting deterministic equivalent reformulation is often referred to as the 'tractable' *robust counterpart* (RC).

Step 1: The worst-case formulation (6) can be equivalently reformulated as

$$\boldsymbol{a}^\top \boldsymbol{x} + \max_{\boldsymbol{\zeta}:\ \boldsymbol{D\zeta}+\boldsymbol{d}\ge 0} (\boldsymbol{B}^\top \boldsymbol{x})^\top \boldsymbol{\zeta} \le 0. \quad (7)$$

We now have a nested optimization problem because we have a maximization inside the constraint. Next, we take the dual the inner maximization problem.

Step 2: Note that by strong duality

$$\max\left\{(\boldsymbol{B}^\top \boldsymbol{x})^\top \boldsymbol{\zeta} \ : \ \boldsymbol{D\zeta}+\boldsymbol{d} \ge 0\right\}$$
$$= \min\left\{\boldsymbol{d}^\top \boldsymbol{y} : \boldsymbol{D}^\top \boldsymbol{y} = -\boldsymbol{B}^\top \boldsymbol{x},\ \boldsymbol{y} \ge 0\right\}.$$

Hence (7) is equivalent to

$$\boldsymbol{a}^\top \boldsymbol{x} + \min_{\boldsymbol{y}\ge 0}\{\boldsymbol{d}^\top \boldsymbol{y} :\ \boldsymbol{D}^\top \boldsymbol{y} = -\boldsymbol{B}^\top \boldsymbol{x}\} \le 0. \quad (8)$$

Step 3: We can remove the *min*imization in (8) because a feasible solution for (8) yields an upper bound for the maximization problem by weak duality (i.e., equivalent at optimality by strong duality because the problem is convex).

$$\exists\, \boldsymbol{y} : \boldsymbol{a}^\top \boldsymbol{x} + \boldsymbol{d}^\top \boldsymbol{y} \le \beta, \quad \boldsymbol{D}^\top \boldsymbol{y} = -\boldsymbol{B}^\top \boldsymbol{x}, \quad \boldsymbol{y} \ge 0.$$

Finally, we obtain the tractable RC of the initial semi-infinite problem (6).

Table 1 presents the RCs of (6) with respect to a class of uncertainty sets. The only difference is that the type of duality in Step 3 changes according to the uncertainty set at hand, e.g., when the uncertainty set is a cone, we use conic duality to obtain the RC; see, the third row of the Table 1.

Table 1. The tractable robust counterparts of uncertain linear constraints

Set	$\mathcal{Z}$	Robust Counterpart	Tractability
Box	$\|\boldsymbol{\zeta}\|_\infty \le \rho$	$\boldsymbol{a}^\top \boldsymbol{x} + \rho\|\boldsymbol{B}^\top \boldsymbol{x}\|_1 \le 0$	LP
Ball	$\|\boldsymbol{\zeta}\|_2 \le \rho$	$\boldsymbol{a}^\top \boldsymbol{x} + \rho\|\boldsymbol{B}^\top \boldsymbol{x}\|_2 \le 0$	CQP
Cone	$\boldsymbol{D\zeta}+\boldsymbol{d} \in K$	$\boldsymbol{a}^\top \boldsymbol{x} + \boldsymbol{d}^\top \boldsymbol{y} \le 0$ $\boldsymbol{D}^\top \boldsymbol{y} = -\boldsymbol{B}^\top \boldsymbol{x}$ $\boldsymbol{y} \in K^*$	Conic

Notice that the three step procedure shall be similarly applied in our setting to derive the tractable RC reformulations of the semi-infinite probability threshold constraint:

$$\sum_{s\in S} p_s y_s \ge \epsilon \quad \forall \boldsymbol{p} \in \mathcal{U} \qquad (\mathbf{SI})$$

for the two different classes of the ambiguity set $\mathcal{U}$. We refer reader to [26, 49] and the references therein for further details on the RO paradigm.

2.2. Robust reformulation of ambiguous chance constraint

In this section, we focus on the robust reformulations of the ambiguous chance constraints for two classes of uncertainty sets, namely, 'p-box' and 'p-ellipsoidal' uncertainty sets that are specifically created for the uncertain probability vector $\boldsymbol{p} \in \{0,1\}^{|S|}$ that resides in the plane sections of box and ellipsoidal regions. To this end, we shall develop the tractable RC reformulations of the semi-infinite probability constraint (SI) in

$$\begin{aligned} & f(\boldsymbol{x}, \boldsymbol{\zeta}^s) \le M(1-y_s) \quad \forall s \in S \\ & \sum_{s\in S} p_s y_s \ge 1-\epsilon \quad \forall \boldsymbol{p} \in \mathcal{U}. \end{aligned} \qquad (re\text{-}5)$$

The formal representations of p-box ($\mathcal{U}_B$) and p-ellipsoidal ($\mathcal{U}_E$) ambiguity sets are given as

$$\mathcal{U}_B = \left\{\boldsymbol{p} = \boldsymbol{p}^0 + \boldsymbol{\xi} \in \mathbb{R}^{|S|} : \boldsymbol{\ell} \le \boldsymbol{\xi} \le \boldsymbol{u}, \boldsymbol{e}^\top \boldsymbol{\xi} = 0\right\}$$

and

$$\mathcal{U}_E = \left\{\boldsymbol{p} = \boldsymbol{p}^0 + \boldsymbol{\xi} \in \mathbb{R}^{|S|} : ||\boldsymbol{Q\xi}||_2 \le \sigma, \boldsymbol{e}^\top \boldsymbol{\xi} = 0\right\},$$

where $\boldsymbol{p}^0$ denotes the nominal probability vector given that $\boldsymbol{p}^0 \ge 0$ and $\sum_{s\in S} p_s^0 = 1$; $\boldsymbol{\xi}$ is the uncertainty vector that determines the dispersion from the nominal probability vector; $\boldsymbol{\ell}$ and $\boldsymbol{u}$ are the upper and lower bound vectors for the p-box; σ denotes the radius (or the worst-case dispersion from the nominal vector $\boldsymbol{p}^0$) in the p-ellipsoidal, $\boldsymbol{Q} \in \mathbb{R}^{|S|\times|S|}(:= \operatorname{diag}(\boldsymbol{q}))$ is a diagonal matrix where vector $\boldsymbol{q} \in \mathbb{R}^{|S|}$ contains the scaling parameters that determine the shape of the ellipsoid, e.g., when $\boldsymbol{q} = \boldsymbol{e}$, the resulting uncertainty set is a ball. Notice that the sum of the elements of the uncertainty vector $\boldsymbol{\xi}$ is zero (i.e., $[\sum_{s\in S} \xi_s = 0]$) in order to guarantee that the sum of the elements of the unknown (or ambiguous) probability vector to be 1 (i.e., $[\sum_{s\in S} p_s = 1]$).

Independent versus dependent data. In some cases, it may be known that the uncertainty parameters ζ_j^s are independent for $j \in \{1,\ldots,L\}$. If this is the case, then the joint probability p_s of the uncertainty vector $[\zeta_1^s, \zeta_2^s, \ldots, \zeta_L^s]$ is being realized is equivalent to the product of the marginal probabilities of the uncertainty parameters for the given scenario, i.e., $[p_s = p_1^{(s)} \cdots p_L^{(s)}]$. This results in complex ambiguity sets. We shall delve into details of such reformulations later in §3.3.

In the remainder, for the sake of simplicity, we assume that the elements of the ambiguous probability vector $\boldsymbol{p}$ are independent and the uncertainty parameter ($\boldsymbol{\zeta}^s$) is realized as a vector. Other assumptions are listed below.

Assumptions. (**A1**) We assume that $f(\boldsymbol{x}, \boldsymbol{\zeta})$ is linear in the decision variable $\boldsymbol{x}$ (extended in §3.2). (**A2**) Without loss of generality, we assume that $\mathcal{U}_{B,E} \subseteq [0,1]^{|S|}$, i.e., the parameters $\boldsymbol{\ell}, \boldsymbol{u}, \boldsymbol{Q}$, and σ are selected such that $[\boldsymbol{p} \geq 0 \quad \forall \boldsymbol{p} \in \mathcal{U}_{B,E}]$ is satisfied.

Selecting the parameters of p-ellipsoidal uncertainty set. The standard form of the ellipsoid inequality is

$$\frac{\xi_1^2}{\alpha_1^2} + \cdots + \frac{\xi_{|S|}^2}{\alpha_{|S|}^2} \leq 1,$$

where α_i denotes the half length of the i^{th} principal semiaxis of the ellipsoid, i.e., $\alpha_i > 0$ for all $i \in \{1, \ldots |S|\}$. Let parameter "$\gamma_i \in (0,1]^{|S|}$" be the percentage of dispersion $[(1-\gamma_i)p_i^0, (1+\gamma_i)p_i^0]$ from the nominal probability p_i^0 for $i = \{1, \ldots, |S|\}$, then we may set the half length α_i to the associated dispersion, i.e., $\alpha_i = \gamma_i p_i^0$ for all $i \in \{1, \ldots, |S|\}$. Eventually, the p-ellipsoidal uncertainty set $\mathcal{U}_E$ that satisfies (A2) can be generated by setting $\sigma = 1$ and

$$q_i = \frac{1}{\gamma_i p_i} \quad \forall i \in \{1, \ldots, |S|\},$$

where $\boldsymbol{Q} = \mathrm{diag}(\boldsymbol{q})$. Notice that one can also set σ and $\boldsymbol{Q}$ using other methods as long as (A2) is satisfied; here we present a systematic method that can be easily implemented in practice.

Theorem 1 and 2 provide the tractable RCs of (SI) for the p-box and p-ellipsoidal uncertainty sets; respectively.

Theorem 1. *The vector* $\boldsymbol{y} \in \{0,1\}^{|S|}$ *satisfies*

$$\sum_{s \in S} p_s y_s \geq 1 - \epsilon \quad \forall \boldsymbol{p} \in \mathcal{U}_B \qquad (\mathbf{SI}_{\mathrm{B}})$$

if and only if $\boldsymbol{y}$, $\boldsymbol{\theta}$, $\boldsymbol{w}$ *and* λ *satisfy the following RC problem:*

$$\begin{aligned} &\boldsymbol{y}^\top \boldsymbol{p}^0 + \boldsymbol{u}^\top \boldsymbol{w} + \boldsymbol{\ell}^\top \boldsymbol{\theta} \geq 1 - \epsilon \\ &\lambda \boldsymbol{e} + \boldsymbol{w} + \boldsymbol{\theta} - \boldsymbol{y} = \boldsymbol{0} \\ &\boldsymbol{\theta} \geq \boldsymbol{0}, \boldsymbol{w} \leq \boldsymbol{0}, \lambda \ urs, \end{aligned}$$

where $\boldsymbol{e}$ *is the all-one vector, and* $\boldsymbol{w}, \boldsymbol{\theta}$, *and* λ *denote the dual variables.*

Proof. As in Step 1 of the three step procedure in §2.1, ($\mathbf{SI}_{\mathrm{B}}$) can be equivalently reformulated as

$$\min_{\boldsymbol{p} \in \mathcal{U}_B} \sum_{s \in S} p_s y_s \geq 1 - \epsilon.$$

The above expression is equivalent to the following

$$\min_{\boldsymbol{\xi}} \left\{ \sum_{s \in S} \xi_s y_s : \boldsymbol{\ell} \leq \boldsymbol{\xi} \leq \boldsymbol{u} \right\} \geq 1 - \epsilon - \boldsymbol{y}^\top \boldsymbol{p}^0.$$

Notice that $\boldsymbol{y}^\top \boldsymbol{p}^0$ is taken out of the minimization because it is a fixed term for given $\boldsymbol{y}$. Let us now focus on the minimization problem in the constraint LHS:

$$\begin{aligned} \min_{\boldsymbol{\xi}} \quad & \sum_{s \in S} \xi_s y_s \\ \text{s.t.} \quad & \sum_{s \in S} \xi_s = 0 \qquad (\lambda) \\ & \boldsymbol{\xi} \leq \boldsymbol{u} \qquad (\boldsymbol{w}) \\ & \boldsymbol{\xi} \geq \boldsymbol{\ell} \qquad (\boldsymbol{\theta}), \end{aligned}$$

where each term in the parentheses denotes the dual variable of the associated constraint.

Next we take the dual of the problem as in Step 2:

$$\begin{aligned} \max_{\boldsymbol{w} \leq \boldsymbol{0},\ \boldsymbol{\theta} \geq \boldsymbol{0},\ \lambda} \quad & \boldsymbol{u}^\top \boldsymbol{w} + \boldsymbol{\ell}^\top \boldsymbol{\theta} \quad (\geq 1 - \epsilon - \boldsymbol{y}^\top \boldsymbol{p}^0) \\ \text{s.t.} \quad & \lambda + w_s + \theta_s = y_s \quad \forall s \in S. \end{aligned}$$

Finally, we remove the *max*imization and obtain the tractable reformulation of ($\mathbf{SI}_{\mathrm{B}}$) □

Consequently, the tractable RC of the robust reformulation of the ambiguous chance constraint (5) with respect to the p-box uncertainty set becomes

$$\begin{aligned} & f(\boldsymbol{x}, \boldsymbol{\zeta}^s) \leq M(1 - y_s) \quad \forall s \in S \\ & \boldsymbol{y}^\top \boldsymbol{p}^0 + \boldsymbol{u}^\top \boldsymbol{w} + \boldsymbol{\ell}^\top \boldsymbol{\theta} \geq 1 - \epsilon \\ & \lambda \boldsymbol{e} + \boldsymbol{w} + \boldsymbol{\theta} - \boldsymbol{y} = \boldsymbol{0} \qquad (\mathbf{RC}_{\mathrm{B}}) \\ & \boldsymbol{x} \in \boldsymbol{X}, \boldsymbol{y} \in \{0,1\}^{|S|} \\ & \boldsymbol{w} \leq 0,\ \boldsymbol{\theta} \geq 0,\ \lambda \ urs. \end{aligned}$$

The resulting problem ($\mathbf{RC}_{\mathrm{B}}$) is a *mixed-integer linear problem* (MILP) that can be solved by commercial solvers (e.g., CPLEX) for moderate sized instances; given that there exists a linear objective function $[\boldsymbol{c}^\top \boldsymbol{x}]$ that we either minimize or maximize.

Similarly, Theorem 2 presents the tractable RC of (**SI**) with respect to the p-ellipsoidal uncertainty set.

Theorem 2. *The vector* $\boldsymbol{y} \in \{0,1\}^{|S|}$ *satisfies*

$$\sum_{s \in S} p_s y_s \geq 1 - \epsilon \quad \forall \boldsymbol{p} \in \mathcal{U}_E \qquad (\mathbf{SI}_{\mathrm{E}})$$

if and only if $\boldsymbol{y}$, β, *and* λ *satisfy the following RC problem:*

$$
\begin{aligned}
&-\boldsymbol{y}_\beta^\top \boldsymbol{p}^0 + 0.25\left(\lambda^2\boldsymbol{e} + \boldsymbol{y} + 2\boldsymbol{y}_\lambda\right)^\top \boldsymbol{q}^{-2} + \dots \\
&\quad \beta^2\sigma^2 + \beta(1-\epsilon) \le 0 \\
&\lambda\boldsymbol{e} - M(\boldsymbol{e}-\boldsymbol{y}) \le \boldsymbol{y}_\lambda \le \lambda\boldsymbol{e} + M(\boldsymbol{e}-\boldsymbol{y}) \\
&\beta\boldsymbol{e} - M(\boldsymbol{e}-\boldsymbol{y}) \le \boldsymbol{y}_\beta \le M\boldsymbol{y} \\
&-M\boldsymbol{y} \le \boldsymbol{y}_\lambda \le M\boldsymbol{y} \\
&\boldsymbol{0} \le \boldsymbol{y}_\beta \le \beta\boldsymbol{e} \\
&\beta \ge \varepsilon,\ \lambda\ urs,
\end{aligned}
$$

where $\boldsymbol{e}$ *is the all-one vector,* $\boldsymbol{y}_\lambda$ *and* $\boldsymbol{y}_\beta$ *are the auxiliary variables to linearize* $\lambda\boldsymbol{y}$ *and* $\beta\boldsymbol{y}$*; respectively,* β *and* λ *are the dual variables, and* ε *is a small positive constant.*

Proof. Similar to the proof of Theorem 1, $(\mathbf{SI}_\mathrm{E})$ can be reformulated as

$$\min_{\boldsymbol{p}\in\mathcal{U}_E} \sum_{s\in S} p_s y_s \ge 1-\epsilon.$$

The Lagrangian dual problem of the minimization problem in the constraint LHS is given by

$$\max_{\beta\ge 0,\ \lambda}\ \min_{\boldsymbol{\xi}}\ \boldsymbol{\xi}^\top\boldsymbol{y} + \beta(||\boldsymbol{Q}\boldsymbol{\xi}||_2^2 - \sigma^2) + \lambda\sum_{s\in S}\xi_s$$

where $\beta \ge 0$ and λ denote the dual variables for the p-ellipsoidal constraints $[||\boldsymbol{Q}\boldsymbol{\xi}||_2^2 \le \sigma^2]$ and $[\sum_{s\in S}\xi_s = 0]$; respectively. From the first-order condition, we have $[\boldsymbol{y} + 2\beta\boldsymbol{Q}^2\boldsymbol{\xi} + \lambda\boldsymbol{e} = 0]$ ($\boldsymbol{Q}^\top\boldsymbol{Q} = \boldsymbol{Q}^2$ because $\boldsymbol{Q}$ is a diagonal matrix), i.e., the optimal $\boldsymbol{\xi}^*$ is

$$\boldsymbol{\xi}^* = -\frac{\boldsymbol{Q}^{-2}(\lambda\boldsymbol{e}+\boldsymbol{y})}{2\beta}.$$

Consequently, we substitute $\boldsymbol{\xi}^*$ for $\boldsymbol{\xi}$ in the dual problem. Next, we can remove the *max*imization as in Step 3 and the LHS becomes

$$
\begin{aligned}
&-\frac{1}{2\beta}\Bigg(\lambda\boldsymbol{e}^\top\boldsymbol{Q}^{-2}\boldsymbol{y} + \boldsymbol{y}^\top\boldsymbol{Q}^{-2}\boldsymbol{y} + \dots \\
&\qquad \lambda^2\boldsymbol{e}^\top\boldsymbol{Q}^{-2}\boldsymbol{e} + \lambda\boldsymbol{y}^\top\boldsymbol{Q}^{-2}\boldsymbol{e}\Bigg) + \dots \\
&\quad \frac{1}{4\beta}\Bigg(\lambda^2\boldsymbol{e}^\top\boldsymbol{Q}^{-2}\boldsymbol{e} + 2\lambda\boldsymbol{e}^\top\boldsymbol{Q}^{-2}\boldsymbol{y} + \dots \\
&\qquad \boldsymbol{y}^\top\boldsymbol{Q}^{-2}\boldsymbol{y}\Bigg) - \beta\sigma^2
\end{aligned}
$$

which is $[\ge 1-\epsilon-\boldsymbol{y}^\top\boldsymbol{p}^0]$. It is important to point out that assuming $\beta > 0$ does not affect the optimum solution because the first constraint is binding at optimality $[||\boldsymbol{Q}\boldsymbol{\xi}^*||_2 - \sigma^2 = 0]$ (also see Assumption A2), i.e., the complementary condition $[\beta^*(||\boldsymbol{Q}\boldsymbol{\xi}^*||_2 - \sigma^2) = 0]$ is satisfied for $\beta^* > 0$. Next we multiply the both sides of the inequality by β (> 0):

$$
\begin{aligned}
&-\left(\frac{\boldsymbol{y}^\top\boldsymbol{Q}^{-2}\boldsymbol{y} + \lambda^2\boldsymbol{e}^\top\boldsymbol{Q}^{-2}\boldsymbol{e}}{4\beta} + \frac{\lambda\boldsymbol{e}^\top\boldsymbol{Q}^{-2}\boldsymbol{y}}{2\beta} + \sigma^2\beta\right) \\
&\quad \ge 1-\epsilon-\boldsymbol{y}^\top\boldsymbol{p}^0\ (\times\beta \text{ both sides})
\end{aligned}
$$

which results in the following inequality

$$
\begin{aligned}
&0.25\left(\boldsymbol{y}^2 + \lambda^2\boldsymbol{e} + 2\lambda\boldsymbol{y}\right)^\top \boldsymbol{q}^{-2} + \dots \\
&\quad \beta^2\sigma^2 + \beta(1-\epsilon) - \beta\boldsymbol{y}^\top\boldsymbol{p}^0 \ \le 0.
\end{aligned}
$$

Notice that since $\boldsymbol{y}$ is a vector of binary variables, $\boldsymbol{y}^\top\boldsymbol{y}$ is equivalent to $\boldsymbol{y}^\top\boldsymbol{e}$, and $\boldsymbol{Q} = \mathrm{diag}(\boldsymbol{q})$. Moreover, we introduce a vector of auxiliary variables $\boldsymbol{y}_\beta \in \mathbb{R}_+^{|S|}$ ($:= \beta\boldsymbol{y}$) and the following group of constraints to linearize $\beta\boldsymbol{y}$:

$$
\begin{aligned}
&\boldsymbol{y}_\beta \ge \beta\boldsymbol{e} - M(\boldsymbol{e}-\boldsymbol{y}) \\
&\boldsymbol{y}_\beta \le M\boldsymbol{y} \\
&\boldsymbol{y}_\beta \le \beta\boldsymbol{e} \\
&\boldsymbol{y}_\beta \ge \boldsymbol{0},
\end{aligned}
$$

where M is a large constant. Similarly, we define $\boldsymbol{y}_\lambda \in \mathbb{R}^{|S|}$ ($:= \lambda\boldsymbol{y}$) and the following constraints to linearize $\lambda\boldsymbol{y}$:

$$
\begin{aligned}
&\boldsymbol{y}_\lambda \le M\boldsymbol{y} \\
&\boldsymbol{y}_\lambda \ge -M\boldsymbol{y} \\
&\boldsymbol{y}_\lambda \le \lambda\boldsymbol{e} + M(\boldsymbol{e}-\boldsymbol{y}) \\
&\boldsymbol{y}_\lambda \ge \lambda\boldsymbol{e} - M(\boldsymbol{e}-\boldsymbol{y}).
\end{aligned}
$$

The final formulation of the RC is obtained after the above mentioned substitutions are made and the additional constraints are included. □

Eventually, the tractable RC of (5) with respect to the p-ellipsoidal uncertainty set becomes

$$
\begin{aligned}
&f(\boldsymbol{x},\boldsymbol{\zeta}^s) \le M(1-y_s) \quad \forall s\in S \\
&\sigma^2\beta^2 + \beta(1-\epsilon) - \boldsymbol{y}_\beta^\top\boldsymbol{p}^0 + \dots \\
&\quad 0.25\left(\boldsymbol{y} + \lambda^2\boldsymbol{e} + 2\boldsymbol{y}_\lambda\right)^\top\boldsymbol{q}^{-2} \le 0 \\
&\lambda\boldsymbol{e} - M(\boldsymbol{e}-\boldsymbol{y}) \le \boldsymbol{y}_\lambda \\
&\lambda\boldsymbol{e} + M(\boldsymbol{e}-\boldsymbol{y}) \ge \boldsymbol{y}_\lambda \\
&\beta\boldsymbol{e} - M(\boldsymbol{e}-\boldsymbol{y}) \le \boldsymbol{y}_\beta \le M\boldsymbol{y} \\
&-M\boldsymbol{y} \le \boldsymbol{y}_\lambda \le M\boldsymbol{y} \\
&\boldsymbol{0} \le \boldsymbol{y}_\beta \le \beta\boldsymbol{e} \\
&\boldsymbol{x}\in\boldsymbol{X}, \boldsymbol{y}\in\{0,1\}^{|S|},\ \beta\ge\varepsilon,\ \lambda \text{ urs.}
\end{aligned}
\qquad (\mathbf{RC}_\mathrm{E})
$$

Notice that $(\mathbf{RC}_\mathrm{E})$ is a *mixed-integer second-order cone problem* (MISOCP) that yields a convex relaxation problem; SOCP is a tractable mathematical optimization class and supported by commercial solvers such as CPLEX.

Remark 1. *We assume that* M *is large enough to guarantee that big-M constraints are equivalent to the constraints in the original formulation. On the other hand, they are also small enough* *to avoid excessive branching, i.e., they must be systematically generated in the numerical experiments.*

Remark 2. *The second constraint in* $(\mathbf{RC}_{\mathrm{E}})$ *can be equivalently reformulated as the following second-order cone constraint:*

$$\left\| 1 - \left(\boldsymbol{y}_\beta^\top \boldsymbol{p}^0 - 0.25\left(\boldsymbol{y} + 2\boldsymbol{y}_\lambda\right)^\top \boldsymbol{q}^{-2} - \beta(1-\epsilon) \right)/2; \; 0.5\lambda \boldsymbol{q}^{-1}; \; \sigma\beta \right\|_2 \leq 1 + \left(\boldsymbol{y}_\beta^\top \boldsymbol{p}^0 - 0.25\left(\boldsymbol{y} + 2\boldsymbol{y}_\lambda\right)^\top \boldsymbol{q}^{-2} - \beta(1-\epsilon) \right)/2.$$

In summary, using Theorem 1 and 2, one may obtain *exact* robust reformulations of *unique* ambiguous chance constraints with discrete probability distributions when the unknown scenario probabilities $[p_1, p_2, \dots p_{|S|}]$ are *independent*. The mathematical optimization complexity of the resulting RC is MILP for the p-box and is MISOCP for the p-ellipsoidal uncertainty set given that f is linear in the decision variable $\boldsymbol{x} \in \boldsymbol{X}$. In §§3.1-3.3, we shall relax some of these properties in order to tackle with more general classes of ambiguous chance constraints. Good news is that our approach straightforwardly extends for these new classes even though it is not necessarily exact but a *safe approximation* method when the elements of the probability vector are *dependent*.

2.3. Safe Approximation Algorithm

Notice that when the number of scenarios ($|S|$) increases, $(\mathbf{RC}_{\mathrm{B}})$ and $(\mathbf{RC}_{\mathrm{E}})$ may be challenging mathematical optimization problems to be solved in a given time limit. This is why, in this section, we present an efficient iterative algorithm that shall yield a safe approximation for ambiguous chance constraints with discrete probability distributions. We illustrate our approach using the following (implicit) notation of the unique ambiguous chance constrained problem:

$$\min_{\boldsymbol{x} \in \boldsymbol{X}} \; \boldsymbol{c}^\top \boldsymbol{x}$$
$$\text{s.t.} \quad \Pr_{\boldsymbol{\zeta} \sim \mathbb{P}} \left\{ \boldsymbol{\zeta} : f(\boldsymbol{x}, \boldsymbol{\zeta}) \leq 0 \right\} \geq 1 - \epsilon \quad \forall \mathbb{P} \in \mathcal{P},$$

where $1-\epsilon$ is the prescribed probability, and $\boldsymbol{\zeta}$ is the *primitive* uncertainty vector. The four main steps of the algorithm are explained in detail below.

Step 0. We scale the uncertainty parameters to $[-1, 1]$. W.l.o.g., an uncertainty parameter $\hat{\zeta}_i = [\ell_i, u_i]$ for $i \in S$ can be scaled to $[-1, 1]$ by adopting the following linear transformation:

$$\hat{\zeta}_i = \mathrm{NV}_i + \mathrm{HL}_i \times \zeta_i, \tag{9}$$

where $\mathrm{NV}_i = 0.5(\ell_i + u_i)$, $\mathrm{HL}_i = 0.5(u_i - \ell_i)$, and $\zeta_i \in \{-1, 1\}$ is the so-called primitive uncertainty parameter.

Step 1. Derive the RC of the problem at hand

$$\max_{\boldsymbol{x} \in \boldsymbol{X}} \; \boldsymbol{c}^\top \boldsymbol{x}$$
$$\text{s.t.} \; f(\boldsymbol{x}, \boldsymbol{\zeta}) \leq 0 \quad \forall \boldsymbol{\zeta} \in \mathcal{U} \tag{10}$$

where $\mathcal{U} \equiv \{\boldsymbol{\zeta} \in [-1,1]^{|L|} : ||\boldsymbol{\zeta}||_2 \leq \Omega\}$. It is important to point out that the associated RC yields SOCP when the f is linear in $\boldsymbol{x}$ and $\boldsymbol{\zeta}$; and it is also tractable for the nonlinear case when f is concave in $\boldsymbol{\zeta}$ for any given $\boldsymbol{x}$ (see, [50]).

Step 2. Next, we find the uncertainty parameter realizations that are satisfied for the optimal solution $\boldsymbol{x}^*$ of (10). Namely,

$$y_s^* = 1 \text{ if } f(\boldsymbol{x}^*, \boldsymbol{\zeta}^s) \leq 0; = 0 \text{ o.w. } \forall s \in S.$$

Step 3. Fix $\boldsymbol{y} = \boldsymbol{y}^*$ and solve $(\mathbf{RC}_{\mathrm{B}})$ if the ambiguity set of the uncertain probability vector $\boldsymbol{p}$ is the p-box; or solve $(\mathbf{RC}_{\mathrm{E}})$ if the associated set is the p-ellipsoidal. If there exists a feasible solution for the RC at hand (for given $\boldsymbol{y} = \boldsymbol{y}^*$) then we terminate the algorithm and record $\boldsymbol{x}^*$ as the final solution of the algorithm. Else, we go to Step 4.

Step 4. We increase Ω by the step size ω and go to Step 1.

The table representation of the so-called *stepwise ellipsoidal algorithm* (SEA) that safely approximates the ambiguous chance constrained problem is given below.

Algorithm 1: Stepwise Ellipsoidal Algorithm	
Inputs:	Probability threshold ϵ, nominal probability distribution $\boldsymbol{p}^0$, step size ω, radius of the ambiguity set σ, realizations $\boldsymbol{\zeta}^1, \dots, \boldsymbol{\zeta}^{|S|}$, optimization problem.
Outputs:	Robust optimal solution x^*.
Step 0:	Scale uncertainty parameters (ζ_i^s) to [-1, 1] and set $\Omega = 0$.
Step 1:	Solve the robust counterpart of the given problem with respect to the uncertainty set $||\zeta||_2 \leq \Omega$ and find the optimal solution x^*.
Step 2:	Check the satisfied scenarios by $\boldsymbol{x}^*$: $f(\boldsymbol{x}^*, \boldsymbol{\zeta}^s) \leq M(1 - y_s) \quad \forall s \in S$. Record these scenarios to vector $\boldsymbol{y}^*$.
Step 3:	Solve $(\mathbf{RC}_{\mathrm{E}})$ for given ϵ, σ, $\boldsymbol{p}^0$ when $\boldsymbol{y} = \boldsymbol{y}^*$. **If** $(\mathbf{RC}_{\mathrm{E}})$ yields a feasible solution **then** terminate the algorithm. **Else go to** Step 4.
Step 4:	Set $\Omega = \Omega + \omega$ and **go to** Step 1.

Extensions of Algorithm 1. 1) The associated algorithm can be easily extended to joint chance constraints and non-linear uncertain inequalities as long as the original problem is tractable, i.e., the algorithm does not introduce additional mathematical optimization complexity to that of the original problem. 2) One may also adopt a box uncertainty set in Step 1. We prefer using the ellipsoidal uncertainty set while we are generating our ambiguity set because it yields more diversified solution to the RC compared with the box uncertainty set; also see, [51]. 3) If the ambiguity set is p-box, in Step 3 we solve ($\mathbf{RC}_\mathrm{B}$) instead of ($\mathbf{RC}_\mathrm{E}$).

Complexity. 1) It is important to point that the mathematical optimization complexities of ($\mathbf{RC}_\mathrm{B}$) and ($\mathbf{RC}_\mathrm{E}$) in Step 3 are reduced to LP and SOCP; respectively, because we fix the binary variable $\boldsymbol{y}$ to $\boldsymbol{y}^*$ that comes out of Step 2. 2) In an L-dimensional uncertainty space, the radius of the ellipsoid (or ball) Ω can be at most $\sqrt{L}$ since the ball shall be larger than the support of the uncertainty parameter $\boldsymbol{\zeta}$, i.e., given by $\boldsymbol{\zeta} \in [-1,1]^L$, when it gets larger than $\sqrt{L}$. Therefore, Ω is updated in at most $\mathrm{O}(\omega^{-1}\sqrt{L})$ iterations of the algorithm. In addition, we need the check $|S|$ scenarios at each iteration of the algorithm in Step 2. Eventually, the total number of iterations of the algorithm is bounded above by $\mathrm{O}(\omega^{-1}\sqrt{L}|S|)$.

3. Extensions

In this section, we present extensions of our approach to joint chance constraints, nonlinear inequalities, and dependent probability vectors. It is important to stress that these extensions are not straightforward in general, nevertheless, our approach can be easily extended to the joint chance constraint with slight modification and it is unaffected from nonlinear inequalities, and we propose safe approximations for the dependent case.

3.1. Joint chance constraints

If we have more than one uncertain constraint and aim to find a solution that jointly satisfies these constraints with at least probability $1-\epsilon$, then we have the following joint (ambiguous) chance constrained formulation:

$$\mathrm{Pr}_{\boldsymbol{\zeta}\sim\mathbb{P}}\left\{\boldsymbol{\zeta} : f_k(\boldsymbol{x},\boldsymbol{\zeta}) \le 0 \ \forall k \in K\right\} \ge 1-\epsilon \quad \forall \mathbb{P} \in \mathcal{P}, \tag{11}$$

where K denotes the set of constraint indexes. Unlike classic approaches, our approach straightforwardly extends to a joint chance joint chance constraint. More precisely, one can equivalently reformulate (11) as

$$\begin{aligned} & f_k(\boldsymbol{x},\boldsymbol{\zeta}^s) \le M(1-y_s) && \forall k \in K,\ \forall s \in S \\ & \sum_{s\in S} p_s y_s \ge 1-\epsilon && \forall \boldsymbol{p} \in \mathcal{U}. \end{aligned} \tag{12}$$

The tractable RC of (12) when $\mathcal{U}$ is the p-box uncertainty set is given in Corollary 1.

Corollary 1. *The vectors $\boldsymbol{x} \in \boldsymbol{X}$ and $\boldsymbol{y} \in \{0,1\}^{|S|}$ satisfy*

$$\begin{aligned} & f_k(\boldsymbol{x},\boldsymbol{\zeta}^s) \le M(1-y_s) && \forall k \in K,\ \forall s \in S \\ & \sum_{s\in S} p_s y_s \ge 1-\epsilon && \forall \boldsymbol{p} \in \mathcal{U}_B \end{aligned}$$

if and only if $\boldsymbol{x}$, $\boldsymbol{y}$, $\boldsymbol{\theta}$, $\boldsymbol{w}$, and λ satisfy the following RC problem:

$$\begin{aligned} & f_k(\boldsymbol{x},\boldsymbol{\zeta}^s) \le M(1-y_s)\ \forall k \in K, \forall s \in S \\ & \boldsymbol{y}^\top \boldsymbol{p}_0 + \boldsymbol{u}^\top \boldsymbol{w} + \boldsymbol{\ell}^\top \boldsymbol{\theta} \ge 1-\epsilon \\ & \lambda \boldsymbol{e} + \boldsymbol{w} + \boldsymbol{\theta} - \boldsymbol{y} = \boldsymbol{0} \\ & \boldsymbol{\theta} \ge \boldsymbol{0}, \boldsymbol{w} \le \boldsymbol{0}, \lambda \ urs, \end{aligned} \tag{j$\mathbf{RC}_\mathrm{B}$}$$

where $\boldsymbol{w}, \boldsymbol{\theta}$, and λ denote the dual variables.

Proof. The first group of constraints $[f_k(\boldsymbol{x},\boldsymbol{\zeta}^s) \le M(1-y_s)\ \forall k \in K, \forall s \in S]$ will not be affected while we are deriving the RC. The tractable RC of the semi-infinite constraint $[\sum_{s\in S} p_s y_s \ge 1-\epsilon\ \forall \boldsymbol{p} \in \mathcal{U}_B]$ is given in Theorem 1. □

The mathematical optimization complexity of the robust reformulation of the joint chance constraint (j$\mathbf{RC}_\mathrm{B}$) is the same with that of ($\mathbf{RC}_\mathrm{B}$); RC of (11) for the p-ellipsoidal ambiguity set can be similarly derived by adopting Theorem 2.

3.2. Nonlinear inequalities

The mathematical optimization complexity of our approach is unaffected when we have nonlinearity in the uncertainty parameter $\boldsymbol{\zeta}$, e.g., when f is linear in $\boldsymbol{x}$. In this case, optimization complexity of the resulting RCs for the p-box and the p-ellipsoidal ambiguity sets are MILP and MISOCP; respectively, as in ($\mathbf{RC}_\mathrm{B}$) and ($\mathbf{RC}_\mathrm{E}$). On the other hand, when f is nonlinear in $\boldsymbol{x}$, the structure of nonlinearity in $\boldsymbol{x}$ determines the problem complexity, i.e., (**SI**) does not introduce additional mathematical optimization complexity to that of the original problem.

3.3. Dependent probability vector

In the previous reformulations, we have assumed that the elements of the ambiguous joint probability vector $\boldsymbol{p}$ that reside in the ambiguity set $\mathcal{U}$ to be independent, e.g., the off-diagonal elements of $\boldsymbol{Q}$ are 0 in p-ellipsoidal ambiguity set. Nevertheless, the probabilities in the ambiguity set $\mathcal{U}$ may be dependent in two ways:

(**D1**) probabilities $[\hat{p}_1, \hat{p}_2, \ldots, \hat{p}_{|S|}]$ of some realizations $\{\boldsymbol{\zeta}^{(1)}, \boldsymbol{\zeta}^{(2)}, \ldots, \boldsymbol{\zeta}^{(|S|)}\}$ are correlated (e.g., when the probability of high demand increases in period t, the probability of high demand may increase or decrease in period $t+1$), or

(**D2**) uncertainty parameters ζ_i are independent for $i = \{1, \ldots, L\}$ and the marginal probabilities follow ambiguous discrete probability distribution.

The dependency in (D1) can be easily formulated by setting the value of $\boldsymbol{Q}$ such that $(\boldsymbol{Q}^\top \boldsymbol{Q})^{-1}$ corresponds to the covariance matrix in the p-ellipsoidal ambiguity set and the RC may be derived similar to Theorem 2; for the sake of brevity, it is skipped. However, the latter dependency (D2) is somewhat more complex, and we propose safe approximations for the associated case in the remainder of this section.

Notice that, when the uncertainty parameters are independent as in (D2), the joint probability is equivalent to the product of the individual probabilities, i.e., probabilities of different uncertainty realizations become dependent because joint probabilities $[\hat{p}_1, \hat{p}_2, \ldots, \hat{p}_{|S|}]$ share common or complementary terms.

Extension of the semi-infinite representation (5) of the ambiguous chance constraint for (D2) is given as follows

$$
\begin{aligned}
f(\boldsymbol{x}, \boldsymbol{\zeta}^{i_1, i_2 \ldots, i_L}) &\leq M(1 - Y_{i_1, i_2 \ldots, i_L}) \\
&\qquad \forall (i_1, i_2 \ldots, i_L) \in S \\
\sum_{(i_1, i_2 \ldots, i_L) \in S} \prod_{j=1}^{L} \left(p_{i_j}^{(j)} + \xi_{i_j}^{(j)}\right) & Y_{i_1, i_2 \ldots, i_L} \geq 1 - \epsilon \\
&\qquad \forall \boldsymbol{\xi}^{(j)} \in \mathcal{U}_{B,E}^{(j)},\ j \in \{1, 2, \ldots, L\},
\end{aligned}
$$

where an aggregate scenario is indexed by $(i_1, i_2 \ldots, i_L)$ for $i_j \in S_j$ for all $j \in \{1, \ldots, L\}$; S_j denotes the set of indexes (i_j) for possible realizations of the j^{th} uncertainty parameter $\zeta_{i_j}^{(j)}$, i.e., an aggregate scenario set S is equivalent to the Cartesian product of the individual sets, i.e., $S := S_1 \times S_2 \ldots \times S_L$; an aggregate uncertainty vector $\boldsymbol{\zeta}^{i_1, i_2 \ldots, i_L} = [\zeta_{i_1}^{(1)}, \zeta_{i_2}^{(2)}, \ldots, \zeta_{i_L}^{(L)}]$ is a collection of uncertainty parameter realizations at scenario $(i_1, i_2 \ldots, i_L)$; $p_{i_j}^{(j)}$ denotes the probability of the i_j^{th} realization of the j^{th} uncertainty parameter $\zeta_{i_j}^{(j)}$ is being realized; $\xi_{i_j}^{(j)}$ denotes the random perturbation in probability $p_{i_j}^{(j)}$ where $\mathcal{U}_B^{(j)}$ and $\mathcal{U}_E^{(j)}$ are the associated uncertainty sets; $Y_{i_1, i_2 \ldots, i_L}$ is a 0-1 variable that takes value 1 if the solution $\boldsymbol{x}$ satisfies the constraint for the associated scenario or 0 otherwise. The formal representations of the p-box and p-ellipsoidal ambiguity sets for probability distributions of the independent uncertainty parameters are as follows.

$$
\begin{aligned}
\mathcal{U}_B^{(j)} = \Bigg\{ & \boldsymbol{p}^{(j)} = \boldsymbol{p}^{0(j)} + \boldsymbol{\xi}^{(j)} \in \mathbb{R}^{|S_j|} : \ldots \\
& \boldsymbol{\ell}^{(j)} \leq \boldsymbol{\xi}^{(j)} \leq \boldsymbol{u}^{(j)}, \ldots \\
& \sum_{i_j \in S_j} \xi_{i_j}^{(j)} = 0 \quad \forall j \in \{1, \ldots, L\} \Bigg\}
\end{aligned}
$$

and

$$
\begin{aligned}
\mathcal{U}_E^{(j)} = \Bigg\{ & \boldsymbol{p}^{(j)} = \boldsymbol{p}^{0(j)} + \boldsymbol{\xi}^{(j)} \in \mathbb{R}^{|S_j|} : \ldots \\
& \left\| \boldsymbol{Q}^{(j)} \boldsymbol{\xi}^{(j)} \right\|_2 \leq \sigma_j, \ldots \\
& \sum_{i_j \in S_j} \xi_{i_j}^{(j)} = 0 \quad \forall j \in \{1, \ldots, L\} \Bigg\}.
\end{aligned}
$$

The probability that the scenario $(i_1, i_2 \ldots, i_L)$, i.e., $[\zeta_{i_1}^{(1)}, \zeta_{i_2}^{(2)}, \ldots, \zeta_{i_L}^{(L)}]$, is being realized is equivalent to the product of the individual probabilities:

$$
P_{i_1, i_2 \ldots, i_L} = \prod_{j=1}^{L} \left(p_{i_j}^{(j)} + \xi_{i_j}^{(j)}\right),
$$

Eventually, the semi-infinite probability threshold constraint for the joint distribution can be reformulated as the following mathematical optimization problem for the p-box uncertainty set.

$$
\begin{aligned}
(\mathbf{IB}) \min_{\boldsymbol{P}, \boldsymbol{p}^{(\cdot)}} & \sum_{(i_1, i_2, \ldots, i_L) \in S} P_{i_1, i_2 \ldots, i_L}\ Y_{i_1, i_2 \ldots, i_L} \\
\text{s.t. } & P_{i_1, i_2 \ldots, i_L} = \prod_{j=1}^{L} \left(p_{i_j}^{(j)} + \xi_{i_j}^{(j)}\right) \\
& \qquad \forall (i_1, i_2, \ldots, i_L) \in S \quad (13) \\
& \sum_{i \in S_j} \xi_{i_j}^{(j)} = 0 \qquad \forall j \in \{1, \ldots, L\} \quad (14) \\
& \ell_{i_j}^{(j)} \leq \xi_{i_j}^{(j)} \leq u_{i_j}^{(j)} \\
& \qquad \forall i \in S_j, \forall j \in \{1, \ldots, L\}, \quad (15)
\end{aligned}
$$

where (13) formulates the joint probability as an equality constraint for the ease of exposition, (14) ensures that probability of each independent uncertainty parameter is summed to 1, and (15) determines the bounds of the box uncertainty sets, and [$\mathbf{val}$(IB)$\geq 1 - \epsilon$]. It is easy to see that (**IB**) is nonconvex and highly nonlinear because of (13), and this is why it cannot be dualized in its current form. The following theorem relaxes the nonlinear structure of (**IB**) and provides a lower bound for **val**(**IB**).

Theorem 3. *Let* $S = S_1 \times S_2 \ldots \times S_L$, $\ell_{i_1, i_2 \ldots, i_\ell} = \prod_{j=1}^{L} \left(p_{i_j}^{(j)} + \ell_{i_j}^{(j)}\right)$ *and* $u_{i_1, i_2 \ldots, i_\ell} =$

$\prod_{j=1}^{L}\left(p_{i_j}^{(j)}+u_{i_j}^{(j)}\right)$ $\forall i \in S_j$ $\forall j \in \{1,\ldots,L\}$ *the following mathematical optimization problem:*

$$\left\{\min_{\boldsymbol{P}} \sum_{s\in S} P_s Y_s : \sum_{s\in S} P_s = 1 \quad \ell_s \le P_s \le u_s \quad \forall s \in S\right\} \qquad (\text{r}\mathbf{IB})$$

*is a relaxation of (**IB**).*

Proof. Let $(\boldsymbol{P}, \boldsymbol{p}^{(1)}, \ldots, \boldsymbol{p}^{(\ell)})$ be a feasible solution of (**IB**). If we prove that $\boldsymbol{P} \in \mathbb{R}^{|S_1|\times|S_2|\ldots\times|S_L|}$ is feasible for (r**IB**), then we can conclude that (r**IB**) is a reduced relaxation of (**IB**).
To begin with, let $\hat{p}_{i_j}^{(j)} = p_{i_j}^{(j)} + \xi_{i_j}^{(j)}$, (14) implies that $\sum_{i_j \in S_{i_j}} \hat{p}_{i_j}^{(j)} = 1$ for all $j \in \{1,\ldots,L\}$ given that $0 \le \hat{p}_{i_j}^{(j)} \le 1$ for all $i_j \in S_{i_j}$ for all $j \in \{1,\ldots,L\}$ (by Assumption 2). Notice that, probability $P_{i_1,i_2\ldots,i_L}$ is the product of independent probabilities $\hat{\boldsymbol{p}}^{(j)}$, i.e., the summation of the elements of $\boldsymbol{P}$ over all combinations of individual probabilities is equivalent to 1. Constraints (13) and (14) imply that $P_{i_1,i_2\ldots,i_L} \ge \prod_{j=1}^{L}\left(p_{i_j}^{(j)}+\ell_{i_j}^{(j)}\right)$ and $P_{i_1,i_2\ldots,i_L} \le \prod_{j=1}^{L}\left(p_{i_j}^{(j)}+u_{i_j}^{(j)}\right)$ for all $i_j \in S_{i_j}$for all $j \in \{1,\ldots,L\}$. As a result, $\boldsymbol{P}$ of (**IB**) satisfies all the constraints in (r**IB**). □

Next, the semi-infinite probability threshold constraint for the joint distribution can be reformulated as the following mathematical optimization problem for the p-ellipsoidal uncertainty set.

$$(\mathbf{IE}) \min_{\boldsymbol{P},\boldsymbol{p}^{(\cdot)}} \sum_{(i_1,i_2,\ldots,i_L)\in S} P_{i_1,i_2\ldots,i_L}\, Y_{i_1,i_2\ldots,i_L}$$

$$\text{s.t. } P_{i_1,i_2\ldots,i_L} = \prod_{j=1}^{L}\left(p_{i_j}^{(j)}+\xi_{i_j}^{(j)}\right) \quad \forall (i_1,i_2,\ldots,i_L)\in S \qquad (16)$$

$$\sum_{i\in S_j} \xi_{i_j}^{(j)} = 0 \qquad \forall j \in \{1,\ldots,L\} \qquad (17)$$

$$\left|\left|\boldsymbol{Q}^{(j)}\boldsymbol{\xi}^{(j)}\right|\right|_2 \le \sigma_j \;\forall j \in \{1,\ldots,L\}, \qquad (18)$$

Similarly, (**IE**) is a nonlinear and non-convex optimization problem that is intractable in its current form. The following theorem yields a tractable reduced relaxation of (**IE**).

Theorem 4. *Let* $S = S_1 \times S_2 \ldots \times S_L$, $\ell_{i_1,i_2\ldots,i_\ell} = \prod_{j=1}^{L}\left(p_{i_j}^{(j)} - \sigma_j/q_{i_j}^{(j)}\right)$ *and* $u_{i_1,i_2\ldots,i_\ell} = \prod_{j=1}^{L}\left(p_{i_j}^{(j)} + \sigma_j/q_{i_j}^{(j)}\right)$ $\forall i \in S_j$ $\forall j \in \{1,\ldots,L\}$ *then (r**IB**) is a relaxation of (**IE**).*

Proof. Constraints (17) and (18) imply that the largest value that $\xi_{i_j}^{(j)}$ can get is $\sigma_j/q_{i_j}^{(j)}$ for all $i_j \in S_{i_j}$for all $j \in \{1,\ldots,L\}$; similarly, the smallest value is $-\sigma_j/q_{i_j}^{(j)}$. The remainder of the proof follows similar to Theorem 3. □

Remark 3. *The ambiguity set $\mathcal{U}$ of the unknown true probability vector $\mathbf{p}$ for the independent uncertainty parameters may also be defined by first calculating the nominal joint probabilities of the uncertainty parameter realizations and then adopting the p-box or p-ellipsoidal ambiguity set over the nominal joint probability vector; notice that this shall result in the RCs that are proposed in §2. The extension that is presented in §3.2 defines the ambiguity sets with respect to the marginal probability vectors of the individual uncertainty parameters and propose safe approximations of* (**SI**) *for the resulting complex ambiguity set of the joint probability vector.*

4. Numerical example: knapsack problem

In this section, we present validity or our approach using toy sized instances of an ambiguous chance constrained knapsack problem. We compare optimality and feasibility performances of the classic and the ambiguous chance constrained versions of the problem.
We focus on a chance constrained knapsack problem:

$$\max_{\boldsymbol{x}\in\{\mathbf{0},\mathbf{1}\}} \sum_{i=1}^{n} v_i x_i$$

$$\text{s.t. } \Pr_{\boldsymbol{\zeta}\sim\mathbb{P}}\left\{\boldsymbol{\zeta} : \sum_{i=1}^{n} \zeta_i x_i \le W\right\} \ge 1-\epsilon,$$

where v_i denotes the value and ζ_i denotes the uncertain weight of item $i = \{1,\ldots,m\}$, x_i is the decision variable that is 1 if item i is included in the knapsack or 0 otherwise, and W is the capacity of the knapsack. The uncertainty parameter $\boldsymbol{\zeta}$ follows a discrete probability distribution $\mathbb{P}$:

$\boldsymbol{\zeta}$	$\in$	$\{\boldsymbol{\zeta}^1$	$\ldots$	$\boldsymbol{\zeta}^{\lvert S\rvert}\}$
$\mathbb{P}(\boldsymbol{\zeta})$	$=$	p_1	$\ldots$	$p_{\lvert S\rvert}$

where the true probability distribution $\boldsymbol{p}$ is unknown or ambiguous but is assumed to reside in a p-box ($\mathcal{U}_B$) or a p-ellipsoidal ($\mathcal{U}_E$) ambiguity set:

$$\mathcal{U}_B = \left\{\boldsymbol{\xi} \in \mathbb{R}^L : \boldsymbol{p} = \boldsymbol{p}^0 + \boldsymbol{\xi},\ \sum_{s\in S}\xi_s = 0, \ldots \quad (1-\gamma)\boldsymbol{p}^0 \le \boldsymbol{p} \le (1+\gamma)\boldsymbol{p}^0\right\},$$

and

$$\mathcal{U}_E = \left\{ \boldsymbol{\xi} \in \mathbb{R}^L : \boldsymbol{p} = \boldsymbol{p}^0 + \boldsymbol{\xi}, \sum_{s \in S} \xi_s = 0, \dots \right.$$
$$\left. \left|\left|\boldsymbol{p} - \boldsymbol{p}^0\right|\right|_2 \le \sigma \right\}.$$

The p-box uncertainty set is symmetric around the nominal probability distribution $\boldsymbol{p}^0$ and its size is determined by the scaling parameter $\gamma \in [0, 1]$; σ denotes the radius of the p-ellipsoidal uncertainty set that is again centered at the nominal data $\boldsymbol{p}^0$.

Notice that the ambiguous chance constrained knapsack problem with a discrete probability distribution can be equivalently reformulated as

$$\begin{aligned} \max_{\boldsymbol{x} \in \{\boldsymbol{0}, \boldsymbol{1}\}} \; & \sum_{i=1}^{n} v_i x_i \\ & \sum_{i=1}^{n} \zeta_i^s x_i - W \le M(1 - y_s) \quad \forall s \in S \\ & \sum_{s \in S} p_s y_s \ge 1 - \epsilon \quad \forall \boldsymbol{p} \in \mathcal{U}_{B \text{ or } E}, \end{aligned}$$

where $M = (\max\{\boldsymbol{e}^\top \boldsymbol{\zeta}^1, \dots, \boldsymbol{e}^\top \boldsymbol{\zeta}^{|S|}\} - W)$. The tractable RCs of the knapsack problem can be derived as in ($\mathbf{RC}_{\mathrm{B}}$) and ($\mathbf{RC}_{\mathrm{E}}$).

Illustrative example. We solve an instance of the knapsack problem with ten items (i.e., $n = 10$). Scenarios for the item weights (i.e., $S = \{1, \dots, 10\}$) are given in Table 2; the realization probabilities are given in the last row of the table (see, $\boldsymbol{p}^0$). The objective coefficients are $v = [37; 43; 53; 67; 44; 57; 69; 45; 54; 66]$, the knapsack capacity is $W = 60$, and the probability threshold is $1 - \epsilon = 0.75$.

Table 2. Uncertainty parameter realizations with probabilities

	$\boldsymbol{\zeta}^1$	$\boldsymbol{\zeta}^2$	$\boldsymbol{\zeta}^3$	$\boldsymbol{\zeta}^4$	$\boldsymbol{\zeta}^5$	$\boldsymbol{\zeta}^6$	$\boldsymbol{\zeta}^7$	$\boldsymbol{\zeta}^8$	$\boldsymbol{\zeta}^9$	$\boldsymbol{\zeta}^{10}$
ζ_1	10	4	5	8	9	5	6	6	7	5
ζ_2	9	4	10	4	9	9	7	8	6	9
ζ_3	8	8	9	7	10	7	8	7	9	7
ζ_4	9	7	10	4	10	9	7	4	9	9
ζ_5	6	5	6	8	8	10	5	7	6	5
ζ_6	9	9	6	6	7	5	5	6	5	5
ζ_7	8	10	5	10	7	5	8	8	6	7
ζ_8	4	4	9	4	8	9	9	8	10	6
ζ_9	10	7	8	10	5	10	5	10	10	5
ζ_{10}	4	5	7	9	8	6	7	9	8	5
$\boldsymbol{p}^0$	0.05	0.025	0.1	0.025	0.15	0.15	0.1	0.2	0.1	0.1

Notice that when $\boldsymbol{p} = \boldsymbol{p}^0$ in the knapsack problem, we have the classic chance constrained version of the problem. The optimal solution and the objective function value for the classic problem are given Table 3. The optimal solution for the chance constrained knapsack problem satisfies the constraint with $1 - \epsilon^* = 0.775$ probability.

Table 3. Optimal solution for the chance constrained problem

x_1^*	x_2^*	x_3^*	x_4^*	x_5^*	x_6^*	x_7^*	x_8^*	x_9^*	x_{10}^*	Obj.
1	0	1	1	1	1	1	0	1	1	<u>447</u>
y_1^*	y_2^*	y_3^*	y_4^*	y_5^*	y_6^*	y_7^*	y_8^*	y_9^*	y_{10}^*	$1 - \epsilon$
0	1	1	0	0	1	1	1	1	1	0.775

Next we solve the ambiguous chance constrained knapsack problem with respect to the p-box ($\mathcal{U}_B$) and p-ellipsoidal ($\mathcal{U}_E$) ambiguity sets when $\gamma = 0.4$; respectively. Notice that σ is determined according to the tightest ball inside the box region, i.e., it is less conservative than the box. The optimal solutions are given in Table 4.

It is easy to see that optimal objective function value for the chance constrained problem that uses the nominal probability vector is greater than these of the ambiguous chance constrained version of the problem with respect to p-box and p-ellipsoidal ambiguity sets. To point out, the classic chance constraint approach is not immunized against the ambiguity in the probability distribution and this is why it yields a progressive objective function value. On the other hand, when the worst-case probability distribution $\boldsymbol{p}^*$ is realized, the nominal solution cannot satisfy the given probability threshold $1 - \epsilon = 0.75$. More precisely, the LHS value for the probability threshold constraint $[\sum_{s \in S} p_s^* y_s \ge 1 - \epsilon]$ is 0.65 for the p-box and 0.746 for the p-ellipsoidal uncertainty sets when $\boldsymbol{y}$ is the nominal optimal solution; compare these values with "$\sum_{s \in S} p_s^* y_s$" column in Table 4.

Table 4. Optimal solutions for the ambiguous chance constrained problem

Set	$\boldsymbol{x}^*$	Obj.
p-box	(1, 0, 1, 1, 1, 1, 1, 1, 0, 1)	<u>438</u>
p-ellip.	(1, 1, 1, 1, 0, 1, 1, 0, 1, 1)	<u>446</u>
	$\boldsymbol{y}^*$	$\sum_{s \in S} p_s^* y_s$
p-box	(1, 1, 1, 1, 0, 1, 1, 1, 1, 1)	0.79
p-ellip.	(0, 1, 1, 1, 0, 1, 1, 1, 1, 1)	0.76

As it is anticipated, the classic approach outperforms the robust approach when the nominal probability distribution is used and the robust approach outperforms the classic approach when the worst-case distribution is used. Nevertheless, it may be known that both approaches are based on unique probability vector realizations, namely, the nominal and the worst-case, out of infinitely many possible options in the ambiguity set, i.e., technically both data points might never be realized. This is why, we also test the average feasibility performances of the nominal and robust solutions via Monte Carlo sampling. Even though, the robust approach does not require any distributional information, we assume in the experiment that probabilities are uniform between $[(1-\gamma_i)p_i^0, (1+\gamma_i)p_i^0]$ for the sampling. Algorithm 1 and Algorithm 2 are used to sample from p-box and p-ellipsoidal ambiguity sets.

Algorithm 2: p-box sampling algorithm

Inputs: the nominal probability vector $\boldsymbol{p}^0 \in [0,1]^S$, the scaling vector $\boldsymbol{\gamma} \in [0,1]^S$, *sample size*

Output: *sample*

```
While # of sampled vectors ≤ sample size
   for   i = 1 : 1 : |S| − 1
      sample p_i ∼ Uniform[(1 − γ_i)p_i^0, (1 + γ_i)p_i^0]
   end
   calculate p_|S| = 1 − Σ_{i=1}^{|S|−1} p_i
   If (1 − γ_i)p_|S|^0 ≤ p_|S| ≤ (1 + γ_i)p_|S|^0
      add p to sample; # of sampled vectors ++
   end
end
```

We sample 1000 probability vectors from p-box and p-ellipsoidal uncertainty sets and the simulation outcomes are presented in Table 5 & 6. Table 5 reports the average LHS value of the probability threshold constraint $[\sum_{i=1}^{1000} \sum_{s\in S} p_s^i y_s]$ when $\boldsymbol{y}$ is fixed to the solution at hand. It is easy to see that the optimal solution for the p-box and the p-ellipsoidal uncertainty sets outperform the feasibility performance of the nominal solution.

Algorithm 3: p-ellipsoidal sampling algorithm

Inputs: the nominal probability vector $\boldsymbol{p}^0 \in [0,1]^S$, the radius of the ellipsoid $\sigma \in \mathbb{R}_+$, *sample size*

Output: *sample*

Initialization: set $\gamma_i = \sigma/p_i^0 \quad \forall i \in S$

```
While # of sampled vectors ≤ sample size
   for   i = 1 : 1 : |S| − 1
      sample p_i ∼ Uniform[(1 − γ_i)p_i^0, (1 + γ_i)p_i^0]
   end
   calculate p_|S| = 1 − Σ_{i=1}^{|S|−1} p_i
   If ||p − p^0||_2 ≤ σ
      add p to sample; # of sampled vectors ++
   end
end
```

As we have pointed out before the p-box uncertainty set is larger than the p-ellipsoidal and this is why its solution is immunized against uncertainty more than that for the p-ellipsoidal uncertainty set. If we compare the average feasibility performance of the p-box approach, we also see that its average performance is better than that of the p-ellipsoidal approach. It is important to point out that all approaches, namely, p-box, p-ellipsoidal, and nominal, yield (on average) feasible results that are (on average) far from being binding to the given probability threshold $1-\epsilon = 0.75$.

Table 5. Feasibility performance of solutions

sample	solution		
sets	box	ellip	nom
p-box	0.85	0.79	0.76
p-ellip	0.85	0.80	0.76

On the other hand, solutions are not feasible for all of the sampled instances. In Table 6, we report the average performances of the solutions for the violating instances. The first three columns in Table 6 denote the number of violating instances (out of 1000). E.g., the numerical result at "row = p-box" and "column = #Vio(ellip)" denotes the number of violated constraints when the solution is fixed to the optimal solution of the RC with respect to the p-box uncertainty set, i.e., the optimal solution of the ambiguous chance constraint for the p-box uncertainty is tested when the probability vectors are sampled from the p-ellipsoidal uncertainty set. The last three columns report the average LHS value of the probability threshold constraint for the violating instances.

Table 6. Feasibility performance of solutions

$\mathcal{U}$	#Vio(box)	#Vio(ellip)	#Vio(nom)
p-box	0	83	283
p-ellip	0	0	25
$\mathcal{U}$	$\overline{\text{Vio}}$(box)	$\overline{\text{Vio}}$(ellip)	$\overline{\text{Vio}}$(nom)
p-box	-	0.73	0.72
p-ellip	-	-	0.74

The numerical results show that the nominal solution cannot satisfy nearly one third of the instances when data comes from p-box uncertainty set. Since the ellipsoidal uncertainty set is less conservative with 83 violations, the feasibility performance of the nominal solution for the p-ellipsoidal uncertainty is less conservative; compare the number of violations in the third column. As it is anticipated, the optimal solution with respect p-box uncertainty set does not violate the probability threshold constraint when data comes from the p-ellipsoidal because p-box is a superset; and both approaches are robust with respect to their own ambiguity sets, e.g., the p-box solution is robust against the p-box ambiguity set by definition. The average violation of the LHS value of the probability constraint for the violating instances ranges between %1 to %3; see the last two columns where p-box solution is fully robust against the uncertainty in the probability distribution; p-ellipsoidal approach violates the constraints for the p-box uncertainty (on average) with %2; and the nominal solution violates the constraint for p-box uncertainty with %3 and for the p-ellipsoidal uncertainty with %1.

Monte Carlo simulation. In the remainder of this section, we shall adopt a Monte Carlo simulation study to compare the optimality and computational performances of the *stepwise ellipsoidal algorithm* (SEA) that is proposed in §2.3 with those of the exact reformulation ($\mathbf{RC}_\mathrm{E}$) and the *randomized algorithm* (RA) that is proposed by [15] for combinations of the instance parameters of the chance constrained knapsack problem. RA is based on random extraction of N realizations ($\{\hat{\boldsymbol{\zeta}}^1, \ldots, \hat{\boldsymbol{\zeta}}^N\}$) of the uncertainty parameter $\boldsymbol{\zeta}$ using the known probability distribution of the parameter, i.e., a discrete probability distribution in our case. Each extraction coincides with a discrete constraint and instead of solving the exact problem, the authors solve the mathematical optimization problem with N constraints, i.e., $[f(x, \hat{\boldsymbol{\zeta}}^i) \leq 0 \ \forall i \in \{1, \ldots, N\}]$. They show that the optimal solution of the randomized approach satisfies the following probabilistic guarantee:

$$\Pr\{V(x^*) > \epsilon\} \leq \textstyle\sum_{i=0}^{L-1} \mathrm{Cb}(N, i)\epsilon^i (1-\epsilon)^{N-i},$$

where the LHS of the inequality is associated with the probability that the chance constraint is violated for the solution at hand ($\boldsymbol{x}_N^*$) when N samples are drawn for an L-dimensional decision space, and the RHS coincides with the worst-case bound for the associated probability, e.g., when $\epsilon = 0.2$, $L = 5$ and RHS $= 0.01$, then $N = 54$ samples have to be drawn. We refer reader to [15] for further details on RA; and to [16] for the formal proof on tightness of the given probability bound.

Data used in the experiment is generated as follows: 1) we randomly sample the lower (ℓ_i) and upper (u_i) bounds of the intervals of the item weights from U[1-10] and U[11-20]; respectively, i.e., $\zeta_i \in [\ell_i, u_i] \ \ \forall i \in L$. 2) Next, we randomly sample $|S|$ scenarios as vectors $\{\boldsymbol{\zeta}^1, \boldsymbol{\zeta}^2, \ldots, \boldsymbol{\zeta}^{|S|}\}$ using the associated intervals. 3) For the sake of simplicity, we assume that all scenarios are equally likely, i.e., $p_s^0 = 1/|S|$ for all $s \in S$. 4) Item values ($\boldsymbol{v}$) are randomly sampled from U[10-20] and the bag capacity (W) is set to %80 of the total nominal weights of the items. The confidence level $[\sum_{i=0}^{L-1} \mathrm{Cb}(N, i)\epsilon^i (1-\epsilon)^{N-i}]$ of RA is set to 0.01; the number of samples to be drawn for $\epsilon \in \{0.1, 0.2\}$. 5) L denotes the number of items and $|S|$ denotes the number of scenario realizations used in discrete probability distribution. For each $L/|S|$ pair 20 different data sets have been generated by following the data generation structure mentioned above. Using the associated data, the optimality and CPU performances of RA, SEA (Algorithm 1) and the exact reformulation ($\mathbf{RC}_\mathrm{E}$) have been compared in Tables 7 & 8.

As we have pointed out above we have generated 20 instances for each $L/|S|$ combination. The asterisk symbol ($*$) denotes that the associated algorithm solves all instances to optimality for the given parameter combination or it denotes the best performing algorithm when the exact reformulation cannot be solved. The tilde symbol ($\sim$) denotes that optimality cannot be attained in 7200 seconds. "Gap" denotes the (average) optimality gap percentage of an algorithm for the instances those cannot be solved to optimality or the (average) optimality gap percentage of an algorithm with respect to the best performing algorithm when the exact reformulation cannot be solved in 7200 seconds; the hash tag symbol (#) denotes the number of instances (out of 20) those cannot be solved to optimality (or worse than the best performing algorithm) by the given algorithm. Finally, CPU is the total computation time of a given algorithm in seconds. All experiments are run on a 64-bit Windows machine equipped with an Intel Quad-Core i7-6700HQ processor with 16 GB of RAM.

Table 7. Comparison of solution approaches when $\epsilon = 0.1$

L/$\lvert S\rvert$	Output	Exact	RA	**SEA**
5/10	Gap (#)	$*$	$*$	$*$
	CPU	0.10	0.02	0.01
10/20	Gap (#)	$*$	%7.6 (18)	%1 (1)
	CPU	76	0.1	0.02
25/50	Gap (#)	-	%6 (19)	%1 (1)
	CPU	$\sim$	0.4	0.02

Table 8. Comparison of solution approaches when $\epsilon = 0.2$

$L/\|S\|$	Output	Exact	RA	**SEA**
5/10	Gap (#)	$*$	%15 (15)	$*$
	CPU	0.10	0.2	0.02
10/20	Gap (#)	$*$	%12.2 (19)	$*$
	CPU	22	0.3	0.02
25/50	Gap (#)	$\sim$	%9.8 (20)	$*$
	CPU	$\sim$	0.4	0.02

The numerical results in Table 7 & 8 show that SEA outperforms RA at all instances both in CPU time and the optimality gap. Improved optimality performance of SEA may be an anticipated result since the algorithm systematically includes the uncertain parameters in the uncertainty set in order to yield the tightest ambiguity set and hence a better objective function value compared with RA that is fully randomized without a systematic objective performance consideration. Improved computational and optimality performances of SEA become more significant when probability threshold ϵ, and hence the size of the feasible region, increases; it is easy to see that when we compare the numerical results (Gap, CPU) in Tables 7 & 8. Notice that $L/|S|$=5/10 instances in Table 7 are kind of redundant since we need to satisfy all uncertainty realizations (i.e., robust) in this case to satisfy $1 - \epsilon = 0.9$ probability threshold. Nevertheless, these are the only instance where we see no significant difference among all alternative approaches. According to these numerical results, we can conclude that SEA is an efficient approximation algorithm to solve the ambiguous chance constrained problem for medium to large sized instances. SEA is almost as good as the exact reformulation (except for 1 instance in Table 7 at $L/|S| = 10/20$ with %1 gap) in optimality performance while yielding high quality solutions in less than a second. Moreover, SEA significantly outperforms RA in increased dimensions where we cannot adopt the exact approach (see rows $L/|S| = 25/50$ in Tables 8 & 9).

5. Conclusion

In this paper, we have proposed robust reformulations of ambiguous chance constraints with discrete probability distributions. We have derived the tractable robust counterparts of the associated class of ambiguous chance constraints using p-box and p-ellipsoidal uncertainty sets that support the ambiguous family of distributions. Our approach can be easily applied in practice where one works with a finite number of scenarios that follow a discrete probability distribution. The associated probabilities are ambiguous by nature because they are forecast or decided by an expert opinion. Proposed methodology aims to find a solution that satisfies the given probability requirement of being feasible while maximizing the utility (or minimizing the cost) and at the same time taking into account the distributional ambiguity. The proposed approach can be easily extended to joint chances constraints, nonlinear inequalities as well as different data structures without introducing additional mathematical optimization complexity to that of tackling a unique ambiguous chance constraint with discrete probability distribution using our method.

Acknowledgment

The author thanks to two anonymous referees for their insightful comments and suggestions which significantly improved the overall quality of the paper. The author also thanks to Farzad Avishan who has generated the data used in the numerical experiments and made the final proofreading.

References

[1] Charnes, A. & Cooper, W.W. (1959). Chance-constrained programming. *Management Science*, 6(1), 73–79.

[2] Charnes, A., Cooper, W.W. & Symonds, G.H. (1958). Cost horizons and certainty equivalents: an approach to stochastic programming of heating oil. *Management Science*, 4(3), 235–263.

[3] Miller, B.L. & Wagner, H.M. (1965). Chance constrained programming with joint constraints. *Operations Research*, 13(6), 930–945.

[4] Prékopa, A. (1970). Efficient robust optimization of metal forming processes using a sequential metamodel based strategy. *In Proceedings of the Princeton Symposium on Mathematical Programming*, Princeton University Press, Princeton, NJ, 113–138.

[5] Burkauskas, A. (1986). On the convexity problem of probabilistic constraint stochastic programming problems. *Alkalmazott Matematikai Lapok*, 12, 77–90.

[6] Prékopa, A. (1974). Programming under probabilistic constraints with a random technology matrix. *Mathematische Operationsforschung und Statistik*, 5, 109–116.

[7] Van de Panne, C. & Popp, W., (1963). Minimum-cost cattle feed under probabilistic protein constraints. *Management Science*, 9(3), 405–430.

[8] Prékopa, A. (1973). On logarithmic concave measures and functions. *Acta Scientiarum Mathematicarum*, 34, 335–343.

[9] Prékopa, A. (1995). *Stochastic Programming* Kluwer Academic Publishers, Dordrecht, The Netherlands.

[10] Nemirovski, A. & Shapiro, A. (2006). Convex approximations of chance constrained programs. *SIAM Journal on Optimization*, 17(4), 969–996.

[11] Ben-Tal, A. & Nemirovski, A. (2000). Robust solutions of linear programming problems contaminated with uncertain data. *Mathematical Programming*, 88(3), 411–424.

[12] Chen, W., Sim, M., Sun, J. & Teo, C.P. (2010). From CVaR to uncertainty set: implications in joint chance-constrained optimization. *Operations Research*, 58(2), 470–485.

[13] Chen, X., Sim, M. & Sun, P. (2007). A robust optimization perspective on stochastic programming. *Operations Research* 55(6), 1058–1107.

[14] Zymler S., Kuhn, D. & Rüstem, B. (2013). Distributionally robust joint chance constraints with second-order moment information. *Mathematical Programming*, 137(1-2), 167–198.

[15] Calafiore, G.C. & Campi, M.C. (2005). Uncertain convex programs: randomized solutions and confidence levels. *Mathematical Programming*, 102, 25–46.

[16] Campi, M.C. & Garatti, S. (2008). The exact feasibility of randomized solutions of robust convex programs. *SIAM Journal on Optimization*, 19(3), 1211–1230.

[17] Birge, J.R. & Wets, R.J.-B. (1986). Designing approximation schemes for stochastic optimization problems, in particular for stochastic programs with recourse. *Mathematical Programming Studies*, 27, 54–102.

[18] Dupačová, J. (2001). Stochastic Programming: minimax approach. In: *Encyclopedia of Optimization*. Kluwer Academic Publishers, Dordrecht, The Netherlands.

[19] Shapiro, A. & Ahmed, S. (2004). On a class of minimax stochastic programs. *SIAM Journal on Optimization*, 14(4), 1237–1252.

[20] Shapiro, A. & Kleywegt, A.J. (2002). Minimax analysis of stochastic problems. *Optimization Methods and Software*, 17, 523–542.

[21] Epstein, L.G. & Schneider, M. (2003). Recursive multiple-priors. *Journal of Economic Theory*, 113(1), 1–31.

[22] Epstein, L.G. & Schneider, M. (2007). Learning under ambiguity. *Review of Economic Studies*, 74(4), 1275–1303.

[23] Hansen, L.P. & Sargent, T.J. (2001). Robust control and model uncertainty. *American Economic Review*, 91, 60–66.

[24] Erdoğan, E. & Iyengar, G. (2006). Ambiguous chance constrained problems and robust optimization. *Mathematical Programming*, 107(1–2), 37–61.

[25] Yanıkoğlu, İ, den Hertog, D. (2013). Safe approximations of ambiguous chance constraints using historical data. *INFORMS Journal on Computing*, 25(4), 666–681.

[26] Ben-Tal, A., El Ghaoui, L., Nemirovski, A. (2009). *Robust Optimization.* Princeton Press, Princeton, NJ.

[27] Nemirovski, A. (2012). On safe tractable approximations of chance constraints. *European Journal of Operations Research*, 219(3), 707–718

[28] Yanıkoğlu, İ & den Hertog, D. & Kleijnen, J.P.C. (2016). Robust dual-response optimization. *IIE Transactions*, 48(3), 298–312.

[29] Luedtke, J. (2014). A branch-and-cut decomposition algorithm for solving chance-constrained mathematical programs with finite support. *Mathematical Programming* 146(1–2), 219-244.

[30] Song, Y., Luedtke, J. R., & Küçükyavuz, S. (2014). Chance-constrained binary packing problems. *INFORMS Journal on Computing*, 26(4), 735-747.

[31] Hanasusanto, G.A., Roitch, V., Kuhn, D. & Wiesemann, W. (2015). A distributionally robust perspective on uncertainty quantification and chance constrained programming. *Mathematical Programming*, 151(1), 35–62.

[32] Hanasusanto, G.A., Roitch, V., Kuhn, D. & Wiesemann, W. (2017). Ambiguous joint chance constraints under mean and dispersion information. *Operations Research*, 65(3), 751–767.

[33] Jiang, R. & Guan, Y. (2016). Data-driven chance constrained stochastic program. *Mathematical Programming*, 158(1-2), 291–327.

[34] Chen, Z., Kuhn, D., & Wiesemann, W. (2018). Data-driven chance constrained programs over Wasserstein Balls. *arXiv preprint*, arXiv:1809.00210.

[35] Ji, R. & Lejeune, M. (2018). Data-driven distributionally robust chance-constrained programming with Wasserstein metric. Available at *Optimization Online*.

[36] Zhang, Y., Jiang, R. & Shen, S. (2016). Distributionally robust chance-constrained bin packing. Available at *Optimization Online*.

[37] Cheng, J., Delage, E. & Lisser, A. (2014). Distributionally robust stochastic knapsack

problem. *SIAM Journal on Optimization*, 24(3), 1485–1506.

[38] Hu, Z. & Hong, L.J. (2013). Kullback-Leibler divergence constrained distributionally robust optimization. Available at *Optimization Online*.

[39] Xie, W. & Ahmed, S. (2018). On deterministic reformulations of distributionally robust joint chance constrained optimization problems. *SIAM Journal on Optimization*, 28(2), 1151–1182.

[40] Xie, W., Ahmed, S. & Jiang, R. (2017). Optimized Bonferroni approximations of distributionally robust joint chance constraints. Available at *Optimization Online*.

[41] Xie, W. (2018). On distributionally robust chance constrained program with wasserstein distance. *arXiv preprint*, arXiv:1806.07418.

[42] Mehrotra, S. & Zhang, H. (2014). Models and algorithms for distributionally robust least squares problems. *Mathematical Programming*, 146(1-2), 123–141.

[43] Özmen, A., Weber, G.W., Batmaz, İ. & Kropat, E. (2011). RCMARS: Robustification of CMARS with different scenarios under polyhedral uncertainty set. *Communications in Nonlinear Science and Numerical Simulation*, 16(12), 4780–4787.

[44] Friedman, J.H. (1991). Multivariate adaptive regression splines. *Annals of Statistics*, 19(1), 1–141.

[45] Weber, G.W., Batmaz, İ., Köksal, G., Taylan, P. & F. Yerlikaya-Özkurt, (2012). CMARS: a new contribution to nonparametric regression with multivariate adaptive regression splines supported by continuous optimization. *Inverse Problems in Science and Engineering*, 20(3), 371–400.

[46] Bemis, C., Hu, X., Lin, W., Moazeni, S., Wang, L., Wang, T. & Zhang, J. (2009). Robust portfolio optimization using a simple factor model. *IMA Preprint Series*, No. 2284, University of Minnesota, Minneapolis, MN.

[47] Kara, G., Özmen, A., & Weber, G. W. (2019). Stability advances in robust portfolio optimization under parallelepiped uncertainty. *Central European Journal of Operations Research*, 27(1), 241–261.

[48] Postek, K., den Hertog, D. & Melenberg, B. (2016). Computationally tractable counterparts of distributionally robust constraints on risk measures. *SIAM Review*, 58(4), 603-–650.

[49] Gorissen, B.L., Yanıkoğlu, İ & den Hertog, D. (2015). A practical guide to robust optimization. *Omega*, 53, 124–137.

[50] Ben-Tal, A., den Hertog, D. & and Vial, J.-P. (2015). Deriving robust counterparts of nonlinear uncertain inequalities. *Mathematical Programming*, 149(1-2), 265–299.

[51] Yanıkoğlu, İ. (2018). Selected Topics in Robust Optimization. In: *Optimization Techniques for Problem Solving in Uncertainty.* IGI Global, PA, USA.

İhsan Yanıkoğlu *is an Assistant Professor of Industrial Engineering at Özyegin University, İstanbul, Turkey. He obtained his Ph.D. in Econometrics and Operations Research at Tilburg University in 2014. His research focuses on developing robust optimization methodologies and applying these methods in real-life problems. In 2017, he has received the Operations Engineering and Analytics Best Paper Award from IIE Transactions Journal with his publication titled "Robust Dual-response Optimization" together with Dick den Hertog and Jack Kleijnen. His research has been published in journals such as SIAM Journal on Optimization, INFORMS Journal on Computing, OMEGA, IIE Transactions, and EJOR.*

An International Journal of Optimization and Control: Theories & Applications
ISSN:2146-0957 eISSN:2146-5703
Vol.9, No.2, pp.253-260 (2019)
http://doi.org/10.11121/ijocta.01.2019.00549

RESEARCH ARTICLE

On Hermite-Hadamard type inequalities for $S_{\varphi}-$preinvex functions by using Riemann-Liouville fractional integrals

Seda Kılınç *, Abdullah Akkurt and Hüseyin Yıldırım

Kahramanmaraş Sütçü İmam University, Department of Mathematics, Kahramanmaraş, Turkey
sedaaa_kilinc@hotmail.com, abdullahmat@gmail.com, hyildir@ksu.edu.tr

This paper is dedicated to the memory of our colleague, Dr. Hatice Yaldız, who recently passed away.

ARTICLE INFO

Article History:
Received 10 October 2017
Accepted 10 December 2018
Available 31 July 2019

Keywords:
Fractional integral
Riemann-Liouville fractional integral
Integral inequalities

AMS Classification 2010:
26A33; 26D10; 26D15; 41A55

ABSTRACT

In this study, we have obtained some Hermite-Hadamard type integral inequalities for $s_{\varphi}-$preinvex functions. These inequalities are a generalization of some of the results in the literature.

1. Introduction

Fractional calculus (see [1–3]) arise in the mathematical modeling of various problems in sciences and engineering such as mathematics, physics, chemistry and biology.

Many authors have been working to fractional integral operators (see [4–7]) due to many applications in differents areas of Mathematics, Engineering and Physics, etc (see [8, 9]). Also, these operators have allow to extended results about integral inequalities of many types (see [4, 10, 11]), for instance, Hermite-Hadamard integral inequalities (see [12–14]), Ostrowski type inequalities (see [7]).

In particular, in recent years, several extensions and generalizations have been considered for classical convexity (see [13, 15, 16]). A significant generalizations of convex functions is that of invex functions introduced by Hanson (see [17]).

In this work we derive several new inequalities of Hermite-Hadamard type for s_{φ} -preinvex function of first and second sense by using fractional integrals.

In this article, we define and recall some basic concepts and results. Let $\mathbb{R}^n$ be the finite dimensional Euclidian space, also $0 \leq \varphi \leq \frac{\pi}{2}$ be a continuous function.

Definition 1. ([7, 8]). *Let $f \in L_1[a,b]$. Then Riemann-Liouville fractional integrals $J^{\alpha}_{a+}f$ and $J^{\alpha}_{b-}f$ of order $\alpha > 0$ with $a \geq 0$ are defined by*

$$J^{\alpha}_{a+}f(x) = \frac{1}{\Gamma(\alpha)} \int_a^x (x-\tau)^{\alpha-1} f(\tau)\, d\tau, \qquad (1)$$

and

$$J^{\alpha}_{b-}f(x) = \frac{1}{\Gamma(\alpha)} \int_x^b (\tau-x)^{\alpha-1} f(\tau)\, d\tau, \qquad (2)$$

where Γ is the classical Gamma function.

Definition 2. *If $K_{\varphi\eta}$ in $\mathbb{R}^n$ set, is said to be $\varphi-$invex at u according to φ, if there exists a bifunction $\eta(.,.) : K_{\varphi\eta} \times K_{\varphi\eta} \to \mathbb{R}^n$, so that,*

$$u + \tau e^{i\varphi}\eta(u,v) \in K_{\varphi\eta},\ \forall u, v \in K_{\varphi\eta}, \tau \in [0,1].$$

*Corresponding Author

The $\varphi-$invex set $K_{\varphi\eta}$ is also called $\varphi\eta-$connected set. Note that the convex set with $\varphi = 0$ and $\eta(u,v) = v-u$ is a $\varphi-$invex set, but the converse is not true.

Theorem 1. *Let $f : I \subseteq \mathbb{R} \to \mathbb{R}$ is a convex function defined on the interval $I = [a,b]$ of real numbers where $a < b$. Then, the following double inequality*

$$f\left(\frac{a+b}{2}\right) \le \frac{1}{b-a}\int_a^b f(x)dx \le \frac{f(a)+f(b)}{2},$$

the above double inequality is known as Hermite-Hadamard type of inequality in the literature.

Let $\mathbb{R}$ be the set of real numbers. During the article $I = [a,b] \subset \mathbb{R}$ be the interval unless otherwise specified, also let $0 \le \varphi \le \dfrac{\pi}{2}$ be a continuous function.

Lemma 1. *Suppose a function $K_{\varphi\eta} \subseteq \mathbb{R}^n$ and $\varphi : K_{\varphi\eta} \to \mathbb{R}$, the $f : [a,b] \to \mathbb{R}$ be twice differentiable function on (a,b) with $a < b$, $\eta(.,.) : K_{\varphi\eta} \times K_{\varphi\eta} \to \mathbb{R}^n$, The $\varphi-$invex set $K_{\varphi\eta}$ and $0 \le \varphi \le \pi/2$ be a continuous function. Let $f'' \in L[a,b]$, afterward, we get the following equality for fractional integrals:*

$$\begin{aligned}
&\tfrac{2^{\alpha-1}\Gamma(\alpha+1)}{(e^{i\varphi}\eta(b,a))^{\alpha}}\left[J^{\alpha,\varphi}_{\left(a+\frac{e^{i\varphi}\eta(b,a)}{2}\right)^-} f(a)\right.\\
&\left.+J^{\alpha,\varphi}_{\left(a+\frac{e^{i\varphi}\eta(b,a)}{2}\right)^+} f(b)\right] - f\left(a+\tfrac{e^{i\varphi}\eta(b,a)}{2}\right)\\
&= \tfrac{\left|e^{i\varphi}\eta(b,a)\right|^2}{8(\alpha+1)}\int_0^1 (1-\tau)^{\alpha+1}\left(f''\left(a+\tfrac{1-\tau}{2}e^{i\varphi}\eta(b,a)\right)\right.\\
&\left.\times + f''\left(a+\tfrac{1+\tau}{2}e^{i\varphi}\eta(b,a)\right)\right)d\tau.
\end{aligned}$$

Proof. Let,

$$\begin{aligned}
&\int_0^1 (1-\tau)^{\alpha+1}\left[f''\left(a+\tfrac{1-\tau}{2}e^{i\varphi}\eta(b,a)\right)\right.\\
&\left.+f''\left(a+\tfrac{1+\tau}{2}e^{i\varphi}\eta(b,a)\right)\right]d\tau\\
&=\int_0^1 (1-\tau)^{\alpha+1} f''\left(a+\tfrac{1-\tau}{2}e^{i\varphi}\eta(b,a)\right)d\tau\\
&+\int_0^1 (1-\tau)^{\alpha+1} f''\left(a+\tfrac{1+\tau}{2}e^{i\varphi}\eta(b,a)\right)d\tau\\
&= I_1 + I_2.
\end{aligned} \tag{3}$$

Integration by part respectively:

$$\begin{aligned}
I_1 &= \int_0^1 (1-\tau)^{\alpha+1} f''\left(a+\tfrac{1-\tau}{2}e^{i\varphi}\eta(b,a)\right)d\tau\\
&= -\left.\tfrac{2(1-\tau)^{\alpha+1}f'\left(a+\frac{1-\tau}{2}e^{i\varphi}\eta(b,a)\right)}{e^{i\varphi}\eta(b,a)}\right|_0^1 - \tfrac{2(\alpha+1)}{e^{i\varphi}\eta(b,a)}\\
&\times \int_0^1 (1-\tau)^{\alpha} f'\left(a+\tfrac{1-\tau}{2}e^{i\varphi}\eta(b,a)\right)d\tau\\
&= \tfrac{2}{e^{i\varphi}\eta(b,a)} f'\left(a+\tfrac{e^{i\varphi}\eta(b,a)}{2}\right)\\
&-\tfrac{2(\alpha+1)}{e^{i\varphi}\eta(b,a)}\left[\tfrac{2}{e^{i\varphi}\eta(b,a)} f\left(a+\tfrac{e^{i\varphi}\eta(b,a)}{2}\right)\right.\\
&\left.-\tfrac{2^{\alpha+1}\Gamma(\alpha+1)}{e^{i\varphi}\eta(b,a)} \times J^{\alpha,\varphi}_{\left(a+\frac{e^{i\varphi}\eta(b,a)}{2}\right)^-} f(a)\right]\\
&= \tfrac{2}{e^{i\varphi}\eta(b,a)} f'\left(a+\tfrac{e^{i\varphi}\eta(b,a)}{2}\right)\\
&-\tfrac{4(\alpha+1)}{\left|e^{i\varphi}\eta(b,a)\right|^2} f\left(a+\tfrac{e^{i\varphi}\eta(b,a)}{2}\right)\\
&+\tfrac{2^{\alpha+2}\Gamma(\alpha+2)}{(e^{i\varphi}\eta(b,a))^{\alpha+2}} J^{\alpha,\varphi}_{\left(a+\frac{e^{i\varphi}\eta(b,a)}{2}\right)^-} f(a),
\end{aligned}$$

and,

$$\begin{aligned}
I_2 &= \int_0^1 (1-\tau)^{\alpha+1} f''\left(a+\tfrac{1+\tau}{2}e^{i\varphi}\eta(b,a)\right)d\tau\\
&= \left.\tfrac{2(1-\tau)^{\alpha+1}f'\left(a+\frac{1+\tau}{2}e^{i\varphi}\eta(b,a)\right)}{e^{i\varphi}\eta(b,a)}\right|_0^1\\
&+\tfrac{2(\alpha+1)}{e^{i\varphi}\eta(b,a)}\int_0^1 (1-\tau)^{\alpha} f'\left(a+\tfrac{1+\tau}{2}e^{i\varphi}\eta(b,a)\right)d\tau\\
&= -\tfrac{2}{e^{i\varphi}\eta(b,a)} f'\left(a+\tfrac{e^{i\varphi}\eta(b,a)}{2}\right)\\
&+\tfrac{2(\alpha+1)}{e^{i\varphi}\eta(b,a)}\left[-\tfrac{2}{e^{i\varphi}\eta(b,a)} f\left(a+\tfrac{e^{i\varphi}\eta(b,a)}{2}\right)\right.\\
&\left.+\tfrac{2^{\alpha+1}\Gamma(\alpha+1)}{e^{i\varphi}\eta(b,a)} J^{\alpha,\varphi}_{\left(a+\frac{e^{i\varphi}\eta(b,a)}{2}\right)^+} f(b)\right]\\
&= -\tfrac{2}{e^{i\varphi}\eta(b,a)} f'\left(a+\tfrac{e^{i\varphi}\eta(b,a)}{2}\right)\\
&-\tfrac{4(\alpha+1)}{\left|e^{i\varphi}\eta(b,a)\right|^2} f\left(a+\tfrac{e^{i\varphi}\eta(b,a)}{2}\right)\\
&+\tfrac{2^{\alpha+2}\Gamma(\alpha+2)}{(e^{i\varphi}\eta(b,a))^{\alpha+2}} J^{\alpha,\varphi}_{\left(a+\frac{e^{i\varphi}\eta(b,a)}{2}\right)^+} f(b).
\end{aligned}$$

Using I_1 and I_2 in (3), and afterwards multiplying both sides by $\dfrac{(e^{i\varphi}\eta(b,a))^2}{8(\alpha+1)}$ the proof is done. □

If we take $\alpha = 1$ in Lemma 1, we obtain to following result.

Lemma 2. *Let $K_{\varphi\eta} \subseteq \mathbb{R}^n$ and $\varphi : K_{\varphi\eta} \to \mathbb{R}$, the $f : [a,b] \to \mathbb{R}$ be twice differentiable function on (a,b) with $a < b$. Let $f'' \in L[a,b]$, afterward, $\eta(.,.) : K_{\varphi\eta} \times K_{\varphi\eta} \to \mathbb{R}^n$, the $\varphi-$invex set $K_{\varphi\eta}$ and $0 \le \varphi \le \frac{\pi}{2}$ be a continuous function. We get the following equality for fractional integrals:*

$$\begin{aligned}
&\tfrac{1}{e^{i\varphi}\eta(b,a)}\int_a^{a+\frac{e^{i\varphi}\eta(b,a)}{2}} f(x)dx - f\left(a+\tfrac{e^{i\varphi}\eta(b,a)}{2}\right)\\
&= \tfrac{\left|e^{i\varphi}\eta(b,a)\right|^2}{16}\int_0^1 (1-\tau)^2\\
&\left[f''\left(a+\tfrac{1-\tau}{2}e^{i\varphi}\eta(b,a)\right) + f''\left(a+\tfrac{1+\tau}{2}e^{i\varphi}\eta(b,a)\right)\right]d\tau.
\end{aligned}$$

If we take $\eta(b,a) = b-a$, $\varphi = 0$, then we have,

$$\left[a, a+e^{i\varphi}\eta(b,a)\right] = [a, a+\eta(b,a)] = [a,b].$$

2. Inequalities for S_φ-preinvex of second sense

In order to obtain main results introduced by [18] the $s_\varphi-$preinvex function of second sense.

Definition 3. *[18] A function f on the set $K_{\varphi\eta}$ is said to be $s_\varphi-$preinvex function of second sense according to φ and η, we get*

$$f\left(u+\tau e^{i\varphi}\eta(v,u)\right)\le(1-\tau)^s f(u)+\tau^s f(v), \quad (4)$$

where $\forall u,v\in K_{\varphi\eta},\tau\in[0,1]$.

Theorem 2. *Suppose a function $K_{\varphi\eta}\subseteq\mathbb{R}^n$ be a open invex set according to bifunction $\eta(.,.):K_{\varphi\eta}\times K_{\varphi\eta}\to\mathbb{R}^n$, The $\varphi-$invex set $K_{\varphi\eta}$ where $\eta(b,a)>0$. Also $\varphi:K_{\varphi\eta}\to\mathbb{R}$. Let $f''\in L_1\left[a,a+e^{i\varphi}\eta(b,a)\right]$ and $|f''|$ is s_φ-preinvex function of second sense, afterward, we get the following inequality for fractional integrals:*

$$\begin{aligned}&\left|\frac{2^{\alpha-1}\Gamma(\alpha+1)}{\left(e^{i\varphi}\eta(b,a)\right)^\alpha}\left[J^{\alpha,\varphi}_{\left(a+\frac{e^{i\varphi}\eta(b,a)}{2}\right)^-}f(a)\right.\right.\\&\left.\left.+J^{\alpha,\varphi}_{\left(a+\frac{e^{i\varphi}\eta(b,a)}{2}\right)^+}f(b)\right]-f\left(a+\frac{e^{i\varphi}\eta(b,a)}{2}\right)\right|\\&\le\frac{\left|e^{i\varphi}\eta(b,a)\right|^2}{2^{s+3}(\alpha+1)}\left\{\left(\frac{1}{s+1}\left[2^{s+1}-1\right]\right)+\frac{1}{s+\alpha+2}\right\}\\&\times\left[\left|f''(a)\right|+\left|f''(b)\right|\right].\end{aligned} \quad (5)$$

Proof. Via Lemma 1 and the fact that $|f''|$ is s_φ-preinvex function of second sense, we get

$$\begin{aligned}&\left|\frac{2^{\alpha-1}\Gamma(\alpha+1)}{\left(e^{i\varphi}\eta(b,a)\right)^\alpha}\left[J^{\alpha,\varphi}_{\left(a+\frac{e^{i\varphi}\eta(b,a)}{2}\right)^-}f(a)\right.\right.\\&\left.\left.+J^{\alpha,\varphi}_{\left(a+\frac{e^{i\varphi}\eta(b,a)}{2}\right)^+}f(b)\right]-f\left(a+\frac{e^{i\varphi}\eta(b,a)}{2}\right)\right|\\&=\left|\frac{\left(e^{i\varphi}\eta(b,a)\right)^2}{8(\alpha+1)}\int_0^1(1-\tau)^{\alpha+1}\right.\\&\times\left[f''\left(a+\tfrac{1-\tau}{2}e^{i\varphi}\eta(b,a)\right)\right.\\&\left.\left.+f''\left(a+\tfrac{1+\tau}{2}e^{i\varphi}\eta(b,a)\right)\right]d\tau\right|\\&\le\left|\frac{\left(e^{i\varphi}\eta(b,a)\right)^2}{8(\alpha+1)}\int_0^1(1-\tau)^{\alpha+1}\right.\\&\left.\times f''\left(a+\tfrac{1-\tau}{2}e^{i\varphi}\eta(b,a)\right)d\tau\right|\\&+\left|\frac{\left(e^{i\varphi}\eta(b,a)\right)^2}{8(\alpha+1)}\int_0^1(1-\tau)^{\alpha+1}\right.\\&\left.\times f''\left(a+\tfrac{1+\tau}{2}e^{i\varphi}\eta(b,a)\right)d\tau\right|\\&\le\frac{\left|e^{i\varphi}\eta(b,a)\right|^2}{8(\alpha+1)}\int_0^1(1-\tau)^{\alpha+1}\\&\times\left|f''\left(a+\tfrac{1-\tau}{2}e^{i\varphi}\eta(b,a)\right)\right|d\tau\\&+\frac{\left|e^{i\varphi}\eta(b,a)\right|^2}{8(\alpha+1)}\int_0^1(1-\tau)^{\alpha+1}\\&\times\left|f''\left(a+\tfrac{1+\tau}{2}e^{i\varphi}\eta(b,a)\right)\right|d\tau\end{aligned}$$

where

$$\int_0^1(1-\tau)^{\alpha+1}(1+\tau)^s d\tau\le\int_0^1(1+\tau)^s d\tau$$

the above selection will be accepted, namely,

$$\begin{aligned}&\le\frac{\left|e^{i\varphi}\eta(b,a)\right|^2}{8(\alpha+1)}\left[\int_0^1(1-\tau)^{\alpha+1}\right.\\&\left.\times\left(\left(\tfrac{1+\tau}{2}\right)^s\left|f''(a)\right|+\left(\tfrac{1-\tau}{2}\right)^s\left|f''(b)\right|\right)d\tau\right]\\&+\frac{\left|e^{i\varphi}\eta(b,a)\right|^2}{8(\alpha+1)}\left[\int_0^1(1-\tau)^{\alpha+1}\right.\\&\left.\times\left(\left(\tfrac{1-\tau}{2}\right)^s\left|f''(a)\right|+\left(\tfrac{1+\tau}{2}\right)^s\left|f''(b)\right|\right)d\tau\right]\\&=\frac{\left|e^{i\varphi}\eta(b,a)\right|^2}{2^{s+3}(\alpha+1)}\left[\left|f''(a)\right|\int_0^1(1-\tau)^{\alpha+1}(1+\tau)^s d\tau\right.\\&\left.+\left|f''(b)\right|\int_0^1(1-\tau)^{\alpha+1}(1-\tau)^s d\tau\right]\\&+\frac{\left|e^{i\varphi}\eta(b,a)\right|^2}{2^{s+3}(\alpha+1)}\left[\left|f''(a)\right|\int_0^1(1-\tau)^{\alpha+1}(1-\tau)^s d\tau\right.\\&\left.+\left|f''(b)\right|\int_0^1(1-\tau)^{\alpha+1}(1+\tau)^s d\tau\right]\\&\le\frac{\left|e^{i\varphi}\eta(b,a)\right|^2}{2^{s+3}(\alpha+1)}\left[\left|f''(a)\right|\left(\frac{1}{s+1}\left(2^{s+1}-1\right)\right)\right.\\&+\left|f''(b)\right|\frac{1}{s+\alpha+2}+\left|f''(a)\right|\frac{1}{s+\alpha+2}\\&\left.+\left|f''(b)\right|\left(\frac{1}{s+1}\left(2^{s+1}-1\right)\right)\right]\\&=\frac{\left|e^{i\varphi}\eta(b,a)\right|^2}{2^{s+3}(\alpha+1)}\left\{\left(\frac{1}{s+1}\left[2^{s+1}-1\right]\right)+\frac{1}{s+\alpha+2}\right\}\\&\times\left[\left|f''(a)\right|+\left|f''(b)\right|\right].\end{aligned}$$

which completes the proof of Theorem. □

Theorem 3. *Suppose a function $K_{\varphi\eta}\subseteq\mathbb{R}^n$ and $\varphi:K_{\varphi\eta}\to\mathbb{R}$, $f:[a,b]\to\mathbb{R}$ be twice differentiable function on (a,b) with $a<b$, $\eta(.,.):K_{\varphi\eta}\times K_{\varphi\eta}\to\mathbb{R}^n$.Also $\mathbb{R}^n$ be the finite dimensional Euclidian space. The $\varphi-$invex set $K_{\varphi\eta}$. Let $f''\in L[a,b]$ and $|f''|^q$ is s_φ-preinvex function of second sense, afterward, we get the following inequality for fractional integrals:*

$$\begin{aligned}&\left|\frac{2^{\alpha-1}\Gamma(\alpha+1)}{\left(e^{i\varphi}\eta(b,a)\right)^\alpha}\left[J^{\alpha,\varphi}_{\left(a+\frac{e^{i\varphi}\eta(b,a)}{2}\right)^-}f(a)\right.\right.\\&\left.\left.+J^{\alpha,\varphi}_{\left(a+\frac{e^{i\varphi}\eta(b,a)}{2}\right)^+}f(b)\right]-f\left(a+\frac{e^{i\varphi}\eta(b,a)}{2}\right)\right|\\&\le\frac{\left|e^{i\varphi}\eta(b,a)\right|^2}{2^{\frac{3q+s}{q}}(\alpha+1)}\left(\frac{1}{p(\alpha+1)+1}\right)^{\frac1p}\left(\frac{1}{s+1}\right)^{\frac1q}\\&\times\left[\left\{\left|f''(a)\right|^q\left(2^{s+1}-1\right)+\left|f''(b)\right|^q\right\}^{\frac1q}\right]\\&+\frac{\left|e^{i\varphi}\eta(b,a)\right|^2}{2^{\frac{3q+s}{q}}(\alpha+1)}\left(\frac{1}{p(\alpha+1)+1}\right)^{\frac1p}\left(\frac{1}{s+1}\right)^{\frac1q}\\&\times\left[\left\{\left|f''(a)\right|^q+\left|f''(b)\right|^q\left(2^{s+1}-1\right)\right\}^{\frac1q}\right].\end{aligned} \quad (6)$$

Proof. From Lemma 1, Holder's inequality and the fact that $|f''|^q$ is s_φ-preinvex function of second sense, we get

$$\begin{aligned}
&\left|\tfrac{2^{\alpha-1}\Gamma(\alpha+1)}{(e^{i\varphi}\eta(b,a))^\alpha}\left[J^{\alpha,\varphi}_{\left(a+\frac{e^{i\varphi}\eta(b,a)}{2}\right)^-}f(a)\right.\right.\\
&\left.\left.+J^{\alpha,\varphi}_{\left(a+\frac{e^{i\varphi}\eta(b,a)}{2}\right)^+}f(b)\right]-f\left(a+\tfrac{e^{i\varphi}\eta(b,a)}{2}\right)\right|\\
&=\left|\tfrac{\left(e^{i\varphi}\eta(b,a)\right)^2}{8(\alpha+1)}\int_0^1(1-\tau)^{\alpha+1}\right.\\
&\times\left[f''\left(a+\tfrac{1-\tau}{2}e^{i\varphi}\eta(b,a)\right)\right.\\
&\left.\left.+\,+f''\left(a+\tfrac{1+\tau}{2}e^{i\varphi}\eta(b,a)\right)\right]d\tau\right|\\
&\leq\left|\tfrac{\left(e^{i\varphi}\eta(b,a)\right)^2}{8(\alpha+1)}\int_0^1(1-\tau)^{\alpha+1}\right.\\
&\left.\times f''\left(a+\tfrac{1-\tau}{2}e^{i\varphi}\eta(b,a)\right)d\tau\right|\\
&+\left|\tfrac{\left(e^{i\varphi}\eta(b,a)\right)^2}{8(\alpha+1)}\int_0^1(1-\tau)^{\alpha+1}\right.\\
&\left.\times f''\left(a+\tfrac{1+\tau}{2}e^{i\varphi}\eta(b,a)\right)d\tau\right|\\
&\leq\tfrac{\left|e^{i\varphi}\eta(b,a)\right|^2}{8(\alpha+1)}\left\{\left(\int_0^1(1-\tau)^{(\alpha+1)p}d\tau\right)^{\frac{1}{p}}\right.\\
&\left.\times\left(\int_0^1\left|f''\left(a+\tfrac{1-\tau}{2}e^{i\varphi}\eta(b,a)\right)\right|^q d\tau\right)^{\frac{1}{q}}\right\}\\
&+\tfrac{\left|e^{i\varphi}\eta(b,a)\right|^2}{8(\alpha+1)}\left\{\left(\int_0^1(1-\tau)^{(\alpha+1)p}d\tau\right)^{\frac{1}{p}}\right.\\
&\left.\times\left(\int_0^1\left|f''\left(a+\tfrac{1+\tau}{2}e^{i\varphi}\eta(b,a)\right)\right|^q d\tau\right)^{\frac{1}{q}}\right\}\\
&\leq\tfrac{\left|e^{i\varphi}\eta(b,a)\right|^2}{8(\alpha+1)}\left(\tfrac{1}{p(\alpha+1)+1}\right)^{\frac{1}{p}}\\
&\times\left\{\left(|f''(a)|^q\int_0^1\left(\tfrac{1+\tau}{2}\right)^s d\tau^{\frac{1}{q}}\right.\right.\\
&\left.+|f''(b)|^q\int_0^1\left(\tfrac{1-\tau}{2}\right)^s d\tau\right)^{\frac{1}{q}}\Bigg\}\\
&+\tfrac{\left|e^{i\varphi}\eta(b,a)\right|^2}{8(\alpha+1)}\left(\tfrac{1}{p(\alpha+1)+1}\right)^{\frac{1}{p}}\\
&\times\left\{\left(|f''(a)|^q\int_0^1\left(\tfrac{1-\tau}{2}\right)^s d\tau^{\frac{1}{q}}\right.\right.\\
&\left.+|f''(b)|^q\int_0^1\left(\tfrac{1+\tau}{2}\right)^s d\tau\right)^{\frac{1}{q}}\Bigg\}\\
&=\tfrac{\left|e^{i\varphi}\eta(b,a)\right|^2}{2^{\frac{3q+s}{q}}(\alpha+1)}\left(\tfrac{1}{p(\alpha+1)+1}\right)^{\frac{1}{p}}\left(\tfrac{1}{s+1}\right)^{\frac{1}{q}}\\
&\times\left[\left\{|f''(a)|^q\left(2^{s+1}-1\right)+|f''(b)|^q\right\}^{\frac{1}{q}}\right]\\
&+\tfrac{\left|e^{i\varphi}\eta(b,a)\right|^2}{2^{\frac{3q+s}{q}}(\alpha+1)}\left(\tfrac{1}{p(\alpha+1)+1}\right)^{\frac{1}{p}}\left(\tfrac{1}{s+1}\right)^{\frac{1}{q}}\\
&\times\left[\left\{|f''(a)|^q+|f''(b)|^q\left(2^{s+1}-1\right)\right\}^{\frac{1}{q}}\right],
\end{aligned}$$

which completes the proof of Theorem. □

Theorem 4. *Suppose a function$K_{\varphi\eta}\subseteq\mathbb{R}^n$ and $\varphi:K_{\varphi\eta}\to\mathbb{R}$, $f:[a,b]\to\mathbb{R}$ be twice differentiable function on (a,b) with $a<b$, $\eta(.,.):K_{\varphi\eta}\times K_{\varphi\eta}\to\mathbb{R}^n$. Also $\mathbb{R}^n$ be the finite dimensional Euclidian space .The $\varphi-$invex set $K_{\varphi\eta}$. Let $f''\in L[a,b]$ and $|f''|^q$ is $s_\varphi-$preinvex function of second sense, afterward, we get the following inequality for fractional integrals:*

$$\begin{aligned}
&\left|\tfrac{2^{\alpha-1}\Gamma(\alpha+1)}{(e^{i\varphi}\eta(b,a))^\alpha}\left[J^{\alpha,\varphi}_{\left(a+\frac{e^{i\varphi}\eta(b,a)}{2}\right)^-}f(a)\right.\right.\\
&\left.+J^{\alpha,\varphi}_{\left(a+\frac{e^{i\varphi}\eta(b,a)}{2}\right)^+}f(b)\right]\\
&\left.-f\left(a+\tfrac{e^{i\varphi}\eta(b,a)}{2}\right)\right|\\
&\leq\tfrac{\left|e^{i\varphi}\eta(b,a)\right|^2}{2^{\frac{3q+s}{q}}(\alpha+1)}\left(\tfrac{1}{\alpha+2}\right)^{1-\frac{1}{q}}\\
&\times\left[\left\{|f''(a)|^q\left(\tfrac{1}{s+1}\left[2^{s+1}-1\right]\right)^{\frac{1}{q}}\right.\right.\\
&\left.\left.+|f''(b)|^q\tfrac{1}{\alpha+s+2}\right\}^{\frac{1}{q}}\right]\\
&+\tfrac{\left|e^{i\varphi}\eta(b,a)\right|^2}{2^{\frac{3q+s}{q}}(\alpha+1)}\left(\tfrac{1}{\alpha+2}\right)^{1-\frac{1}{q}}\\
&\times\left[|f''(a)|^q\tfrac{1}{\alpha+s+2}\right\}\\
&\left.+|f''(b)|^q\left(\tfrac{1}{s+1}\left[2^{s+1}-1\right]\right)\right\}^{\frac{1}{q}}\Bigg].
\end{aligned} \tag{7}$$

Proof. From Lemma 1, power-mean inequality and the fact that $|f''|^q$ is $s_\varphi-$preinvex function of second sense, we get

$$\begin{aligned}
&\left|\tfrac{2^{\alpha-1}\Gamma(\alpha+1)}{(e^{i\varphi}\eta(b,a))^\alpha}\left[J^{\alpha,\varphi}_{\left(a+\frac{e^{i\varphi}\eta(b,a)}{2}\right)^-}f(a)\right.\right.\\
&\left.+J^{\alpha,\varphi}_{\left(a+\frac{e^{i\varphi}\eta(b,a)}{2}\right)^+}f(b)\right]\\
&\left.-f\left(a+\tfrac{e^{i\varphi}\eta(b,a)}{2}\right)\right|\\
&=\left|\tfrac{\left(e^{i\varphi}\eta(b,a)\right)^2}{8(\alpha+1)}\int_0^1(1-\tau)^{\alpha+1}\left[f''\left(a+\tfrac{1-\tau}{2}e^{i\varphi}\eta(b,a)\right)\right.\right.\\
&\left.\left.+f''\left(a+\tfrac{1+\tau}{2}e^{i\varphi}\eta(b,a)\right)\right]d\tau\right|\\
&\leq\left|\tfrac{\left(e^{i\varphi}\eta(b,a)\right)^2}{8(\alpha+1)}\int_0^1(1-\tau)^{\alpha+1}f''\left(a+\tfrac{1-\tau}{2}e^{i\varphi}\eta(b,a)\right)d\tau\right|\\
&+\left|\tfrac{\left(e^{i\varphi}\eta(b,a)\right)^2}{8(\alpha+1)}\int_0^1(1-\tau)^{\alpha+1}f''\left(a+\tfrac{1+\tau}{2}e^{i\varphi}\eta(b,a)\right)d\tau\right|\\
&\leq\tfrac{\left|e^{i\varphi}\eta(b,a)\right|^2}{8(\alpha+1)}\left\{\left(\int_0^1(1-\tau)^{\alpha+1}d\tau\right)^{1-\frac{1}{q}}\right.\\
&\left.+\left(\int_0^1(1-\tau)^{\alpha+1}\left|f''\left(a+\tfrac{1-\tau}{2}e^{i\varphi}\eta(b,a)\right)\right|^q d\tau\right)^{\frac{1}{q}}\right\}\\
&\tfrac{\left|e^{i\varphi}\eta(b,a)\right|^2}{8(\alpha+1)}\left\{\left(\int_0^1(1-\tau)^{\alpha+1}d\tau\right)^{1-\frac{1}{q}}\right.\\
&\left.+\left(\int_0^1(1-\tau)^{\alpha+1}\left|f''\left(a+\tfrac{1+\tau}{2}e^{i\varphi}\eta(b,a)\right)\right|^q d\tau\right)^{\frac{1}{q}}\right\}\\
&\leq\tfrac{\left|e^{i\varphi}\eta(b,a)\right|^2}{2^{\frac{3q+s}{q}}(\alpha+1)}\left(\tfrac{1}{\alpha+2}\right)^{1-\frac{1}{q}}\\
&\times\left[\left\{|f''(a)|^q\left(\tfrac{1}{s+1}\left[2^{s+1}-1\right]\right)+|f''(b)|^q\tfrac{1}{\alpha+s+2}\right\}^{\frac{1}{q}}\right]\\
&+\tfrac{\left|e^{i\varphi}\eta(b,a)\right|^2}{2^{\frac{3q+s}{q}}(\alpha+1)}\left(\tfrac{1}{\alpha+2}\right)^{1-\frac{1}{q}}\\
&\times\left[\left\{|f''(a)|^q\tfrac{1}{\alpha+s+2}+|f''(b)|^q\left(\tfrac{1}{s+1}\left[2^{s+1}-1\right]\right)\right\}^{\frac{1}{q}}\right]
\end{aligned}$$

which completes the proof of Theorem. □

Remark 1. *If we take $\varphi = 0$ in Theorem 4, we obtain the results in [7].*

3. Inequalities for S$_\varphi$-convex funstions of first sense

In order to obtain main results introduced by [18] the $s_\varphi-$preinvex function of first sense.

Definition 4. *[18] Suppose a function f on the set $K_{\varphi\eta}$ is said to be $s_\varphi-$preinvex function of first sense according to φ and η, let*

$$f\left(u+\tau e^{i\varphi}\eta\left(v,u\right)\right)\leq\left(1-\tau^{s}\right)f(u)+\tau^{s}f(v), \tag{8}$$

$\forall u,v\in K_{\varphi\eta},\tau\in[0,1]$.

Theorem 5. *Suppose a function $K_{\varphi\eta}\subseteq\mathbb{R}^n$ and $\varphi : K_{\varphi\eta}\to\mathbb{R}$, the $f:[a,b]\to\mathbb{R}$ be twice differentiable function on (a,b) with $a<b$, $\eta(.,.) : K_{\varphi\eta}\times K_{\varphi\eta}\to\mathbb{R}^n$.Also $\mathbb{R}^n$ be the finite dimensional Euclidian space. The $\varphi-$invex set $K_{\varphi\eta}$. Let $f''\in L[a,b]$ and $|f''|$ is s_φ-preinvex function of second sense, afterward, we get the following inequality for fractional integrals:*

$$\begin{aligned}&\left|\frac{2^{\alpha-1}\Gamma(\alpha+1)}{(e^{i\varphi}\eta(b,a))^{\alpha}}\left[J^{\alpha,\varphi}_{\left(a+\frac{e^{i\varphi}\eta(b,a)}{2}\right)^-}f(a)\right.\right.\\&\left.+J^{\alpha,\varphi}_{\left(a+\frac{e^{i\varphi}\eta(b,a)}{2}\right)^+}f(b)\right]\\&\left.-f\left(a+\frac{e^{i\varphi}\eta(b,a)}{2}\right)\right|\\&\leq\frac{\left|e^{i\varphi}\eta(b,a)\right|^2}{8(\alpha+1)(\alpha+2)}\left[|f''(a)|+|f''(b)|\right].\end{aligned}$$

Proof. From Lemma 1 and the fact that $|f''|$ is s_φ-preinvex function of first sense, we get

$$\begin{aligned}&\left|\frac{2^{\alpha-1}\Gamma(\alpha+1)}{(e^{i\varphi}\eta(b,a))^{\alpha}}\left[J^{\alpha,\varphi}_{\left(a+\frac{e^{i\varphi}\eta(b,a)}{2}\right)^-}f(a)\right.\right.\\&\left.+J^{\alpha,\varphi}_{\left(a+\frac{e^{i\varphi}\eta(b,a)}{2}\right)^+}f(b)\right]\\&\left.-f\left(a+\frac{e^{i\varphi}\eta(b,a)}{2}\right)\right|\\&=\left|\frac{\left(e^{i\varphi}\eta(b,a)\right)^2}{8(\alpha+1)}\int_0^1(1-\tau)^{\alpha+1}\left[f''\left(a+\tfrac{1-\tau}{2}e^{i\varphi}\eta(b,a)\right)\right.\right.\\&\left.\left.+f''\left(a+\tfrac{1+\tau}{2}e^{i\varphi}\eta(b,a)\right)\right]d\tau\right|\\&\leq\left|\frac{\left(e^{i\varphi}\eta(b,a)\right)^2}{8(\alpha+1)}\int_0^1(1-\tau)^{\alpha+1}f''\left(a+\tfrac{1-\tau}{2}e^{i\varphi}\eta(b,a)\right)d\tau\right|\\&+\left|\frac{\left(e^{i\varphi}\eta(b,a)\right)^2}{8(\alpha+1)}\int_0^1(1-\tau)^{\alpha+1}f''\left(a+\tfrac{1+\tau}{2}e^{i\varphi}\eta(b,a)\right)d\tau\right|\\&\leq\frac{\left|e^{i\varphi}\eta(b,a)\right|^2}{8(\alpha+1)}\int_0^1(1-\tau)^{\alpha+1}\left|f''\left(a+\tfrac{1-\tau}{2}e^{i\varphi}\eta(b,a)\right)\right|d\tau\\&+\frac{\left|e^{i\varphi}\eta(b,a)\right|^2}{8(\alpha+1)}\int_0^1(1-\tau)^{\alpha+1}\left|f''\left(a+\tfrac{1+\tau}{2}e^{i\varphi}\eta(b,a)\right)\right|d\tau\\&\leq\frac{\left|e^{i\varphi}\eta(b,a)\right|^2}{8(\alpha+1)}\int_0^1(1-\tau)^{\alpha+1}\left\{1-\left(\tfrac{1-\tau}{2}\right)^s\right\}|f''(a)|\Big]d\tau\\&+\left(\tfrac{1-\tau}{2}\right)^s|f''(b)|\Big]d\tau\\&+\frac{\left|e^{i\varphi}\eta(b,a)\right|^2}{8(\alpha+1)}\left[\int_0^1(1-\tau)^{\alpha+1}\left(\tfrac{1-\tau}{2}\right)^s|f''(a)|\right.\\&\left.+\left(1-\left(\tfrac{1-\tau}{2}\right)^s\right)|f''(b)|\right]d\tau\\&=\frac{\left|e^{i\varphi}\eta(b,a)\right|^2}{8(\alpha+1)}\frac{1}{\alpha+2}\left[|f''(a)|+|f''(b)|\right]\end{aligned}$$

which completes the proof of Theorem.. □

Theorem 6. *Suppose a function $K_{\varphi\eta}\subseteq\mathbb{R}^n$ and $\varphi : K_{\varphi\eta}\to\mathbb{R}$, the $f:[a,b]\to\mathbb{R}$ be twice differentiable function on (a,b) with $a<b$, $\eta(.,.) : K_{\varphi\eta}\times K_{\varphi\eta}\to\mathbb{R}^n$, Also $\mathbb{R}^n$ be the finite dimensional Euclidian space. The $\varphi-$invex set $K_{\varphi\eta}$. If $f''\in L[a,b]$ and $|f''|^q$ is s_φ-preinvex function of second sense, afterward, we get the following inequality for fractional integrals:*

$$\begin{aligned}&\left|\frac{2^{\alpha-1}\Gamma(\alpha+1)}{(e^{i\varphi}\eta(b,a))^{\alpha}}\left[J^{\alpha,\varphi}_{\left(a+\frac{e^{i\varphi}\eta(b,a)}{2}\right)^-}f(a)\right.\right.\\&\left.+J^{\alpha,\varphi}_{\left(a+\frac{e^{i\varphi}\eta(b,a)}{2}\right)^+}f(b)\right]\\&\left.-f\left(a+\frac{e^{i\varphi}\eta(b,a)}{2}\right)\right|\\&\leq\frac{\left|e^{i\varphi}\eta(b,a)\right|^2}{2^{\frac{3q+s}{q}}(\alpha+1)}\left(\frac{1}{p(\alpha+1)+1}\right)^{\frac{1}{p}}\left(\frac{1}{s+1}\right)^{\frac{1}{q}}\\&\times\left\{\left(|f''(a)|^q\left(2^s(s+1)-1\right)+|f''(b)|^q\right)^{\frac{1}{q}}\right\}\\&+\frac{\left|e^{i\varphi}\eta(b,a)\right|^2}{2^{\frac{3q+s}{q}}(\alpha+1)}\left(\frac{1}{p(\alpha+1)+1}\right)^{\frac{1}{p}}\left(\frac{1}{s+1}\right)^{\frac{1}{q}}\\&\times\left\{\left(|f''(a)|^q+|f''(b)|^q\left(2^s(s+1)-1\right)\right)^{\frac{1}{q}}\right\}.\end{aligned}$$

Proof. From Lemma 1, Hölder inequality and the fact that $|f''|^q$ is s_φ-preinvex function of second sense, we get

$$\begin{aligned}&\left|\frac{2^{\alpha-1}\Gamma(\alpha+1)}{(e^{i\varphi}\eta(b,a))^{\alpha}}\left[J^{\alpha,\varphi}_{\left(a+\frac{e^{i\varphi}\eta(b,a)}{2}\right)^-}f(a)\right.\right.\\&\left.+J^{\alpha,\varphi}_{\left(a+\frac{e^{i\varphi}\eta(b,a)}{2}\right)^+}f(b)\right]\\&\left.-f\left(a+\frac{e^{i\varphi}\eta(b,a)}{2}\right)\right|\\&=\left|\frac{\left(e^{i\varphi}\eta(b,a)\right)^2}{8(\alpha+1)}\int_0^1(1-\tau)^{\alpha+1}\left[f''\left(a+\tfrac{1-\tau}{2}e^{i\varphi}\eta(b,a)\right)\right.\right.\\&\left.\left.+f''\left(a+\tfrac{1+\tau}{2}e^{i\varphi}\eta(b,a)\right)\right]d\tau\right|\\&\leq\left|\frac{\left(e^{i\varphi}\eta(b,a)\right)^2}{8(\alpha+1)}\int_0^1(1-\tau)^{\alpha+1}f''\left(a+\tfrac{1-\tau}{2}e^{i\varphi}\eta(b,a)\right)d\tau\right|\\&+\left|\frac{\left(e^{i\varphi}\eta(b,a)\right)^2}{8(\alpha+1)}\int_0^1(1-\tau)^{\alpha+1}f''\left(a+\tfrac{1+\tau}{2}e^{i\varphi}\eta(b,a)\right)d\tau\right|\\&\leq\frac{\left|e^{i\varphi}\eta(b,a)\right|^2}{8(\alpha+1)}\left(\int_0^1(1-\tau)^{(\alpha+1)p}d\tau\right)^{\frac{1}{p}}\\&\times\left(\int_0^1\left|f''\left(a+\tfrac{1-\tau}{2}e^{i\varphi}\eta(b,a)\right)\right|^q d\tau\right)^{\frac{1}{q}}\end{aligned}$$

$$+\frac{\left|e^{i\varphi}\eta(b,a)\right|^2}{8(\alpha+1)}\left(\int_0^1(1-\tau)^{(\alpha+1)p}d\tau\right)^{\frac{1}{p}}$$
$$\times\left(\int_0^1\left|f''\left(a+\frac{1+\tau}{2}e^{i\varphi}\eta(b,a)\right)\right|^q d\tau\right)^{\frac{1}{q}}$$
$$\leq\frac{\left|e^{i\varphi}\eta(b,a)\right|^2}{8(\alpha+1)}\left(\frac{1}{p(\alpha+1)+1}\right)^{\frac{1}{p}}\left(|f''(a)|^q\right.$$
$$\left.\times\int_0^1\left(1-\left(\frac{1-\tau}{2}\right)^s\right)d\tau+|f''(b)|^q\int_0^1\left(\frac{1-\tau}{2}\right)^s d\tau\right)^{\frac{1}{q}}$$
$$+\frac{\left|e^{i\varphi}\eta(b,a)\right|^2}{8(\alpha+1)}\left(\frac{1}{p(\alpha+1)+1}\right)^{\frac{1}{p}}\left(|f''(a)|^q\int_0^1\left(\frac{1-\tau}{2}\right)^s d\tau\right.$$
$$\left.+|f''(b)|^q\int_0^1\left\{1-\left(\frac{1-\tau}{2}\right)^s\right\}d\tau\right)^{\frac{1}{q}}$$
$$\leq\frac{\left|e^{i\varphi}\eta(b,a)\right|^2}{2^{\frac{3q+s}{q}}(\alpha+1)}\left(\frac{1}{p(\alpha+1)+1}\right)^{\frac{1}{p}}\left(\frac{1}{s+1}\right)^{\frac{1}{q}}$$
$$\times\left\{\left(|f''(a)|^q\left(2^s(s+1)-1\right)+|f''(b)|^q\right)^{\frac{1}{q}}\right\}$$
$$+\frac{\left|e^{i\varphi}\eta(b,a)\right|^2}{2^{\frac{3q+s}{q}}(\alpha+1)}\left(\frac{1}{p(\alpha+1)+1}\right)^{\frac{1}{p}}\left(\frac{1}{s+1}\right)^{\frac{1}{q}}$$
$$\times\left\{\left(|f''(a)|^q+|f''(b)|^q\left(2^s(s+1)-1\right)\right)^{\frac{1}{q}}\right\},$$

which completes the proof of Theorem. □

Theorem 7. *Suppose a function $K_{\varphi\eta}\subseteq\mathbb{R}^n$ and $\varphi:K_{\varphi\eta}\to\mathbb{R}$, the $f:[a,b]\to\mathbb{R}$ be twice differentiable function on (a,b) with $a<b$, $\eta(.,.):K_{\varphi\eta}\times K_{\varphi\eta}\to\mathbb{R}^n$. Also $\mathbb{R}^n$ be the finite dimensional Euclidian space. The $\varphi-$invex set $K_{\varphi\eta}$. Let $f''\in L[a,b]$ and $|f''|^q$ is s_φ-preinvex function of second sense, afterward, we get the following inequality for fractional integrals:*

$$\left|\frac{2^{\alpha-1}\Gamma(\alpha+1)}{\left(e^{i\varphi}\eta(b,a)\right)^\alpha}\left[J^{\alpha,\varphi}_{\left(a+\frac{e^{i\varphi}\eta(b,a)}{2}\right)^-}f(a)\right.\right.$$
$$\left.+J^{\alpha,\varphi}_{\left(a+\frac{e^{i\varphi}\eta(b,a)}{2}\right)^+}f(b)\right]$$
$$\left.-f\left(a+\frac{e^{i\varphi}\eta(b,a)}{2}\right)\right|$$
$$\leq\frac{\left|e^{i\varphi}\eta(b,a)\right|^2}{8(\alpha+1)}\left(\frac{1}{\alpha+2}\right)^{1-\frac{1}{q}}$$
$$\times\left(|f''(a)|^q\left(\frac{1}{\alpha+2}-\frac{1}{2^s}\frac{\Gamma(s+\alpha+2)}{\Gamma(s+\alpha+3)}\right)\right.$$
$$\left.+|f''(b)|^q\frac{1}{2^s}\frac{\Gamma(s+\alpha+2)}{\Gamma(s+\alpha+3)}\right)^{\frac{1}{q}}$$
$$+\frac{\left|e^{i\varphi}\eta(b,a)\right|^2}{8(\alpha+1)}\left(\frac{1}{\alpha+2}\right)^{1-\frac{1}{q}}$$
$$\times\left[|f''(a)|^q\frac{1}{2^s}\frac{1}{\alpha+s+2}\right.$$
$$\left.+|f''(b)|^q\left(\frac{1}{\alpha+2}-\frac{1}{2^s}\frac{1}{\alpha+s+2}\right)\right]^{\frac{1}{q}}.$$

Proof. From Lemma 1, power-mean inequality and the fact that $|f''|^q$ is s_φ-preinvex function of second sense, we get

$$\left|\frac{2^{\alpha-1}\Gamma(\alpha+1)}{\left(e^{i\varphi}\eta(b,a)\right)^\alpha}\left[J^{\alpha,\varphi}_{\left(a+\frac{e^{i\varphi}\eta(b,a)}{2}\right)^-}f(a)\right.\right.$$
$$\left.+J^{\alpha,\varphi}_{\left(a+\frac{e^{i\varphi}\eta(b,a)}{2}\right)^+}f(b)\right]$$
$$\left.-f\left(a+\frac{e^{i\varphi}\eta(b,a)}{2}\right)\right|$$
$$=\left|\frac{\left(e^{i\varphi}\eta(b,a)\right)^2}{8(\alpha+1)}\int_0^1(1-\tau)^{\alpha+1}\left[f''\left(a+\frac{1-\tau}{2}e^{i\varphi}\eta(b,a)\right)\right.\right.$$
$$\left.\left.+f''\left(a+\frac{1+\tau}{2}e^{i\varphi}\eta(b,a)\right)\right]d\tau\right|$$
$$\leq\left|\frac{\left(e^{i\varphi}\eta(b,a)\right)^2}{8(\alpha+1)}\int_0^1(1-\tau)^{\alpha+1}f''\left(a+\frac{1-\tau}{2}e^{i\varphi}\eta(b,a)\right)d\tau\right|$$
$$+\left|\frac{\left(e^{i\varphi}\eta(b,a)\right)^2}{8(\alpha+1)}\int_0^1(1-\tau)^{\alpha+1}f''\left(a+\frac{1+\tau}{2}e^{i\varphi}\eta(b,a)\right)d\tau\right|$$
$$\leq\frac{\left|e^{i\varphi}\eta(b,a)\right|^2}{8(\alpha+1)}\left(\int_0^1(1-\tau)^{\alpha+1}d\tau\right)^{1-\frac{1}{q}}$$
$$\times\left(\int_0^1(1-\tau)^{\alpha+1}\left|f''\left(a+\frac{1-\tau}{2}e^{i\varphi}\eta(b,a)\right)\right|^q d\tau\right)^{\frac{1}{q}}$$
$$+\frac{\left|e^{i\varphi}\eta(b,a)\right|^2}{8(\alpha+1)}\left(\int_0^1(1-\tau)^{\alpha+1}d\tau\right)^{1-\frac{1}{q}}$$
$$\times\left(\int_0^1(1-\tau)^{\alpha+1}\right.$$
$$\left.\times\left|f''\left(a+\frac{1+\tau}{2}e^{i\varphi}\eta(b,a)\right)\right|^q d\tau\right)^{\frac{1}{q}}$$
$$\leq\frac{\left|e^{i\varphi}\eta(b,a)\right|^2}{8(\alpha+1)}\left(\frac{1}{\alpha+2}\right)^{1-\frac{1}{q}}\left\{\int_0^1(1-\tau)^{\alpha+1}\right.$$
$$\times\left[\left(1-\left(\frac{1-\tau}{2}\right)^s\right)\right.$$
$$\left.\left.\times|f''(a)|^q+\left(\frac{1-\tau}{2}\right)|f''(b)|^q\right]d\tau\right\}^{\frac{1}{q}}$$
$$+\frac{\left|e^{i\varphi}\eta(b,a)\right|^2}{8(\alpha+1)}\left(\frac{1}{\alpha+2}\right)^{1-\frac{1}{q}}$$
$$\times\left\{\int_0^1(1-\tau)^{\alpha+1}\left[\left(1-\left(\frac{1-\tau}{2}\right)^s\right)|f''(b)|^q\right.\right.$$
$$\left.\left.+\left(\frac{1-\tau}{2}\right)|f''(a)|^q\right]d\tau\right\}^{\frac{1}{q}}$$
$$=\frac{\left|e^{i\varphi}\eta(b,a)\right|^2}{8(\alpha+1)}\left(\frac{1}{\alpha+2}\right)^{1-\frac{1}{q}}$$
$$\times\left(|f''(a)|^q\left(\frac{1}{\alpha+2}-\frac{1}{2^s}\frac{1}{\alpha+s+2}\right)\right.$$
$$\left.+|f''(b)|^q\frac{1}{2^s}\frac{1}{\alpha+s+2}\right)^{\frac{1}{q}}$$
$$+\frac{\left|e^{i\varphi}\eta(b,a)\right|^2}{8(\alpha+1)}\left(\frac{1}{\alpha+2}\right)^{1-\frac{1}{q}}$$
$$\times\left(|f''(a)|^q\frac{1}{2^s}\frac{1}{\alpha+s+2}\right.$$
$$\left.+|f''(b)|^q\left(\frac{1}{\alpha+2}-\frac{1}{2^s}\frac{1}{\alpha+s+2}\right)\right)^{\frac{1}{q}}$$

which completes the proof of Theorem. □

References

[1] Katugampola, U. N. (2011). New Approach to a generalized fractional integral. *Applied Mathematics and Computation*, 218(3), 860-865.

[2] Kilbas, A., Srivastava, H. M. and Trujillo, J.J. (2006). *Theory and applications of fractional differantial equations.* Elsevier B.V., Amsterdam Netherlands.

[3] Samko, S. G., Kilbas, A. A. and Marichev, O. I. (1993). *Fractional Integral and Derivatives, Theory and Applications.* Gordon and Breach, Yverdon et alibi.

[4] Ozdemir, M. E., Yildiz, C. and Kavurmaci, H. (2015). Fractional integral inequalities for different functions. `New Trends in Mathematical Sciences`, 3(2)2, 110-117.

[5] Sarikaya, M. Z., Set, E., Yaldiz, H. and Basak, N. (2013). Hermite-Hadamard's. inequalities for fractional integrals and related fractional inequalities. `Mathematical and Computer Modelling` 57, 2403-2407.

[6] Wang, J., Li, X., Feckan, M. and Zhou, Y. (2012). Hermite-Hadamard type inequalities for Riemann-Liouville fractional integrals via two kinds of convexity. *Applicable Analysis*, doi:10.1080/00036811.2012.727986.

[7] Yıldırım, H. and Kırtay, Z. (2014). Ostrowski Inequality for Generalized Fractional Integral and Related Inequalities. *Malaya Journal of Mathematics*, 2(3) 322-329.

[8] Das, S. (2011). *Functional Fractional Calculus.* Springer-Verlag, Berlin Heidelberg.

[9] Sarikaya, M. Z., Dahmani, Z., Kiris, M. and Ahmad, F. (2016). $(k,s)-$Riemann-Liouville fractional integral and applications. *Hacettepe Journal of Mathematics and Statistics*, 45(1), 77 − 89.

[10] Akkurt, A. and Yıldırım, H. (2013). On Feng Qi type integral inequalities for generalized fractional integrals. I*nternational Anatolia Academic Online Journal, Scientific Science*, 1(2), 22-25.

[11] Noor, M. A. and Awan, M. U. (2013). Some Integral inequalities for two kinds of convexities via fractional integrals. *Transylvanian Journal of Mathematics and Mechanics*, 5(2), 129-136.

[12] Cristescu, G. (2004). Hadamard type inequalities for $\varphi-$convex functions, Annals of the University of Oradea, Fascicle of Management and Technological Engineering, CD-Rom Edition, III (XIII).

[13] Dragomir, S. S. and Pearce, C. E. M. (2000). Selected topics on Hermite-Hadamard inequalities and applications, Victoria University, Australia.

[14] Dragomir, S. S., Pećarić, J. and Persson, L. E. (1995). Some inequalities of Hadamard type. *Soochow Journal of Mathematics*, 21, 335-341.

[15] Cristescu, G. (2005). Improved integral inequalities for products of convex functions. *Journal of Inequalities in Pure and Applied Mathematics*, 6(2).

[16] Zhang, T. Y., Ji, A. P. and Qi, F. (2013). Some inequalities of Hermite-Hadamard type for s-convex functions with applications to means, Le Matematiche LXVIII, Fasc. I, 229-239, doi:10.4418/2013.68.1.17.

[17] Hanson, M. A. (1981). On sufficiency of the Kuhn-Tucker conditions. *Journal of Mathematical Analysis and Applications*, 80(2), 545-550.

[18] Noor, M. A., Awan, M. U., Noor, K. I. and Khan, S. (2015). Hermite–Hadamard type inequalities for differentiable hφ-preinvex functions. *Arabian Journal of Mathematics*, 4, 63-76.

Seda Kılınç *graduated from Kahramanmaraş Sütçü İmam University in 2014. In 2016, she received a master's degree from Kahramanmaraş Sütçü İmam University. In 2017, she started her Doctor of Philosophy (Ph.D) degree programme at Kahramanmaraş Sütçü İmam University.*

Abdullah Akkurt *holds Bachelor of Mathematics and Master of Science degrees from the University of Kahramanmaraş Sütçü İmam, Turkey. He is an Research Assistant in the Department of Mathematics in the University of Kahramanmaraş Sütçü İmam. His research interests are in special functions and integral inequalities. Presently, he is undertaking his Doctor of Philosophy (Ph.D) degree programme at University of Kahramanmaraş Sütçü İmam.*

Hüseyin Yıldırım *received his BSc (Maths) degree from Atatürk University, Erzurum, Turkey in 1986. He received his M.Sc. degree from Van Yüzüncü Yıl University in 1990. In 1995, he received a PhD (Maths) degrees from Ankara University. At present, he is working as a professor in the Department of Mathematics at Kahramanmaraş Sütçü İmam University (Turkey) and is the head of the department. He is the author or coauthor of more than 100 papers in the field of theory of inequalities, potential theory, integral equations and transforms, special functions, time-scales.*

INSTRUCTIONS FOR AUTHORS

Aims and Scope

This journal shares the research carried out through different disciplines in regards to optimization, control and their applications.

The basic fields of this journal are linear, nonlinear, stochastic, parametric, discrete and dynamic programming; heuristic algorithms in optimization, control theory, game theory and their applications. Problems such as managerial decisions, time minimization, profit maximizations and other related topics are also shared in this journal.

Besides the research articles expository papers, which are hard to express or model, conference proceedings, book reviews and announcements are also welcome.

Journal Topics

- Applied Mathematics,
- Financial Mathematics,
- Control Theory,
- Game Theory,
- Fractional Calculus,
- Fractional Control,
- Modeling of Bio-systems for Optimization and Control,
- Linear Programming,
- Nonlinear Programming,
- Stochastic Programming,
- Parametric Programming,
- Conic Programming,
- Discrete Programming,
- Dynamic Programming,
- Optimization with Artificial Intelligence,
- Operational Research in Life and Human Sciences,
- Heuristic Algorithms in Optimization,
- Applications Related to Optimization on Engineering.

Submission of Manuscripts

New Submissions

Solicited and contributed manuscripts should be submitted to IJOCTA via the journal's online submission system. You need to make registration prior to submitting a new manuscript (please click here to register and do not forget to define yourself as an "Author" in doing so). You may then click on the "New Submission" link on your User Home.

IMPORTANT: If you already have an account, please click here to login. It is likely that you will have created an account if you have reviewed or authored for the journal in the past.

On the submission page, enter data and answer questions as prompted. Click on the “Next” button on each screen to save your work and advance to the next screen. The names and contact details of at least four internationally recognized experts who can review your manuscript should be entered in the "Comments for the Editor" box.

You will be prompted to upload your files: Click on the “Browse” button and locate the file on your computer. Select the description of the file in the drop down next to the Browse button. When you have selected all files you wish to upload, click the “Upload” button. Review your submission before sending to the Editors. Click the “Submit” button when you are done reviewing. Authors are responsible for verifying all files have uploaded correctly.

You may stop a submission at any phase and save it to submit later. Acknowledgment of receipt of the manuscript by IJOCTA Online Submission System will be sent to the corresponding author, including an assigned manuscript number that should be included in all subsequent correspondence. You can also log-on to submission web page of IJOCTA any time to check the status of your manuscript. You will receive an e-mail once a decision has been made on your manuscript.

Each manuscript must be accompanied by a statement that it has not been published elsewhere and that it has not been submitted simultaneously for publication elsewhere.

Manuscripts can be prepared using LaTeX (.tex) or MSWord (.docx). However, manuscripts with heavy mathematical content will only be accepted as LaTeX files.

Preferred first submission format (for reviewing purpose only) is Portable Document File (.pdf). Please find below the templates for first submission.

Click here to download Word template for first submission (.docx)

Click here to download LaTeX template for first submission (.tex)

Revised Manuscripts

Revised manuscripts should be submitted via IJOCTA online system to ensure that they are linked to the original submission. It is also necessary to attach a separate file in which a point-by-point explanation is given to the specific points/questions raised by the referees and the corresponding changes made in the revised version.

To upload your revised manuscript, please go to your author page and click on the related manuscript title. Navigate to the "Review" link on the top left and scroll down the page. Click on the "Choose File" button under the "Editor Decision" title, choose the revised article (in pdf format) that you want to submit, and click on the "Upload" button to upload the author version. Repeat the same steps to upload the "Responses to Reviewers/Editor" file and make sure that you click the "Upload" button again.

To avoid any delay in making the article available freely online, the authors also need to upload the source files (Word or LaTex) when submitting revised manuscripts. Files can be compressed if necessary. The two-column final submission templates are as follows:

Click here to download Word template for final submission (.docx)

Click here to download LaTeX template for final submission (.tex)

Authors are responsible for obtaining permission to reproduce copyrighted material from other sources and are required to sign an agreement for the transfer of copyright to IJOCTA.

Article Processing Charges

There are no charges for submission and/or publication.

English Editing

Papers must be in English. Both British and American spelling is acceptable, provided usage is consistent within the manuscript. Manuscripts that are written in English that is ambiguous or incomprehensible, in the opinion of the Editor, will be returned to the authors with a request to resubmit once the language issues have been improved. This policy does not imply that all papers must be written in "perfect" English, whatever that may mean. Rather, the criteria require that the intended meaning of the authors must be clearly understandable, i.e., not obscured by language problems, by referees who have agreed to review the paper.

Presentation of Papers

Manuscript style

Use a standard font of the **11-point type: Times New Roman** is preferred. It is necessary to single line space your manuscript. Normally manuscripts are expected not to exceed 25 single-spaced pages including text, tables, figures and bibliography. All illustrations, figures, and tables are placed within the text at the appropriate points, rather than at the end.

During the submission process you must enter: (1) the full title, (2) names and affiliations of all authors and (3) the full address, including email, telephone and fax of the author who is to check the proofs. Supply a brief **biography** of each author at the end of the manuscript after references.

- Include the name(s) of any **sponsor(s)** of the research contained in the paper, along with **grant number(s)**.
- Enter an **abstract** of no more than 250 words for all articles.

Keywords

Authors should prepare no more than 5 keywords for their manuscript.

Maximum five **AMS Classification number** (http://www.ams.org/mathscinet/msc/msc2010.html) of the study should be specified after keywords.

Writing Abstract

An abstract is a concise summary of the whole paper, not just the conclusions. The abstract should be no more than 250 words and convey the following:

1. An introduction to the work. This should be accessible by scientists in any field and express the necessity of the experiments executed.
2. Some scientific detail regarding the background to the problem.
3. A summary of the main result.
4. The implications of the result.
5. A broader perspective of the results, once again understandable across scientific disciplines.

It is crucial that the abstract conveys the importance of the work and be understandable without reference to the rest of the manuscript to a multidisciplinary audience. Abstracts should not contain any citation to other published works.

Reference Style

Reference citations in the text should be identified by numbers in square brackets "[ ]". All references must be complete and accurate. Please ensure that every reference cited in the text is also present in the reference list (and vice versa). Online citations should include date of access. References should be listed in the following style:

Journal article

Author, A.A., & Author, B. (Year). Title of article. Title of Journal, Vol(Issue), pages.

Castles, F.G., Curtin, J.C., & Vowles, J. (2006). Public policy in Australia and New Zealand: The new global context. Australian Journal of Political Science, 41(2), 131–143.

Book

Author, A. (Year). Title of book. Publisher, Place of Publication.

Mercer, P.A., & Smith, G. (1993). Private Viewdata in the UK. 2nd ed. Longman, London.

Chapter

Author, A. (Year). Title of chapter. In: A. Editor and B. Editor, eds. Title of book. Publisher, Place of publication, pages.

Bantz, C.R. (1995). Social dimensions of software development. In: J.A. Anderson, ed. Annual review of software management and development. CA: Sage, Newbury Park, 502–510.

Internet document

Author, A. (Year). Title of document [online]. Source. Available from: URL [Accessed (date)].

Holland, M. (2004). Guide to citing Internet sources [online]. Poole, Bournemouth University. Available from: http://www.bournemouth.ac.uk/library/using/guide_to_citing_internet_sourc.html [Accessed 4 November 2004].

Newspaper article

Author, A. (or Title of Newspaper) (Year). Title of article. Title of Newspaper, day Month, page, column.

Independent (1992). Picking up the bills. Independent, 4 June, p. 28a.

Thesis

Author, A. (Year). Title of thesis. Type of thesis (degree). Name of University.

Agutter, A.J. (1995). The linguistic significance of current British slang. PhD Thesis. Edinburgh University.

Illustrations

Illustrations submitted (line drawings, halftones, photos, photomicrographs, etc.) should be clean originals or digital files. Digital files are recommended for highest quality reproduction and should follow these guidelines:

- 300 dpi or higher
- Sized to fit on journal page
- TIFF or JPEG format only
- Embedded in text files and submitted as separate files (if required)

Tables and Figures

Tables and figures (illustrations) should be embedded in the text at the appropriate points, rather than at the end. A short descriptive title should appear above each table with a clear legend and any footnotes suitably identified below.

Proofs

Page proofs are sent to the designated author using IJOCTA EProof system. They must be carefully checked and returned within 48 hours of receipt.

Offprints/Reprints

Each corresponding author of an article will receive a PDF file of the article via email. This file is for personal use only and may not be copied and disseminated in any form without prior written permission from IJOCTA.

Submission Preparation Checklist

As part of the submission process, authors are required to check off their submission's compliance with all of the following items, and submissions may be returned to authors that do not adhere to these guidelines.

1. The submission has not been previously published, nor is it before another journal for consideration (or an explanation has been provided in Comments for the Editor).
2. The submission file is in Portable Document Format (.pdf).
3. The ORCID profile numbers of "all" authors are ready to enter in the step of Article Metadata (visit https://orcid.org for more details).
4. The text is single line spaced; uses a 11-point font; employs italics, rather than underlining (except with URL addresses); and all illustrations, figures, and tables are placed within the text at the appropriate points, rather than at the end.
5. The text adheres to the stylistic and bibliographic requirements outlined in the Author Guidelines, which is found in "About the Journal".
6. Maximum five AMS Classification number (http://www.ams.org/mathscinet/msc/msc2010.html) of the study have been provided after keywords.
7. After the acceptance of manuscript (before copy editing), Word (.docx) or LaTeX (.tex) version of the paper will be presented.
8. The names and email addresses of at least four (4) possible reviewers have been indicated in "Comments for the Editor" box in Paper Submission Step 1. Please note that at least two of the recommendations should be from different countries. Avoid suggesting reviewers who are at arms-length from you or your co-authors. This includes graduate advisors, people in your current department, or any others with a conflict of interest.

Peer Review Process

All contributions, prepared according to the author guidelines and submitted via IJOCTA online submission system are evaluated according to the criteria of originality and quality of their scientific content. The corresponding author will receive a confirmation e-mail with a reference number assigned to the paper, which he/she is asked to quote in all subsequent correspondence.

All manuscripts are first checked by the Technical Editor using plagiarism detection software (iThenticate) to verify originality and ensure the quality of the written work. If the result is not satisfactory (i.e. exceeding the limit of 30% of overlapping), the submission is rejected and the author is notified.

After the plagiarism check, the manuscripts are evaluated by the Editor-in-Chief and can be rejected without reviewing if considered not of sufficient interest or novelty, too preliminary or out of the scope of the journal. If the manuscript is considered suitable for further evaluation, it is first sent to the Area Editor. Based on his/her opinion the paper is then sent to at least two independent reviewers. Each reviewer is allowed up to four weeks to return his/her feedback but this duration may be extended based on his/her availability. IJOCTA has instituted a blind peer review process where the reviewers' identities are not known to authors. When the reviews are received, the Area Editor gives a decision and lets the author know it together with the reviewer comments and any supplementary files.

Should the reviews be positive, the authors are expected to submit the revised version usually within two months the editor decision is sent (this period can be extended when the authors contact to the editor and let him/her know that they need extra time for resubmission). If a revised paper is not resubmitted within the deadline, it is considered as a new submission after all the changes requested by reviewers have been made. Authors are required to submit a new cover letter, a response to reviewers letter and the revised manuscript (which ideally shows the revisions made in a different color or highlighted). If a change in authorship (addition or removal of author) has occurred during the revision, authors are requested to clarify the reason for change, and all authors (including the removed/added ones) need to submit a written consent for the change. The revised version is evaluated by the Area editor and/or reviewers and the Editor-in-Chief brings a decision about final acceptance based on their suggestions. If necessary, further revision can be asked for to fulfil all the requirements of the reviewers.

When a manuscript is accepted for publication, an acceptance letter is sent to the corresponding author and the authors are asked to submit the source file of the manuscript conforming to the IJOCTA two-column final submission template. After that stage, changes of authors of the manuscript are not possible. The manuscript is sent to the Copyeditor and a linguistic, metrological and technical revision is made, at which stage the authors are asked to make the final corrections in no more than a week. The layout editor prepares the galleys and the authors receive the galley proof for final check before printing. The authors are expected to correct only typographical errors on the proofs and return the proofs within 48 hours. After the final check by the layout editor and the proofreader, the manuscript is assigned a DOI number, made publicly available and listed in the forthcoming journal issue. After printing the issue, the corresponding metadata and files published in this issue are sent to the databases for indexing.

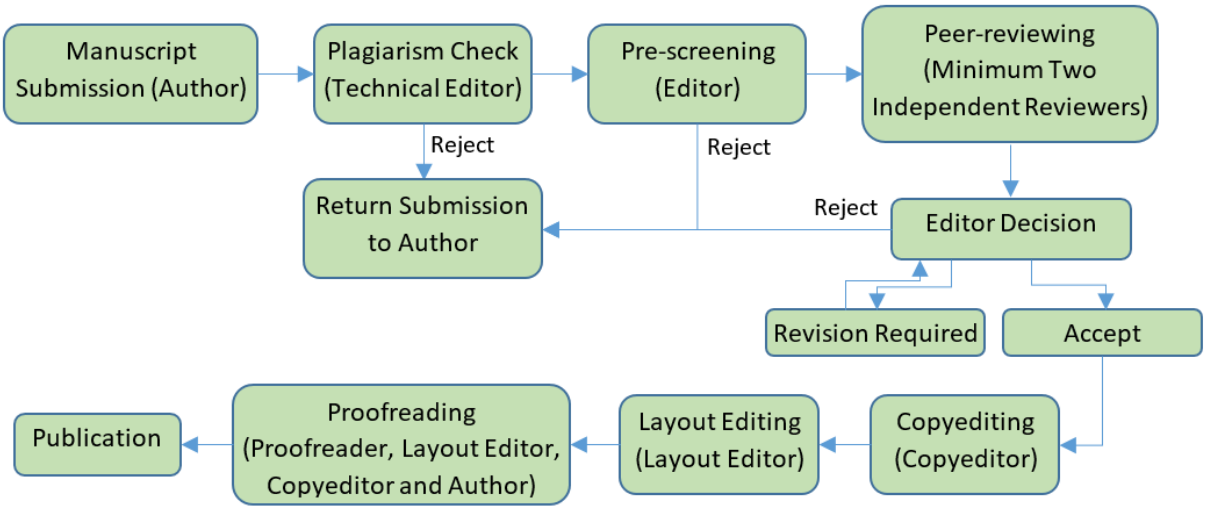

Publication Ethics and Malpractice Statement

IJOCTA is committed to ensuring ethics in publication and quality of articles. Conforming to standards of expected ethical behavior is therefore necessary for all parties (the author, the editor(s), the peer reviewer) involved in the act of publishing.

International Standards for Editors

The editors of the IJOCTA are responsible for deciding which of the articles submitted to the journal should be published considering their intellectual content without regard to race, gender, sexual orientation, religious belief, ethnic origin, citizenship, or political philosophy of the authors. The editors may be guided by the policies of the journal's editorial board and constrained by such legal requirements as shall then be in force regarding libel, copyright infringement and plagiarism. The editors may confer with other editors or reviewers in making this decision. As guardians and stewards of the research record, editors should encourage authors to strive for, and adhere themselves to, the highest standards of publication ethics. Furthermore, editors are in a unique position to indirectly foster responsible conduct of research through their policies and processes.

To achieve the maximum effect within the research community, ideally all editors should adhere to universal standards and good practices.

- Editors are accountable and should take responsibility for everything they publish.
- Editors should make fair and unbiased decisions independent from commercial consideration and ensure a fair and appropriate peer review process.
- Editors should adopt editorial policies that encourage maximum transparency and complete, honest reporting.
- Editors should guard the integrity of the published record by issuing corrections and retractions when needed and pursuing suspected or alleged research and publication misconduct.
- Editors should pursue reviewer and editorial misconduct.
- Editors should critically assess the ethical conduct of studies in humans and animals.
- Peer reviewers and authors should be told what is expected of them.
- Editors should have appropriate policies in place for handling editorial conflicts of interest.

Reference:

Kleinert S & Wager E (2011). Responsible research publication: international standards for editors. A position statement developed at the 2nd World Conference on Research Integrity, Singapore, July 22-24, 2010. Chapter 51 in: Mayer T & Steneck N (eds) Promoting Research Integrity in a Global Environment. Imperial College Press / World Scientific Publishing, Singapore (pp 317-28). (ISBN 978-981-4340-97-7) [Link].

International Standards for Authors

Publication is the final stage of research and therefore a responsibility for all researchers. Scholarly publications are expected to provide a detailed and permanent record of research. Because publications form the basis for both new research and the application of findings, they can affect not only the research community but also, indirectly, society at large. Researchers therefore have a responsibility to ensure that their publications are honest, clear, accurate, complete and balanced, and should avoid misleading, selective or ambiguous reporting. Journal editors also have responsibilities for ensuring the integrity of the research literature and these are set out in companion guidelines.

- The research being reported should have been conducted in an ethical and responsible manner and should comply with all relevant legislation.
- Researchers should present their results clearly, honestly, and without fabrication, falsification or inappropriate data manipulation.
- Researchers should strive to describe their methods clearly and unambiguously so that their findings can be confirmed by others.
- Researchers should adhere to publication requirements that submitted work is original, is not plagiarised, and has not been published elsewhere.
- Authors should take collective responsibility for submitted and published work.
- The authorship of research publications should accurately reflect individuals' contributions to the work and its reporting.

- Funding sources and relevant conflicts of interest should be disclosed.
- When an author discovers a significant error or inaccuracy in his/her own published work, it is the author's obligation to promptly notify the journal's Editor-in-Chief and cooperate with them to either retract the paper or to publish an appropriate erratum.

Reference:

Wager E & Kleinert S (2011) Responsible research publication: international standards for authors. A position statement developed at the 2nd World Conference on Research Integrity, Singapore, July 22-24, 2010. Chapter 50 in: Mayer T & Steneck N (eds) Promoting Research Integrity in a Global Environment. Imperial College Press / World Scientific Publishing, Singapore (pp 309-16). (ISBN 978-981-4340-97-7) [Link].

Basic principles to which peer reviewers should adhere

Peer review in all its forms plays an important role in ensuring the integrity of the scholarly record. The process depends to a large extent on trust and requires that everyone involved behaves responsibly and ethically. Peer reviewers play a central and critical part in the peer-review process as the peer review assists the Editors in making editorial decisions and, through the editorial communication with the author, may also assist the author in improving the manuscript.

Peer reviewers should:

- respect the confidentiality of peer review and not reveal any details of a manuscript or its review, during or after the peer-review process, beyond those that are released by the journal;
- not use information obtained during the peer-review process for their own or any other person's or organization's advantage, or to disadvantage or discredit others;
- only agree to review manuscripts for which they have the subject expertise required to carry out a proper assessment and which they can assess within a reasonable time-frame;
- declare all potential conflicting interests, seeking advice from the journal if they are unsure whether something constitutes a relevant conflict;
- not allow their reviews to be influenced by the origins of a manuscript, by the nationality, religion, political beliefs, gender or other characteristics of the authors, or by commercial considerations;
- be objective and constructive in their reviews, refraining from being hostile or inflammatory and from making libellous or derogatory personal comments;
- acknowledge that peer review is largely a reciprocal endeavour and undertake to carry out their fair share of reviewing, in a timely manner;
- provide personal and professional information that is accurate and a true representation of their expertise when creating or updating journal accounts.

Reference:

Homes I (2013). COPE Ethical Guidelines for Peer Reviewers, March 2013, v1 [Link].

An International Journal of Optimization and Control: Theories & Applications

Volume: 9 Number: 2
July 2019

CONTENTS

(see inside for the full list)

ISSN 2146-0957

www.ijocta.com
info@ijocta.com